UILU-ENG-82-2009

CIVIL ENGINEERING STUDIES

STRUCTURAL RESEARCH SERIES NO. 500

EFFECT OF GROUND MOTION CHARACTERISTICS ON THE SEISMIC RESPONSE OF TORSIONALLY COUPLED ELASTIC SYSTEMS

by
SHYH-YUAN KUNG
and
D. A. PECKNOLD

A Technical Report of
Research Supported by the
NATIONAL SCIENCE FOUNDATION
under Grant Nos. ENV 77-07190
and
PFR 80-02582

DEPARTMENT OF CIVIL ENGINEERING
UNIVERSITY OF ILLINOIS
AT URBANA-CHAMPAIGN
URBANA, ILLINOIS

JUNE 1982

EFFECT OF GROUND MOTION CHARACTERISTICS ON THE SEISMIC RESPONSE OF TORSIONALLY COUPLED ELASTIC SYSTEMS

By

SHYH-YUAN KUNG
and
D. A. PECKNOLD

A Report on a Research Project Sponsored by the
NATIONAL SCIENCE FOUNDATION
Research Grant Nos. ENV 77-07190 and PFR 80-02582

University of Illinois at Urbana-Champaign
Urbana, Illinois
June 1982

50272-101

REPORT DOCUMENTATION PAGE	1. REPORT NO. UILU - ENG-82-2009	2.	3. Recipient's Accession No.

4. Title and Subtitle
Effect Of Ground Motion Characteristics On The Seismic Response Of Torsionally Coupled Elastic Systems

5. Report Date
June 1982

6.

7. Author(s)
Shyh-Yuan Kung and D. A. Pecknold

8. Performing Organization Rept. No.
SRS 500

9. Performing Organization Name and Address
University of Illinois at Urbana-Champaign
Department of Civil Engineering
208 N. Romine Street
Urbana, Illinois 61801

10. Project/Task/Work Unit No.

11. Contract(C) or Grant(G) No.
(C) ENV 77-07190
(G) PFR 80-02582

12. Sponsoring Organization Name and Address
National Science Foundation
Washington, D.C. 20550

13. Type of Report & Period Covered

14.

15. Supplementary Notes

16. Abstract (Limit: 200 words)

This study presents a systematic investigation of the effects of ground motion characteristics, especially its multi-directional character, on the response of torsionally coupled elastic structural systems. The ground motion model is probabilistic and is founded on the assumption of the existence of ground motion principal directions. The structural systems considered are single-story and multi-story elastic shear beam models with stiffness eccentricity.

17. Document Analysis a. Descriptors
Dynamic Response, Earthquake Resistant Design, Ground Motion, Multi-directional, Seismic, Structural Dynamics, Torsion, Torsional Coupling.

b. Identifiers/Open-Ended Terms

c. COSATI Field/Group 13M

18. Availability Statement	19. Security Class (This Report)	21. No. of Pages
Release Unlimited	UNCLASSIFIED	339
	20. Security Class (This Page) UNCLASSIFIED	22. Price

ACKNOWLEDGMENT

This report was prepared as a doctoral dissertation by Mr. Shyh-Yuan Kung and was submitted to the Graduate College of the University of Illinois at Urbana-Champaign in partial fulfillment of the requirements for the Ph.D. degree. The study was directed by D. A. Pecknold, Professor of Civil Engineering.

The investigation was part of a research program sponsored by the National Science Foundation under Grants ENV 77-07190, Engineering Design for Natural Hazards and PFR 80-02582, Earthquake Engineering Design Investigations. Any opinions, findings, and conclusions or recommendations expressed in this publication are those of the authors and do not necessarily reflect the views of the National Science Foundation.

The authors wish to thank William J. Hall, Professor of Civil Engineering, for his suggestions and constructive comments throughout the course of the Study. The authors are also grateful for the assistance provided by the Office of Computing Services of the University of Illinois.

TABLE OF CONTENTS

Page

LIST OF TABLES

LIST OF FIGURES

Figure Page

Figure Page

CHAPTER 1

INTRODUCTION

This study presents a systematic investigation of the effects of ground motion characteristics, especially its multi-directional character, on the response of torsionally coupled elastic structural systems. The ground motion model is probabilistic and is founded on the assumption of the existence of ground motion principal directions. The structural systems considered are single-story and multi-story elastic shear beam models with stiffness eccentricity.

1.1 General Remarks

Conventional dynamic response analyses of structures to earthquake ground motions have often employed planar structural models and a single horizontal component of earthquake ground motions. There certainly exist many situations in which this approach furnishes sufficiently accurate information for design. However, there are cases in which planar structural models are not adequate and in which, in addition, the multi-directional character of the ground motion should be considered. Nuclear reactor components, pipelines, bridges, and buildings with asymmetric plan configurations are important examples. It has also been widely recognized that multi-story buildings which are nominally symmetric in layout are seldom actually so. As a result, such buildings respond in coupled translational and

torsional motion when subjected to horizontal ground motions. Building codes usually recognize such torsional response effects by specifying an eccentricity (a given percentage of the longest plan dimension of the structure) at which design horizontal forces are to be applied. The effects of multi-directional ground motions are also recognized by recent codes of practice (3,6). ATC-3-06 [6] requires that structural elements be designed for 100 percent of the effects of seismic forces in one principal direction combined with 30 percent of the effects of seismic forces in the orthogonal direction. For offshore platforms, the API Recommended Practice [3] specifies that 2/3 of the spectral acceleration for the principal horizontal axis be applied in the direction of the minor horizontal axis. Each of the two principal axes must be considered as possible directions for the larger horizontal ground motion.

1.2 Previous Work

The effects of torsion in buildings appears to have first been considered by Ayre [7, 8] who examined coupled translational and torsional vibration in discrete and continuous shear beam models. Most of the research in the area has been done in the last four decades, either mathematically for specific models of building structures or through experiments, and much insight has been gained.

A strong coupling effect can occur if corresponding natural

frequencies are close together, even when eccentricities are small [34, 47, 66, 77, 79]. A 95% increase in shear at the corner of a rectangular building was reported by Hoerner [34], as compared with 30% implied by 5% eccentricity in the code. The dynamic torque may be significantly larger than the product of horizontal shear times the eccentricity [47, 66, 71]. This effect arises from differences between dynamic and static methods of analysis, and is often associated with the term "dynamic magnification" of eccentricity. Rosenblueth and other authors [16, 47, 71] have concluded that horizontal shears are reduced as a result of torsional coupling. A second, distinct, cause of torsional response is "accidental" eccentricity resulting from inaccurate or imprecise knowledge of stiffness or mass distributions and the effects of the rotational components of ground motion (Newmark [58]). However, all these results are based on the assumption that ground motions are in the principal directions of the structure, and are uncorrelated. The overall response of buildings is sensitive to the orientation of the structure with respect to ground motion [26, 55].

Many papers have dealt with random process models for earthquake excitation. Commonly used models are discussed in standard texts [62]. Most early work modeled the ground motions as stationary random processes. The frequency characteristics are often modeled as white noise [17, 35] or filtered white noise [48, 81]. The time varying intensity is often handled by

modulating the stationary random process with a deterministic time varying function [2, 78].

Attention has only recently been given to modeling multi-directional ground motion [67]. Arias noted the existence of principal axes of ground motion. Later, Penzien and his colleagues [49, 67] found that "the uncorrelated components should be directed along a set of principal axes with the major principal axis being directed toward the expected epicenter and minor principal axis directed vertically". Thus, it may be reasonable to assume ground motion has principal axes, but these need not coincide with structure axes. With respect to the principal axes of the structure, the ground motion components are then statistically correlated.

Recent studies [22, 47] of single story elastic systems have provided valuable insight into the general features of torsional coupling. These studies employ either a smoothed design spectrum or actual recorded earthquake motions to describe the ground motion input. They also deal primarily with "one-way" torsional coupling and consider only a single component of ground motion. In addition, most previous work employs certain rules for combining modal responses [71]. Such combination rules may not be accurate enough when frequencies are closely spaced and ground motion correlations are present. Therefore, a method which can account for the correlation between components of ground motion and which does not rely on an arbitrary rule for the combination of modal responses is

desirable.

1.3 Object and Scope

The object of this study is to systematically investigate the effect of ground motion characteristics on the response of torsionally coupled elastic systems. It was desired to arrive at results which are as generally applicable as possible. Therefore, a probabilistic approach was selected so that the use of a limited number of specific recorded earthquake motions could be avoided.

The multi-directional ground motion model was based on the premise that a fixed set of ground motion principal directions exist, along which the ground motion components are statistically uncorrelated. Other important characteristics of earthquake ground motions which were addressed were frequency content, and time-varying intensity and duration. Limited attention was also given to some peripheral issues: lack of spatial correlation of ground motion components resulting in an effective rotational ground motion input; and the presence of large isolated acceleration pulses in the ground motion. Before carrying out the primary objective, a concerted effort was made to examine the ground motion model and compare its predictions, behavior, and features with the existing body of knowledge on recorded earthquake motions and response spectra.

In Chapter 2, the basic ground motion models used in this

study are presented. The characteristics of ground motions are discussed, commonly used stochastic models are re-examined and some properties necessary for later work are derived. Frequency content, time varying intensity and duration, and directionality are modeled. A previously unreported defect is revealed in a general class of ground motion models in which time varying intensity is modeled by modulating a stationary random process with a deterministic envelope function. Isolated acceleration pulses and ground motion spatial correlation characteristics are illustrated with a simple white noise model.

In Chapter 3, the methods used for computing structural responses to the ground motion models are described. An efficient solution algorithm is devised for evaluating the nonstationary response statistics of general multi-degree-of-freedom (MDOF) systems to the excitations of various ground motion models.

In Chapter 4, the effects of various ground motion characteristics on single-degree-of-freedom (SDOF) systems are discussed. Three frequency-content models described in Chapter 2 are evaluated by comparing computed SDOF response spectra with typical deterministic earthquake response spectra. Relations between mean square ground acceleration, velocity and displacement predicted by the ground motion model are compared with corresponding estimates proposed by Newmark and Hall [57]. Effects of ground motion frequency content and duration and

the presence of large acceleration pulses in the ground motion are also examined.

In Chapter 5, the effects of ground motion on the response of single-story torsionally coupled systems are investigated. A wide range of structural parameters is considered using a white noise model. The effects of frequency content and time-varying intensity of the ground motion are also examined. Ground motion correlation and directionality effects are studied and compared with the provisions of a recent recommended code of practice.

Lack of spatial correlation in the ground motion input is treated and related to the "accidental eccentricity" approach of Newmark [58].

In Chapter 6, the response of a special class of torsionally coupled tall buildings is considered and a numerical example for an 8 story structure is given. An approximate solution which yields a good approximation using only a few modes is discussed.

CHAPTER 2

RANDOM PROCESS MODELS OF EARTHQUAKE GROUND MOTIONS

2.1 Introduction

Selection of an appropriate earthquake ground motion is an old and persistent problem facing earthquake engineering researchers who wish to carry out either analytical or experimental studies of structural response and behavior. Two common approaches to defining ground motion are: 1). to assume that certain recorded ground motions are representative of future site ground motions. 2). to consider them as being sample funtions from stochastic processes having specified intensities and frequency contents.

The use of a (small) set of recorded accelerograms has disadvantages. The question immediately arises as to how many accelerograms must be used in order that the results will not be unduly biased. There is also no guarantee that future ground motions at a given site will resemble ground motions previously observed at that site. The task of selecting a suitable set of recorded accelerograms would be much easier if more were known about the significant characteristics of earthquake ground motions as they relate to structural response and behavior. Thus the selection of a set of recorded accelerograms is often made in the hope rather than the certainty that the important characteristics of ground motions are represented.

The second approach involves stochastic modelling of ground motion. The stochastic models are devised to possess similar characteristics, insofar as they are known, to recorded ground motions. The obvious pitfall in this procedure is that, at the present state of knowledge, the significant characteristics may not have been fully recognized and so are not incorporated in the ground motion model. However, despite this, the advantage of using a stochastic ground motion model is that its properties are well defined. As a result general conclusions regarding structural response can be drawn within the context of that well defined set of premises. It seems essential in such an approach to investigate carefully the characteristics of the stochastic ground motion model to make sure that it does in fact represent as well as possible the known characteristics of recorded ground motions. This is all the more important if the ground motion model is to used to study effects on structural response of ground motion characteristics, since in effect such a study becomes a study of variations of the parameters defining the model.

Two important characteristics which have received the most attention are: 1). frequency content 2). variation of intensities with time (nonstationarity). Many records have been analyzed to obtain information about these two characteristics and numerous models have been suggested [2, 10, 13, 14, 42, 48, 78, 83]. In this chapter, some commonly used models

which are employed in this work will be summarized. Some properties associated with these models will be examined, and a previously unreported defect in a widely used class of ground motion models will be pointed out. Interested readers should refer to the original references for additional details.

The model of ground motion acceleration, $a(t)$, is taken in the general form

$$a(t) = I(t)\ \xi(t) \tag{2.1}$$

where $\xi(t)$ is a zero mean stationary random process, and $I(t)$ is a deterministic envelope function. $\xi(t)$ gives the desired frequency content defined by a specified power spectral density function (PSDF) (Appendix [A]), while $I(t)$ accounts for the variation of ground motion intensity with time. The process $a(t)$ in Eq. (2.1) is called a "locally stationary process". This process has been successfully used to model nonstationary random phenomena by many researchers [53, 64, 68]. The autocorrelation function [Appendix A] of $a(t)$ is

$$R_a(t_1,t_2) = I(t_1)I(t_2)R_\xi(|t_1-t_2|) \tag{2.2}$$

where $R_\xi(|t_1-t_2|)$ is the autocorrelation function of $\xi(t)$.

2.2 Duration

The envelope function I(t) accounts for the variation of ground motion intensity with time. The simplest choice for the envelope function I(t) is a constant value. In this case, the ground motion is stationary. This assumption is not entirely reasonable from a physical standpoint. Nevertheless, it is of great importance because it leads to simple results which provide a great deal of insight. In addition, it often yields conservative estimates of the response of structural systems.

A number of envelope functions which give time-varying intensities have been proposed [2, 13, 14, 43, 78]. In this study, the envelope function proposed by Shinozuka and Sato [78] is employed. This choice was made because the Shinozuka and Sato envelope function is simple, and involves only a single analytical expression which makes it possible to analytically evaluate responses in many cases. The envelope function has a double exponential form given by

$$I(t) = C_e(e^{-\alpha t} - e^{-\beta t}) \tag{2.3}$$

in which

$$C_e = \frac{1}{(\frac{\alpha}{\beta})^{\frac{\alpha}{\beta-\alpha}} - (\frac{\alpha}{\beta})^{\frac{\beta}{\beta-\alpha}}}$$

is a normalizing constant chosen to make $I(t)_{max} = 1$.

In the limiting case $\alpha \to 0$, $\beta \to \infty$, $a(t)$ is stationary. The envelope functions for $\alpha = 0.25/\text{sec}$, $\beta = 0.75/\text{sec}$ and $\alpha = 0.10/\text{sec}$, $\beta = 0.20/\text{sec}$ are shown in Fig. 2.1. These two sets of parameters were chosen to provide a "short duration" and a "long duration" ground motion for the subsequent numerical work.

The time at which $I(t_{max}) = 1$ is

$$t_{max} = \frac{\ln(\frac{\beta}{\alpha})}{\beta - \alpha} \tag{2.4}$$

Fig. 2.2 and Table 2.1 show the variation of αt_{max} with the ratio β/α of envelope parameters for a range of values of α and β.

In order to describe the variation of ground motion intensity with time by a single index with some physical meaning, the concept of "duration" of strong ground motion is often used. Many definitions have been proposed, all of them rather arbitrary.

Husid [40] proposed a method for studying the evolution of ground shaking intensity with time. He suggested that the expression

$$h(t) = \frac{\int_0^t a^2(t)dt}{\int_0^{t_f} a^2(t)dt} \tag{2.5}$$

be used as a measure of time-dependent intensity. In Eq. (2.5), t_f is the total duration of the record.

Trifunac and Brady [82] and Dobry et al [25] define significant duration as the time interval between h(t) = 0.05 and h(t) = 0.95.

A parallel definition for time-dependent intensity for a probabilistic ground motion model is given by

$$h(t) = \frac{\int_0^t E[a^2(t)]dt}{\int_0^\infty E[a^2(t)]dt} \tag{2.6}$$

For the ground motion model described by Eq. (2.1), the intensity h(t) reduces to the simple expression

$$h(t) = \frac{\int_0^t I^2(t)dt}{\int_0^\infty I^2(t)dt} \tag{2.7}$$

in terms of the envelope function alone.

Note that $0 \leq h(t) \leq 1$. For the ground motion model described by Eqs. (2.1) and (2.3), it can easily be shown that

$$h(t) = \frac{\frac{1}{2\alpha}[1-e^{-2\alpha t}] + \frac{1}{2\beta}[1-e^{-2\beta t}] - \frac{2}{\alpha+\beta}[1-e^{-(\alpha+\beta)t}]}{[\frac{1}{2\alpha} + \frac{1}{2\beta} - \frac{2}{(\alpha+\beta)}]} \qquad (2.8)$$

The intensities h(t) for the two envelopes shown in Fig. 2.1, are given in the "Husid Plots" shown in Fig. 2.3. The "short duration" envelope reaches the 95 percent intensity level after about 8 seconds, while the "long duration" envelope reaches the 95 percent intensity level after about 23 seconds.

The corresponding Trifunac-Brady durations for the two envelope functions shown in Fig. 2.1 were calculated from Eq. (2.8) and are shown in the table below.

Envelope	Trifunac-Brady Duration D_{TB} (Sec)
Short Duration	7.24
Long Duration	20.41

Trifunac-Brady Durations for "Short" and "Long" Duration Envelopes

Table 2.1 shows the variation of duration D_{TB} with the envelope parameters α and β and Fig. 2.2 shows the ratio t_{max}/D_{TB} as a function of β/α, for a range of values of α and β.

Fig. 2.2 shows that the shape of the envelope (t_{max}/D_{TB}) is primarily controlled by the ratio β/α. The peak time t_{max} is then determined by the parameter α, given the desired shape of the envelope as specified by t_{max}/D_{TB}.

A more commonly used envelope in earthquake engineering is the well known three segment envelope consisting of a segment with parabolic buildup, followed by a segment of constant intensity and a segment of exponential decay. However, the envelope I(t) given in Eq.(2.3) was much more convenient for the purpose of this study since many of the results were then obtainable in closed form.

2.3 Frequency Content

The frequency content of the ground motion model is accounted for by the stationary random process $\xi(t)$ in Eq. (2.1). In this section several models for $\xi(t)$, with different levels of complexity and realism are presented.

2.3.1 White Noise

The simplest stochastic model for $\xi(t)$ is white noise. The white noise has a constant power spectral density function (PSDF),

$$S_{\xi}(\omega) = S_0 \tag{2.9}$$

The corresponding autocorrelation function is

$$R_{\xi}(\tau) = S_0 \delta(\tau) \tag{2.10}$$

where $\delta(\tau)$ is the Dirac delta function.

2.3.2 Filtered White Noise

2.3.2.1 Kanai-Tajimi Spectrum

Frequency domain analyses of recorded strong motion accelerograms demonstrate that earthquake power spectra are not

independent of frequency. They tend to have predominant frequencies. This suggests that stationary filtered white noise is a more reasonable assumption for $\xi(t)$ than is stationary white noise. Kanai and Tajimi [48, 81] have proposed a semi-empirical power spectral density function

$$S_{\xi}(\omega) = \frac{1 + 4\zeta_g^2 (\frac{\omega}{\omega_g})^2}{(1-(\frac{\omega}{\omega_g})^2)^2 + 4\zeta_g^2 (\frac{\omega}{\omega_g})^2} S_0 \qquad (2.11)$$

where ω_g and ζ_g are low pass filter parameters. These parameters can be thought of as foundation properties in a situation where a white noise disturbance is applied at bedrock and the motion is transmitted to the ground surface through a soil layer. The corresponding ground surface motion $\xi(t)$ can be obtained by passing white noise of spectral density S_0 through a low-pass filter [Appendix C]. The autocorrelation function of $\xi(t)$ [Appendix C] is

$$R_{\xi}(\tau) = \frac{S_0 \omega_g^2}{4\omega_g \zeta_g} \sqrt{\frac{1+8\zeta_g^2}{1-\zeta_g^2}} \{e^{-\omega_g \zeta_g |\tau|} \cos(\omega_g^d |\tau| - \phi)\} \qquad (2.12)$$

where

$$\omega_g^d = \omega_g \sqrt{1 - \zeta_g^2}$$

$$\phi = \tan^{-1} \frac{\zeta_g (1-4\zeta_g^2)}{\sqrt{1-\zeta_g^2}\,(1+4\zeta_g^2)}$$

For firm soil conditions, $\omega_g = 15.56$ rad/sec, $\zeta_g = 0.64$ have been recommended by Housner and Jennings [37] in the frequency range from $\omega = 2.1$ rad/sec to $\omega = 21$ rad/sec, corresponding to a period range from $T = 0.3$ sec to $T = 3$ sec. $S_\xi(\omega)$ and $R_\xi(\tau)$ are shown in Fig. 2.4.

The variance, $\sigma_\xi^2 \equiv R_\xi(0)$, can be easily obtained as

$$\sigma_\xi^2 = \frac{\omega_g}{4\zeta_g} (1 + 4\zeta_g^2) S_0 \qquad (2.13)$$

2.3.2.2 Clough-Penzien Spectrum

If ground acceleration $\xi(t)$ is modeled as described in the previous section, then an inconsistency arises because the variances of ground velocity and ground displacement become infinite as $\omega \to 0$. This can be seen from the relationships between power spectra for ground acceleration, velocity and displacement

$$S_v(\omega) = \frac{S_\xi(\omega)}{\omega^2} \qquad S_d(\omega) = \frac{S_\xi(\omega)}{\omega^4} \tag{2.14}$$

In Eq. (2.14) $S_v(\omega)$ and $S_d(\omega)$ are respectively the ground velocity power spectrum and the ground displacement power spectrum. To remove the singularity at $\omega = 0$, Clough and Penzien modified the Kanai-Tajimi formulation. Clough and Penzien suggest the power spectral density function

$$S_\xi(\omega) = \left[\frac{1 + 4\zeta_g^2 (\frac{\omega}{\omega_g})^2}{(1 - (\frac{\omega}{\omega_g})^2)^2 + 4\zeta_g^2 (\frac{\omega}{\omega_g})^2}\right]\left[\frac{(\frac{\omega}{\omega_f})^4 \quad S_0}{(1 - (\frac{\omega}{\omega_f})^2)^2 + 4\zeta_f^2 (\frac{\omega}{\omega_f})^2}\right] \tag{2.15}$$

where ω_f and ζ_f are high-pass filter parameters [Appendix C]. The ground acceleration $\xi(t)$ can be obtained by passing white noise successively through the Kanai-Tajimi filter and then through the Clough-Penzien filter. The corresponding autocorrelation function $R_\xi(\tau)$ has the general form

$$R_\xi(\tau) = S_0 \{ A_\xi e^{-\omega_g \zeta_g |\tau|} \cos(\omega_g^d |\tau| - \phi) + B_\xi e^{-\omega_f \zeta_f |\tau|} \cos(\omega_f^d |\tau| - \theta) \} \tag{2.16}$$

where $A_\xi, B_\xi, \phi, \theta$ are functions of ω_g, ζ_g, ω_f, and ζ_f. Analytical expressions for these parameters are given in Appendix [C].

The variance of ξ is equal to $R_\xi(0)$.

Ruiz and Penzien [75] analyzed several ground acceleration records for firm soil site conditions and obtained an average transfer function linking the motions of bedrock and ground surface [Fig. 2.5]. The two horizontal components of the four ground acceleration records indicated in Fig. 2.5 were used. They were normalized to unit spectral intensity as defined by Housner [39]. An optimization routine was used in [33] to fit the Clough-Penzien spectrum to the average transfer function. The filter parameters obtained in this way are ω_g = 15.46 rad /sec, ζ_g = 0.623, ω_f = 1.636 rad/sec, ζ_f = 0.619. For these filter parameters and S_0 = 1.0 m^2/sec^3,

A_ξ = 16.0895 m^2/sec^4 $\quad$ ϕ = -0.1657 rad

B_ξ = 0.8459 m^2/sec^4 $\quad$ θ = 4.2591 rad

The corresponding $S_\xi(\omega)$ and $R_\xi(\tau)$ are shown in Fig 2.6.

For the same filter parameters, the autocorrelation function corresponding to the Kanai-Tajimi spectrum gives

$$R_\xi(\tau) = 16.0690\ e^{-\omega_g \zeta_g |\tau|} \cos(\omega_g^d |\tau| - (-0.1724))$$

which is almost identical to the first term in Eq. (2.16). The second term of Eq. (2.16), although quite small in magnitude, contributes significantly to the response of systems with low natural frequency. The curve for $\omega_g = 5\pi$ rad/sec, $\zeta_g = 0.6$, $\frac{\omega_f}{\omega_g} = 0.1$, $\frac{\zeta_f}{\zeta_g} = 1$ is also shown in Fig. 2.4. For these rounded parameters and $S_0 = 1.0\ m^2/sec^3$, $A_\xi = 16.1416\ m^2/sec^4$, $\phi = -0.1291$ rad, $B_\xi = 0.8228\ m^2/sec^4$, and $\theta = 4.3336$ rad.

The auto-correlation function of ground velocity and ground displacement for the Clough-Penzien spectrum are

$$\begin{aligned} R_v(\tau) = -\{&A_\xi C_\xi e^{-\omega_g \zeta_g \tau} \cos(\omega_g^d \tau - \phi) + A_\xi D_\xi e^{-\omega_g \zeta_g \tau} \sin(\omega_g^d \tau - \phi) \\ &+ B_\xi E_\xi e^{-\omega_f \zeta_f \tau} \cos(\omega_f^d \tau - \theta) + B_\xi F_\xi e^{-\omega_f \zeta_f \tau} \sin(\omega_f^d \tau - \theta)\} S_0 \end{aligned} \tag{2.17}$$

$$\begin{aligned} R_d(\tau) = &A_\xi \{(C_\xi^2 - D_\xi^2) e^{-\omega_g \zeta_g \tau} \cos(\omega_g^d \tau - \phi) + 2C_\xi D_\xi e^{-\omega_g \zeta_g \tau} \sin(\omega_g^d \tau - \phi)\} S_0 \\ &+ B_\xi \{(E_\xi^2 - F_\xi^2) e^{-\omega_f \zeta_f \tau} \cos(\omega_f^d \tau - \theta) + 2E_\xi F_\xi e^{-\omega_f \zeta_f \tau} \sin(\omega_f^d \tau - \theta)\} S_0 \end{aligned}$$

where $\tau \geq 0$, and

$$C_\xi = \frac{\zeta_g^2}{\omega_g^2} - \frac{(\omega_g^d)^2}{\omega_g^4} \qquad D_\xi = -\frac{2\omega_g^d \zeta_g}{\omega_g^3}$$

$$E_\xi = \frac{\zeta_f^2}{\omega_f^2} - \frac{(\omega_f^d)^2}{\omega_f^4} \qquad F_\xi = -\frac{2\omega_f^d \zeta_f}{\omega_f^3}$$

In order to relate the properties of the probabilistic ground motion model to the body of existing information on recorded ground motions, three sets of filter parameters for the Clough-Penzien spectrum are chosen as follows:

Ground Motion No.	Filter Parameters				
	S_0	$\omega_g(\frac{rad}{sec})$	ζ_g	$\omega_f(\frac{rad}{sec})$	ζ_f
1	1.0	2π	0.400	0.2π	0.400
2	1.0	15.46	0.623	1.636	0.619
3	1.0	10π	0.800	π	0.800

The three cases are selected to represent ground motions having different characteristic frequencies, The corresponding spectrum shapes are shown in Fig. 2.7.

The variances of these ground motions are

Ground Motion No.	Variance				
	σ_ξ^2	σ_v^2	σ_d^2	$\frac{\sigma_\xi \sigma_d}{\sigma_v^2}$	$\frac{\sigma_v}{\sigma_\xi}$ (in/sec/g)
1	6.63	1.101	2.5695	3.75	157.44
2	15.50	0.270	0.0941	4.48	50.96
3	33.36	0.107	0.0102	5.49	21.84

in which $\sigma_\xi^2 = R_\xi(0)$, $\sigma_v^2 = R_v(0)$, $\sigma_d^2 = R_d(0)$

A parameter equal to the product of peak acceleration times peak displacement divided by the square of peak velocity is found to be about 6 for a large number of recorded earthquakes [30]. However, the value appears to be somewhat less for close-in earthquakes and the value was taken as 4 in the development of design spectra for the Diablo Canyon reactor facility [60]. Newmark and Hall [61] recommended the ratio of maximum velocity to maximum acceleration be taken as 48 in/sec/g and 36 in/sec/g for competent soil conditions and rock respectively. These values, based on analyses of recorded earthquakes, are intended for use in constructing smooth design spectra, given an estimate of peak ground acceleration. The coefficients $\sigma_\xi \sigma_d / \sigma_v$ and σ_v / σ_ξ for ground motion No. 2 show good agreement with the corresponding deterministic quantities recommended by Newmark and Hall. Fig. 2.8 shows the R.M.S. ground motion on a tripartite logarithmic plot (see also Figs. 4.1 and 4.2)

From the above discussion, one can see that the Clough-Penzien spectrum is quite flexible and can realistically model the frequency content of earthquake ground motions. Analytical expressions for the statistics (variances) of the ground motion can be easily obtained as functions of the filter parameters.

2.4 Low Frequency Behavior

In this section, the adequacy of the class of ground motion models specified by Eq. (2.1), for studying the response of very low frequency structural systems is examined. It appears that there is a fundamental defect in this class of ground motion models which has not previously been noted.

It is well known [62] that elastic response spectra for real ground motions exhibit a certain asymptotic behavior at low and high system frequencies. For very low system frequency the spectral displacement S_d approaches the peak ground displacement. For very high system frequency, the spectral pseudo-acceleration approaches the peak ground acceleration.

The low frequency behavior of the elastic response spectrum is dependent on the fact that for any real ground motion the relation

$$\int_0^T a(t)\, dt = v(T) - v(0) = 0 \qquad (2.18)$$

must hold, where T is the total duration of the ground motion.

Recorded accelerograms may not precisely satisfy this relation for a variety of reasons, including the presence of recording and digitizing errors. As a result, it is necessary to perform base-line adjustments on recorded accelerograms. If accelerograms are not adjusted to satisfy Eq. (2.18), then below some limiting frequency response calculations for low frequency systems are unreliable. The limiting frequency is dependent on the tolerance to which Eq. (2.18) is satisfied. If the tolerance is kept small enough, the limiting frequency can be kept below frequencies of practical interest. Pecknold and Riddell [65] estimate the limiting frequency as

$$f_\ell \cong v_o/2\pi d_m \tag{2.19}$$

where $$v_o = \left| \int_0^T a(t)\, dt \right|$$

and d_m = peak ground displacement

Chopra and Lopez [18] recently evaluated the suitability of simulated ground motions for studying response of long period structures. They developed a set of 8 simulated ground motions by generating samples of stationary Gaussian white noise, applying the 3-segment duration function described earlier and then passing the signal through a second order filter corresponding to the Kanai-Tajimi spectrum. They then applied two different base line correction procedures to the simulated motions and computed elastic response spectra.

Comparisons were made with elastic response spectra for a set of 8 recorded ground motions which had been subjected to the same base line correction procedures. The low frequency behavior of the set of simulated ground motions was quite different from that of the set of recorded ground motions, which was inevitable since they had different maximum ground displacements.

It should be expected that the simulated motions would not behave particularly well at low frequency since, as already noted, the Kanai-Tajimi spectrum is not realistic at low frequency. Perhaps all that the findings quoted above mean, in the context of this study, is that the base line correction procedures studied by Chopra and Lopez can not completely correct a gross vilation of relation Eq.(2.18) as was probably the case for the simulated ground motions.

The surprising fact which emerged during the course of this study is that even if the Clough-Penzien spectrum is used, which gives realistic behavior at low frequency, the basic form of the ground motion model

$$a(t) = I(t)\xi(t) \qquad (2.1)$$

introduces some low frequency error.

This may be shown as follows. Systems with extremely low natural frequencies "see" the ground motion as an impulse.

Consider then the impulse

$$\chi \equiv \int_0^\infty a(t)dt = \int_0^\infty I(t)\xi(t)dt \tag{2.20}$$

Note that $E[\chi] = 0$. However, the M.S. value of χ is

$$E[\chi^2] = \int_0^\infty \int_0^\infty I(t)I(s)R_\xi(t-s)dtds \tag{2.21}$$

If $I(t) = 1$, then $E[\chi^2] = 0$ for the Clough-Penzien spectrum. If a time varying envelope $I(t)$ is used, it seems extremely unlikely that $E[\chi^2] = 0$. For the double exponential envelope function and the Clough-Penzien spectrum, Eq.(2.21) can be put in the form

$$E[\chi^2] = C_e^2 \{ f(\alpha,\alpha) - f(\alpha,\beta) - f(\beta,\alpha) + f(\beta,\beta) \} \tag{2.22}$$

in which

$$f(\alpha,\beta) = 2 A_\xi C_P \{ [\frac{\omega_g\zeta_g - \beta}{\alpha+\beta} + \frac{\omega_g^{d_2} - (\alpha+\omega_g\zeta_g)(\omega_g\zeta_g-\beta)}{C_M}] \cos(\phi)$$

$$+ [\frac{\omega_g^d}{\alpha+\beta} - \frac{\omega_g^d(\alpha-\beta+2\omega_g\zeta_g)}{C_M}] \sin(\phi)\} S_0$$

$$+ 2B_\xi D_P \{ [\frac{\omega_f\zeta_f - \beta}{\alpha+\beta} + \frac{\omega_f^{d_2} - (\alpha+\omega_f\zeta_f)(\omega_f\zeta_f-\beta)}{D_M}] \cos(\theta)$$

$$+ [\frac{\omega_f^d}{\alpha+\beta} - \frac{\omega_f^d(\alpha-\beta+2\omega_f\zeta_f)}{D_M}] \sin(\theta)\} S_0$$

and

$$C_P = \frac{1}{(\omega_g\zeta_g-\beta)^2+\omega_g^{d_2}} \qquad C_M = \{(\alpha+\omega_g\zeta_g)^2 + \omega_g^{d_2}\}$$

$$D_P = \frac{1}{(\omega_f\zeta_f-\beta)^2+\omega_f^{d_2}} \qquad D_M = \{(\alpha+\omega_f\zeta_f)^2 + \omega_f^{d_2}\}$$

Thus the impulse χ is a zero mean random variable with a non-zero variance, which is evaluated explicitly for the Clough-Penzien spectrum and double exponential envelope function.

While it has not been explicitly evaluated for any other cases, it seems virtually certain that

$$E[\chi^2] > 0$$

is a general property of the class of ground motion models

$$a(t) = I(t)\xi(t) \tag{2.1}$$

The manner in which this quantity is related to structural response of low frequency systems is explained below.

If the system frequency is very low, the ground motion impulse becomes an initial velocity for the free vibration response of the system [65]. If the initial velocity is

$$v_o = \sqrt{E[\chi^2]}$$

the maximum displacement of the system is

$$S_d = \frac{\sqrt{E[\chi^2]}}{\omega} f_1(\zeta) \qquad (2.23)$$

where $f_1(\zeta) = \exp\{-(\frac{\pi}{2} - \arcsin\zeta)\zeta/\sqrt{1-\zeta^2}\}$

is a factor which depends on system damping as shown in the table below

Fraction of Critical Damping ζ	Function $f_1(\zeta)$
0	1.0
.01	.9845
.05	.9267
.10	.8626

thus the spectral pseudo velocity

$$S_v = \omega S_d = \sqrt{E[\chi^2]}\, f_1(\zeta)$$

is independent of system frequency at low frequency.

Therefore the R.M.S. response spectrum asymptotically approaches the limit

$$S_v \rightarrow \sqrt{E[\chi^2]}\, f_1(\zeta)$$

at low frequency, rather than the limit

$$S_d \rightarrow \sigma_d$$

These asymptotes are shown in Fig. 2.9, for the Clough-Penzien Ground Motion No. 2 and the short duration envelope.

An estimate of the frequency at which this spurious asymptotic behavior is likely to become evident can be made by finding the frequency at which the two asymptotes (for zero damping) intersect. This gives the frequency limit

$$f_\ell = \frac{\sqrt{E[\chi^2]}}{2\pi\sigma_d} \qquad (2.24)$$

which is analagous to the result quoted by Pecknold and Riddell [65].

f_ℓ (Hertz)	Clough-Penzien Ground Motion		
	No. 1	No. 2	No. 3
Short Duration	.104	.151	.171
Long Duration	.053	.058	.060

Fig. 2.10 shows the variation of the low frequency limit f_ℓ with a range of values of the envelope parameters α and β for the Clough-Penzien Ground Motion No. 2. (see also Table 2.1).

The frequency limit, f_ℓ, seems to be primarily a function of t_{max} and the "spurious" low frequency behavior is quite evident for ground motions with small t_{max}.

With the aid of Figs. 2.2 and 2.10 it is possible to choose a set of envelope parameters which provide the desired envelope shape, and to immediately determine an approximate system frequency above which the "spurious effect" mentioned above will be insignificant.

2.5 Individual Large Pulses

There has been speculation from time to time about the effect on structures of large isolated acceleration pulses in ground motions. For example, the 1971 Pacoima Dam record contains three acceleration pulses each lasting about 2/3 seconds between 2-4 seconds after the start of the record. These pulses have peak accelerations ranging from about 0.2 g to 0.7 g and contribute greatly to the structural response (Bertero [12]). In this study an attempt was made to incorporate pulses in the ground motion model and to study the effects of such motions on simple structural systems. This phase of the study is rather limited because no satisfactory method was found of relating model parameters describing the pulses to actual ground motion characteristics. Chopra and Lopez [18] compared a set of 8 artificially generated earthquake with a set of 8 recorded earthquakes. They found that

the ensemble of artifically generated earthquake had more zero crossings than the ensemble of recorded earthquakes and that the ensemble of recorded earthquakes had a greater number of large acceleration pulses (defined as the area under the accelerogram between successive zero crossings) than did the ensemble of artficial earthquakes.

This section outlines a method for including the effects of pulses in the ground motion model. A later section presents a limited parameter study on the effects of pulses on structural response.

The three ground motion models discussed above can all be obtained by passing white noise through linear filters. If the probability distribution of the white noise is Gaussian, then the linearly filtered motions are also Gaussian. In this case, the second-order moment statistics are sufficient to characterize the probability distribution of the ground motion. Previous studies of earthquake response [2, 52, 62] have assumed that the earthquake acceleration consists of a series of (filtered) impulses distributed randomly in time. If the average number of impulses per second, λ, tends to infinity, and the variance of the impulse magnitude σ^2 tends to zero in such a manner that $\lambda\sigma^2$ is constant, then the impulses can be shown using the central limit theorem [64] to be Gaussian white noise. Therefore, small impulses with a relatively high incidence rate are properly modeled as Gaussian white

noise. However, large less frequent pulses are not well represented as Gaussian white driven processes. A filtered compound Poisson process provides a better model for large pulses [Appendix D]. Therefore, it is perhaps more realistic to model ground motions as a combination of (filtered) Gaussian white noise and (filtered) compound Poisson impulses.

The Poisson pulses are white, that is, they have a constant PSDF; however, they do not have a Gaussian probability distribution. Hence, the response to this input is not Gaussian and the second order statistics do not therefore provide a complete description of the response. The details of the compound Poisson process are presented in Appendix D. Response of SDOF systems to this ground motion model are presented in Chapter 4.

2.6 Multi-Directional Ground Motion

An important factor in the response of structures to earthquakes is the multi-directional character of the ground motion. Recent recommended codes of practice such as ATC-3-06 [6] and API RP2A [3] provide methods for accounting for effects of multi-directional ground motions. However, these recommendations are not as solidly based on experience or research results as are other aspects of earthquake resistant design procedures. In this study, the effects of multi-directional ground motion on simple structures is studied in a systematic manner. This section presents the multi-directional ground motion model which was used.

Modelling of multi-directional ground motion is much more complicated than one-directional motion because the correlation between the components in various directions must be taken into account.

At any instant of time, the covariance matrix for multi-directional ground motion is symmetric and positive definite. Therefore, a set of orthogonal axes can always be found along which the components are uncorrelated statistically. These axes are defined as principal axes for ground motion. The determination of principal axes of ground motion is identical to that for principal axes of stress via Mohr's circle, which is familiar to structural engineers.

Unfortunately, the directions of principal axes for ground motion are time dependent. However, Penzien and his coworkers [49, 67] examined the San Fernando accelerograms and found that the directions of ground motion principal axes are relatively constant over time, particularly during the period of high intensity ground motion. They conclude that "the major principal direction points in the general direction of the epicentre and the minor principal axis is nearly vertical. It is concluded that artifically generated components of ground motion need not be correlated statistically provided that they are directed along a set of principal axes". Therefore, it seems reasonable to assume that translational ground motion has principal axes with constant directions, but these obviously need not coincide with the principal axes of the

structure.

Because insufficient data are available on rotational components of ground motion, they are not considered in this study. The only exception to this is the case in which spatial variability of translational ground motion can produce, for structures with large horizontal dimensions, an effective rotational ground motion input to the structure. This is discussed in Section 2.7. Since this work is focused on the interaction of lateral-torsional motions, vertical motions are also not considered. Hence, two uncorrelated horizontal components of ground motion directed along a set of principal axes are considered in this study. Each component is modeled as indicated in Eq. (2.1), with the same envelope function and frequency content.

Let e and d be the ground motion principal directions as shown in Fig. 2.11 Then the ground motion accelerations in these directions are modeled as

$$\begin{Bmatrix} a_e(t) \\ a_d(t) \end{Bmatrix} = \begin{Bmatrix} \bar{a}_e \\ \bar{a}_d \end{Bmatrix} I(t)\xi(t)$$

The autocorrelation functions for $a_e(t)$ and $a_d(t)$ are

$$\begin{aligned} R_{a_e}(t_1,t_2) &= I_e(t_1)I_e(t_2)R_{\xi_e}(|t_1-t_2|) \\ R_{a_d}(t_1,t_2) &= I_d(t_1)I_d(t_2)R_{\xi_d}(|t_1-t_2|) \end{aligned} \qquad (2.25)$$

where subscripts e and d indicate that the quantities are associated with e and d directions respectively.

The assumption of constant principal axis directions implies only that the cross-correlation function is zero at a given instant of time. It is further assumed in this study that the cross-correlation function

$$R_{a_e a_d}(t_1,t_2) = 0 \tag{2.26}$$

at different times t_1, t_2. There is not sufficient information available about the cross-correlation function to clearly justify this assumption. However, real earthquake accelerograms demonstrate a rapid loss in correlation with increasing values $|t_1 - t_2|$. This suggests that the influence of $R_{a_e a_d}(t_1,t_2)$ is negligible and that the assumption given in Eq. (2.26) is reasonable.

Let X and Y denote the principal axes of the structure, and let δ be the angle between the X direction and the e direction (Fig. 2.11). Then, the correlation functions of ground motions, $a_x(t)$ and $a_y(t)$, in the structure principal axes are

$$\begin{aligned} R_{a_x}(t_1,t_2) &= R_{a_e}(t_1,t_2)\cos^2(\delta) + R_{a_d}(t_1,t_2)\sin^2(\delta) \\ R_{a_y}(t_1,t_2) &= R_{a_e}(t_1,t_2)\sin^2(\delta) + R_{a_d}(t_1,t_2)\cos^2(\delta) \\ R_{a_x a_y}(t_1,t_2) &= \{R_{a_e}(t_1,t_2) - R_{a_d}(t_1,t_2)\}\sin(\delta)\cos(\delta) \end{aligned} \tag{2.27}$$

The covariance $R_{a_x a_y}(t,t)$ achieves its maximum value $(R_{a_e}(t,t) - R_{a_d}(t,t))/2$ at $\delta = \pi/4$. The normalized covariance, the cross-correlation coefficient, $\rho_{xy}(t)$ is obtained through the relation

$$\rho_{xy}(t) = \frac{R_{a_x a_y}(t,t)}{\sqrt{R_{a_x}(t,t) R_{a_y}(t,t)}} \qquad (2.28)$$

and takes values in the range (-1, 1). ρ_{xy} is a good indicator of linear dependency of two random variables. Kubo and Penzien [49] studied the San Fernando 3-directional ground motion records and determined statistical properties of principal variances for different geological classifications. These properties are summarized in Tables 2.2 and 2.3. Since the minor principal direction is nearly vertical during the strong motion period, the major and intermediate principal directions are approximately horizontal. Table 2.3 shows that for hard soil conditions the average major principal variance is about .61/.26 = 2.35 times the average intermediate principal variance. This corresponds to an average cross-correlation coefficient $(R_1-R_2)/(R_1+R_2)$ = 1.35/3.35 = 0.40 for ground motions in a set of axes rotated 45 degrees with respect to the ground motion principal directions. Therefore, treating ground motions

as independent quantities in the structure principal directions may sometimes be quite unconservative.

The variances $R_{a_x}(t,t)$ and $R_{a_y}(t,t)$ are plotted as functions of angle of incidence δ in Fig. 2.12, in which the principal variances $R_{a_e}(t,t)$ and $R_{a_d}(t,t)$ are assigned values 1 and 1/2.35 = .4255 respectively. As shown in Fig. 2.12, at $\delta = \pi/4$ and $\delta = \pi/8$ $R_{a_x}(t,t)$ and $R_{a_y}(t,t)$ are equal and $R_{a_x a_y}(t,t)$ reaches its maximum absolute value.

2.7 Spatial Correlation

For structures which have large horizontal dimensions, spatial differences in translational ground motion can produce an effective rotational ground motion input to the structure. Newmark [55, 59] used a travelling wave model to derive an expression for rotational ground motion input.

In this section, the spatial correlation of translation ground motion components is accounted for, which results in a probabilistic model for rotational ground motion, analogous to that of Newmark [59].

The ground motion models discussed up to this point are assumed to be uniform over the structure base. Previous research on spatial correlation [1, 33] showed that correlation of ground motion decays with the increase in distance. Therefore, the full correlation assumption is probably not appropriate for structures with very large base dimensions. The

partial correlation of ground motion may cause torsional excitation. To illustrate this, consider a structure being subjected to a one-directional translational base excitation shown in Fig. 2.13. The foundation is assumed to be rigid. The free-field ground motion at location y is designated as $\xi_x(t,y)$. The effective translational excitation $\hat{\xi}_x(t)$ averaged over the foundation dimension, is

$$\hat{\xi}_x(t) = \frac{1}{b}\int_{-b/2}^{b/2} \xi_x(t,y)\,dy \tag{2.29}$$

The effective torsional excitation $\hat{\xi}_\phi(t)$ is obtained by finding a $\xi_\phi(t)$ which minimizes the expression

$$\int_{-b/2}^{b/2} [\xi_x(t,y) - \hat{\xi}_x(t) - y\xi_\phi(t)]^2 dy \tag{2.30}$$

After simple calculations, $\hat{\xi}_\phi(t)$ is obtained as

$$\hat{\xi}_\phi(t) = \frac{12}{b^3}\int_{-b/2}^{b/2} \xi_x(t,y)\,y\,dy \tag{2.31}$$

It is emphasized that this effective torsional excitation is due to the smoothing effect of a rigid structural base on free-field translational ground motion which is not perfectly correlated spatially. It is also assumed that the wave shape is not affected by the presence of the structure, which may be questionable.

If ground motion $\xi_x(t,y)$ is assumed to be stationary and spatially homogeneous, then the PSDF of $\xi_x(t,y)$ can be denoted as $S_{\xi_x}(\tau,r)$, where r is $|y_1-y_2|$. The PSDF of $\hat{\xi}_x(t)$ and $\hat{\xi}_\theta(t) \equiv b\hat{\xi}_\phi$ are then

$$S_{\hat{\xi}_x}(\omega) = \frac{1}{b^2}\int_{-b/2}^{b/2}\int_{-b/2}^{b/2} S_{\xi_x}(\omega,|y_1-y_2|)dy_1dy_2$$

$$S_{\hat{\xi}_\theta}(\omega) = \frac{144}{b^4}\int_{-b/2}^{b/2}\int_{-b/2}^{b/2} y_1y_2S_{\xi_x}(\omega,|y_1-y_2|)dy_1dy_2 \qquad (2.32)$$

In the absence of information about the form of spatial correlation, a convenient expression is chosen. Suppose $S_{\xi_x}(\omega,r)$ takes the form

$$S_{\xi_x}(\omega,r) = S(\omega)R(\omega,r) \qquad (2.33)$$

where $S(\omega)$ is a local spectrum and $R(\omega,r)$ is a normalized cross spectrum. $R(\omega,r)$ is conveniently described by

$$R(\omega,r) = \exp[-c_s(\frac{r|\omega|}{V_s})^m] \qquad (2.34)$$

where V_s = shear wave velocity of soil and c_s = a constant. The shear wave velocity, V_s, is in general greater than 600 m/sec for firm soil conditions and is less than 600 m/sec for soft soil conditions. The parameter c_s accounts for the spatial correlation effects. A value of $c_s = 0$ corresponds to perfect spatial correlation. A value of $c_s = 0.5/2\pi$ was used in the study by Hindy and Novak [33] and is shown to be acceptable according to some ray measurements. This value corresponds to a correlation length of about (10 sec) x V_s for acceleration and (45 sec) x V_s for displacement. The correlation length is a characteristic length indicating how fast the spatial correlation decays. Interested readers should refer to Hindy and Novak et al [33] for details.

For m = 1, the following relations result

$$S_{\hat{\xi}_x}(z) = \frac{2}{z}\{1 + \frac{1}{z}(e^{-z} - 1)\} S(\omega)$$

$$S_{\hat{\xi}_\theta}(z) = 288\{\frac{1}{12z} - \frac{1}{z^3}(e^{-z}) - \frac{1}{4z^2}(1+e^{-z}) + \frac{1}{z^4}(1-e^{-z})\} S(\omega) \quad (2.35)$$

in which the dimensionless variable $z \equiv \frac{bc_s\omega}{V_s}$. For example, if $c_s = 0.5/2\pi$, $V_s = 600$ m/sec, $b = 100$ m, $\omega = 10\pi$ rad/sec, then $z = 0.41667$ and $S_{\hat{\xi}_x}(z) = 0.874$ and $S_{\hat{\xi}_\theta}(z) = 0.844$. Therefore, for systems with a large natural frequency and huge base dimensions, the torsional excitation is quite significant. $S_{\hat{\xi}_x}(z)$ and $S_{\hat{\xi}_\theta}(z)$ are plotted in Fig. 2.14 against z. $S_{\hat{\xi}_x}(z)$ decreases with increasing z. However, $S_{\hat{\xi}_\theta}(z)$ increases with increasing z up to $z = \sqrt{11.5} = 3.39$ and then decreases afterward. It is noted that the radius of gyration of a bar element is $r = \sqrt{\frac{b}{12}}$, so the torsional spectrum reaches a maximum approximately when the relation $\frac{V_s}{c_s} = \frac{b}{\sqrt{12}} = r$ holds.

2.8 Summary and Discussion

In this chapter, a class of stochastic ground motion models (Eq. (2.1)) was examined.

(1) Time varying intensity was modeled by means of a double exponential envelope proposed by Shinozuka and Sato. Time to peak intensity, t_{max}, and Trifunac-Brady duration, D_{TB} were related to the envelope parameters.

(2) Three different frequency content models were

considered: white noise, the Kanai-Tajimi spectrum, and the Clough-Penzien spectrum. Ground motion R.M.S. accelerations, velocities and displacements were calculated and appropriate ratios were compared with values recommended by Newmark and Hall for use in constructing smoothed design spectra given an estimate of peak ground acceleration.

(3). It was shown that ground motion acceleration models of the general form of Eq. (2.1) possess a previously unreported deficiency. Care should be taken in using such stochastic ground motion models in studies of structural response of very low frequency elastic systems.

(4). A multi-directional ground motion model based on the premise of the existence of fixed ground motion principal directions was discussed.

(5). The presence of large individual acceleration pulses in the ground motion was modeled, although there is not sufficient information available to select a reasonable range of parameters.

(6). Lack of spatial correlation in the translational ground acceleration resulting in an effective rotational ground motion input was modeled using a travelling wave model originally introduced by Newmark [59].

CHAPTER 3

RESPONSE OF LINEAR SYSTEMS TO SEISMIC EXCITATION

3.1 Introduction

This chapter introduces and summarizes the methods used in this study for computing structural responses to the ground motion models described in Chapter 2.

The ground motion models used in this study are zero mean random processes. The response to this ground motion of any linear structural system is therefore also random and has zero mean. Therefore, a great deal of information is contained in the second-order moment statistics of the response. Most of the response calculations carried out in this study involve determination of displacement and velocity response covariances.

Special consideration is given to systems with closely spaced frequencies, since such a situation arises in systems with lateral-torsional coupling. It is well known that conventional procedures experience accuracy problems when applied to systems with nearly equal natural frequencies [41, 47, 58, 71].

In this chapter, the effect on response of close frequencies is illustrated by considering the stationary response of systems excited by white noise; expressions are derived for covariances of response for general multi-DOF systems in terms of system properties and ground motion parameters; an efficient and accurate time domain response calculation procedure is

developed; and the probable response, which blends information on various response covariances into a better indicator of structural response is discussed.

It is assumed that damping in the structural model may be specified as a fraction of critical damping in each mode of vibration . For simplicity it is assumed that each mode has the same value of damping. Therefore, the well known normal mode method is employed. Throughout the study, the systems are assumed to have zero initial conditions. However, other initial conditions can be incorporated into the analysis if so desired.

3.2 Normal Mode Method for Multi-DOF Systems

This section contains a brief summary of the well known normal mode method for linear systems, in order to introduce notation.

Consider a general discrete, lumped mass system with N DOF subjected to ground motion excitation a(t). The equation of motion of the system is

$$[M]\{\ddot{u}\} + [C]\{\dot{u}\} + [K]\{u\} = -[M]\{r\}a \qquad (3.1)$$

where [M], [K] and [C] are mass, stiffness, and damping matrices of order NxN. {u}, {$\dot{u}$} and {$\ddot{u}$} are respectively displacement, velocity, and acceleration vectors relative

to the base. $\{r\}$ is a vector which represents the displacements resulting from a unit base displacement.

Let $\{\psi_j\}$ be the j-th free vibration mode of the system satisfying

$$[K]\{\psi_j\} = \omega_j^2[M]\{\psi_j\} \tag{3.2}$$

and the orthogonality conditions

$$\{\psi_j\}^T[M]\{\psi_k\} = \{\psi_j\}^T[K]\{\psi_k\} = 0 \qquad \text{if } j \neq k \tag{3.3}$$

where ω_j is the natural frequency of mode j.

Let $[\psi]$ denote the modal matrix whose columns contain the mode shapes

$$[\Psi] \equiv [\{\psi_1\}|\{\psi_2\}|\ldots|\{\psi_j\}|\ldots|\{\psi_N\}]$$

The displacement $\{u\}$ is transformed into mode shape coordinates $\{q\}$ through

$$\{q\} = [\Psi]^{-1}\{u\}$$

or (3.4)

$$\{u\} = [\Psi]\{q\}$$

where $\{q\}$ is a vector of modal displacements. Eq. (3.1) becomes

$$[M][\Psi]\{\ddot{q}\} + [C][\Psi]\{\dot{q}\} + [K][\Psi]\{q\} = -\ddot{y}[M]\{r\}a \tag{3.5}$$

Premultiplication of Eq. (3.5) by $[\psi]^T$, produces

$$[M^m]\{\ddot{q}\} + [C^m]\{\dot{q}\} + [K^m]\{q\} = -[\Psi]^T[M]\{r\}a \tag{3.6}$$

where

$$[M^m] = [\Psi]^T[M][\Psi]$$

$$[C^m] = [\Psi]^T[C][\Psi]$$

$$[K^m] = [\Psi]^T[K][\Psi]$$

$[M^m]$, $[C^m]$ and $[K^m]$ are respectively modal mass, damping and stiffness matrices. They are all diagonal matrices as a result of the orthogonality property of the mode shape vectors, and the modal damping assumption. Therefore, the method trans-

forms complicated systems into a set of N independent SDOF systems in the mode shape coordinates. From Eq. (3.2), one has $k^m_{jj} / m^m_{jj} = \omega_j^2$, in which k_{jj} and m_{jj} are j-th diagonal elements of $[K^m]$ and $[M^m]$ matrices respectively.

3.3 Multi DOF Systems with Closely Spaced Frequencies

In dynamic analyses of structures, closely spaced modes typically arise from symmetry or near-symmetry in buildings. The interaction between modes with nearly coincident frequencies may account for a significant increase in response. To illustrate the effect of close natural frequencies, consider linear systems excited by white noise. The equation of motion in the mode shape coordinates can be written as

$$\begin{Bmatrix} \ddot{q}_1 \\ \vdots \\ \ddot{q}_i \\ \vdots \\ \ddot{q}_j \\ \vdots \\ \ddot{q}_N \end{Bmatrix} + \begin{bmatrix} c_{11} & & & & \\ & \ddots & & 0 & \\ & & c_{ii} & & \\ & & & \ddots & \\ & 0 & & & c_{jj} \\ & & & \ddots & \\ & & & & c_{NN} \end{bmatrix} \begin{Bmatrix} \dot{q}_1 \\ \vdots \\ \dot{q}_i \\ \vdots \\ \dot{q}_j \\ \vdots \\ \dot{q}_N \end{Bmatrix} + \begin{bmatrix} \omega_{11}^2 & & & & \\ & \ddots & & 0 & \\ & & \omega_{ii}^2 & & \\ & & & \ddots & \\ & 0 & & & \omega_{jj}^2 \\ & & & \ddots & \\ & & & & \omega_{NN}^2 \end{bmatrix} \begin{Bmatrix} q_1 \\ \vdots \\ q_i \\ \vdots \\ q_j \\ \vdots \\ q_N \end{Bmatrix} = \begin{Bmatrix} \dot{W}_1 \\ \vdots \\ \dot{W}_i \\ \vdots \\ \dot{W}_j \\ \vdots \\ \dot{W}_N \end{Bmatrix} = \underline{\dot{W}} \tag{3.7}$$

where $c_{kk} \equiv 2\omega_{kk}\zeta$, $\underline{\dot{W}}$ is a vector of white noises with

$$E[\underline{\dot{W}}(t)\underline{\dot{W}}(s)] = \begin{bmatrix} S_{11} & \cdots & S_{1N} \\ & S_{ij} & \\ \text{symm.} & & S_{NN} \end{bmatrix} \delta(t-s) \tag{3.8}$$

where S_{ij} is cross-spectral intensity.

Rewrite Eq. (3.7) in a state variable representation and consider only the i-th and j-th modes, leading to

$$d \begin{Bmatrix} q_i \\ \dot{q}_i \\ q_j \\ \dot{q}_j \end{Bmatrix} = \begin{bmatrix} 0 & 1 & 0 & 0 \\ -\omega_{ii}^2 & -c_{ii} & 0 & 0 \\ 0 & 0 & 0 & 1 \\ 0 & 0 & -\omega_{jj}^2 & -c_{jj} \end{bmatrix} \begin{Bmatrix} q_i \\ \dot{q}_i \\ q_j \\ \dot{q}_j \end{Bmatrix} dt + \begin{Bmatrix} 0 \\ \dot{W}_i \\ 0 \\ \dot{W}_j \end{Bmatrix} dt \tag{3.9}$$

Applying Eq. (B.18), the second moment evolutionary equations, which give the time variation of the second moments of response, are written as follows

$$\frac{\partial}{\partial t} E[q_i q_j] = E[\dot{q}_i q_j] + E[q_i \dot{q}_j] \tag{3.10}$$

$$\frac{\partial}{\partial t} E[\dot{q}_i q_j] = E[\dot{q}_i \dot{q}_j] - \omega_{ii}^2 E[q_i q_j] - c_{ii} E[\dot{q}_i q_j] \tag{3.11}$$

$$\frac{\partial}{\partial t} E[q_i \dot{q}_j] = E[\dot{q}_i \dot{q}_j] - \omega_{jj}^2 E[q_i q_j] - c_{jj} E[q_i \dot{q}_j] \qquad (3.12)$$

$$\frac{\partial}{\partial t} E[\dot{q}_i \dot{q}_j] = -\omega_{ii}^2 E[q_i \dot{q}_j] - \omega_{jj}^2 E[\dot{q}_i q_j] \qquad (3.13)$$

$$- (c_{ii} + c_{jj}) E[\dot{q}_i \dot{q}_j] + S_{ij}$$

If only stationary response is considered, the time derivatives appearing in Eq. (3.10) to Eq. (3.13) are replaced by zero. These equations can then be easily solved for the covariances as follows. From Eq. (3.10)

$$E[\dot{q}_i q_j] = - E[q_i \dot{q}_j] \qquad (3.14)$$

Subtraction of Eq. (3.11) from Eq. (3.12) and use of Eq. (3.14) yields

$$E[q_i \dot{q}_j] = \frac{(\omega_{ii}^2 - \omega_{jj}^2)}{(c_{ii} + c_{jj})} E[q_i q_j] \qquad (3.15)$$

Addition of c_{jj} times Eq. (3.11) plus c_{ii} times Eq. (3.12), yields

$$E[\dot{q}_i \dot{q}_j] = \frac{(c_{jj}\omega_{ii}^2 + c_{ii}\omega_{jj}^2)}{(c_{ii} + c_{jj})} E[q_i q_j] \qquad (3.16)$$

Substitution of Eqs. (3.14), (3.15), and (3.16) into Eq. (3.13), then gives

$$E[q_i q_j] = \frac{S_{ij}}{T_{ij}} \tag{3.17}$$

in which

$$T_{ij} = c_{ii}\omega_{jj}^2 + c_{jj}\omega_{ii}^2 + \frac{(\omega_{ii}^2-\omega_{jj}^2)^2}{c_{ii}+c_{jj}}$$

$$= [2\zeta(\omega_{ii}\omega_{jj}) + \frac{1}{2\zeta}(\omega_{ii}-\omega_{jj})^2](\omega_{ii}+\omega_{jj})$$

T_{ij}, which is completely determined by system properties, is analogous to stiffness in static analysis, while S_{ij} is analogous to force description.

For the variance, i = j and

$$T_{ii} = T_{jj} = 2c_{ii}\omega_{ii} = 4\zeta\omega_{ii}^3 \tag{3.18}$$

which is a familiar result for SDOF systems.

Consider the effect on the response of mode i of a second mode j with the same frequency, $\omega_{jj} = \omega_{ii}$. If the cross term S_{ij} in the input spectrum is of the same order of magnitude as S_{ii}, then $E[q_i q_j]$ is of the same order of magnitude as $E[q_i^2]$ and has an important effect on the response.

To see the effect of nearly equal frequencies, define the parameter γ

$$\gamma \equiv \frac{T_{ij}}{4\zeta\omega_{ii}^3} = \{\frac{1}{2}(\frac{\omega_{jj}}{\omega_{ii}}) + \frac{1}{8\zeta^2}(1-\frac{\omega_{jj}}{\omega_{ii}})^2\}(1+\frac{\omega_{jj}}{\omega_{ii}}) \qquad (3.19)$$

which is the ratio of $E[q_i^2]$ to $E[q_i q_j]$ if $S_{ii} = S_{ij}$.

The parameter γ is shown in Fig. 3.1 as a function of ω_{jj}/ω_{ii} for damping ζ = .02, .05, and .10. The figure shows clearly that γ increases rapidly with increasing $\frac{\omega_{jj}}{\omega_{ii}}$ for small damping, thus, it is reasonable to omit cross modal response for systems having separated natural frequencies providing that damping is small. Eq. (3.19) can be used as a quantitative measure of the feasibility of omitting the cross modal response.

3.4 Covariance of Responses

Since modal damping is assumed, a system is completely characterized by mode shapes and natural frequencies. Let

ψ_{ij} = i-th element of j-th mode shape

q_{1j} = j-th element of modal response $\{q_1\}$

q_{2k} = k-th element of modal response $\{q_2\}$

Q_j = j-th generalized input

X_i = i-th component of response $\{X\}$

Y_p = p-th component of response $\{Y\}$

F_j = j-th component of input

M_j = j-th modal mass

N = number of degrees of freedom of structure.

h_{1j} = impulse response function of modal response q_{1j}

h_{2k} = impulse response function of modal response q_{2k}

For displacement response

$$h_{z_j}(\tau) = \frac{1}{\omega_j^d} e^{-\omega_j \zeta \tau} \sin(\omega_j^d \tau)$$

For velocity response (3.20)

$$h_{z_j}(\tau) = e^{-\omega_j \zeta \tau} \cos(\omega_j^d \tau) - \omega_j \zeta \frac{1}{\omega_j^d} e^{-\omega_j \zeta \tau} \sin(\omega_j^d \tau)$$

where

$$\omega_j^d = \omega_j \sqrt{1 - \zeta^2} \qquad z = 1 \text{ or } 2$$

Then

$$X_i(t) = \sum_j \psi_{ij} q_{1j}(t) \qquad Y_p(t) = \sum_k \psi_{pk} q_{2k}(t)$$

$$q_{1j}(t) = \int_0^t h_{1j}(t-\tau)\frac{1}{M_j} Q_j(\tau)\,d\tau$$

$$q_{2k}(t) = \int_0^t h_{2k}(t-\tau)\frac{1}{M_k} Q_k(\tau)\,d\tau \tag{3.21}$$

$$Q_j(t) = \sum_\ell \psi_{j\ell} F_\ell \qquad Q_k(t) = \sum_m \psi_{km} F_m$$

The covariance of X_i and Y_p is then

$$R_{x_i y_p}(t,t) = \sum_{jk\ell m}\sum\sum\sum \psi_{ij}\psi_{pk}\psi_{\ell j}\psi_{mk}\frac{1}{M_j M_k}\gamma_{jk,\ell m}(t)$$

(3.22)

$$\gamma_{jk,\ell m}(t) = \int_0^t \int_0^t h_{1j}(t-\tau_1)h_{2k}(t-\tau_2)R_{F_\ell F_m}(\tau_1,\tau_2)\,d\tau_1 d\tau_2$$

If the input is stationary, the stationary form of Eq. (3.22) can be written as

$$R_{x_i y_p\ t\to\infty}(t,t) = \frac{1}{2\pi}\int_{-\infty}^{\infty} \sum_{jk\ell m}\sum\sum\sum \psi_{ij}\psi_{pk}\psi_{\ell j}\psi_{mk} \cdot$$

$$\frac{1}{M_j M_k} H_{1j}(\omega) H_{2k}^*(\omega) S_{F_\ell F_m}(\omega)\,d\omega \tag{3.23}$$

where $H(\omega)$ is the transfer function of the response and $*$ denotes complex conjugation.

Eq. (3.22) involves double integrals. It is prohibitive to evaluate these integrals numerically due to high computational cost. In the past, the covariances of responses have been obtained via frequency domain analysis. Since ground motions are assumed to be locally stationary, the evolutionary power spectral technique by Priestley enables one to evaluate Eq. (3.22) numerically by performing a series of one-dimensional discrete Fourier transforms and numerical integrations rather than by evaluating double integrals [68, 69, 89]. Nevertheless these procedures are still quite expensive and numerical errors are difficult to assess. In order to evaluate nonstationary covariance of responses efficiently and accurately, it is desirable to obtain an analytical expression for double integrals. For the ground motion considered, this can be done in a straightforward manner due to the simple, well structured, integrable autocorrelation function of the input. Therefore, computational cost can be cut drastically.

In seismic building analysis, one significant advantage associated with normal mode analysis is that a good approximation of displacement or velocity can usually be achieved using only a few modes. Hence, another reduction in computational cost can be made by establishing criteria for selection of significant mode pairs to yield results with the specified accuracy. More details will be discussed in Chapter 6.

3.5 Analytical Evaluation of Response Covariances

If $\xi(t)$ is white, the double integrals in Eq. (3.22) automatically reduce to single integrals which can easily be carried out analytically. If the Kanai-Tajimi or Clough-Penzien spectra are used, it is only necessary to evaluate expressions of the form

$$\hat{\gamma}_{jk}(t) = \int_0^t\int_0^t h_{1j}(t-\tau_1)h_{2k}(t-\tau_2) \cdot e^{-\omega_g\zeta_g|\tau_1-\tau_2|} \cdot \cos(\omega_g^d|\tau_1-\tau_2| - \phi)I(\tau_1)I(\tau_2)d\tau_1 d\tau_2 \tag{3.24}$$

For most envelope functions which have been proposed, Eq. (3.24) can be integrated. The analytical expressions for displacement response, velocity response, and displacement-velocity joint response are given in Appendix E, in which the Shinozuka-Sato envelope function is employed.

3.6 Maximum Response

In previous sections, the covariances of various responses are derived. These response statistics contain much of the information concerning structural response characteristics. They represent the mean square responses. However, in structural analyses, maximum responses are of particular importance. Since the structural response in this formulation is random, maximum response can only be discussed in terms of probability. A meaningful way to phrase the problem of finding extreme res-

ponses is to determine the probability that a prescribed displacement threshold, d*, will not be exceeded by structural random response [Fig. 3.2]. This is known as the First-Passage problem. It is perhaps more useful to solve the problem the other way around; prescribe a probability of no exceedance and to determine the corresponding threshold (level). The response threshold associated with a fixed probability of no exceedance will be called Probable Response. For instance, the threshold corresponding to 90 percent probability of no exceedance is called 90 percent Probable Response and denoted as $d^*_{0.9}$.

3.6.1 Probability of No Exceedance (Reliability)

Let d be the random response of interest. Then the probability of no exceedance $\Lambda(d^*, t)$ of level d* in the time interval $0 \leq \tau \leq t$ is defined by

$$\Lambda(d^*,t) = p\{\tau>t : d(\tau) \geq d^* \text{ for the first time}\} \qquad (3.25)$$

If the ground motion is assumed to be Gaussian, then all response quantities are Gaussian. However, so far no solution has been obtained for $\Lambda(d^*, t)$. Consequently, it is necessary to employ approximate methods. A number of approximation methods have been devised [54, 70, 84]. In this study the Poisson process (crossing assumption) approximation is used because of its

simplicity. This approximation is often conservative for narrow band Gaussian processes [21] which is the case in this study. The approximation assumes that the number of crossings at time t is a Poisson process. Accordingly, the probability of no exceedance is

$$\Lambda(d^*,t) = \exp\left[-\int_0^t \nu_{d^*}(\tau)\, d\tau\right] \tag{3.26}$$

where $\nu_{d^*}(\tau)$ is expected rate of upcrossings of level d* given by [70]

$$\begin{aligned}\nu_{d^*}(\tau) = \; & \left\{\frac{1}{\sqrt{2\pi}\sigma_d(\tau)} \exp\left[-\frac{d^{*2}}{2\sigma_d^2(\tau)}\right]\right\} \cdot \\ & \left\{\frac{\sigma_{\dot d}(\tau)}{\sigma_d(\tau)}\, \rho_{d\dot d}(\tau) \cdot d^* \Phi\left[\frac{\rho_{d\dot d}(\tau) d^*}{\sigma_d(\tau)\sqrt{1-\rho_{d\dot d}^2}}\right]\right. \\ & \left. + \frac{1}{\sqrt{2\pi}}\, \sigma_{\dot d}(\tau)\sqrt{1-\rho_{d\dot d}^2(\tau)} \exp\left[-\frac{\rho_{d\dot d}^2(\tau) d^{*2}}{2\sigma_d^2(1-\rho_{d\dot d}^2(\tau))}\right]\right\}\end{aligned} \tag{3.27}$$

where $\sigma_d(\tau)$, and $\sigma_{\dot d}(\tau)$ are respectively the standard deviation of d and $\dot d$, and $\rho_{d\dot d}(\tau)$ is the correlation coefficient. $\Phi[\cdot]$ denotes the cumulative distribution function of the unit normal distribution. In structural analysis, the absolute value of d, $|d|$, is of particular concern and

$$\nu_{|d^*|} = 2\,\nu_{d^*}$$

$$\Lambda(|d^*|,t) = \exp\left[-\int_0^t \nu_{|d^*|}(\tau)\,d\tau\right] \tag{3.28}$$

The above approximation involves only response covariances (first order probability information), and correlation information for two different time instants is not considered.

For stationary response, $\rho_{d\dot{d}}$ in Eq. (3.27) is zero, and $\Lambda(|d^*|, t)$ becomes

$$\Lambda(|d^*|,t) = \exp\left\{-2t\,\frac{\sigma_{\dot{d}}}{2\pi\sigma_d}\exp\left[-\frac{d^{*2}}{2\sigma_d^2}\right]\right\} \tag{3.29}$$

In Eq. (3.29), knowledge of σ_d, $\sigma_{\dot{d}}$ and duration t is required. In the nonstationary case, the response will die out eventually and duration of response can be omitted. However, $\rho_{d\dot{d}}$ is no longer zero for the nonstationary case.

3.6.2 Probable Response

For a fixed duration, $\Lambda(|d^*|, t)$ is a monotonic increasing function of $|d^*|$. Therefore, $|d^*|$ can always be obtained numerically by an iteration process. Let $|d^*|$ be expressed in

terms of M.S. displacement as

$$|d^*| = c\ \sigma_d \qquad \text{for stationary case}$$

$$|d^*| = c\ (\sigma_d)_{max} \qquad \text{for nonstationary case}$$

in which c will be termed the Multiplication Constant. From Eq. (3.29), c for stationary response is

$$c = \left[\ 2\ \ln \frac{\frac{\sigma_{\dot{d}}}{\sigma_d}\, t}{-\pi \ln \Lambda}\ \right]^{1/2} \tag{3.30}$$

3.7 Summary and Discussion

The methods used in this study for computing structural response of linear MDOF systems to ground motion input were presented.

For stationary white noise input, modal covariances were computed using Eq. (B.18). For stationary and nonstationary response to Kanai-Tajimi and Clough-Penzien spectra input, responses were computed using the auto-correlation function. Expressions for time-varying modal displacement and velocity

variances and covariances were evaluated analytically. Eq. (3.22) gives the general form for time-varying response covariance, and Eq.(3.23) gives the stationary response covariance. The canonical form of the double integrals which are involved in the analytical evaluation of covariances, is displayed in Eq. (3.24) and evaluated in Appendix E.

The closed form expressions for response covariances were incorporated into a normal mode analysis procedure for linear elastic MDOF systems.

Rice's approximation [70] for maximum response (with a specified probability of no exceedence) was also summarized.

CHAPTER 4

EFFECTS OF GROUND MOTION CHARACTERISTICS ON THE RESPONSE OF SINGLE DEGREE OF FREEDOM (SDOF) ELASTIC SYSTEMS

4.1 Introduction

In this chapter, the ground motion models described in Chapter 2 are used as input to single degree of freedom (SDOF) elastic oscillators.

SDOF systems are studied in order to provide some insight, in as simple a context as possible, into the effects on response of various ground motion characteristics. In addition, a thorough understanding of the response of SDOF systems is fundamental to the understanding of more complicated systems.

Response spectra, which contain important information on the response characteristics of SDOF systems, have been widely used in earthquake engineering . A typical response spectrum (El Centro (1940 EW)) is shown in Fig. 4.1. The smoothed design spectrum obtained by applying the rules due to Newmark and Hall [57] and Newmark [56] is shown in Fig. 4.2. This spectrum may be thought of as an expected response spectrum . The figures indicate the general pattern of response of SDOF systems to ground motion shaking. The spectral shape illustrated in Figures 4.1 and 4.2 is typical of earthquake ground motions recorded at medium epicentral distances on firm soil or rock sites. These deterministic spectra provide a frame of reference for evaluating the stochastic ground motion models

used in this study.

The most important general characteristics of the ground motion models discussed in Chapter 2 are frequency content and nonstationarity or duration.

Three commonly used models for the frequency content of strong ground motions were discussed in Chapter 2. These models provide varying degrees of realism in spectral shape when compared with response spectra of recorded motions. The three models, ranked in order from most realistic to least realistic, are:

1) Clough-Penzien spectrum
2) Kanai-Tajimi spectrum
3) White noise

Conversely, a ranking of the models on the basis of simplicity and convenience would reverse the order shown above.

Likewise, the introduction of a nonstationary envelope function may provide a realistic variation of ground motion intensity at the expense of complicating the problem. In structural analyses, it is the response that really counts. The use of a more realistic model may (sometimes) lead to analytical difficulties and make it impossible to draw useful general conclusions. On the other hand, the simpler models may not yield reasonable results in the range of interest. A balance must be reached between these conflicting objectives. Therefore, the ranges of applicability and the adequacy of the models must be carefully investigated.

In this chapter, R.M.S. responses to the ground excitations are computed and plotted on tripartite spectral charts so that 1). the effects of ground motion characteristics (frequency content and duration) on structural response can be clearly seen, and 2). comparision can be made with actual earthquake response spectra, so that the models can be evaluated.

Since linear structures are of concern, the responses are proportional to the spectral level, S_0. Another advantage of plotting the results on tripartite logarithmic paper is that the response spectra are merely shifted when different spectral levels S_0 are used, and therefore, S_0 can be chosen quite arbitarily.

The effect of individual large pulses on the response will be illustrated using the white noise model because its simplicity.

4.2 Response of SDOF System

Consider the SDOF system shown in Fig. 4.3. The equation of motion is

$$\ddot{u} + 2\omega_0 \zeta \dot{u} + \omega_0^2 u = -a(t) \tag{4.1}$$

where u is the displacement of the mass relative to the base, ω_0 and ζ are respectively natural circular frequency and

damping, and a(t) is the ground acceleration. In earthquake engineering applications, the natural frequency f_0 (= $\omega_0/2\pi$) is normally in the range from 0.05 cps to 20 cps. The damping coefficient ζ depends on the type and condition of the structure. In this chapter, only 5 percent critical damping (ζ = 0.05) is considered.

4.2.1 M.S. Responses

As will be seen later, the effect of frequency content and duration (nonstationarity) will be illustrated through the stationary and nonstationary R. M.S. displacement and velocity responses of SDOF systems. The stationary response is the response at $t\to\infty$ to a stationary excitation. The nonstationary response discussed in this research implies that the oscillator is at rest initially and the excitation is a locally stationary process as descibed in Eq. (2.1).

For the convenience of later discussion, let $\sigma_u(t)$ and $\sigma_{\dot{u}}(t)$ denote respectively the R.M.S. displacement and velocity response. $(\sigma_\cdot(t))_{max}$ denotes the maximum over the time history and t_p denotes the time at which the maximum occurs. $\sigma_\cdot(\infty)$ denotes the stationary result.

If the ground acceleration a(t) is Gaussian white noise, applying Eq. (B.18), the second moment evolutionary equations, which are a set of coupled ordinary differential equations which give the time history of the second moments of response, can be derived as follows

$$\frac{\partial}{\partial t}\begin{Bmatrix} E[u^2] \\ E[u\dot{u}] \\ E[\dot{u}^2] \end{Bmatrix} = \begin{bmatrix} 0 & 2 & 0 \\ -\omega_0^2 & -2\omega_0\zeta & 1 \\ 0 & -2\omega_0^2 & -4\omega_0\zeta \end{bmatrix} \begin{Bmatrix} E[u^2] \\ E[u\dot{u}] \\ E[\dot{u}^2] \end{Bmatrix} + \begin{Bmatrix} 0 \\ 0 \\ I^2(t)S_0 \end{Bmatrix} \quad (4.2)$$

where S_0 is the spectral level of $\xi(t)$. If stationary responses are of concern, one immediately obtains the familiar result

$$\sigma_u^2(\infty) = E[u^2] = \frac{S_0}{4\omega_0^3\zeta}$$
$$\sigma_{\dot{u}}^2(\infty) = E[\dot{u}^2] = \frac{S_0}{4\omega_0\zeta} \quad (4.3)$$

After some calculation, the nonstationary response can be expressed as

$$\begin{Bmatrix} E[u^2] \\ E[u\dot{u}] \\ E[\dot{u}^2] \end{Bmatrix} = S_0\int_0^t \begin{Bmatrix} \phi_{13}(t-\tau) \\ \phi_{23}(t-\tau) \\ \phi_{33}(t-\tau) \end{Bmatrix} I^2(\tau)d\tau \quad (4.4)$$

in which

$$\phi_{13}(t) = \frac{e^{-2\omega_0\zeta t}}{2\omega_0^2(1-\zeta^2)}\{1 - \cos(2\omega_0\sqrt{1-\zeta^2}\,t)\}$$

$$\phi_{23}(t) = \frac{e^{-2\omega_0\zeta t}}{\omega_0^2(1-\zeta^2)}\left\{\frac{\omega_0\zeta}{2}\left[\cos\left(2\omega_0\sqrt{1-\zeta^2}\,t\right) - 1\right] + \frac{\omega_0\sqrt{1-\zeta^2}}{2}\sin\left(2\omega_0\sqrt{1-\zeta^2}\,t\right)\right\}$$

$$\phi_{33}(t) = \frac{e^{-2\omega_0\zeta t}}{\omega_0^2(1-\zeta^2)}\left\{\frac{\omega_0^2(1-2\zeta^2)}{2}\cos\left(2\omega_0\sqrt{1-\zeta^2}\,t\right) - \omega_0^2\zeta\sqrt{1-\zeta^2}\sin\left(2\omega_0\sqrt{1-\zeta^2}\,t\right) + \frac{\omega_0^2}{2}\right\} \tag{4.5}$$

Eq. (4.4) can be evaluated analytically [Appendix F].

The M.S. responses of systems to ground motions having Kanai-Tajimi or Clough-Penzien spectrum characteristics can be obtained by specializing Eqs. (3.22-3.24) and Appendix E. The stationary results are obtained by keeping only those terms involving $e^{\lambda t}$ in Appendix E since all the other terms die out as $t\to\infty$.

The stationary R.M.S. displacement and velocity responses to ground motion with the Kanai-Tajimi spectrum characteristics can then be arranged in the following simple forms:

$$\sigma_u = E[u^2] = \frac{-1}{\omega_0^2\Delta}\left\{\omega_g^2\left(1+\frac{\omega_g\zeta_g}{\omega_0\zeta}\right)\Delta_1 + \left[\frac{\omega_g^2(1-4\zeta_g^2)}{2\omega_0\zeta} - 2\omega_g\zeta_g\right]\Delta_2\right\}$$

$$\sigma_{\dot{u}} = E[\dot{u}^2] = \frac{-1}{2\omega_0\zeta\Delta}\left\{2\zeta_g\omega_g^3\Delta_1 + \omega_g^2(1-4\zeta_g^2)\Delta_2\right\} \tag{4.6}$$

in which

$$\Delta = -(\omega_0^2-\omega_g^2)^2 - 4(\omega_g\zeta_g\omega_0^2+\omega_0\zeta\omega_g^2)(\omega_0\zeta+\omega_g\zeta_g)$$

$$\Delta_1 = \frac{S_0}{4\omega_g\zeta_g}\{\omega_0^2 - \omega_g^2 + 8\omega_g\zeta_g(\omega_0\zeta+\omega_g\zeta_g)\}$$

$$\Delta_2 = \frac{S_0}{4\omega_g\zeta_g}\{4\omega_g^3\zeta_g + 2\omega_0\omega_g(\omega_g\zeta-\omega_0\zeta_g)\}$$

The stationary R.M.S. displacement and velocity responses to ground motion with Clough-Penzien spectral characteristics can be evaluated using the expressions given in Appedix E but are too lengthy to repeat here.

4.3 Effects of Ground Motion Characteristics

4.3.1 Effect of Frequency Content

In this section the stationary responses to the three types of input spectra (white noise, Kanai-Tajimi, Clough-Penzien) are examined to determine how well the general characteristics of the response spectra agree with the response spectra computed from actual earthquakes. Then, using the Clough-Penzien input spectrum, the effect of dominant ground motion frequency is examined.

The stationary responses $\sigma_u(\infty)$ and $\sigma_{\dot{u}}(\infty)$ to ground motions with white noise, Kanai-Tajimi, and Clough-Penzien frequency content characteristics are shown in Figs. 4.4

and 4.5. In these figures, S_0= 10000 in²/sec³ and filter parameters of ω_g = 15.46 rad/sec, ζ_g = 0.623, ω_f = 1.636 rad/sec, and ζ_f = 0.619 are used.

The figures reveal that the general shape of the R.M.S. displacement and velocity response spectra for the Clough-Penzien input closely resembles the El Centro response spectrum shown in Fig. 4.1. This general shape is typical of earthquake response spectra. As expected, the response spectra for the Kanai-Tajimi and white noise input tend to diverge as the natural frequency approaches zero. However, for very low frequency systems, the displacement response should be equal to the ground displacement. For the Clough-Penzien spectrum with rounded parameters ω_g=5π rad/sec, ω_g=0.6, ω_f/ω_g=0.1, ζ_f/ζ_g=1.0, and S_0=1.0 in²/sec³ (Fig. 2.5), the R.M.S. ground displacement is computed as 0.3308 in. from Eq. (2.17). For the same set of parameters, the R.M.S. displacement response for a system with very low natural frequency, say f_0 = 0.01/2π cps, is obtained through Eq.(3.24) and expressions given in Appendix E as 0.3426 in. This confirms that the Clough-Penzien spectrum provides a reasonable ground motion model especially in the low frequency range.

The responses $\sigma_u(\infty)$ and $\sigma_{\dot{u}}(\infty)$ due to white noise are identical straight lines on the spectral charts. This can easily be seen from Eq.(4.3) which shows that the pseudo-velocity response (defined as $\omega_0\sigma_u$) is equal to velocity

response $\sigma_{\dot{u}}(\infty)$. For the same spectral level, the white noise input yields higher response in the low and high frequency range, but smaller response in the mid-frequency range when compared with those from Clough-Penzien spectrum input.

The response for the Kanai-Tajimi spectrum input are virtually the same as those for white noise in the low frequency range. In the mid and high frequency range, the responses are very close to those for the Clough-Penzien spectrum input.

From the above discussion and in view of Figs. 4.4 and 4.5, it is clear that the white noise model represents the effects of ground motion well only if the natural frequencies of the structural system fall within a very limited range. The Kanai-Tajimi spectrum yields reasonable results if the system natural frequencies are not in the low frequency range. In much of the subsequent work reported in this study, the Clough-Penzien spectrum will be used to represent ground motion frequency content. However, in a few cases, the white noise model will be used for the sake of simplicity.

The displacement and velocity response spectra for Clough-Penzien spectrum input are in general quite similar. In the mid frequency range, the pseudo-velocity $\omega_0 \sigma_u(\infty)$ is approximately the same as velocity $\sigma_{\dot{u}}(\infty)$. The pseudo-velocity $\omega_0 \sigma_u(\infty)$ underestimates the velocity $\sigma_{\dot{u}}(\infty)$ in the low frequency range, but overestimates the velocity in the

high frequency range.

To compare the effect of ground motion dominant frequency, the R.M.S. displacement response spectra for the three ground motions with Clough-Penzien spectra (Fig. 2.7) are plotted in Figs. 4.6 to 4.8. Applying the Newmark-Hall approach [57] for the construction of spectra, R.M.S. ground acceleration, R.M.S. ground velocity, and R.M.S. ground displacement are employed as control parameters to separate the frequency range into three regions. Amplification factors are indicated in the figures. It is evident that the amplification patterns over the three regions are quite similar for the three spectra used despite the fact that the spectral shapes of the three ground motion inputs are quite different. This suggests that one can adequately estimate response spectra using only M.S. ground acceleration, velocity, and displacement. These quantities can be obtained analytically for the ground motion model with Clough-Penzien spectrum characteristics using Eqs.(2.16) and (2.17).

The relations $\sigma_\xi \sigma_d / \sigma_v^2$ and σ_v / σ_ξ are quite different for the three ground motions used (Refer to Sec. 2.3.2.2). Therefore, a single set of numerical value of these quantities does not seem appropriate for ground motions with significantly different frequency content.

4.3.2 Effect of Duration

In this section, the effect on response of ground motion duration is considered.

First, a short-duration earthquake (Trifunac-Brady duration = 7.2 sec., Sec. 2.2) is considered, with frequency content characteristics corresponding to white noise, Kanai-Tajimi and Clough-Penzien spectra. For the same set of filter parameters used in the previous section and $S_0 = 10000$ in^2/sec^3 , the maximum responses $(\sigma_u(t))_{max}$ and $(\sigma_{\dot{u}}(t))_{max}$ are shown in Figs. 4.9 and 4.10. In all cases, the stationary response levels are attained if the system natural frequency is in the high frequency range. (Compare Figs. 4.4 and 4.9 and Figs. 4.5 and 4.10) In the mid and low frequency ranges, the maximum nonstationary responses are generally smaller than the corresponding stationary results.

Unlike the response for white noise or the Kanai-Tajimi spectrum, the maximum displacement response $(\sigma_u(t))_{max}$ for the Clough-Penzien spectrum exhibits some unusual behavior. $(\sigma_u(t))_{max}$ starts to depart from the stationary response $\sigma_u(\infty)$ at about $f_0 = 2$ cps. As f_0 decreases further the divergence first becomes larger, then becomes smaller. This can be explained by the fact that the transient response of low frequency systems can greatly overshoot the stationary response. This is demonstrated in Fig.4.11 which shows the response history of a SDOF system having $f_0 = 0.05$ cps to stationary input with the Clough-Penzien spectrum (Ground Motion No. 2). Note that the M.S. impulse of the ground motion (Chapter 2) is zero for the stationary Clough-Penzien spectrum input so that at low frequency the correct asymptotic

behavior is observed.

Second, a ground motion with Clough-Penzien spectral characteristics is considered. Two durations, designated as "short" and "long" in Sec. 2.2 with Trifunac-Brady durations equal to 7.2 seconds and 20.4 seconds, respectively, are used. Figs 4.12 and 4.13 show displacement and velocity response spectra, i.e., $(\sigma_u(t))_{max}$ and $(\sigma_{\dot{u}}(t))_{max}$, for $S_0=10000$ in^2/sec^3.

In Fig. 4.12, the short duration response curve is beginning to show evidence of approaching its (spurious) horizontal low frequency asymptote, which for 5 per cent damping, is $S_v=27.03$. The low frequency limit f_ℓ (Eq.(2.24)) gives 0.151 cps as an estimate of the frequency below which the nonstationary responses are likely to be inaccurate because of deficiencies in the ground motion model. This estimate appears to agree well with one's visual impression of Fig. 4.12.

The probable response has been discussed in Sec. 3.6 as a more useful quantity than R.M.S. response in structural engineering. It blends the information of the statistics of structural random responses and duration into a single meaningful index. For convenience, the probable response is often expressed in terms of R.M.S. response, $\sigma_u(\infty)$ or $(\sigma_u(t))_{max}$ by introducing the multiplication constant described in Sec. 3.6.2.

The 90 percent probable responses of SDOF oscillators are obtained for the aforementioned ground motions according to the formula and approximation described in Sec. 3.6. For the nonstationary cases (short duration and long duration) the "t" in Eq.(3.26) is chosen to be sufficiently large so that $\nu_d^*(t)$ in Eq.(3.26) becomes virtually zero. The probable response for the stationary case is obtained through Eq.(3.30) using t=10 seconds. The multiplication constants for the three cases are shown in Table 4.1. Table 4.1 shows that the multiplication constant for a system is greater if earthquake duration is longer as expected.

It is worth noting that the probability of no exceedance according to a instant response probability distribution (shaded area in Fig. 4.14) should be greater than the probability of no exceedance over an entire duration. The probabilty obtained from a instant response distribution will be refered as Instant Probability of No Exceedance. For example, a multiplication constant c = 2.807 is obtained for f_0 = 1 cps, short duration, and 90 percent probable response (Table 4.1). This corresponds to a 99.75 percent instant probability of no exceedance if the Gaussian assumption is valid.

The 90 percent probable responses are shown in Fig.4.15. The figure shows that in the frequency range plotted, the probable responses are consistently larger for the long duration motion than for the short duration motion. At lower frequencies,

the spurious low frequency behavior due to the short duration envelope is again evident.

Since many important structures such as pipelines and offshore platforms may have very low natural frequencies, care should be taken in using stochastic ground motion models of the form given by Eq.(2.1) for studies of such structures. It is entirely possible that the more commonly used 3-segment intensity envelope may not produce as severe an effect at low frequencies. This remains to be demonstrated however.

4.3.3 Effect of Pulses

In this section, the effect of large acceleration pulses in the ground motion is considered. As mentioned in Sec. 2.4, no satisfactory way was found to relate the parameters of the pulse model to observable properties of recorded ground motions. Thus, in the absence of a method of determining a reasonable range for the ground motion model parameters, only a very limited study of the effects of acceleration pulses on system response was undertaken. Nevertheless, the results do show that pulses increase the probable response of SDOF elastic systems.

Unless the response is assumed to have a Gaussian Probability distribution, the M.S. response is not sufficient to characterize the response distribution. For non-Gaussian cases, besides M.S. response, Skewness (third moment), and

Kertosis (fourth moment) are quite important in determining the response probability distribution. As discussed in Sec. 2.4, let the ground acceleration a(t) consist of a combination of Gaussian white noise (continuous) with spectral level S_0, and marked poisson pulses (discontinuous) with intensity λ, and zero mean symmetrically distributed mark H. The marked poisson pulses are employed to model individual large acceleration pulses in the ground motion with random arrival time.

Applying Eq.(B.18), the second moment evolutionary equations are the same as Eq.(4.4) except that S_0 is replaced by $S_0 + \lambda E[H^2]$. Since all quantities are assumed to be zero mean and symmetrically distributed, all third moments are zero. The fourth moment evolutionary equations are as follows

$$\frac{\partial}{\partial t}\begin{Bmatrix} E[u^4] \\ E[u^3\dot{u}] \\ E[u^2\dot{u}^2] \\ E[u\,\dot{u}^3] \\ E[\dot{u}^4] \end{Bmatrix} = \begin{bmatrix} 0 & 4 & 0 & 0 & 0 \\ -\omega_0^2 & -2\dot{\omega}_0\zeta & 3 & 0 & 0 \\ 0 & -2\omega_0^2 & -4\omega_0\zeta & 2 & 0 \\ 0 & 0 & -3\omega_0^2 & -6\omega_0\zeta & 1 \\ 0 & 0 & 0 & -4\omega_0^2 & -8\omega_0\zeta \end{bmatrix} \begin{Bmatrix} E[u^4] \\ E[u^3\dot{u}] \\ E[u^2\dot{u}^2] \\ E[u\,\dot{u}^3] \\ E[\dot{u}^4] \end{Bmatrix}$$

$$+ I^4(t) \begin{Bmatrix} 0 \\ 0 \\ 0 \\ 0 \\ E[H^4] \end{Bmatrix} + S_0' \begin{Bmatrix} 0 \\ 0 \\ E[u^2\ \ ] \\ 3E[u\ \dot{u}\ ] \\ 6E[\dot{u}^2\ \ ] \end{Bmatrix} I^2(t) \qquad (4.7)$$

in which $S_0' = S_0 + \lambda E[H^2]$

The contribution to $E[u^4]$ of $I^2(t)S_0'\{E[u^2],3E[u\dot{u}],6E[\dot{u}^2]\}^T$ is denoted as $E[u^4]_G$ and is equal to $3E^2[u^2]$ (as in the Gaussian case). i.e., $E[u^4]_G$ is the fourth moment of response u excited by Gaussian white noise of spectral density S_0'. The contribution to $E[u^4]$ of $I^4(t)E[H^4]$ is denoted as $E[u^4]_P$ and is equal to

$$E[u^4]_P = \lambda E[H^4] \int_0^t \phi_P(t-\tau) I^4(\tau) d\tau \qquad (4.8)$$

It can be shown that the transfer function $\phi_P(t)$ is

$$\phi_P(t) = \frac{e^{-4\omega_0 \zeta t}}{\omega_0^4 (1-\zeta^2)^2} \{ \frac{1}{8} \cos(4\omega_0 \sqrt{1-\zeta^2}\ t) - \qquad (4.9)$$

$$\frac{1}{2} \cos(2\omega_0 \sqrt{1-\zeta^2}\ t) + \frac{3}{8} \}$$

The fourth moment $E[u^4]_P$ is always positive and Eq. (4.8) can be integrated in closed form [Appendix F]. Thus, for same total input spectral level, the existence of acceleration pulses produces a response distribution which is flatter than a gaussian distribution (as illustrated in Fig. 4.16). The increase of fourth moment of response can be expressed by the ratio

$$r = \frac{E[u^4]_P}{E[u^4]_G} \tag{4.10}$$

For the stationary case

$$E[u^4]_G = \frac{3}{16} \frac{S_0^2}{\omega_0^6 \zeta^2}$$

$$E[u^4]_P = \frac{3}{32} \frac{\lambda E[H^4]}{\omega_0^5 \zeta (1+3\zeta^2)} \tag{4.11}$$

Let $E[H^2] = \mu S_0'$, $E[H^4] = qE^2[H^2] = q\mu^2 (S_0'/\lambda)^2$

then

$$r = \frac{1}{2} q\mu^2 \frac{\omega_0}{\lambda} \frac{\zeta}{(1+3\zeta^2)} \tag{4.12}$$

The parameter p is a measure of the proportion of the ground motion power contained in the pulses. The parameter q characterizes the probability distribution of the pulse intensity.

In order to compute probable responses, a response probability distribution must be assumed. A family of distributions due to Karl Pearson is selected for this purpose. Some background on the Pearson family of distributions is given in Appendix G.

As mentioned above, the presence of pulses always yields a response distribution which is flatter than a gaussian distribution if the total spectral level is fixed. However, the M.S. response $\sigma_u(t)$ remains the same. Therefore, the response level corresponding to a fixed instant probability of no exceedance is always greater than if the response was Gaussian [Fig. 4.16]. Fig. 4.17 shows the probable stationary response(99.75 percent instant probability of no exceedance) to white noise excitation. In the figure, the pulses are assumed to account for one third of the total spectral level, i.e., $p = 1/3$, and H is assumed to have a wide distribution with $q = 9$ ($q = 3$ for a gaussian distribution). The intensity of pulses is assumed to be $\lambda = 0.5$/sec. It is emphasized that the choice $p = 1/3$ is entirely arbitrary and is made simply to demonstrate the positive effect of large pulses on response.

These limited results show that acceleration pulses do increase the probable response, although it is difficult to conclude very much more than that until a way is found to

establish physically reasonable values for the parameters p and q which characterize the pulse model used in this study.

4.4 An Approximation - Equivalent White Noise

The stationary response to white noise excitation, Eqs.(3.15-3.17) or Eq.(4.3), is easily computed. Since the response transfer function is narrow banded and the ground motion model has a broad spectrum, (except for the Clough-Penzien spectrum in the low frequency range) Eq.(3.23) may be approximated as

$$R_{x_i y_p}(t,t) = \frac{1}{2\pi} \sum_{\ell m} \sum_{jk} EQ_{\ell,m}(\omega_j,\omega_k)\ \psi_{ij}\psi_{pk}\psi_{\ell j}\psi_{mk}\ \frac{1}{M_j M_k} \cdot \int_{-\infty}^{\infty} H_{x_j}(\omega) H^*_{y_k}(\omega)\, d\omega \tag{4.13}$$

If $\xi(t)$ has the Kanai-Tajimi spectrum characteristics with filter parameters ω_g and ζ_g, $S_{F_\ell F_m}(\omega)$ in Eq.(3.23) can be in general expressed as (Refer to Eqs. (2.11), (2.27) and (3.21-3.23))

$$S_{F_\ell F_m}(\omega) = \frac{1 + 4\zeta_g^2 (\frac{\omega}{\omega_g})^2}{(1-(\frac{\omega}{\omega_g})^2)^2 + 4\zeta_g^2 (\frac{\omega}{\omega_g})^2}\ S_{\ell m} \tag{4.14}$$

in which $S_{\ell m}$ is the spectral level.

In this case, $EQ_{\ell,m}(\omega_j,\omega_k)$ in Eq.(4.13) can be chosen as

$$EQ_{\ell,m}(\omega_j,\omega_k) = S_{\ell,m} \sqrt{\frac{1 + 4\zeta_g^2(\frac{\omega_j}{\omega_g})^2}{[1-(\frac{\omega_j}{\omega_g})^2]^2 + 4\zeta_g^2(\frac{\omega_j}{\omega_g})^2}} \cdot \sqrt{\frac{1 + 4\zeta_g^2(\frac{\omega_k}{\omega_g})^2}{[1-(\frac{\omega_k}{\omega_g})^2]^2 + 4\zeta_g^2(\frac{\omega_k}{\omega_g})^2}} \qquad (4.15)$$

Eq.(4.13) physically means that the system is excited by white noise with a frequency dependent spectral level equal to $EQ_{\ell,m}(\omega_j,\omega_k)$ [Fig.4.18]. Table 4.2 shows the displacement response computed using the equivalent white noise approximation, for a series of SDOF systems with different natural frequencies and damping. The results are expressed as a ratio of exact to approximate M.S. responses.

The approximation appears to be quite good.

4.5 Summary and Discussion

Effects of ground motion characteristics on the response of SDOF elastic systems were examined.

(1) The SDOF elastic response spectra computed using the Clough-Penzien input ground motion agree qualitatively with actual earthquake response spectra. The ground motion model also predicts relations between mean square ground acceleration, velocity and displacement which agree well with corresponding estimates proposed by Newmark and Hall [57].

(2) To study the effects of variations in ground motion frequency content on the response of SDOF elastic systems, the filter parameters controlling the Clough-Penzien spectrum were varied to simulate different "predominant" ground motion frequencies. The corresponding response spectra exhibited response amplification factors (relative to mean square ground motions) which were insensitive to quite large changes in ground motion frequency content. It is noted that this is a prediction of the model rather than an established fact, and it remains to be verified by comparison with recorded earthquake motions.

(3) The effect of time-varying intensity and duration of the ground acceleration was modelled by means of an exponential envelope function proposed by Shinozuka and Sato. Mean square responses were sensitive to duration only for medium and low frequency systems. Mean square displacement response to the long duration motion consistently exceeded the response to the short duration motion except

for very low frequency systems in which the "spurious" low frequency behavior mentioned in Chapter 2 is quite evident. Maximum (90% probability of no exceedence) responses show a slight dependence on duration for high frequency systems as well.

(4) Limited results obtained using a white noise ground motion model suggest that for ground motions of the same general intensity level, those containing large individual acceleration pulses produce large maximum responses than those without such acceleration pulses.

CHAPTER 5

EFFECTS OF MULTI-DIRECTIONAL GROUND MOTION ON THE RESPONSE OF ONE-STORY TORSIONALLY COUPLED ELASTIC SYSTEMS

5.1 Introduction

An understanding of the response characteristics of SDOF-systems is prerequisite to understanding the behavior of more complex systems. For this reason, torsional coupling in a simple one-story structure is investigated in this chapter. A subsequent chapter (Chapter 6) will consider torsional coupling in multi-story structures.

Newmark and Rosenblueth [62] separate the causes of torsional coupling in buildings into two categories.

The first category arises even in nominally symmetric buildings and includes calculation errors, inaccuracies or imprecise knowledge of stiffness and mass distributions, and also the effects of rotational components of ground motion which are normally not considered. These are termed "accidental eccentricities". On the basis of studies of idealized single story systems, combined with estimates of the effect of rotational ground motion components, Newmark [58] found that an accidental eccentricity of 5 per cent of the longer plan building dimension was reasonable for framed buildings with fundamental period greater than about 0.6 seconds or shear wall buildings with fundamental period

exceeding about 1.0 seconds. For shorter fundamental periods, accidental eccentricities of about 10 to 15 per cent of the longer plan building dimension were reasonable. These accidental eccentricities compensate for the torsional effects of rotational ground motion components only.

Accidental eccentricity due to rotational ground motion components is studied in this chapter. The rotational component of ground motion is assumed to arise from the lack of spatial correlation in the translational component of ground motion. This is the stochastic counterpart of the model for rotational ground motion introduced by Newmark [58].

The second category involves the difference between static and dynamic methods of analysis, and is termed "dynamic magnification" of eccentricity.

The dynamic magnification of eccentricity is studied in detail by considering a series of single story structures with a full range of structural parameters and eccentricities.

The effect of torsion in buildings has beeen studied in the past either mathematically for specific models of building structures or through experiments [7, 8, 16, 26, 29, 34, 41, 47, 58, 71, 79, 89]. However, previous studies are based on the assumption that ground motions are in the principal directions of the structure, and are uncorrelated. The overall response of a building is sensitive to the orientation of the structure with respect to the ground motion [26, 55]. A systematic evaluation of the effects of ground motion cor-

relation and incidence direction is not available in the literature. This chapter addresses this need. In addition, most previous work employs a certain rule for combining modal responses [16, 41, 47]. Such combination rules may not be accurate enough when structural frequencies are closely spaced and ground motion correlations are present. In this chapter, single story buildings modeled as a lumped mass shear beam subjected to the ground excitations described in Chapter 2 are analyzed. The M.S. responses of systems are obtained without recourse to modal combination rules, and both system and ground motion coupling are incorporated in the analysis. Parameter studies are conducted of stationary system response to white noise excitation to serve as a bench mark for other more realistic excitations. Since the Clough-Penzien spectrum was shown in Chapter 4 to accurately model actual ground excitations, stationary and nonstationary responses of the system to the Clough-Penzien spectrum input are then calculated and compared with the white noise results.

5.2 Equations of Motion

A one-story structure (Fig. 5.1) idealized as a rigid diaphragm on massless columns is considered. Throughout this study, only elastic systems are considered.

The structure principal directions are designated as the X, Y axes. The system has 3 DOF. They are:

u_x = translational displacement of the mass center in the X direction.

u_y = translational displacement of the mass center in the Y direction.

u_θ = rotation about the vertical (Z) axis.

The stiffnesses of the i-th resistance element (column) are:

$(k_x)_i$ = translational stiffness in X direction

$(k_y)_i$ = translational stiffness in Y direction

The coordinates of the i-th resistance element with respect to the center of mass are (x_i, y_i).

The structure stiffness properties are then expressed in terms of element properties as:

K_x = stiffness in X direction = $\sum_i (k_x)_i$

K_y = stiffness in Y direction = $\sum_i (k_y)_i$

K_θ = rotational stiffness about the mass center

$= \sum_i x_i^2 (k_y)_i + y_i^2 (k_x)_i$

The coordinates of the center of rigidity (C.R.) with respect to the mass center are (e_x, e_y).

The idealized lumped mass, three dimensional shear beam model is shown schematically in Fig. 5.2. Three dashpots with linear damping constants C_x, C_y, and C_θ are used to take account of structural damping. Let M denote the mass and I denote moment of inertia of the rigid diaphragm. The equations of motion of the system are

$$M\ddot{u}_x + C_x(\dot{u}_x - e_y\dot{u}_\theta) + K_x(u_x - e_y u_\theta) = -Ma_x$$

$$I\ddot{u}_\theta + C_\theta\dot{u}_\theta - C_x\dot{u}_x e_y + C_y\dot{u}_y e_x + K_\theta u_\theta - K_x e_y u_x + K_y e_x u_y = -Ia_\theta$$

$$M\ddot{u}_y + C_y(\dot{u}_y + e_x\dot{u}_\theta) + K_y(u_y + e_x u_\theta) = -Ma_y \qquad (5.1)$$

in which

a_x = ground acceleration in X direction.

a_y = ground acceleration in Y direction.

a_θ = rotational ground acceleration

In terms of the parameters ω_x, ω_y, ω_θ, r defined by

$$\omega_x = \sqrt{\frac{K_x}{M}}$$

$$\omega_y = \sqrt{\frac{K_y}{M}}$$

$$\omega_\theta = \sqrt{\frac{K_\theta}{I}}$$

$$r = \sqrt{\frac{I}{M}} = \text{radius of gyration}$$

Eqs. (5.1) can be expressed as

$$\{\ddot{U}\} + [C]\{\dot{U}\} + [K]\{U\} = -\{a\} \qquad (5.2)$$

in which

$$\{U\} = \{u_x,\ ru_\theta,\ u_y\}^T$$

$$\{a\} = \{a_x,\ ra_\theta,\ a_y\}^T$$

and

$$[K] = \omega_x^2 \begin{bmatrix} 1 & -\frac{e_y}{r} & 0 \\ -\frac{e_y}{r} & (\frac{\omega_\theta}{\omega_x})^2 & (\frac{\omega_y}{\omega_x})^2 \frac{e_x}{r} \\ 0 & (\frac{\omega_y}{\omega_x})^2 \frac{e_x}{r} & (\frac{\omega_y}{\omega_x})^2 \end{bmatrix}$$

$$[C] = 2\omega_x\zeta \begin{bmatrix} 1 & -\frac{e_y}{r} & 0 \\ -\frac{e_y}{r} & \frac{\omega_\theta}{\omega_x} & (\frac{\omega_y}{\omega_x}) \frac{e_x}{r} \\ 0 & (\frac{\omega_y}{\omega_x}) \frac{e_x}{r} & \frac{\omega_y}{\omega_x} \end{bmatrix}$$

in which

$$\zeta = \frac{C_x}{2\omega_x M} = \frac{C_y}{2\omega_y M} = \frac{C_\theta}{2\omega_\theta I}$$

ω_x, ω_y and ω_θ are respectively the natural frequencies in the X, Y and θ directions for the case when eccentricities vanish ($e_x = e_y = 0$). They will be termed "uncoupled natural frequencies" in the X, Y, and θ directions. The matrices [K] and [C] will be termed "stiffness" and "damping" matrices although they have been normalized with respect to mass M.

The foregoing relationships can also be written in terms of displacements referred to the center of rigidity (C.R.). Let the displacements of the C.R. be denoted

$$\{\bar{U}\} = \{\bar{u}_x,\ r\bar{u}_\theta,\ \bar{u}_y\}^T$$

The quantities $\{\bar{U}\}$ are related to the displacement $\{U\}$ referred to the center of mass (C.M.) by the relationships

$$\{U\} = [A]\{\bar{U}\} \tag{5.3}$$

in which

$$[A] = \begin{bmatrix} 1, & \frac{e_y}{r}, & 0 \\ 0, & 1, & 0 \\ 0, & -\frac{e_x}{r}, & 1 \end{bmatrix}$$

Eq. (5.2) can then be easily transformed to

$$[\bar{M}]\{\ddot{\bar{U}}\} + [\bar{C}]\{\dot{\bar{U}}\} + [\bar{K}]\{\bar{U}\} = \{\bar{F}\}$$

in which

$$[\bar{M}] = [A]^T[I][A] = \begin{bmatrix} 1, & \frac{e_y}{r}, & 0 \\ \frac{e_y}{r}, & 1+(\frac{e_x}{r})^2+(\frac{e_y}{r})^2, & -\frac{e_x}{r} \\ 0, & -\frac{e_x}{r}, & 1 \end{bmatrix}$$

$$[\bar{K}] = [A]^T[K][A] = \begin{bmatrix} 1, & 0 & , & 0 \\ 0, & \frac{\bar{\omega}_\theta^2}{\omega_x^2} & , & 0 \\ 0, & 0 & , & (\frac{\omega_y}{\omega_x})^2 \end{bmatrix}$$

$$[\bar{C}] = [A]^T[C][A]$$

$$\{\bar{F}\} = [A]^T\{a\} = \begin{Bmatrix} -a_x \\ -a_x \frac{e_y}{r} \quad -ra_\theta \quad +a_y \frac{e_x}{r} \\ -a_y \end{Bmatrix}$$

and

$$\bar{\omega}_\theta^2 \equiv \omega_\theta^2 - (\frac{e_x}{r})^2 \omega_y^2 - (\frac{e_y}{r})^2 \omega_x^2$$

The equations of motion are therefore in a form (by referring quantities to the C.R.) in which the stiffness terms uncouple. However, if this is done, mass coupling is introduced and in addition the input acceleration vector has a more complicated form, with translational accelerations and eccentricity terms entering the rotational equation of motion.

In dynamic analysis, modal damping is normally used, and the damping matrix is implicitly specified in the mode shape coordinates. In the following, the damping matrix in Eq. (5.2) will be referred to as the "special damping" matrix. The frequency ratios, as will be seen later are quite important in determining the degree of torsional coupling. Three common types of layout of the resistance elements of buildings are shown in Fig. 5.3. In general, buildings with a central core, uniformly distributed columns, or peripheral shear walls tend to have respectively lower, nearly equal or higher torsional frequencies than corresponding lateral natural frequencies. Frequency ratios for one story buildings with resistance patterns shown in Fig. 5.4 are tabulated in Table 5.1.

As a result of interaction between lateral and torsional motions, columns at the perimeter of buildings may have significantly larger displacements than when the motion is uncoupled. Consider the columns at locations E, W, N, S shown in Fig. 5.5 The displacements in the X direction are

$$(u_E)_x = (u_W)_x = u_x$$

$$(u_S)_x = u_x + (b/2)\, u_\theta = u_x + (b/2r)(ru_\theta)$$

$$(u_N)_x = u_x - (b/2r)(ru_\theta) \qquad (5.4)$$

The displacements in the Y direction are

$$(u_E)_y = u_y + (a/2r)(ru_\theta)$$

$$(u_W)_y = u_y - (a/2r)(ru_\theta)$$

$$(u_N)_y = (u_S)_y = u_y$$

Thus the shape of the floor diaphragm and the distances to the outer columns are also quite important. For the same systems shown in Fig. 5.4, the ratio of the floor dimension to radius of gyration of the floor, $\frac{b}{r}$, are listed in Table 5.2.

5.3 Stationary Response to White Noise Excitation

From the discussion in the previous section, it is evident that there are many parameters involved even for the idealized model of a one story building. A great deal of simplicity in the presentation of results can be achieved by examining the stationary response to white noise excitation. In this case, the results depend only on ratios of system frequencies and not on their absolute values. This is due, of course, to the frequency independent white noise power spectrum. Although the white noise model for ground excitation has some deficiencies , as discussed in Section 4.3, it provides a convenient framework within which to study response to the more reasonable Clough-Penzien spectrum.

The solution algorithm has been discussed in Sections

3.2 and 3.3 for modal damping. Therefore, the derivation which follows, unless otherwise specified, is for special damping (Section 5.2).

In Eq. (5.2), let the ground acceleration, {a}, be stationary and white with covariance

$$R_{\underline{a}}(t_1,t_2) = \begin{bmatrix} S_{xx} & S_{x\theta} & S_{xy} \\ S_{x\theta} & S_{\theta\theta} & S_{y\theta} \\ S_{xy} & S_{y\theta} & S_{yy} \end{bmatrix} \delta(t_2 - t_1) \qquad (5.5)$$

Then, it can be shown (see Appendix H) that the stationary displacement responses are given by the solution of the system of linear equations

$$[\Gamma]\{\S\} = \{P\} \qquad (5.6)$$

in which

$$\{\S\} = \{ E[u_x^2], E[r^2u_\theta^2], E[u_y^2], E[u_x ru_\theta], E[u_x u_y], E[u_y ru_\theta] \}^T$$

$$\{P\} = \{ \frac{S_{xx}}{2}, \frac{S_{\theta\theta}}{2}, \frac{S_{yy}}{2}, S_{x\theta}, S_{xy}, S_{y\theta} \}^T$$

$[\Gamma]$ is a symmetric (6 x 6) matrix with constant elements given in Appendix H.

The M.S. response quantities of Eq. (5.4) can then be obtained. For example,

$$E[(u_S)_x^2] = E[u_x^2] + (\frac{1}{4})(\frac{b}{r})^2 E[(ru_\theta)^2] + (\frac{b}{r}) E[(u_x ru_\theta)]$$

$$E[(u_N)_x^2] = E[u_x^2] + (\frac{1}{4})(\frac{b}{r})^2 E[(ru_\theta)^2] - (\frac{b}{r}) E(u_x ru_\theta)] \quad (5.7)$$

In addition to the M.S. translational and rotational responses of the center of mass, the correlation between them is also important in determining the response of the columns on the periphery.

Let

F_x = Base shear in X direction.

F_y = Base shear in Y direction.

T = Torque about C.M.[1]

Then the covariance of forces can be expressed as

$$\begin{bmatrix} E[F_x^2], & E[F_x \frac{T}{r}], & E[F_x F_y] \\ & E[(\frac{T}{r})^2], & E[F_y \frac{T}{r}] \\ \text{symm.} & & E[F_y^2] \end{bmatrix} = [K] \begin{bmatrix} E[u_x^2], & E[ru_\theta u_x], & E[u_x u_y] \\ & E[r^2 u_\theta^2], & E[ru_\theta u_y] \\ \text{symm.} & & E[u_y^2] \end{bmatrix} [K]^T \quad (5.8)$$

(1) The torque $\bar{T}$ about the C.R. is $\bar{T} = T + e_y F_x - e_x F_y$

5.3.1 One-Way Torsionally Coupled Systems

To obtain a better intuitive understanding about the effects of torsional coupling on response, an even simpler one-way torsionally coupled system is first considered. In this model torsional motion is coupled with lateral motion in only one direction. Most previous studies on torsional coupling have been concerned with this special system [7, 8, 26, 71, 77]. However, the previous work on this class of torsionally coupled systems has employed a deterministic approach.

In this section, one-way torsionally coupled systems are investigated in depth using random white noise excitation. Both special damping and modal damping are discussed, and comparisons of responses with these two forms of damping are made. Figure 5.6 shows the one-way torsionally coupled system in which $e_x = 0$. In this case, the coefficient matrix $[\Gamma]$ of Eq. (5.6) takes the special form

$$[\Gamma] = \begin{bmatrix} \Gamma_{11} & \Gamma_{12} & 0 & \Gamma_{14} & 0 & 0 \\ & \Gamma_{22} & 0 & \Gamma_{24} & 0 & 0 \\ & & \Gamma_{33} & 0 & 0 & 0 \\ & & & \Gamma_{44} & 0 & 0 \\ \text{sym.} & & & & \Gamma_{55} & \Gamma_{56} \\ & & & & & \Gamma_{66} \end{bmatrix} \tag{5.9}$$

where the Γ_{ij} are given in Appendix H. As expected, the M.S. torsional response is coupled with the M.S. translational response in the X direction. The M.S. response in the Y direction is uncoupled. In the following discussion, only quantities associated with torsional and X direction motion are considered. Since Eq. (5.6) is a set of linear equations, superposition holds. Therefore, the responses due to individual components of $\{P\}$ can be considered separately. It should, however, be clearly understood that cross spectral levels $S_{x\theta}$, S_{xy}, and $S_{y\theta}$ in $\{P\}$ cannot, on a physical basis, exist alone without proper spectral levels S_{xx}, $S_{\theta\theta}$, and S_{yy}. The responses due to individual cross spectral levels should be interpreted as response influence functions for the various input spectral values, from which responses to physically realizable inputs can be constructed by superposition.

5.3.1.1 The Effect of Spectral Level S_x

One-dimensional ground motion input in the X direction corresponds to a nonzero value of S_x with other spectral inputs equal to zero. S_x induces lateral response in the X direction as well as torsional response because of coupling. For special damping, the analytical expression for the displacement responses are obtained in a straight forward manner and are given by

$$E[r^2 u_\theta^2] = \frac{\Delta_\theta}{\omega_x^3 \Delta} \qquad E[u_x^2] = \frac{\Delta_x}{\omega_x^3 \Delta}$$

$$E[u_x r u_\theta] = \frac{\Delta_{\theta x}}{\omega_x^3 \Delta} \tag{5.10}$$

where

$$\Delta = 8\beta_*^4(1+\beta_*)\zeta^3 + 2\beta_*^3(\beta_*-1)(\beta_*^2-1)\zeta +$$

$$(\frac{e_Y}{r})^2 [(-8\beta_*^2-32\beta_*^3-8\beta_*^4)\zeta^3 + (-2\beta_*+12\beta_*^3-6\beta_*^4)\zeta] +$$

$$(\frac{e_Y}{r})^4 [24\beta_*(\beta_*+1)\zeta^3 + (-\frac{4}{(\beta_*+1)} + 6 - 14\beta_* +$$

$$4\beta_*^3 \frac{1}{(\beta_*+1)})\zeta] + (\frac{e_Y}{r})^6 [-16\zeta^3 + 8\frac{\zeta}{(\beta_*+1)}]$$

$$\beta_* \equiv \frac{\omega_\theta}{\omega_x}$$

$$\Delta_\theta = -\frac{S_x}{2}\{(\frac{e_y}{r})^2[-4\beta_*(\beta_*+1)\zeta^2 - 1 + \beta_* - \beta_*^2] + (\frac{e_y}{r})^4[8\zeta^2 - \frac{2}{(\beta_*+1)}]\}$$

$$\Delta_x = \frac{S_x}{2}\{\beta_*^3(\beta_*+1)[4\beta_*\zeta^2 + (\beta_*-1)^2] + (\frac{e_y}{r})^2[-4\beta_*^2(\beta_*^2+1)\zeta^2 - \beta_* + 2\beta_*^3] + (\frac{e_y}{r})^4[\frac{2}{(\beta_*+1)}]\}$$

$$\Delta_{\theta x} = +\frac{S_x}{2}\{(\frac{e_y}{r})[8\beta_*^3\zeta^2 + \beta_*^3(\beta_*-1)] + (\frac{e_y}{r})^3[\frac{2}{(\beta_*+1)} - 1 + 2\beta_* - 4\beta_*(\beta_*+1)\zeta^2]\}$$

The base shear and torque can then be obtained through Eq. (5.8) as

$$E[F_x^2] = \omega_x \frac{1}{\Delta}\{(\frac{e_y}{r})^2\Delta_\theta - 2(\frac{e_y}{r})\Delta_{\theta x} + \Delta_x\} \qquad (5.11)$$

$$E[(\frac{T}{r})^2] = \omega_x \frac{1}{\Delta}\{\beta_*^4 \Delta_\theta - 2\beta_*^2(\frac{e_y}{r})\Delta_{\theta x} + (\frac{e_y}{r})^2 \Delta_x\}$$

Computed responses are plotted against $\frac{\omega_\theta}{\omega_x}$ for three small eccentricities (e_y/r = 0.05, 0.10, 0.15) in Fig. 5.7 and three relatively large eccentricities (e_y/r = 0.2, 0.3, 0.4) in Fig. 5.8 for special damping. Figures 5.9 and 5.10 present similar results for modal damping. Section 5.3.1.1.3 presents the computational procedure for modal damping using a Mohr's circle approach. Damping values ζ = 0.02 (solid-line) and 0.05 (dashed-line) are used for special damping, and damping equal to 2 percent (solid-line) and 5 percent (dashed-line) of critical damping are used for modal damping. All responses are normalized by the M.S. X directional response of the uncoupled system, so that the effects of coupling can be better visualized. For displacement response, the normalizing constant is $\frac{S_x}{4\zeta\omega_x^3}$. For force response, the normalizing constant is $\frac{\omega_x S_x}{4\zeta}$. The normalized results are denoted as $E_N(\cdot)$. The general characteristics of response with the two types of damping are similar. However, numerical differences between the two cases increase with increasing eccentricity.

5.3.1.1.1 Force Responses for One-Dimensional Input

Before discussing individual force responses, an interesting interaction relationship for the forces given by Kan and Chopra for the deterministic case [47] is presented.

Define

$$\text{SUMP} = \frac{F_x^2 + F_y^2 + (\frac{T}{r})^2}{(F_x)^2_{\text{uncoupled}}}$$

in which $(F_x)_{\text{uncoupled}}$ denotes the base shear in the X direction for the corresponding uncoupled systems (no eccentricity). They have shown that SUMP based on the combination rule given by Rosenblueth [71] is always equal to one for two types of response spectra (hyperbolic and constant).

A quantity parallel to SUMP in the stochastic sense is

$$\text{SUMF} = \frac{\{ E[(\frac{T}{r})^2] + E[F_x^2] + E[F_y^2] \}}{(\frac{\omega_x S_x}{4\zeta})} \qquad (5.12)$$

in which $\frac{\omega_x S_x}{4\zeta}$ is the M.S. base shear in the X direction for the corresponding uncoupled systems.

In one-way torsionally coupled systems, $E(F_y^2) = 0$. For special damping, SUMF can be analytically expressed as

$$\frac{E[(\frac{T}{r})^2] + E[F_y^2]}{(\frac{\omega_y S_y}{4\zeta})} = 1 + \frac{1}{\Delta}\{(\frac{e_x}{r})^2[(8\beta_*^6-16\beta_*^5+8\beta_*^2)\zeta^3 - 2(\beta_*^5-3\beta_*^4+\beta_*^3+2\beta_*^2-\beta_*)\zeta] + (\frac{e_x}{r})^4 \cdot [1 - 8\beta_*^2(\beta_*-1)^2\zeta^3 + 2\beta_*(1-\beta_*)\zeta]\} \quad (5.13)$$

If there is no eccentricity, SUMF is always one. SUMF is also equal to one if $\frac{\omega_\theta}{\omega_x} = 1$. For other values of $\frac{\omega_\theta}{\omega_x}$, SUMF is close to 1 if the eccentricity is not large. (Fig. 5.7.e and 5.8.e). For modal damping, SUMF is very close to 1 for all values of $\frac{\omega_\theta}{\omega_x}$ and $\frac{e_y}{r}$ (Fig. 5.9.e and 5.10.e). These results show that the existence of eccentricity produces a redistribution of forces. This relation implies that the base shear is reduced as a result of torsional coupling, which has also been found in several other studies [16, 47, 71]. The question is how much of the force is transferred to the torsional mode. From the numerical results, the M.S. torsional force reaches its maximum when $\frac{\omega_\theta}{\omega_x}$ is close to one. Consider an extreme case in which the eccentricity is so large that the system is almost unstable, i.e., $\frac{e_y}{r}$ is just slightly less than $\frac{\omega_\theta}{\omega_x}$. If $\frac{\omega_\theta}{\omega_x} = 1$, then $\Delta_\theta \cong \Delta_x \cong \Delta_{\theta x}$ and is independent of damping. From Eq. (5.11), $E[(\frac{T}{r})^2] \cong E[F_x^2]$ and is independent of damping. This shows that a maximum of about 50 percent of the M.S. force may be transfered to the torsional mode as a result of torsional coupling. For small eccentricity, the amount of redistribution is quite sensitive to damping. This sensitivity decreases with increasing eccentricity. From Eqs. (5.10) and

(5.11), it can easily be verified that for $\frac{\omega_\theta}{\omega_x} = 1$ and $\zeta \to 0$, the normalized torsional force is 0.5. Therefore, the coupling may be quite strong for small damping even if the eccentricity is very small. The results show that the normalized torsional force may be close to 0.5 for small eccentricity if the damping is small and $\frac{\omega_\theta}{\omega_x}$ is near 1 (Fig. 5.7.a, 5.9.a). For larger values of eccentricity (Fig 5.8.a, 5.10.a), the normalized torsional force can approach 0.5 over a wider interval of frequency ratio $\frac{\omega_\theta}{\omega_x}$. The ratio, R, of dynamic torque about the center of rigidity to the product of uncoupled base shear times eccentricity is defined as

$$R = \frac{\sqrt{E_N[T_{CR}^2]}}{e_y} = \sqrt{E_N[(\frac{T_{CR}}{r})^2](\frac{r}{e_y})} = (\frac{\omega_\theta}{\omega_x})^2 \sqrt{E_N[(ru_\theta)^2]}(\frac{r}{e_y}) \qquad (5.14)$$

in which T_{CR} denotes the torsional force about the center of rigidity.

The product $R \cdot e_y$ can be interpreted as a "dynamic eccentricity". When the maximum amount of redistribution occurs, the normalized torsional force approaches 0.5. In this case, the dynamic eccentricity can greatly exceed the static eccentricity. The dynamic amplification of eccentricity, R, can approach $(0.707)/(e_y/r)$ for small damping, when ω_θ/ω_x is near 1.

The table below shows values of R at $\omega_\theta/\omega_x = 1$, for different values of damping and eccentricity.

ζ	e_y/r		
	.05	.10	.15
0.02	11.08	6.64	4.66
0.05	6.38	5.09	4.04
0.10	3.53	3.28	2.98

Dynamic Amplification of Eccentricity (R) for One-Way Torsionally Coupled System ($\omega_\theta/\omega_x = 1$)

Rosenblueth and Elorduy [71] presented a plot of dynamic magnification factor for eccentricity for a one-way torsionally coupled system subjected to flat and hyperbolic ground acceleration spectra.

5.3.1.1.2 Displacement Responses for One-Dimensional Input

A relationship for the change due to torsional coupling of total M.S. displacement response exists which is similar to that for SUMF. Define

$$SUMD = \frac{\{ E[(ru_\theta)^2] + E[u_x^2] + E[u_y^2] \}}{\left(\frac{S_x}{4\zeta\omega_x^3}\right)} \qquad (5.15)$$

SUMD is always greater than one and asympototically approaches one as $\frac{\omega_\theta}{\omega_x}$ tends to ∞ (Fig 5.7f). SUMD increases greatly with increasing eccentricity (Fig 5.8f) and is almost independent of damping. This implies that the system is effectively softer due to torsional coupling. The phenomenon can be explained using Mohr's circle plots presented later. The value of SUMD for special damping is generally greater than that for modal damping for the frequency ratios of interest.

The figures show that there is a peak in torsional response near $\frac{\omega_\theta}{\omega_x} = 1$ for small eccentricities. However, the peak becomes less pronounced as eccentricity increases. For small eccentricities, the two system natural frequencies are quite close, so the large torsional response is the result of beating. For large eccentricity, the beating phenomenon is less significant. However, in this case the lowest natural frequency is much lower than the uncoupled natural frequency. Therefore, the response is significantly greater than that of the uncoupled system because of the fact that the response to white noise is proportional to the inverse of natural frequency to the third power.

No consistent trend is found for lateral displacement at the center of mass when eccentricity is large (Fig. 5.8.d). M.S. displacement at the center of rigidity is obtained through the relation,

$$E(u_x)^2_{C.R.} = E(u_x^2) + (\frac{e_y}{r})^2 E(r^2u_\theta^2) - 2(\frac{e_y}{r})E[u_x r u_\theta] \qquad (5.16)$$

The normalized result is, of course, the same as the normalized lateral force (Eqs. (5.10),(5.11)).

The M.S. displacement responses at locations N and S are obtained through Eq. (5.7). The maximum of the two responses, $E[u_x^2]_{max}$, is plotted against $\frac{\omega_\theta}{\omega_x}$ in Figs. 5.7 - 5.10 (g&h) for square and rectangular floor geometry. For a square floor diaphragm, $b/r = \sqrt{6} = 2.45$, and values of $\frac{e_y}{r} = 0.05, 0.10, 0.15$ then correspond to $\frac{e_y}{b} = 0.0204, 0.0408$, and 0.0612 respectively. An aspect ratio of $\frac{b}{a} = 2$ is used for the rectangular floor geometry. In this case, $\frac{b}{r} = 3.10$ and $\frac{e_y}{r} = 0.05, 0.10$, and 0.15 corresponds respectively to $\frac{e_y}{b} = 0.016, 0.032$ and 0.048. The figures indicate that the response at the outer edges of the building is significantly increased. For large eccentricity the results are again insensitive to damping. The figures also show that the greatest response of the outer columns may not occur near $\frac{\omega_\theta}{\omega_x} = 1$, although the greatest torsional response occurs at around $\frac{\omega_\theta}{\omega_x} = 1$.

5.3.1.1.3 Use of Mohr's Circle Plots for Presentation and Interpretation of Responses - Modal Damping

For one-way torsionally coupled systems with modal damping, the eigenvalue analysis and coordinate transformations involved in the modal analysis method can be represented by means of Mohr's Circle.

Let eccentricity in the X direction, $e_x = 0$. The equations of motion for a one-way torsionally coupled system subjected to white noise excitation, $\dot{W}_x$, in the X direction are

$$\{\ddot{u}\} + [\text{modal damping matrix}]\{\dot{u}\} + [K]\{u\} = \begin{Bmatrix} \dot{W}_x \\ 0 \end{Bmatrix} \qquad (5.17)$$

in which

$$[K] = \omega_x^2 \begin{bmatrix} 1 & -\frac{e_y}{r} \\ -\frac{e_y}{r} & (\frac{\omega_\theta}{\omega_x})^2 \end{bmatrix}$$

$$E[\dot{W}_x(t)\dot{W}_x(s)] = S_x\delta(t-s)$$

With reference to Eqs. (3.2) to (3.6), the stiffness matrix and correlation function of white noise excitation in the mode shape coordinate, $[K^m]$ and $[R^m(t-s)]$ can be expressed in the form of

$$[K^m] = [\Psi]^T[K][\Psi] = \begin{bmatrix} \omega_1^2 , & 0 \\ 0 , & \omega_2^2 \end{bmatrix} \tag{5.18}$$

$$\begin{aligned} [R^m(t-s)] &= [\Psi]^T \begin{bmatrix} S_x , & 0 \\ 0 , & 0 \end{bmatrix} [\Psi]\delta(t-s) \\ &= \begin{bmatrix} S_{11}, & S_{12} \\ S_{12}, & S_{22} \end{bmatrix} \delta(t-s) \end{aligned} \tag{5.19}$$

The modal matrix $[\Psi]$ in Eqs. (5.18) and (5.19) can in general be expressed as

$$[\Psi] = \begin{bmatrix} \cos\theta, & \sin\theta \\ -\sin\theta, & \cos\theta \end{bmatrix}$$

in which θ is a properly determined rotation angle. The M.S. displacement responses $E[\{q\}\{q\}^T]$ in the mode shape coordinates can then be obtained from Eq. (3.17). From Eq. (3.4), the M.S. displacement response $E[\{u\}\{u\}^T]$ is

$$E[\{u\}\{u\}^T] = [\Psi]\, E[\{q\}\{q\}^T]\, [\Psi]^T \tag{5.20}$$

Eqs (5.18) to (5.20) involve a similarity transformation of the following form:

$$\begin{bmatrix} a_{11}, & a_{12} \\ a_{12}, & a_{22} \end{bmatrix} = \begin{bmatrix} \cos\phi, & -\sin\phi \\ \sin\phi, & \cos\phi \end{bmatrix} \begin{bmatrix} a_{xx}, & a_{xy} \\ a_{xy}, & a_{yy} \end{bmatrix} \begin{bmatrix} \cos\phi, & \sin\phi \\ -\sin\phi, & \cos\phi \end{bmatrix}$$

(5.21)

$$= \begin{bmatrix} \frac{a_{xx}+a_{yy}}{2} + \frac{1}{2}(a_{xx}-a_{yy})\cos(2\phi) & \\ \quad - a_{xy}\sin(2\phi) & \text{symm.} \\ \left(\frac{a_{xx}-a_{yy}}{2}\right)\sin(2\phi) & \frac{a_{xx}+a_{yy}}{2} + \frac{1}{2}(a_{yy}-a_{xx})\cos(2\phi) \\ \quad + a_{xy}\cos(2\phi) & + a_{xy}\sin(2\phi) \end{bmatrix}$$

It is noted that the similarity transformation in Eq. (5.21) can be done graphically on a Mohr's circle plot shown in Fig. 5.11.

The natural frequencies ω_1^2 and ω_2^2 are (refer to Fig. 5.12.a):

$$\omega_1^2 = \omega_x^2 \lambda_1^2$$

$$\omega_2^2 = \omega_x^2 \lambda_2^2 \qquad (5.22)$$

in which

$$\lambda_1^2 = \frac{1}{2}\left[1 + \left(\frac{\omega_\theta}{\omega_x}\right)^2\right] + R$$

$$\lambda_2^2 = \frac{1}{2}\left[1 + \left(\frac{\omega_\theta}{\omega_x}\right)^2\right] - R$$

and

$$R = \sqrt{\left[\frac{\left(\frac{\omega_\theta}{\omega_x}\right)^2 - 1}{2}\right]^2 + \left(\frac{e_y}{r}\right)^2}$$

Note that $\lambda_1 \geq \lambda_2$. For zero eccentricity, if $\omega_\theta > \omega_x$ then λ_1 corresponds to the torsional mode and λ_2 to the translational mode. If $\omega_\theta < \omega_x$, λ_1 corresponds to the translational mode and λ_2 to the torsional mode.

The white noise spectral levels in the mode shape coordinates can be easily obtained as (Refer to Fig. 5.12.b)

$$S_{11} = C_{11} S_x, \quad S_{22} = C_{22} S_x, \quad S_{12} = C_{12} S_x$$

in which

$$C_{11} = \frac{1}{2}\left[1 - \frac{\left(\frac{\omega_\theta}{\omega_x}\right)^2 - 1}{2R}\right]$$

$$C_{22} = \frac{1}{2}\left[1 + \frac{\left(\frac{\omega_\theta}{\omega_x}\right)^2 - 1}{2R}\right]$$

$$C_{12} = \frac{1}{2}\left[\frac{(\frac{e_Y}{r})}{R}\right]$$

From Eq. (3.17), the M.S. displacement responses in the mode shape coordinates normalized by the M.S. displacement in the X direction of the corresponding uncoupled system, $\frac{S_x}{4\omega_x^3\zeta}$, are

$$E_N[q_1^2] = \frac{C_{11}}{\lambda_1^3}$$

$$E_N[q_2^2] = \frac{C_{22}}{\lambda_2^3} \qquad (5.23)$$

$$E_N[q_1 q_2] = \frac{C_{12}}{(\frac{\lambda_1+\lambda_2}{2})[\lambda_1\lambda_2 + \frac{(\lambda_1-\lambda_2)^2}{4\zeta^2}]}$$

The normalized M.S. displacement responses, $E_N[u_x^2]$ and $E_N[r^2u_\theta^2]$, can then be obtained with the Mohr's Circle plot shown in Fig. 5.12c.

Note that the sum of M.S. responses is equal to the sum of modal responses, i.e., SUMD = $E_N[u_x^2] + E_N[(ru_\theta)^2] = E_N[q_1^2] + E_N[q_2^2]$. The sum is

$$SUMD = \frac{C_{11}}{\lambda_1^3} + \frac{C_{22}}{\lambda_2^3} \qquad (5.24)$$

$$= \frac{1}{2}\left[\frac{1}{\lambda_1^3} + \frac{1}{\lambda_2^3}\right] + \frac{\left[\left(\frac{\omega_\theta}{\omega_x}\right)^2 - 1\right]}{4R}\left[\frac{1}{\lambda_2^3} - \frac{1}{\lambda_1^3}\right]$$

The sum is always greater than one and is independent of damping.

Consider the special case in which $\omega_\theta = \omega_x$, The sum is

$$SUMD = \frac{1}{2}\left[\frac{1}{\left(\sqrt{1 + \left(\frac{e_y}{r}\right)}\right)^3} + \frac{1}{\left(\sqrt{1 - \left(\frac{e_y}{r}\right)}\right)^3}\right] \qquad (5.25)$$

The sum is greater than or equal to one (Fig. 5.14).

When $\omega_\theta = \omega_x$, λ_1 and λ_2 in Eq. (5.22) become

$$\lambda_1 = \sqrt{1 + \left(\frac{e_y}{r}\right)}$$

$$\lambda_2 = \sqrt{1 - \left(\frac{e_y}{r}\right)}$$

and $C_{11} = C_{22} = C_{12} = 0.5$

Then Eq. (5.23) reduces to

$$E_N[q_1^2] = \frac{1}{2} \frac{1}{\left[\sqrt{1+\left(\frac{e_y}{r}\right)}\right]^3}$$

$$E_N[q_2^2] = \frac{1}{2} \frac{1}{\left[\sqrt{1-\left(\frac{e_y}{r}\right)}\right]^3} \tag{5.26}$$

$$E_N[q_1 q_2] = \frac{1}{(\lambda_1+\lambda_2)\left[\lambda_1\lambda_2 + \frac{(\lambda_1-\lambda_2)^2}{4\zeta^2}\right]}$$

$$= \frac{2\zeta^2}{\left[\sqrt{1+\left(\frac{e_y}{r}\right)} + \sqrt{1-\left(\frac{e_y}{r}\right)}\right]\left[1 - \sqrt{1-\left(\frac{e_y}{r}\right)^2} + 2\zeta^2\sqrt{1-\left(\frac{e_y}{r}\right)^2}\right]}$$

The M.S. displacement responses [Fig. (5.13.c)] are

$$E_N[u_x^2] = \frac{1}{2}\{E_N[q_1^2] + E_N[q_2^2]\} + E[q_1 q_2]$$

$$E_N[r^2 u_\theta^2] = \frac{1}{2}\{E_N[q_1^2] + E_N[q_2^2]\} - E[q_1 q_2] \tag{5.27}$$

$$E_N[u_x r u_\theta] = \frac{1}{2}\{E_N[q_2^2] - E_N[q_1^2]\}$$

Eq. (5.27) shows again that for very small damping, $E_N[r^2u_\theta^2]$ tends to $E[u_x^2]$.

For square floor geometry, $\frac{b}{r} = \sqrt{6}$, the maximum of the two M.S. displacements, max ($E_N[(u_S)_x^2]$, $E_N[(u_N)_x^2]$) , at the outer edges of the building is [Eq. (5.7)]

$$E_N[(u_S)_x^2] = E_N[u_x^2] + \frac{3}{2} E_N[(ru_\theta)^2] + \sqrt{6}\, E_N[(u_x ru_\theta)]$$

$$= (\frac{5-2\sqrt{6}}{4}) E_N[q_1^2] + (\frac{5+2\sqrt{6}}{4}) E_N[q_2^2] - \frac{1}{2} E[q_1 q_2] \qquad (5.28)$$

$$= \frac{1}{8} \{ (5-2\sqrt{6}) \frac{1}{[\sqrt{1+(\frac{e_y}{r})}]^3} + (5+2\sqrt{6}) \frac{1}{[\sqrt{1-(\frac{e_y}{r})}]^3} \}$$

$$- \frac{\zeta^2}{\{\sqrt{1+(\frac{e_y}{r})} + \sqrt{1-(\frac{e_y}{r})}\}\{1 - \sqrt{1-(\frac{e_y}{r})^2} + 2\zeta^2\sqrt{1-(\frac{e_y}{r})^2}\}}$$

Since the last term in Eq. (5.28) tends to zero for small damping ($\zeta \leq 0.1$), thus for small damping

$$E_N[(u_S)_x^2] \cong \frac{1}{8} \{ (5-2\sqrt{6}) \frac{1}{[\sqrt{1+(\frac{e_y}{r})}]^3} + (5+2\sqrt{6}) \frac{1}{[\sqrt{1-(\frac{e_y}{r})}]^3} \} \qquad (5.29)$$

5.3.1.2 The Effect of Cross Spectral Level $S_{x\theta}$

Although the effect of $S_{x\theta}$ is not of primary concern in this research, this section is presented for completeness.

The M.S. displacement responses due to $S_{x\theta}$ are given by for special damping by

$$E[(ru_\theta)^2] = \frac{S_{x\theta}}{\omega_x^3\Delta}\{-(\frac{e_y}{r})[4\beta_*(\beta_*+1)\zeta^2 + (1-\beta_*)] + (\frac{e_y}{r})^3[8\zeta^2 - 1 - \frac{2}{\beta_*+1}]$$

$$E[u_x^2] = -\frac{S_{x\theta}}{\omega_x^3\Delta}\{(\frac{e_y}{r})[\beta_*^3(8\zeta^2+\beta_*-1)] + (\frac{e_y}{r})^3[-4\beta_*(\beta_*+1)\zeta^2 - 1 + 2\beta_* + \frac{2}{(\beta_*+1)}]\} \quad (5.30)$$

$$E[(u_x ru_\theta)] = -\frac{S_{x\theta}}{\omega_x^3\Delta}\{4\beta_*^3\zeta^2 + (\frac{e_y}{r})^2\frac{\beta_*^3+1}{\beta_*+1} + (\frac{e_y}{r})^4[-4\zeta^2 + \frac{2}{\beta_*+1}]\}$$

The sum of M.S. forces due to $S_{x\theta}$, normalized by $\frac{S_{x\theta}\omega_x}{4\zeta}$ is given by

$$\frac{\Delta(E[(\frac{T}{r})^2] + E[F_x^2])}{(\frac{\omega_x S_{x\theta}}{4\zeta})} = \frac{4\zeta}{\Delta}\{(\frac{e_y}{r})[(-4\beta_*^6+4\beta_*^5)\zeta^2 - \beta_*^4(1-\beta_*)] + (\frac{e_y}{r})^3[8\beta_*^3(\beta_*-1)\zeta^2 + \frac{-4\beta_*^4+2\beta_*^3+\beta_*^2+1}{\beta_*+1}] + (\frac{e_y}{r})^5[(-4\beta_*^2+4\beta_*)\zeta^2 - 2\beta_* + \frac{4\beta_*^2}{\beta_*+1}]\} \quad (5.31)$$

When $\frac{\omega_\theta}{\omega_x} = 1$, the sum of M.S. forces due to $S_{x\theta}$ is exactly zero. For other $\frac{\omega_\theta}{\omega_x}$, the normalized sum of M.S. forces is close to zero if the eccentricity is not very large (Table 5.3). This indicates that excitation correlation also redistributes the forces. This relation will be further discussed in the next section.

5.3.2 Two-Way Torsionally Coupled Systems

For a particular value of damping and stationary white noise excitation in the X direction, the effects of one-way torsional coupling on stationary responses depend on $\frac{\omega_\theta}{\omega_x}$ and $\frac{e_y}{r}$. In two-way torsionally coupled systems, the results depend also on $\frac{\omega_y}{\omega_x}$ and $\frac{e_x}{r}$. In this section, numerical results are obtained for 5 percent modal damping. As in one-way torsionally coupled systems, torsional coupling is very sensitive to damping at low damping levels.

For convenience, the influence on response of the components of the input spectrum are obtained separately and combined later, as appropriate.

5.3.2.1 The Effect of Spectral Level S_x on Response

The responses due to S_x for 5 percent modal damping are shown in Fig. 5.15 to Fig. 5.18 for $\frac{\omega_y}{\omega_x} = 1$ and $\frac{\omega_y}{\omega_x} = \sqrt{2}$ as

functions of $\frac{\omega_\theta}{\omega_x}$. In the figures, $\frac{e_y}{r}$ is fixed, and three values of $\frac{e_x}{r}$ are used. In all cases, the quantity SUMF is virtually equal to 1. This again shows that torsional coupling simply redistributes the force. A similar relation was found by Kan and Chopra [47]. As in one-way coupled systems, SUMD is always greater than 1. For fixed $\frac{e_y}{r}$, the peak torsional response decreases with increasing $\frac{e_x}{r}$. This decrease is more pronounced when $\frac{\omega_y}{\omega_x}$ is near 1. This trend was also observed by Kan and Chopra. They also concluded that 1) the base shear in the direction of ground motion is essentially independent of $\frac{\omega_y}{\omega_x}$ and $\frac{e_x}{r}$, i.e., this component of base shear is about the same as in the corresponding one-way torsionally coupled system. 2) except for a relatively narrow band of $\frac{\omega_y}{\omega_x}$, around $\frac{\omega_y}{\omega_x} = 1$, the normalized torque is about the same as in a corresponding one-way coupled system. However, the results of this study show that these conclusions hold only when eccentricities are relatively small. Figures 5.15b, 5.16b, 5.17b, and 5.18b pertain to conclusion (1) above. Figures 5.17a and 5.18a pertain to conclusion (2) above.

In addition, it may be noted that the value of $\frac{\omega_\theta}{\omega_x}$ for peak torsional response shifts away from that of the corresponding uncoupled system as $\frac{e_x}{r}$ increases [Fig. 5.18].

5.3.2.2 The Effect of Cross Spectral Level S_{xy} on Response

Since the ground motion may be correlated with respect

to the structure principal directions, it is necessary to examine the effect on structural response of this correlation. Once again it is emphasized that a spectrum level S_{xy} cannot exist by itself. A physically realizable ground motion input which has uncorrelated components in directions which do not coincide with the structure principal directions, will in general have nonzero values of S_x, S_y, S_{xy}. Results obtained separately for inputs S_x, S_{xy} are combined appropriately to give results for general ground motions. Numerical results for the same systems discussed in the previous section are shown in Figs. 5.19 to Fig. 5.22. SUMF due to S_{xy} is essential zero for general torsionally coupled systems. This shows that the ground motion correlation only redistributes the force. The effect on torsional response of the ground motion correlation may be very significant for systems having very close uncoupled frequencies and equal eccentricities in both principal directions, i.e., $\omega_x = \omega_y = \omega_\theta$ and $e_x = \pm e_y$ (Fig. 5.19.a and Fig. 5.20.a).

5.3.3 Effect on Response of Ground Motion Directionality

The principal directions of ground motion obviously need not coincide with the structure principal directions. This section examines the effect on response of ground motion directionality (Fig. 2.11).

Symmetric structures ($\omega_x = \omega_y$) with square geometry ($b/r = \sqrt{6}$) are considered. Numerical results are obtained

for the following two structures:

STRUCTURE I - $\frac{e_x}{r} = 0.2$ $\frac{e_y}{r} = 0.$

STRUCTURE II - $\frac{e_x}{r} = 0.2$ $\frac{e_y}{r} = 0.2$

modal damping 5% of critical

Let S_E and S_D be major and minor (intermediate) principal intensities. They can be decomposed into spectral levels S_x and S_y and a cross-spectral level S_{xy} in the structural principal axes [Eq. (2.27)]. The structural response to this excitation is a linear superposition of the responses to individual spectral levels. [Figs. 5.15 to 5.22].

The R.M.S. displacement responses are normalized by $\sqrt{S_E/4\omega_x^3\ \zeta}$. The maximum normalized displacement responses in the X and Y directions over all ω_θ/ω_x of interest for the four locations N, S, E, W at the perimeter of the building are denoted as $(\sigma_x)_{max}$ and $(\sigma_y)_{max}$. $(\sigma_x)_{max}$ and $(\sigma_y)_{max}$ for STRUCTURE I and STRUCTURE II are shown in Figs. 5.23 and 5.24 as functions of the angle of incidence δ (Fig. 2.11). In the figures, ratios of principal variances S_D/S_E = 1.0, 0.5 and 0.0 are used.[2]

The figures show that the values of $(\sigma_x)_{max}$ and $(\sigma_y)_{max}$ increase with increasing S_D/S_E ratio for a fixed angle of

(2) Note that these ratios correspond to "relative strengths" of the ground motion components equal to 1, .707, 0 respectively.

incidence δ. When S_D and S_E are of equal strength ($S_D/S_E = 1$), as is easily seen, the response is the same for all angles of incidence.

In practice, the angle of incidence δ is not known. However, design must allow for the worst case. The figures show that the response for the worst case $S_D/S_E = 1$ is not that much greater than the response for $S_D/S_E = 0$. In Fig. 5.23 (STRUCTURE I), the worst case for $(\sigma_y)_{max}$ occurs at $\delta = 90°$. At $\delta = 90°$ the response is the same for all S_D/S_E since it really just the one-way system response to S_E excitation. For STRUCTURE II, the worst case obtained for $S_D/S_E = 0$ is about 90% of the worst case for $S_D/S_E = 1$. Therefore, the use of $S_D/S_E = 1$ leads to results which are not overly conservative.

STRUCTURE I and II are in fact one-way torsionally coupled systems (rotate the axes of STRUCTURE II by 45°) with eccentricities 0.2 and $\sqrt{2} \times 0.2$ respectively. The response for $S_D/S_E = 1$ can be obtained through the equations in Sec. 5.3.1. The analytical expressions for the responses of structures with frequency ratio $\frac{\omega_\theta}{\omega_x} = 1$ are quite simple [Eq. (5.25) - (5.29)]. Although the maximum response at the outer edges of buildings does not occur at a frequency ratio $\frac{\omega_\theta}{\omega_x} = 1$ [Figs. (5.7) - (5.10) g & h], the results obtained by setting $\frac{\omega_\theta}{\omega_x} = 1$ estimate the maximum responses reasonably well. $(\sigma_x)_{max}$ and $(\sigma_y)_{max}$ for STRUCTURE I are respectively 1.31 and 1.39. The results obtained by setting $\frac{\omega_\theta}{\omega_x} = 1$ give 1.29 and 1.30. For

STRUCTURE II, $(\sigma_x)_{max} = (\sigma_y)_{max} = 1.44$ and the X and Y R.M.S. response at E and S for $\frac{\omega_\theta}{\omega_x} = 1$ is 1.42.

With reference to Fig. 5.25, the normalized displacement response u_{SW} at south west corner for $\frac{\omega_\theta}{\omega_x} = 1$ can be easily obtained from Eqs. (5.25) - (5.27) as

$$E_N[(u_{SW})^2] = \frac{1}{2}\{(2-\sqrt{3})\frac{1}{[\sqrt{1+(\frac{e}{r})}]^3} + (2+\sqrt{3})\frac{1}{[\sqrt{1-(\frac{e}{r})}]^3}\} - \frac{4\zeta^2}{[\sqrt{1+(\frac{e}{r})} + \sqrt{1-(\frac{e}{r})}][1-\sqrt{1-(\frac{e}{r})^2} + 2\zeta^2\sqrt{1-(\frac{e}{r})^2}} \quad (5.32)$$

in which $e = \sqrt{2}\, e_x = \sqrt{2}\, e_y$

For STRUCTURE II ($\frac{e_x}{r} = \frac{e_y}{r} = 0.2$), $\sigma_{u_{SW}} = \sqrt{E_N[(u_{SW})^2]}$ equals 1.75 which is 1.23 times the X or Y R.M.S. response at W or S. Note that $\frac{e}{r} = \sqrt{2}\,\frac{e_x}{r} = 0.283$ corresponds to $\frac{e}{b} = 0.115$, and more than a 75 percent increase may arise as a result of torsional coupling.

The orthogonal effects have been considered by current codes. In the ATC-3 code [6], it is required that structural elements be designed for 100 percent of the effects of seismic forces in one principal direction combined with 30 percent of the effects of seismic forces in the orthogonal direction.

The maximum of the two responses

$$\left\{\begin{array}{l}\sigma.(\delta = 0) + 0.3\sigma.(\delta = 90°) \\ \sigma.(\delta = 90°) + 0.3\sigma.(\delta = 0°)\end{array}\right\} \qquad (5.33)$$

for the case $S_D/S_E = 0$ corresponds to the ATC-3 recommendation. For STRUCTURE I, $(\sigma_x)_{max}$ and $(\sigma_y)_{max}$ obtained from Eq. (5.33) are 1.25 and 1.39. The worst case from the analysis gives respectively 1.31 and 1.39. For STRUCTURE II, Eq. (5.33) gives $(\sigma_x)_{max} = (\sigma_y)_{max} = 1.49$. The worst case shown in Fig. 5.22 is 1.44. Therefore, the method of accounting for orthogonal effects proposed in the ATC-3 code seems quite reasonable.

Rosenblueth [72] assumed equal intensity ground motions in two orthogonal directions, and excluded the case of closely spaced frequencies. He recommended combining 100 percent of the seismic force effect in one direction with 30 percent in the orthogonal direction except for towers and chimney stacks. In that case, he recommended that 50 percent of the seismic force effect in the second direction be used.

5.4 Response to Clough-Penzien Spectrum Excitation

As discussed, the effects of torsion are dependent only on the frequency ratios, $\frac{\omega_\theta}{\omega_x}$ and $\frac{\omega_y}{\omega_x}$, when white noise excitation is used. This is due to the uniform frequency content of white noise. This section considers the effect of non-uniform frequency content and time varying intensity in the ground motion input on the response of torsionally coupled systems.

5.4.1 One-Way Torsionally Coupled Systems

The normalized results for systems with $\frac{e_y}{r} = 0.15$ subjected to ground motion excitation in the X direction are shown in Fig. 5.26 to Fig. 5.31. Three uncoupled frequencies in X direction, $f_x = 0.2$ cps, 1.0 cps, and 5 cps are employed to represent respectively soft, medium, and stiff systems. 5 percent modal damping is assumed. For nonstationary response, the short duration envelope is used ($\alpha = 0.25$, $\beta = 0.75$). The M.S. responses are normalized by the (maximum) M.S. response of the corresponding uncoupled system. The response of the systems to white noise excitation is also presented in the figures for comparison. The figures show that in general the stationary white noise results can be used to predict the effects of coupling for the Clough-Penzien spectrum input. The effect of coupling for $f_x = 1$ cps is quite close to that of white noise especially when stationary responses are of concern. However, for the stiff system, $f_x = 5$ cps, the white noise result under-estimates the outer edge response. For the soft system, $f_x = 0.2$ cps, the effect of coupling is not as strong as for white noise. The effect of coupling on the soft system is even less important when nonstationary response is considered. This can be seen from the response time history shown in Fig. 5.32 in which $\frac{\omega_\theta}{\omega_x} = 1.0$ is used. It shows that there is a time lag (about 1.5 period) between the maximum torsional response and maximum lateral response.

From the figures, one may observe that the frequency ratio at which peak torsional response occurs shifts to the

right for soft systems and to the left for stiff systems when compared with white noise results.

The multiplication constants, c, for the probable responses of the outer edge columns are tabulated in Table 5.3 and Table 5.4. For a fixed probability of no exceedance, the constants are almost the same as those of the corresponding uncoupled system. This suggests that the probable response of torsionally coupled systems can be approximately obtained as the product of the M.S. displacement and the multiplication constant of the corresponding uncoupled systems. Therefore M.S. displacement response is a good indicator of maximum response.

5.5 The Effects of Spatial Correlation

To illustrate the effect of (the lack of) ground motion spatial correlation on response, we consider only one story structures with no eccentricity and the ground motion described in Section 2.7.

The translational M.S. response and rotational M.S. responses are

$$E[u_x^2] = \frac{1}{2\pi} \int_{-\infty}^{\infty} S_{\hat{\xi}_x}(\omega) |H_x(\omega)|^2 \, d\omega$$

$$E[(ru_\theta)^2] = \frac{1}{2\pi} \int_{-\infty}^{\infty} S_{\hat{\xi}_\theta}(\omega) |H_\theta(\omega)|^2 \, d\omega \qquad (5.34)$$

where $H_x(\omega)$ and $H_\theta(\omega)$ are transfer functions.

If the ground motion is fully spatially correlated, i.e., $c_s = 0$, then $S_{\hat{\xi}_x}(\omega) = S_0$ and $S_{\hat{\xi}_\theta}(\omega) = 0$. This leads to the familiar result $E[u_x^2] = S_0/4\omega_x^3\zeta$, $E[r^2u_\theta^2] = 0$. If the ground motion is partially correlated, the responses are approximately

$$E[u_x^2] \cong S_{\hat{\xi}_x}(\omega_x)\ \frac{1}{2\pi}\int_{-\infty}^{\infty} |H_x(\omega)|^2\, d\omega = \frac{S_{\hat{\xi}_x}(\omega_x)}{4\omega_x^3\zeta}$$

$$E[(ru_\theta)^2] \cong S_{\hat{\xi}_\theta}(\omega_\theta)\ \frac{1}{2\pi}\int_{-\infty}^{\infty} |H_\theta(\omega)|^2\, d\omega = \frac{S_{\hat{\xi}_\theta}(\omega_\theta)}{4\omega_\theta^3\zeta} \qquad (5.35)$$

Therefore, the lack of correlation of ground motion results in torsional response and a reduction of translational response. By referring to Eq. (2.29), (2.31) and (2.35) and Fig. (2.14), one can see immediately that the magnitude of the torsional response and the reduction of translational response increases with building size and frequency.

"Accidental eccentricity" $\tilde{e}_y$ is defined so that the translational force times $\frac{\tilde{e}_y}{r}$ applied as a torsional force to the uncoupled system produces the same torsional response as the rotational ground motion component [58]. Using the approximate responses of Eq. (5.35),

$$\frac{\tilde{e}_y}{b} = \left(\frac{r}{b}\right)\sqrt{\frac{\omega_\theta}{\omega_x}}\sqrt{\frac{S_{\hat{\xi}_\theta}\left(\frac{\omega_\theta}{\omega_x} z\right)}{S_{\hat{\xi}_x}(z)}} \tag{5.36}$$

in which $z = \frac{bc_s\omega_x}{V_s} = 2\pi c_s t_b f_x$, $t_b = \frac{b}{V_s}$

Plots of accidental eccentricity are shown in Figs. 5.33 and 5.34 for $c_s = \frac{0.5}{2\pi}$, together with Newmark's results [53].

Newmark's results, which are based on realistic response spectral shapes, show a roughly linear relationship between accidental eccentricity $\tilde{e}_y/b$ and the parameter $t_b f_x$. The white noise model used here does not have a very realistic ground motion frequency content, and in addition, the spatial correlation parameter c_s has been arbitarily selected. Although the white noise model does not predict a straight line relationship between $\tilde{e}_y/b$ and $t_b f_x$, the white noise results are in general agreement with Newmark's results over the significant range of $t_b f_x$.

5.6 Summary and Discussion

The effect of torsion in one-story systems was studied. The stationary responses to white noise excitation for one-way and two-way torsionally coupled systems were evaluated and plotted as functions of $\frac{\omega_\theta}{\omega_x}$.

The following results are drawn based on the numerical results :

(1) One-way torsionally coupled systems show an increase in torsional response and a reduction in translational response when the uncoupled torsional and translational frequencies are nearly equal. The peak torsional response increases as eccentricity increases and damping decreases. (See, for example, Fig. 5.9)

(2) The sum of the mean square torsional and translational forces (normalized by the value for zero eccentricity) remains essentially equal to one indicating that the torsional coupling merely produces a redistribution of forces.

(3) The maximum normalized torsional force is 0.5 and this large redistribution occurs even when the eccentricity is small, if the damping is small and the torsional/translational frequency ratio is near one.

(4) The sum of the normalized mean square torsional and translational displacement responses is independent of damping and always greater than one indicating that the system is effectively softened by the torsional coupling.

(5) The dynamic eccentricity (defined as the eccentricity at which the base shear in the uncoupled system must be applied in order to produce the dynamic torsional force) can greatly exceed the static eccentricity if $\frac{\omega_\theta}{\omega_x}$ is near 1 and the damping and static eccentricity are small. (For example, the dynamic eccentricity is 11.08 times as large as the static eccentricity for $\frac{e_y}{r} = 0.05$ and 2 percent modal damping)

(6) Compared to uncoupled translational response, the maximum root mean square responses at the periphery of the single story model are increased by about 40 percent for an eccentricity equal to about 6 percent of the floor plan dimension. For a two-way coupled system with equal eccentricities equal to about 8 percent of the floor plan dimension, the maximum root mean square response at the corner of the floor diaphragm increased by about 75 percent.

(7) For two-way torsionally coupled systems subjected to one-directional ground motion, eccentricities in the direction of the ground motion reduce the peak torsional response. Some conclusions drawn by Kan and Chopra [47] relating the response of two-way torsionally coupled systems to one-way torsionally coupled systems were shown to be valid only when the eccentricities are quite small.

(8) Ground motion directionality was considered by varying the incidence angle of the ground motion principal directions with respect to the structure. Results computed for different relative strengths of the two ground motion components showed that when the governing incidence angle for each case is taken

into account the maximum responses at the periphery of the floor diaphragm are relatively insensitive to the relative strengths of the two ground motion components. The "worst case", that of two components of ground motion of equal intensity, is not grossly overconservative. Comparison with the procedure recommended by the ATC-3 Code for recognizing orthogonal effects showed that that procedure is quite reasonable.

(9) The stationary and nonstationary responses of a one-way torsionally coupled system with $\frac{e_y}{r} = 0.15$ to Clough-Penzien spectrum excitation were computed and compared with the corresponding white noise results. The comparison showed that in general the stationary white noise results can be used to predict the effect of coupling for more realistic (Clough-Penzien spectrum) inputs. However, the white noise result tends to underestimate the outer edge response for stiff systems. The effect of coupling for soft systems is overestimated by the white noise results. The effect is further reduced for soft systems when nonstationary response is considered.

(10) The effect of ground spatial correlation was considered using an approximate solution. The response due to the resulting rotational component of ground motion input was determined in terms of an accidental eccentricity. A comparison with results given by Newmark [58] shows general agreement.

CHAPTER 6

THE EFFECT OF EARTHQUAKES ON TORSIONALLY COUPLED MULTI-STORY BUILDINGS

6.1 Introduction

The response of tall buildings under earthquake excitations has drawn much attention recently because the number of tall buildings in seismic regions has increased rapidly. Previous chapters have shown that the response at the outer edges of a one-story building is significantly increased by the existence of coupling between translation and rotation. Most previous studies of torsional coupling have also involved only single story systems ([47], [58], [71]) and the general results have been assumed to be valid for multi-story systems. The purpose of this chapter is to investigate the effect of torsional coupling on the response of a multi-story building and to verify that the general trends observed for single story systems can indeed be extrapolated to multi-story structures.

A particular class of buildings excited by two horizontal ground motion components is considered. The ground motions are assumed to be uniform over the base of the structure, however, they may have principal axes different from those of the structure. In the numerical example presented, the ground motion is assumed to have equal intensity in two orthogonal directions since that assumption was shown previously to produce not overly conservative "worst case" results. The frequency content of the

ground motion is described by the Clough Penzien spectrum and its time varying intensity by the short duration envelope.

Since torsional coupling may result in a significant increase in response at the perimeter of the building, the interstory drifts at the outer edges of a torsionally coupled building are obtained and compared with those of a corresponding uncoupled building. As was mentioned in Section 3.4, it is desirable to consider dominant participating mode pairs from which response can be obtained with sufficient accuracy. In this chapter, some general guidelines concerning the selection of modes are discussed.

6.2 Equations of Motion

Consider a particular class of N-story buildings (Figure 6.1) in which the floor mass centers lie on a single vertical axis and which has identically oriented principal axes in all stories. The buildings are idealized as lumped mass, shear beams with two translational DOFs and one rotational DOF associated with each mass. Let K_{xi}, K_{yi} and $K_{\theta i}$ represent respectively the translational stiffnesses in the structure principal directions X and Y and the torsional stiffness of the i-th story. Then

$$K_{xi} = \sum_j k_{xi}(j) \quad , \qquad K_{yi} = \sum_j k_{yi}(j) \quad ,$$

$$K_{\theta i} = \sum_j [\, k_{xi}(j) y_i^2(j) + k_{yi}(j) X_i^2(j) \,] \tag{6.1}$$

where $k_{xi}(j)$ and $k_{yi}(j)$ are the translational stiffnesses of the j-th resisting element connecting floors (i-1) and i. $(x_i(j), y_i(j))$ is the position of the element with respect to the line of mass centers. Let e_{xi} and e_{yi} be the static eccentricities of the stiffness elements connecting floors (i-1) and i.

$$e_{xi} = \frac{1}{K_{yi}} \sum_j x_i(j) k_{yi}(j) \tag{6.2}$$

$$e_{yi} = \frac{1}{K_{xi}} \sum_j y_i(j) k_{xi}(j)$$

The undamped equations of motion for the structure subjected to horizontal ground accelerations $a_x(t)$ and $a_y(t)$, are

$$\begin{bmatrix} \underline{m} & & \\ & \underline{m} & \\ & & \underline{m} \end{bmatrix} \begin{Bmatrix} \ddot{\underline{u}}_x \\ \ddot{\underline{u}}_\theta \\ \ddot{\underline{u}}_y \end{Bmatrix} + \begin{bmatrix} \underline{K}_{xx} & \underline{K}_{x\theta} & \underline{0} \\ \underline{K}_x^T & \underline{K}_{\theta\theta} & \underline{K}_y^T \\ \underline{0} & \underline{K}_{y\theta} & \underline{K}_{yy} \end{bmatrix} \begin{Bmatrix} \underline{u}_x \\ \underline{u}_\theta \\ \underline{u}_y \end{Bmatrix} = - \begin{Bmatrix} \underline{m}\ \underline{1}\ a_x \\ \underline{0} \\ \underline{m}\ \underline{1}\ a_y \end{Bmatrix} \tag{6.3}$$

In Eq. (6.3), the displacement sub-vectors are

$$\underline{u}_x = \begin{Bmatrix} u_{1x} \\ u_{2x} \\ \cdot \\ \cdot \\ \cdot \\ u_{Nx} \end{Bmatrix}, \quad \underline{u}_\theta = \begin{Bmatrix} r_1 \; u_{1\theta} \\ r_2 \; u_{2\theta} \\ \cdot \\ \cdot \\ \cdot \\ r_N \; u_{N\theta} \end{Bmatrix}, \quad \underline{u}_y = \begin{Bmatrix} u_{1y} \\ u_{2y} \\ \cdot \\ \cdot \\ \cdot \\ u_{Ny} \end{Bmatrix}$$

where r_i is the radius of gyration of the i-th floor about a vertical axis through the center of mass; the mass sub-matrix

$$\underline{m} = \begin{bmatrix} m_1 & & & & \\ & m_2 & & & \\ & & \cdot & & \\ & & & \cdot & \\ & & & & \cdot \\ & & & & & m_N \end{bmatrix}$$

where m_i is the lumped mass of floor i; all elements of the column vector $\underline{1}$ are unity; and the stiffness sub-matrices are

$$\underline{K}_{xx} = \begin{bmatrix} (K_{x1} + K_{x2}) & -K_{x2} & & & \\ -K_{x2} & (K_{x2} + K_{x3}) & -K_{x3} & & \\ & -K_{x3} & (K_{x3} + K_{x4}) & & \\ & & & \ddots & -K_{xN} \\ & & & -K_{xN} & K_{xN} \end{bmatrix}$$

$$\underline{K}_{yy} = \begin{bmatrix} (K_{y1} + K_{y2}) & -K_{y2} & & & \\ -K_{y2} & (K_{y2} + K_{y3}) & -K_{y3} & & \\ & -K_{y3} & (K_{y3} + K_{y4}) & & \\ & & & \ddots & -K_{yN} \\ & & & -K_{yN} & K_{yN} \end{bmatrix}$$

$$\underline{K}_{\theta\theta} = \begin{bmatrix} (\frac{1}{r_1})^2 (K_{\theta 1}+K_{\theta 2}) & -\frac{1}{r_1 r_2} K_{\theta 2} & & & \\ -\frac{1}{r_1 r_2} K_{\theta 2} & (\frac{1}{r_2})^2 (K_{\theta 2}+K_{\theta 3}) & -\frac{1}{r_2 r_3} K_{\theta 3} & & \\ & -\frac{1}{r_2 r_3} K_{\theta 3} & \ddots & & \\ & & & -\frac{1}{r_{N-1} r_N} K_{\theta N} & (\frac{1}{r_N})^2 K_{\theta N} \end{bmatrix}$$

$$\underline{K}_{x\theta} = -\begin{bmatrix} \frac{1}{r_1}(e_{y1}K_{x1}+e_{y2}K_{x2}) & -\frac{1}{r_2}e_{y2}K_{x2} & & & \\ -\frac{1}{r_1}e_{y2}K_{x2} & \frac{1}{r_2}(e_{y2}K_{x2}+e_{y3}K_{x3}) & -\frac{1}{r_3}e_{y3}K_{x3} & & \\ & -\frac{1}{r_2}e_{y3}K_{x3} & \ddots & & \\ & & & -\frac{1}{r_{N-1}}e_{yN}K_{xN} & \frac{1}{r_N}e_{yN}K_{xN} \end{bmatrix}$$

$$\underline{K}_{y\theta} = \begin{bmatrix} \frac{1}{r_1}(e_{x1}K_{y1}+e_{x2}K_{y2}) & -\frac{1}{r_2}e_{x2}K_{y2} & & & \\ -\frac{1}{r_1}e_{x2}K_{y2} & \frac{1}{r_2}(e_{x2}K_{y2}+e_{x3}K_{y3}) & -\frac{1}{r_3}e_{x3}K_{y3} & & \\ & -\frac{1}{r_2}e_{x3}K_{y3} & \ddots & & \\ & & & -\frac{1}{r_{N-1}}e_{xN}K_{yN} & \frac{1}{r_N}e_{xN}K_{yN} \end{bmatrix}$$

6.3 Response Covariances

6.3.1 Frequencies and Mode Shapes

The response covariances of the system can be obtained by using the formulas given in sections 3.4 and 3.5. The first step is to find the natural frequencies and mode shapes of the system. In general this requires the solution of an eigen-problem of order 3N. However, if all stories have the same radius of gyration, eccentricities, and stiffness ratios, then the eigen problem can be split into two smaller problems, one of order N and the other of order 3. Such simplification in modal extraction was noticed by Shiga [76] and employed in the work of Kan and Chopra [47]. More specifically, let $r_1 = r_2 = \cdots = r_N = r$, $e_{x1} = e_{x2} = \cdots = e_{xN} = e_x$, $e_{y1} = e_{y2} = \cdots = e_{yN} = e_y$, $\underline{K}_{\theta\theta} = \beta_\theta \underline{K}_{xx}$, $\underline{K}_{yy} = \beta_y \underline{K}_{xx}$. Then the natural frequencies, ω_{mn}, and mode shapes of the coupled system, ψ_{mn}, can be obtained as follows:

$$\omega_{mn} = \Omega_m \, \omega_{xn}$$

$$\underline{\psi}_{mn} = \begin{Bmatrix} \phi_{xm} \, \underline{\psi}_{xn} \\ \phi_{\theta m} \, \underline{\psi}_{xn} \\ \phi_{ym} \, \underline{\psi}_{xn} \end{Bmatrix} \qquad \begin{matrix} m = 1,2,3 \\ n = 1,2,3,\cdots N \end{matrix} \qquad (6.4)$$

where ω_{xn} and $\underline{\psi}_{xn}$ are the natural frequencies and mode shapes of the N DOF system

$$(\underline{K}_x - \omega_{xn}^2 \underline{m})\ \underline{\psi}_{xn} = \underline{0} \qquad n = 1, 2, \cdots N \qquad (6.5)$$

and Ω_m and $\{\phi_{xm}, \phi_{\theta m}, \phi_{ym}\}^T$ are determined from the 3 DOF eigen-value problem

$$\begin{bmatrix} (1 - \Omega_m^2), & -\frac{e_y}{r}, & 0 \\ -\frac{e_y}{r}, & (\beta_\theta - \Omega_m^2), & \frac{e_x}{r}\beta_y \\ 0, & \frac{e_x}{r}\beta_y, & (\beta_y - \Omega_m^2) \end{bmatrix} \begin{Bmatrix} \phi_{xm} \\ \phi_{\theta m} \\ \phi_{ym} \end{Bmatrix} = \underline{0} \quad m = 1,2,3 \qquad (6.6)$$

For a uniform structure, i.e., $m_1 = m_2 = \cdots = m_N = m$, $K_{x1} = K_{x2} = \cdots = K_{xN} = K$; the eigenvalues and eigenvectors of the N DOF system of Eq. (6.5) can be analytically expressed as

$$\omega_{xn} = 2\sqrt{\frac{K}{m}} \sin\left(\frac{\beta_n}{2}\right)$$
$$\underline{\psi}_{xn} = \{\psi_{n1}, \psi_{n2}, \cdots \psi_{ni} \cdots \psi_{nN}\}^T \qquad (6.7)$$

in which $$\psi_{ni} = B \sin(\beta_n \cdot i)$$

and $$\beta_n = \frac{(2n - 1)\pi}{2N + 1} \qquad n = 1, 2, \cdots N$$

6.3.2 Input Cross Correlation Function

For the systems described in Eq. (6.3), the input correlation function in Eq. (3.22) is

$$R_{F_\ell F_m}(\tau_1, \tau_2) = m_\ell m_m R_{a_x}(\tau_1, \tau_2) \qquad \begin{matrix} \ell = 1, 2, \cdots N \\ m = 1, 2, \cdots N \end{matrix}$$

$$R_{F_\ell F_m}(\tau_1, \tau_2) = m_{\ell-2N} \cdot m_{m-2N} R_{a_y}(\tau_1, \tau_2)$$

$$\begin{matrix} \ell = 2N+1, 2N+2, \cdots 3N \\ m = 2N+1, 2N+2, \cdots 3N \end{matrix}$$

$$R_{F_\ell F_m}(\tau_1, \tau_2) = m_{\ell-2N} m_m R_{a_x a_y}(\tau_1, \tau_2)$$

$$\begin{matrix} \ell = 2N+1, 2N+2, \cdots 3N \\ m = 1, 2, \cdots N \end{matrix}$$

$$R_{F_\ell F_m}(\tau_1, \tau_2) = m_\ell m_{m-2N} R_{a_x a_y}(\tau_1, \tau_2)$$

$$\begin{matrix} \ell = 1, 2, \cdots N \\ m = 2N+1, 2N+2, \cdots 3N \end{matrix}$$

$$R_{F_\ell F_m}(\tau_1, \tau_2) = 0 \qquad \text{Otherwise}$$

where $R_{a_x}(\tau_1, \tau_2)$, $R_{a_y}(\tau_1, \tau_2)$ and $R_{a_x a_y}(\tau_1, \tau_2)$ are described in Eq. (2.21)

6.3.3 Displacement Covariances and Interstory-Drifts

The displacement (of centers of mass relative to base) covariance can be obtained by Eq. (3.22). The interstory drifts, in the structure principal axes, of i-th story at center of mass are

$$\begin{aligned} d_{xi}(0,0) &= u_{xi} - u_{xi-1} \\ d_{yi}(0,0) &= u_{yi} - u_{yi-1} \end{aligned} \tag{6.9}$$

at location E, W are (refer to Fig. 5.5)

$$\begin{aligned} d_{yi}(\pm \frac{a_i}{2}, 0) &= (u_{yi} \pm \frac{a_i}{2} u_{\theta i}) - (u_{yi-1} \pm \frac{a_i}{2} u_{\theta i-1}) \\ &= (u_{yi} - u_{yi-1}) \pm (u_{\theta i} - u_{\theta i-1})(\frac{a_i}{2}) \end{aligned} \tag{6.10}$$

and at location N, S are

$$d_{xi}(0, \pm\frac{b}{2}) = (u_{xi} \mp \frac{b_i}{2} u_{\theta i}) - (u_{xi-1} \mp \frac{b_i}{2} u_{\theta i-1})$$
$$= (u_{xi} - u_{xi-1}) \mp (u_{\theta i} - u_{\theta i-1})(\frac{b_i}{2}) \qquad (6.11)$$

Therefore, the M. S. interstory drifts can be obtained with the knowledge of mass center displacement covariances. In this study the M.S. interstory drifts $d_{yi}(\pm a/2,0)$ and $d_{xi}(0, \pm b/2)$ are obtained and compared with the M.S. drifts of the corresponding uncoupled system to show the importance of torsional coupling.

6.4 Approximate Solution

For tall building analyses, a good approximation of displacement response can be achieved by considering only a few of the lower modes. Some general guidelines regarding the selection of modes are suggested so that a good approximation

can be obtained using a small fraction of the computation time and storage needed for an exact solution.

In the low frequency end of the response spectrum, the displacement responses are nearly constant. For this reason all the modes in the low frequency range are considered, although, strictly speaking, the contribution of each mode to the response depends also on the modal participation factor. The knee frequency, f*, below which the displacement response is nearly constant is dependent on the ground motion characteristics and can be determined in advance. For the Clough-Penzien spectrum parameters used previously, the knee frequency is about 0.33 cps. For those modes having frequencies above f*, say f_1, the displacement response is close to that of the Kanai-Tajimi spectrum. Using the equivalent white noise analogy, the M.S. modal displacement is (refer to Section 4.4)

$$E[u^2] = EQ(2\pi f_1,\ 2\pi f_1)\ \frac{S_1}{4(2\pi f_1)^3\,\zeta} \qquad (6.12)$$

where S_1 is the modal spectral level.

For the filter parameters used, $EQ(2\pi f_1,\ 2\pi f_1)$ is less than 1.75. Let f_c (reference frequency) be the maximum of f_0 and f* in which f_0 is the fundamental natural frequency. Then

the ratio

$$\frac{EQ(2\pi f_1,\ 2\pi f_1)\ \dfrac{S_1}{4(2\pi f_1)^3\,\zeta}}{EQ(2\pi f_c,\ 2\pi f_c)\ \dfrac{S_c}{4(2\pi f_c)^3\,\zeta}} \leq 1.75\ \left(\frac{f_c}{f_1}\right)^3 \frac{S_1}{S_c} \qquad (6.13)$$

For the shear beam structural model, the participation factors, $\{\psi_i\}^T[M]\{1\}$, of the first few modes are generally greater than those of higher modes. Therefore, the contribution of the higher modes is approximately inversely proportional to frequency raised to the third power.

In Eq. (3.21), Eq. (3.22), in order to obtain covariance, one needs to calculate the double integrals for all participating mode pairs. It is desirable to calculate only those participating mode pairs which have a significant influence on response. Using white noise results and considering the mode pair (i,j), one can see immediately that

$$\frac{\Gamma_{ij}}{4(2\pi f_c)^3\,\zeta} > \frac{(f_i+f_j)(f_i-f_j)^2}{8\zeta^2 f_c^3} \qquad (6.14)$$

For the same modal intensity, the contribution due to the mode pair satisfying $\frac{(f_i+f_j)(f_i-f_j)^2}{8\zeta f_c^3} > p^*$ is approximately less than $1.75/p^*$ of that of reference mode.

With these guide rules, most of the terms in Eq. (3.22) can be eliminated without seriously affecting the accuracy of the results. This saves a great deal of computational time as well as data storage.

6.5 Numerical Example

An 8-story building with a special type of stiffness "taper" is now considered. It is assumed that the ground motion has equal intensity in the two principal directions. This assumption was shown in Section 5.3.3 to produce reasonable upper bounds to the responses due to other ground motion intensity ratios for the governing ground motion incidence angle. The ground motion frequency content is described by the Clough-Penzien spectrum (Ground Motion No.2 of Chapter 2) and the short duration envelope is used for the nonstationary results. The system properties are:

1). $m_1 = m_2 = \text{---} = m_N = m$

2). $\frac{K_i}{m} = 1075, 1045, 985, 896, 776, 627, 448, 239$

3). $\underline{K}_{\theta\theta} = \beta_\theta \underline{K}_{xx}$ and $\beta_\theta = (1.3)^2 = 1.69$

$\underline{K}_{yy} = \beta_y \underline{K}_{xx}$ and $\beta_y = (1.15) = 1.3225$

4). $\frac{e_{xi}}{r} = 0.2 \qquad \frac{e_{yi}}{r} = 0.3$ for all floors

5). damping is 5% critical

6). all floors are assumed to be square. i.e., $\frac{a_i}{b_i} = \frac{a}{b}$ $= 1.$

The floor to floor variation of stiffness is such that the system has a linear first mode for the corresponding uncoupled system. The mode shapes and natural frequencies for the uncoupled system are shown in Fig. 6.2.

For this example, the results of eigen-value problem in Eq. (6.6) are

$$\Omega_1 = 0.9305, \ \Omega_2 = 1.113, \ \Omega_3 = 1.381;$$

and

$$\begin{bmatrix} \phi_{x1}, & \phi_{x2}, & \phi_{x3} \\ \phi_{\theta 1}, & \phi_{\theta 2}, & \phi_{\theta 3} \\ \phi_{y1}, & \phi_{y2}, & \phi_{y3} \end{bmatrix} = \begin{bmatrix} 0.8884, & 0.3573, & -0.2882 \\ 0.3972, & -0.2837, & 0.8728 \\ -0.2301, & 0.8899, & 0.3940 \end{bmatrix}$$

The natural frequencies and mode shape of the coupled system are obtained through Eq. (6.4). The natural frequencies of the system are 5.08, 6.08, 7.55, 12.46, 14.90, 18.49, 19.69, 23.55, 26.91, 29.24, 32.18, 34.11, 39.95, 40.79, 41.31, 48.50, 49.40, 50.64, 55.70, 58.00, 61.32, 66.60, 72.01, and 82.69 rad/sec. The mode shape for the first mode is obtained as

$$\underline{\psi}_{11}^{T} = \{0.062,\ 0.124,\ 0.187,\ 0.249,\ 0.311,\ 0.373,\ 0.435,\ 0.498,\ 0.028,\ 0.056,\ 0.083,\ 0.111,\ 0.139,\ 0.167,\ 0.195,\ 0.223,\ -0.016,\ -0.032,\ -0.048,\ -0.064,\ -0.081,\ -0.097,\ -0.113,\ -0.129\}$$

The structural responses to ground excitation are summarized in Tables 6.1 to 6.5 and Figs. 6.3 and 6.4. The Clough-Penzien spectrum and filter parameters $\omega_g = 15.46$ rad/sec, $\zeta_g = 0.623$, $\omega_f = 1.636$ rad/sec, $\zeta_f = 0.619$ and $S_0 = 1\ m^2/sec^3$ are used (Ground motion No. 2 of Chapter 2). Non-stationary responses are computed using the "short duration" envelope ($\alpha = 0.25$/sec, $\beta = 0.75$/sec, see Chapter 2). Notation used in the tables is defined as follows:

$$\sigma_{xi} = \sqrt{E[d_{xi}^2(0,0)]} \qquad \sigma_{yi} = \sqrt{E[d_{yi}^2(0,0)]}$$

$$\sigma_{Ei} = \sqrt{E[d_{yi}^2(\tfrac{a}{2},0)]} \qquad \sigma_{Wi} = \sqrt{E[d_{yi}^2(-\tfrac{a}{2},0)]}$$

$$\sigma_{Ni} = \sqrt{E[d_{xi}^2(0,\tfrac{b}{2})]} \qquad \sigma_{Si} = \sqrt{E[d_{xi}^2(0,-\tfrac{b}{2})]}$$

The results show that the interstory drifts are quite uniform below the 6th floor. In the top story, the drifts are about 25 percent larger than the average values. The smallest interstory drifts occur between the 3rd and 4th floor and exceed the corresponding results for a single story structure by about 1 percent. The largest interstory drift, at the top story, exceeds the single story structure drift by about 35 percent in the stationary case and 42 percent in the nonstationary case. The spatial distribution of response drifts is undoubtedly dependent on the fact that the stiffness distribution was selected to produce a linear fundamental mode shape.

It is of greater significance to establish whether or not the relative effects of torsional coupling in the multistory structure are predicted by the results for single story structures. As in single story systems, the translational displacements at the center of the mass decrease as the result of torsional coupling. The responses at the outer edges of the building are significantly greater than those of the corresponding uncoupled system by amounts ranging from 39 percent to 55 percent (Fig. 6.3 and 6.4). In the corresponding single story system (Table 6.5) the outer edge responses exceed the uncoupled responses by 39 - 50 percent. The amplification of response due to torsional coupling is virtually the same for the short duration motion as for the stationary case (compare Figs. 6.3 and 6.4). However, the magnitudes of the interstory

drifts for the short duration motion are reduced by about 15 - 20 percent as compared to the stationary case (compare Table 6.1 and 6.2). For the single story structure the short duration drifts are reduced by about 12 - 16 percent as compared to the stationary case.

From these comparisons, it is apparent that the general trends which were observed for torsionally coupled single story structures carry over to multistory structures, in which there is not much variability of response from story to story. That is , the average response in the multistory structure is well predicted by the single story model. For multistory structures with significant changes of stiffness, mass, or eccentricity from floor to floor, the spatial distribution of interstory drifts would be expected to be quite nonuniform. In such cases, extrapolation of single story results is questionable.

A good approximation is obtained by considering only a few important modes (pairs). The numerical results shown in Tables 6.3 and 6.4 are obtained by neglecting all the modes satisfying $(f_1 / f_c) \geq 4.0$ and all the mode pairs satisfying $\frac{(f_i+f_j)(f_i-f_j)^2}{8\zeta f_c^3} \geq 250$. The approximate results are very close to the exact results. Table 6.5 shows the results obtained by considering only the first three modes (one in each direction). The approximation is quite good except at the top two floors, and the drifts are the same at every floor.

6.5.2 Computational Considerations

In order to obtain the exact solution, all 24 modes are considered. If advantage is taken of symmetry , 300 mode pairs in Eq. (3.22) are needed. If one is interested in the results for 10 instants of time, there are 3000 double integrals to be calculated. The cost of such calculation would be prohibitive. With the algorithm described in Chapter 3, all the covariance of displacement responses at the mass center and all drift information (stationary and nonstationary) sampled at 10 arbitrary time instants was obtained in less than 20 seconds of CPU time on the University of Illinois Cyber 175. The approximate solution (15 mode pairs involved) takes only about 1 second of CPU time to obtain the same information. Therefore the algorithm which has been presented is very efficient for the calculation of the response of general M-DOF systems to earthquake ground excitations. A significant advantage of this algorithm is that one can directly obtain the responses at the time instant of interest. One can always use the approximate solution to compute the nonstationary results cheaply, and then compute the exact solution in a reduced time interval of interest.

makes it feasible to systematically investigate the structural response characteristics for a variety of ground motion input and structural characteristics. The effects of various ground motion characteristics on the response of SDOF elastic system are discussed in Chapter 4. These include the effects of frequency content, temporal variation of intensity, duration and the presence of individual large acceleration pulses in the ground motion. In Chapter 5, the effects of modal coupling and multi-directional ground motions are studied through simple one story torsionally coupled structural systems. An extensive parameter study is conducted with white noise input. Effects of ground motion frequency content and duration are also investigated.

A class of tall buildings is considered in Chapter 6. Numerical comparisons for interstory drifts between coupled and uncoupled systems are presented. Exact solutions as well as approximate solutions are obtained and the accuracy and computational cost are discussed.

7.2 Conclusions

The following conclusions are drawn based on the results of this study:

1. Ground Motion Model

a) The ground motion model with frequency content specified by the Clough-Penzien spectrum realistically models

CHAPTER 7

SUMMARY AND CONCLUSIONS

7.1 Summary

The effects of ground motion characteristics on the response of simple elastic structural systems are systematically investigated using stochastic ground motion models.

The characteristics of commonly used stochastic models for ground motion are first investigated in Chapter 2. These include white noise and filtered white noise models (Kanai-Tajimi spectrum and Clough-Penzien spectrum) for frequency content and a double exponential envelope function for intensity and duration. Qualitative comparisons are made with recorded ground motions. Multi-directional ground motions are considered assuming the existence of ground motion principal directions.

Time domain nonstationary response analysis is considered in Chapter 3. Modelling of isolated large acceleration pulses and ground motion spatial correlation are illustrated by white noise model in Chapter 2 and their effects are discussed respectively in Chapter 4 and Chapter 5. The effect of close natural freqeuncies is illustrated with white noise input in Chapter 3. In the same chapter, an efficient solution algorithm is obtained for evaluating nonstationary response of systems to Kanai-Tajimi and Clough-Penzien spectrum excitation. This

high frequency systems as well.

It was demonstrated that when the ground motion is modeled using a time varying intensity function as an envelope to modulate a stationary random process, a previously unreported defect appears in the ground motion model. The behavior of very low frequency elastic systems may not be accurately portrayed using such ground motion models.

d) Limited results obtained using a white noise ground motion model suggest that for ground motions of the same general intensity level, those containing large individual acceleration pulses produce larger maximum responses than those without such acceleration pulses.

2. Response of Single Story Torsionally Coupled System

The response of a single story elastic system with stiffness eccentricity was studied extensively using both a white noise and a Clough-Penzien frequency content model for the ground motion.

Some general results obtained in previous studies [47] using a deterministic approach were confirmed.

a) One-way torsionally coupled systems show an increase in torsional response and a reduction in translational response when the uncoupled torsional and translational frequencies are nearly equal. The peak torsional response increase as eccentricity increases and damping decreases. (See, for example, Fig. 5.9)

earthquake ground motions. SDOF elastic response spectra computed using this input ground motion agree qualitatively with actual earthquake response spectra. The ground motion model also predicts relations between mean square ground acceleration, velocity and displacement which agree well with corresponding estimates proposed by Newmark and Hall [57].

b) Effects of variations in ground motion frequency content and duration on the response of SDOF elastic systems were studied. The filter parameters controlling the Clough-Penzien spectrum were varied to simulate different "Predominant" ground motion frequencies. The corresponding response spectra exhibited response amplification factors (relative to mean square ground motions) which were insensitive to quite large changes in ground motion frequency content. It is noted that this is a prediction of the model rather than an established fact, and it remains to be verified by comparison with recorded earthquake motions.

c) The effect of time-varying intensity and duration of the ground acceleration was modelled by means of an exponential envelope function proposed by Shinozuka and Sato. Mean square responses were sensitive to duration only for medium and low frequency systems. Mean square displacement response to the long duration motion consistently exceeded the response to the short duration motion. Maximum (90% probability of exceedence) responses show a slight dependence on duration for

eccentricities equal to about 8 percent of the floor plan dimension, the maximum root mean square responses at the corner of the floor diaphragm increased by about 75 percent.

g) For two-way torsionally coupled systems subjected to one-directional ground motion, eccentricities in the direction of the ground motion reduce the peak torsional response. Some conclusions drawn by Kan and Chopra [47] relating the response of two-way torsionally coupled systems to one-way torsionally coupled systems were shown in this study to be valid only when the eccentricities are quite small.

h) Ground motion directionality was considered by varying the incidence angle of the ground motion principal directions with respect to the structure. Results computed for different relative strengths of the two ground motion components showed that when the governing incidence angle for each case is taken into account the maximum responses at the periphery of the floor diaphragm are relatively insensitive to the relative strengths of the two ground motion components. The "worst case", that of two components of ground motion of equal intensity, is not grossly overconservative. Comparison with the procedure recommended by the ATC-3 Code for recognizing orthogonal effects showed that that procedure is quite reasonable for this simple structural model.

j) Effects of ground motion frequency content and duration were investigated to determine whether the general

b) The sum of the mean square torsional and translational forces (normalized by the value for zero eccentricity) remains essentially equal to one indicating that the torsional coupling merely produces a redistribution of forces.

c) The maximum normalized torsional force is 0.5 and this large redistribution occurs even when the eccentricity is small, if the damping is small and the torsional/translational frequency ratio is near one.

d) The sum of the normalized mean square torsional and translational displacement responses is always greater than one and is independent of damping indicating that the system is effectively softened by the torsional coupling.

e) The dynamic eccentricity, defined as the eccentricity at which the base shear in the uncoupled system must be applied in order to produce the dynamic torque, can greatly exceed the static eccentricity if the torsional/translational frequency ratio is near one and the damping and static eccentricity are small. For example, for 2 percent modal damping and static eccentricity $\frac{e_y}{r} = 0.05$, the dynamic eccentricity is 11.08 times the static eccentricity.

f) Compared to uncoupled translational response, the maximum root mean square displacement responses at the periphery of the single story model are increased by about 40 percent for an eccentricity equal to about 6 percent of the floor plan dimension. For a two-way coupled system with equal

f = 0.81 cps, and with a stiffness "taper" such that the first mode was linear for the uncoupled system. The Clough-Penzien spectrum and the short duration envelope were used to model the ground motion.

Root mean square interstory drifts computed at the periphery of the floor diaphragms were greater than those of the uncoupled system by amounts ranging from 39% to 55%. Interstory drifts were quite uniform except in the top two stories, and the effects of torsional coupling were well predicted by the responses of the corresponding single story structure. However, for multi-story structures with significant changes of stiffness mass or eccentricity from story to story the extrapolation of single story results is not justified.

trends found for the white noise ground motion model can be assumed to hold for the more realistic ground motion models. The results for the medium frequency system (f_x = 1 cps) were quite close to the white noise results. For the stiff system (f_x = 5 cps) the column response at the periphery is underestimated by the white noise model. For the soft system (f_x = 0.2 cps) the effect of coupling is overemphasized by the white noise model. When the time-varying intensity of the ground motion is considered, the effect of torsional coupling on soft systems is reduced further due to the time lag between maximum torsional and translational response. The frequency ratio at which peak torsional response occurs shifts toward $\omega_\theta > \omega_x$ for soft systems and towards $\omega_\theta < \omega_x$ for stiff systems.

(j) Accidental eccentricity arising from lack of spatial correlation of ground motion was calculated using a white noise approximation. The results show general agreement with those of Newmark [58].

3. Response of Multi-story Torsionally Coupled Systems

A special class of multi-story structures was considered in which floor mass centers lie on a single vertical axis and floor mass principal axes have identical orientations at all floors.

A computationally efficient procedure for computing the responses was developed, and a numerical example was presented for an 8 story structure, with fundemantal frequency

t_{max} (sec) D_{TB} (sec) f_ℓ (cps)		β/α				
		1.5	2.0	3.0	5.0	10.0
α	0.05	16.22 45.40 0.026	13.86 40.83 0.030	10.99 36.20 0.039	8.05 32.75 0.054	5.12 30.63 0.085
	0.10	8.11 22.82 0.050	6.93 20.40 0.058	5.49 18.09 0.073	4.02 16.41 0.098	2.56 15.33 0.141
	0.25	3.24 9.11 0.112	2.77 8.16 0.127	2.20 7.24 0.151	1.61 6.56 0.184	1.02 6.15 0.225
	0.50	1.62 4.58 0.185	1.39 4.08 0.203	1.10 3.62 0.227	0.80 3.25 0.250	0.51 3.06 0.269
	1.00	0.81 2.27 0.261	0.69 2.04 0.272	0.55 1.81 0.282	0.40 1.65 0.286	0.26 1.53 0.283

Table 2.1 Variation of t_{max}, D_{TB} and f_ℓ with the Envelope Parameters α and β

TABLES

GEOLOGICAL CLASSIFICATION			HARD	INTERMEDIATE	SOFT	
NUMBER OF SAMPLES			3	8	14	25
Cross Correlation Coefficients	Mean	ρ_{23}	0.33	0.65	0.53	0.54
		ρ_{13}	0.63	0.73	0.72	0.71
		ρ_{12}	0.40	0.16	0.28	0.26
	Standard deviation	ρ_{23}	0.07	0.15	0.19	0.19
		ρ_{13}	0.16	0.11	0.09	0.11
		ρ_{12}	0.19	0.09	0.14	0.15
	Coefficient of Variation	ρ_{23}	0.20	0.23	0.36	0.35
		ρ_{13}	0.26	0.15	0.13	0.15
		ρ_{12}	0.47	0.58	0.50	0.58

Table 2.3 Statistical Properties of Cross Correlation Coefficients During the Strong Motion - San Fernando (1971) Earthquake (after Kubo and Penzien [49])

GEOLOGICAL CLASSIFICATION			HARD	INTERMEDIATE	SOFT	
NUMBER OF SAMPLES			3	8	14	25
Ratios of Principal Variances to the Sum of the Principal Variances	Mean	Major	0.61	0.53	0.58	0.57
		Inter.	0.26	0.39	0.33	0.34
		Minor	0.13	0.08	0.10	0.10
	Standard deviation	Major	0.12	0.05	0.06	0.07
		Inter.	0.07	0.05	0.07	0.07
		Minor	0.05	0.04	0.04	0.04
	Coefficient of Variation	Major	0.19	0.08	0.10	0.12
		Inter.	0.27	0.12	0.21	0.22
		Minor	0.39	0.44	0.36	0.40
Ratios of the Intermediate and Minor Principal Variances to the Major Principal Variance	Mean	Inter.	0.44	0.74	0.58	0.61
		Minor	0.23	0.16	0.17	0.17
	Standard deviation	Inter.	0.18	0.13	0.16	0.18
		Minor	0.12	0.07	0.06	0.07
	Coefficient of Variation	Inter.	0.41	0.18	0.28	0.29
		Minor	0.52	0.46	0.38	0.43

Table 2.2 Statistical Properties of Principal Variances During the Strong Motion - San Fernando (1971) Earthquake (after Kubo and Penzien [49])

Condition		Quantity	Resistance Pattern			
a/b	$\Sigma k_y / \Sigma k_x$		Uniform	Perimeter	9-Column	4-Column
1.0	1.0	ω_θ/ω_x	1	1.732	1.414	1.732
0.5	1.0	ω_θ/ω_x	1	1.897	1.414	1.732
0.0	all	ω_θ/ω_x	1	1.732	1.414	1.732

Table 5.1 Frequency Ratios for Building Resistance Patterns shown in Fig. 5.4 (After Newmark [62])

a/b	b/r
1.0	$\sqrt{6} = 2.45$
0.5	$\sqrt{48/5} = 3.10$
0.0	$\sqrt{12} = 3.46$

Table 5.2 Ratio of Floor Dimension to Radius of Gyration for Rectangular Floor Diaphragms

	System Natural Frequency (cps)							
	0.05	0.10	0.20	0.50	1.00	2.00	5.00	10.00
Short Duration	2.01	2.23	2.51	2.67	2.807	2.95	3.17	3.34
Long Duration	2.54	2.67	2.73	2.90	3.07	3.25	3.48	3.63
Stationary (10 sec.)	2.61	2.60	2.74	3.03	3.24	3.44	3.68	3.83

Table 4.1 The Multiplication Constant c for 90% Probability of No Exceedance

$$\zeta_g = 0.64 \quad \omega_g = 15.6/\text{sec} \quad r = \frac{E[u^2]_{\text{Kanai}}}{E[u^2]_{\text{Eq.White}}} = \frac{\text{Exact}}{\text{Approx.}}$$

ζ \ ω_θ r	System Natural Frequency (rad/sec)						
	1.0	5.0	10.0	14.0	20.0	24.0	30.0
Damping 0.02	1.000	0.998	0.988	0.985	1.008	1.030	1.060
0.05	1.000	0.995	0.970	0.964	1.019	1.071	1.144
0.10	1.000	0.989	0.944	0.934	1.032	1.128	1.270

Table 4.2 Equivalent White Noise Approximation for M.S. Response to Ground Motion with Kanai-Tajimi Spectral Characteristics

	f_0 (cps)	$\frac{\omega_\theta}{\omega_x}$	UNCOUPLED SYSTEM				COUPLED SYSTEM								90%	
			σ_{max}	c_o			σ_{max} at N	c_1			σ_{max} at S	c_2			$\frac{c_1}{c_o}$	$\frac{c_2}{c_o}$
				80%	90%	95%		80%	90%	95%		80%	90%	95%		
$S_0 = 1.$	0.10	1.0	0.64	1.96	2.23	2.48	0.60	2.10	2.36	2.61	0.68	1.93	2.19	2.43	1.06	0.98
	0.15	1.0	0.57	2.14	2.40	2.64	0.57	2.20	2.46	2.69	0.59	2.14	2.39	2.62	1.02	1.00
	0.20	0.9					0.63	2.37	2.63	2.86	0.54	2.08	2.35	2.60	1.05	0.94
	0.20	1.0	0.55	2.24	2.51	2.75	0.56	2.30	2.56	2.78	0.57	2.27	2.54	2.77	1.02	1.01
	0.20	1.1					0.51	2.20	2.48	2.73	0.62	2.37	2.63	2.86	0.99	1.05
	0.20	1.2					0.50	2.12	2.41	2.66	0.65	2.31	2.58	2.81	0.96	1.03
	0.30	1.0	0.49	2.33	2.60	2.84	0.49	2.38	2.64	2.87	0.53	2.35	2.62	2.86	1.02	1.01
	0.40	1.0	0.40	2.36	2.62	2.86	0.39	2.43	2.69	2.92	0.45	2.38	2.64	2.88	1.03	1.01
$S_0 = 100$	0.50	1.0	3.16	2.41	2.67	2.90	3.05	2.47	2.73	2.96	3.68	2.42	2.68	2.91	1.02	1.00
	0.70	1.0	2.14	2.48	2.74	2.97	2.09	2.52	2.78	3.01	2.54	2.48	2.73	2.97	1.02	1.00
	1.00	0.9					1.73	2.55	2.80	3.03	1.40	2.51	2.76	2.99	1.00	0.98
	1.00	1.0	1.42	2.55	2.81	3.03	1.40	2.59	2.84	3.07	1.69	2.55	2.80	3.02	1.01	1.00
	1.00	1.1					1.12	2.52	2.77	3.00	1.86	2.55	2.80	3.02	0.99	1.00
	1.00	1.2					1.03	2.56	2.81	3.03	1.84	2.53	2.78	3.01	1.00	0.99
	1.50	1.0	0.89	2.65	2.90	3.12	0.89	2.67	2.91	3.13	1.07	2.64	2.88	3.10	1.01	0.99
	2.00	1.0	0.62	2.72	2.95	3.17	0.61	2.74	2.98	3.18	0.76	2.70	2.94	3.16	1.01	1.00
$S_0 = 10000$	3.00	1.0	3.04	2.82	3.05	3.26	2.81	2.84	3.07	3.28	3.90	2.81	3.04	3.25	1.01	1.00
	4.00	1.0	1.58	2.89	3.13	3.33	1.42	2.92	3.15	3.34	2.08	2.88	3.10	3.31	1.01	0.99
	5.00	0.8					1.11	2.96	3.19	3.39	1.06	2.89	3.11	3.32	1.01	0.98
	5.00	0.9					1.02	2.98	3.19	3.39	1.10	2.90	3.14	3.34	1.01	0.99
	5.00	1.0	0.92	2.95	3.10	3.38	0.82	2.98	3.20	3.40	1.22	2.93	3.16	3.36	1.01	1.00
	5.00	1.1					0.65	2.96	3.19	3.39	1.25	2.95	3.17	3.38	1.01	1.00
	5.00	1.2					0.67	2.95	3.17	3.38	1.19	2.95	3.17	3.38	1.00	1.00
	7.00	1.0	0.40	3.04	3.26	3.47	0.36	3.07	3.29	3.49	0.53	3.02	3.24	3.44	1.01	0.99
	10.0	1.0	1.72	3.13	3.34	3.55	1.51	3.15	3.37	3.56	2.24	3.11	3.33	3.52	1.01	1.00

($\omega_\theta/\omega_x = 1$, $e_y/r = 0.15$, $b/a = 1$)

Table 5.4 Multiplication Constants - Input: Clough-Penzien Spectrum, Nonstationary ("Short Duration" Ground Motion, Trifunac-Brady Duration = 7.2 sec)

	f_0	$\frac{\omega_\theta}{\omega_x}$	UNCOUPLED SYSTEM				COUPLED SYSTEM							90%	
				c_o				c_1				c_2		$\frac{c_1}{c_o}$	$\frac{c_2}{c_o}$
			σ_{max}	80%	90%	95%	σ_{max} at N	80%	90%	95%	σ_{max} at S	80%	90%	95%	
$S_0 = 1$	0.10	1.0	0.73	2.30	2.60	2.87	0.81	2.29	2.60	2.86	2.76	2.27	2.58	2.85	1.00	0.99
	0.15	1.0	0.85	2.37	2.67	2.92	0.94	2.38	2.67	2.93	0.89	2.34	2.64	2.90	1.00	0.99
	0.20	0.9					1.13	2.45	2.74	2.99	0.73	2.43	2.72	2.98	1.00	1.00
	0.20	1.0	0.90	2.45	2.74	2.99	0.77	2.47	2.75	3.00	0.97	2.42	2.71	2.96	1.01	0.99
	0.20	1.1					0.73	2.49	2.78	3.03	1.12	2.42	2.71	2.97	1.02	0.99
	0.20	1.2					0.67	2.49	2.78	3.03	1.12	2.43	2.72	2.97	1.02	0.99
	0.30	1.0	0.76	2.59	2.86	3.10	0.78	2.61	2.88	3.12	0.89	2.55	2.83	3.08	1.01	0.99
	0.40	1.0	0.56	2.69	2.95	3.19	0.56	2.71	2.98	3.21	0.68	2.66	2.92	3.16	1.01	0.99
$S_0 = 100$	0.50	1.0	4.20	2.77	3.03	3.25	4.13	2.79	3.05	3.28	5.12	2.74	3.00	3.23	1.01	0.99
	0.70	1.0	2.64	2.88	3.13	3.35	2.59	2.91	3.15	3.38	3.22	2.85	3.11	3.33	1.01	0.99
	1.00	0.9					1.97	3.01	3.25	3.47	1.63	2.96	3.20	3.42	1.00	0.99
	1.00	1.0	1.63	3.00	3.24	3.46	1.61	3.03	3.26	3.48	1.98	2.97	3.22	3.43	1.01	0.99
	1.00	1.1					1.21	3.03	3.27	3.48	2.16	2.99	3.23	3.44	1.01	1.00
	1.00	1.2					1.17	3.02	3.26	3.47	2.10	2.99	3.24	3.45	1.01	1.00
	1.50	1.0	0.98	3.13	3.36	3.57	0.96	3.15	3.38	3.59	1.18	3.11	3.34	3.55	1.01	0.99
	2.00	1.0	0.66	3.22	3.44	3.65	0.64	3.24	3.46	3.67	0.81	3.19	3.42	3.63	1.01	0.99
$S_0 = 10000$	3.00	1.0	3.13	3.33	3.55	3.75	2.88	3.36	3.57	3.77	4.04	3.31	3.53	3.73	1.01	0.99
	4.00	1.0	1.61	3.41	3.62	3.82	1.44	3.43	3.65	3.84	2.12	3.39	3.61	3.80	1.01	1.00
	5.00	0.8					1.12	3.48	3.69	3.88	1.08	3.40	3.62	3.81	1.00	0.98
	5.00	0.9					1.03	3.49	3.70	3.89	1.11	3.43	3.64	3.83	1.01	0.99
	5.00	1.0	0.93	3.47	3.68	3.87	0.83	3.49	3.70	3.89	1.23	3.45	3.66	3.85	1.01	1.00
	5.00	1.1					0.66	3.48	3.69	3.88	1.26	3.46	3.67	3.87	1.00	1.00
	5.00	1.2					0.68	3.46	3.67	3.86	1.20	3.47	3.68	3.87	1.00	1.00
	7.00	1.0	0.41	3.55	3.76	3.94	0.36	3.58	3.78	3.97	0.54	3.53	3.74	3.93	1.01	1.00
	10.0	1.0	1.73	3.63	3.83	4.02	1.52	3.66	3.86	4.04	2.25	3.62	3.82	4.01	1.01	1.00

($\omega_\theta/\omega_x = 1$, $e_y/r = 0.15$, $b/a = 1$)

Table 5.3 Multiplication Constants - Input: Clough-Penzien Spectrum, Stationary (t = 10 sec)

STORY	STORY DRIFTS (UNCOUPLED)		STORY DRIFTS (COUPLED)						
	$(\sigma_x)_{max}$	$(\sigma_y)_{max}$	$(\sigma_x)_{max}$	$(\sigma_T)_{max}$	$(\sigma_y)_{max}$	$(\sigma_E)_{max}$	$(\sigma_W)_{max}$	$(\sigma_N)_{max}$	$(\sigma_S)_{max}$
7-8	0.0405	0.0332	0.0386	0.0218	0.0314	0.0296	0.0505	0.0321	0.0581
6-7	0.0342	0.0286	0.0326	0.0180	0.0270	0.0253	0.0425	0.0284	0.0479
5-6	0.0314	0.0265	0.0300	0.0165	0.0250	0.0234	0.0392	0.0265	0.0437
4-5	0.0301	0.0256	0.0288	0.0159	0.0240	0.0226	0.0378	0.0256	0.0420
3-4	0.0297	0.0252	0.0283	0.0158	0.0237	0.0224	0.0373	0.0252	0.0414
2-3	0.0298	0.0253	0.0284	0.0159	0.0237	0.0224	0.0375	0.0253	0.0416
1-2	0.0301	0.0256	0.0287	0.0161	0.0240	0.0226	0.0379	0.0256	0.0421
0-1	0.0305	0.0259	0.0291	0.0162	0.0243	0.0228	0.0384	0.0259	0.0426

Table 6.2 The Interstory Drifts (Exact, Nonstationary)

STORY	STORY DRIFTS (UNCOUPLED)		STORY DRIFTS (COUPLED)						
	σ_x	σ_y	σ_x	$r\sigma_\theta$	σ_y	σ_E	σ_W	σ_N	σ_S
7-8	0.0457	0.0369	0.0438	0.0244	0.0353	0.0323	0.0568	0.0359	0.0657
6-7	0.0394	0.0324	0.0379	0.0204	0.0310	0.0281	0.0488	0.0321	0.0556
5-6	0.0367	0.0303	0.0353	0.0189	0.0289	0.0263	0.0454	0.0302	0.0515
4-5	0.0354	0.0294	0.0340	0.0184	0.0280	0.0256	0.0439	0.0292	0.0497
3-4	0.0350	0.0290	0.0336	0.0182	0.0277	0.0253	0.0434	0.0288	0.0492
2-3	0.0351	0.0291	0.0337	0.0183	0.0277	0.0254	0.0436	0.0289	0.0494
1-2	0.0355	0.0294	0.0340	0.0185	0.0280	0.0255	0.0440	0.0292	0.0499
0-1	0.0359	0.0297	0.0344	0.0186	0.0283	0.0258	0.0445	0.0295	0.0504

Table 6.1 The Interstory Drifts (Exact, Stationary)

STORY	STORY DRIFTS (UNCOUPLED)		STORY DRIFTS (COUPLED)						
	$(\sigma_x)_{max}$	$(\sigma_y)_{max}$	$(\sigma_x)_{max}$	$(r\sigma_\theta)_{max}$	$(\sigma_y)_{max}$	$(\sigma_E)_{max}$	$(\sigma_W)_{max}$	$(\sigma_N)_{max}$	$(\sigma_S)_{max}$
7-8	0.0404	0.0320	0.0383	0.0215	0.0304	0.0289	0.0491	0.0313	0.0579
6-7	0.0338	0.0283	0.0322	0.0178	0.0267	0.0250	0.0422	0.0281	0.0474
5-6	0.0311	0.0262	0.0297	0.0164	0.0246	0.0230	0.0388	0.0262	0.0434
4-5	0.0299	0.0252	0.0285	0.0159	0.0237	0.0223	0.0374	0.0253	0.0417
3-4	0.0295	0.0251	0.0281	0.0158	0.0235	0.0222	0.0371	0.0251	0.0412
2-3	0.0298	0.0253	0.0284	0.0159	0.0237	0.0225	0.0375	0.0253	0.0416
1-2	0.0303	0.0257	0.0289	0.0161	0.0241	0.0227	0.0381	0.0257	0.0423
0-1	0.0307	0.0259	0.0293	0.0162	0.0243	0.0229	0.0384	0.0259	0.0428

Table 6.4 The Interstory Drifts (Approximation, Nonstationary)

STORY	STORY DRIFTS (UNCOUPLED)		STORY DRIFTS (COUPLED)						
	σ_x	σ_y	σ_x	$r\sigma_\theta$	σ_y	σ_E	σ_W	σ_N	σ_S
7-8	0.0457	0.0359	0.0436	0.0241	0.0343	0.0318	0.0556	0.0350	0.0657
6-7	0.0391	0.0322	0.0375	0.0203	0.0307	0.0279	0.0484	0.0318	0.0552
5-6	0.0364	0.0300	0.0350	0.0188	0.0286	0.0260	0.0450	0.0299	0.0511
4-5	0.0352	0.0290	0.0338	0.0183	0.0276	0.0253	0.0435	0.0289	0.0495
3-4	0.0348	0.0288	0.0334	0.0182	0.0275	0.0252	0.0432	0.0286	0.0490
2-3	0.0351	0.0291	0.0336	0.0183	0.0277	0.0254	0.0436	0.0289	0.0493
1-2	0.0356	0.0295	0.0341	0.0185	0.0281	0.0256	0.0441	0.0293	0.0500
0-1	0.0360	0.0297	0.0346	0.0187	0.0283	0.0258	0.0445	0.0296	0.0506

Table 6.3 The Interstory Drifts (Approximation, Stationary)

FIGURES

	STORY DRIFTS (UNCOUPLED)		STORY DRIFTS (COUPLED)						
	$(\sigma_x)_{max}$	$(\sigma_y)_{max}$	$(\sigma_x)_{max}$	$(r\sigma_\theta)_{max}$	$(\sigma_y)_{max}$	$(\sigma_E)_{max}$	$(\sigma_W)_{max}$	$(\sigma_N)_{max}$	$(\sigma_S)_{max}$
STATIONARY (1)	0.0347	0.0288	0.0332	0.0181	0.0274	0.0251	0.0431	0.0286	0.0487
NONSTATIONARY (2)	0.0294	0.0251	0.0280	0.0157	0.0235	0.0222	0.0371	0.0250	0.0410
(2)/(1) (%)	84.7	86.8	84.3	86.7	85.4	88.0	86.0	87.4	84.2

Table 6.5 The First Three Modes Contribution to the Interstory Drifts

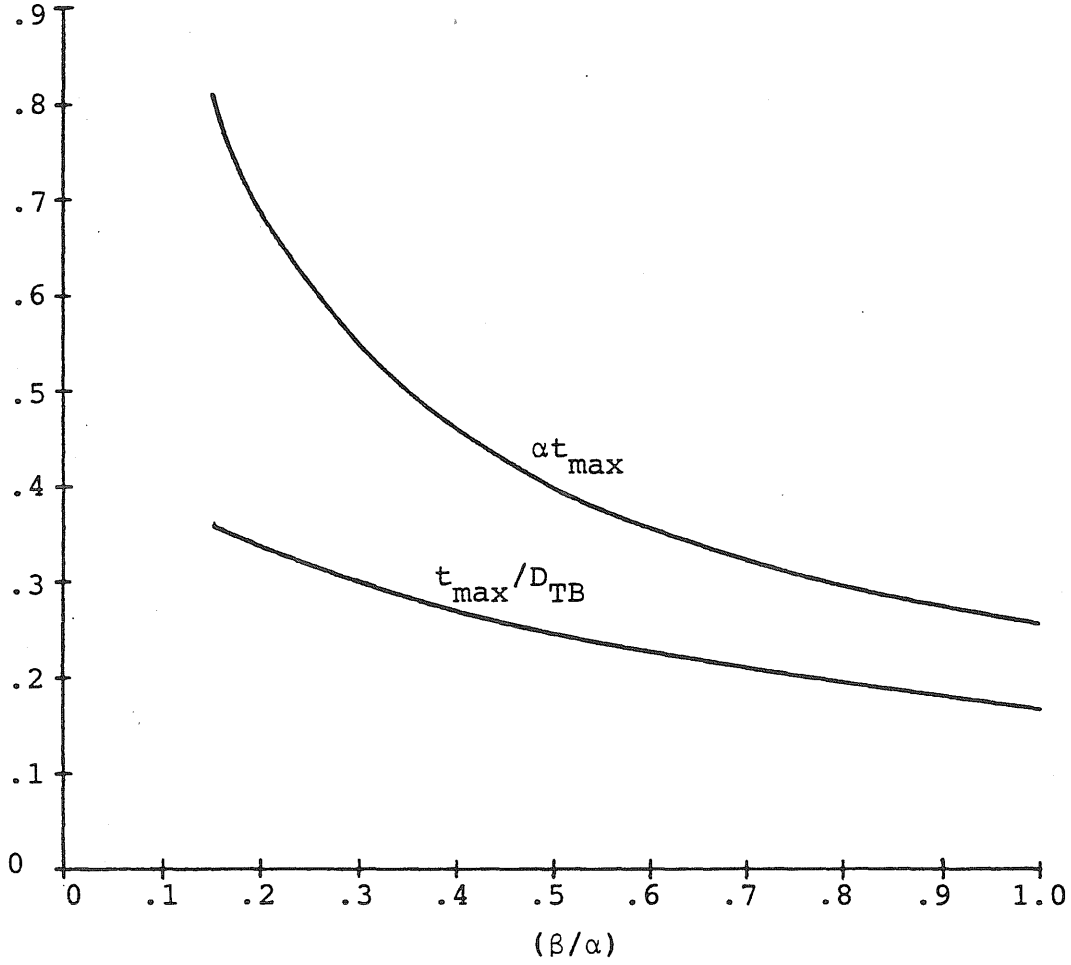

Fig. 2.2 Variation of αt_{max} and t_{max}/D_{TB} with the ratio β/α of envelope parameters

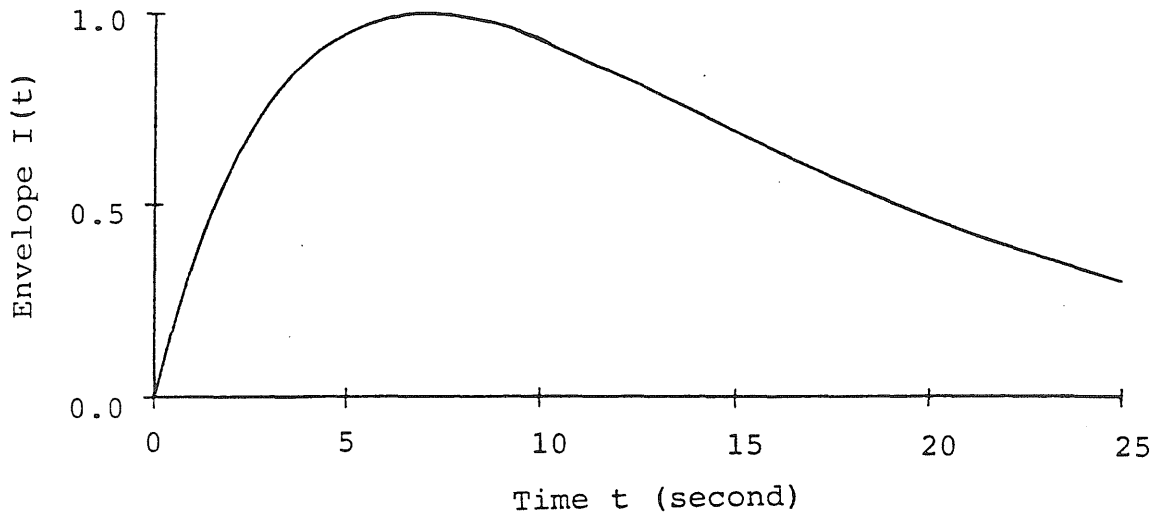

(a)

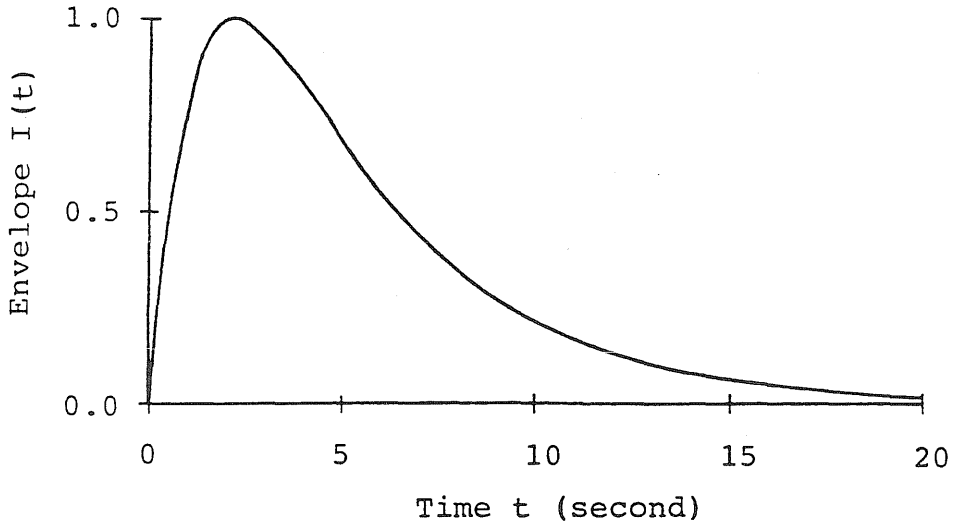

(b)

Fig. 2.1 Shinozuka and Sato Envelope Functions

(a) Long Duration (α=0.10, β=0.20)

(b) Short Duration (α=0.25, β=0.75)

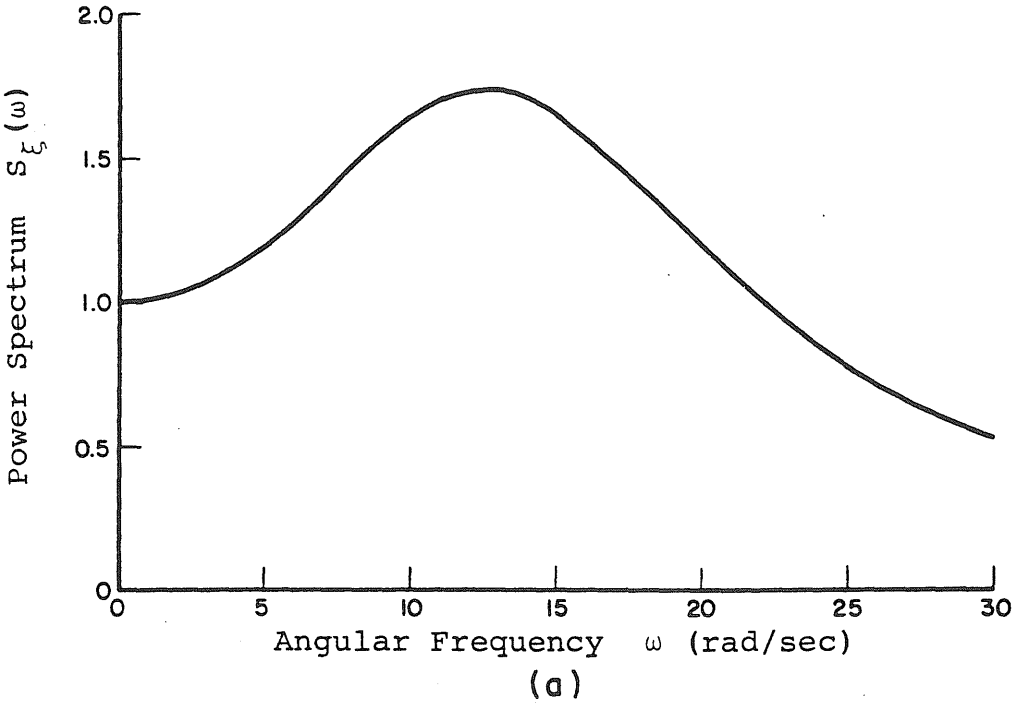

(a)

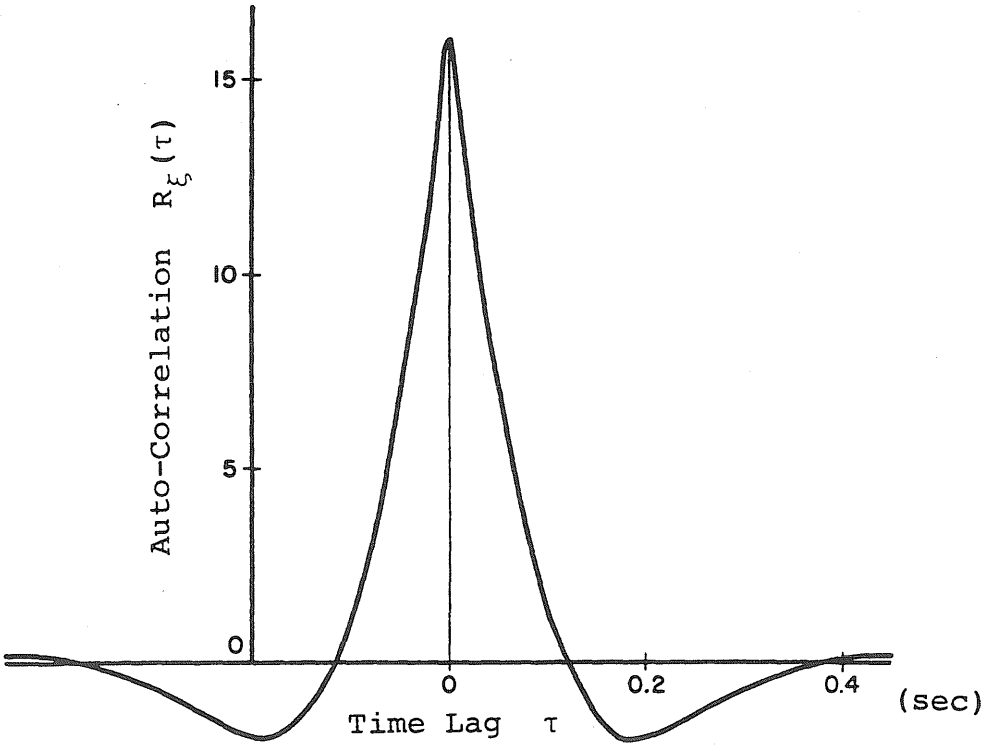

(b)

Fig. 2.4 Kanai-Tajimi Spectrum for Filter Parameters $\omega_g = 15.56$ rad/sec, $\zeta_g = 0.64$

(a) Spectrum (b) Autocorrelation

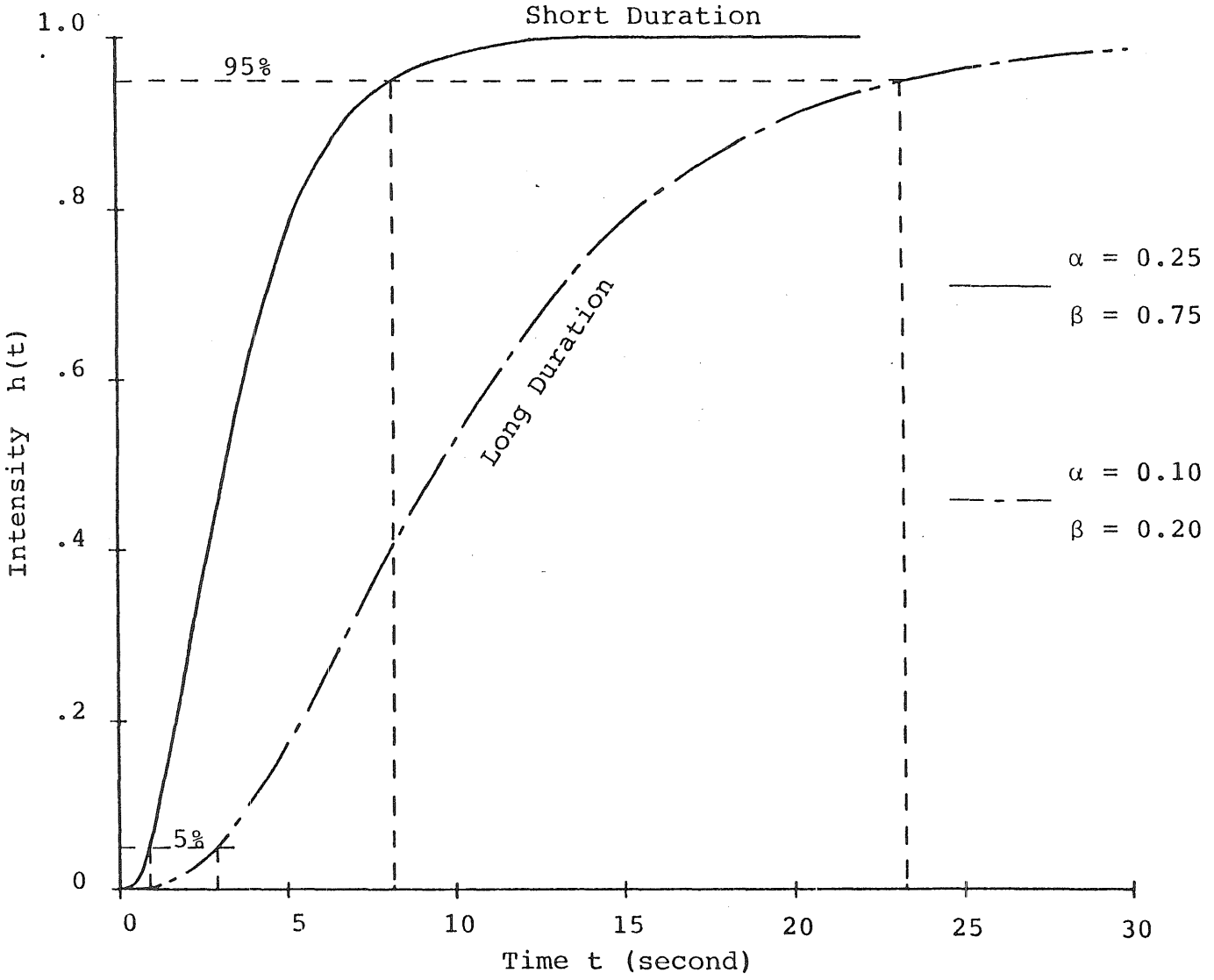

Fig. 2.3 Husid Plots for Two Envelopes

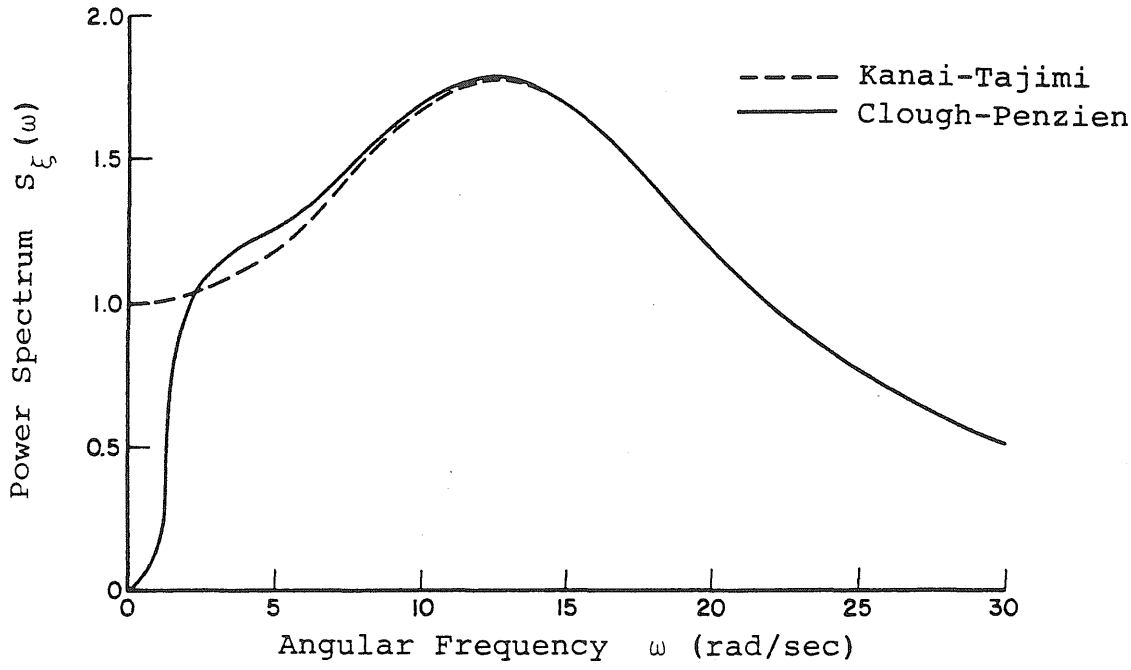

(a)

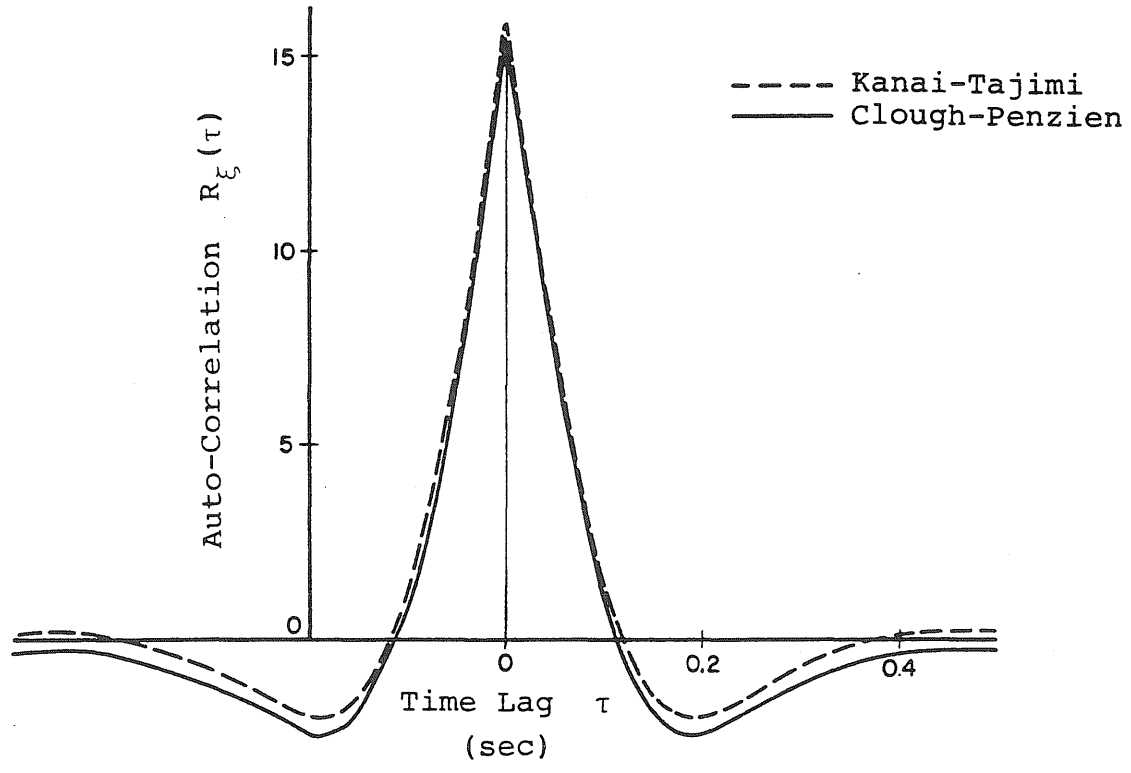

(b)

Fig. 2.6 Clough-Penzien and Kanai-Tajimi Spectra for Filter Parameters ω_g=15.46 rad/sec, ζ_g=0.623, ω_f=1.636 rad/sec, ζ_f=0.619
(a) Spectra (b) Autocorrelation

Strong Motion Earthquake Records Used for Determination of Clough-Penzien Filter Parameters

Location and Date	Components	S.I.* (ft)
El Centro, Calif. Dec. 12, 1934	N and W	1.9
El Centro, Calif. May 18, 1940	N and W	2.7
Olympia, Wash. April 13, 1949	N80E and N10W	1.9
Taft, Calif. June 21, 1952	N69W and S21W	1.6

* S.I. : Spectrum Intensity

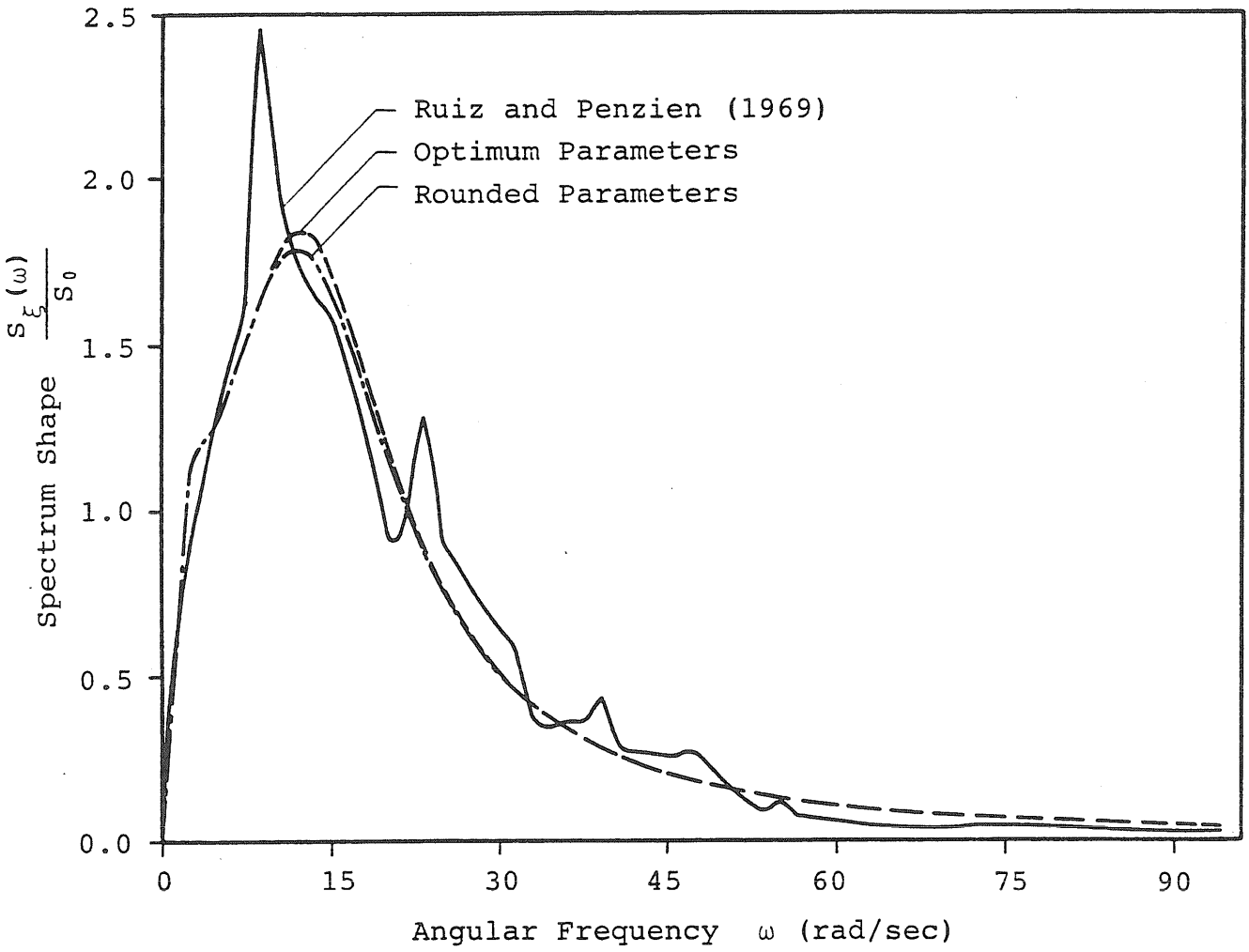

Fig. 2.5 Power Spectrum from Analysis of Strong Motion Earthquakes

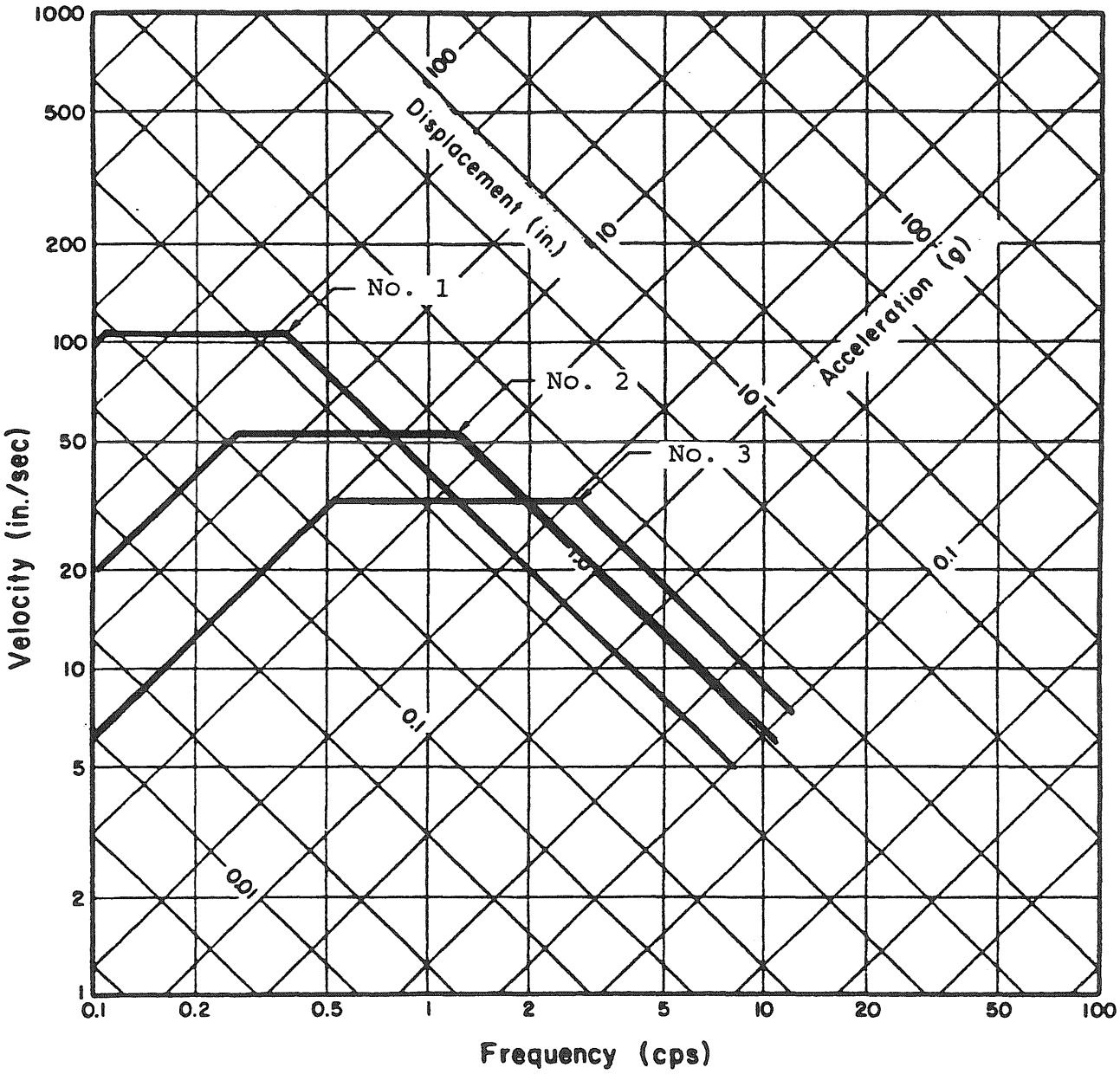

Fig. 2.8 R.M.S. Ground Displacements, Velocities and Accelerations (Clough-Penzien Spectra, S_0=10000 in^2/sec^3)

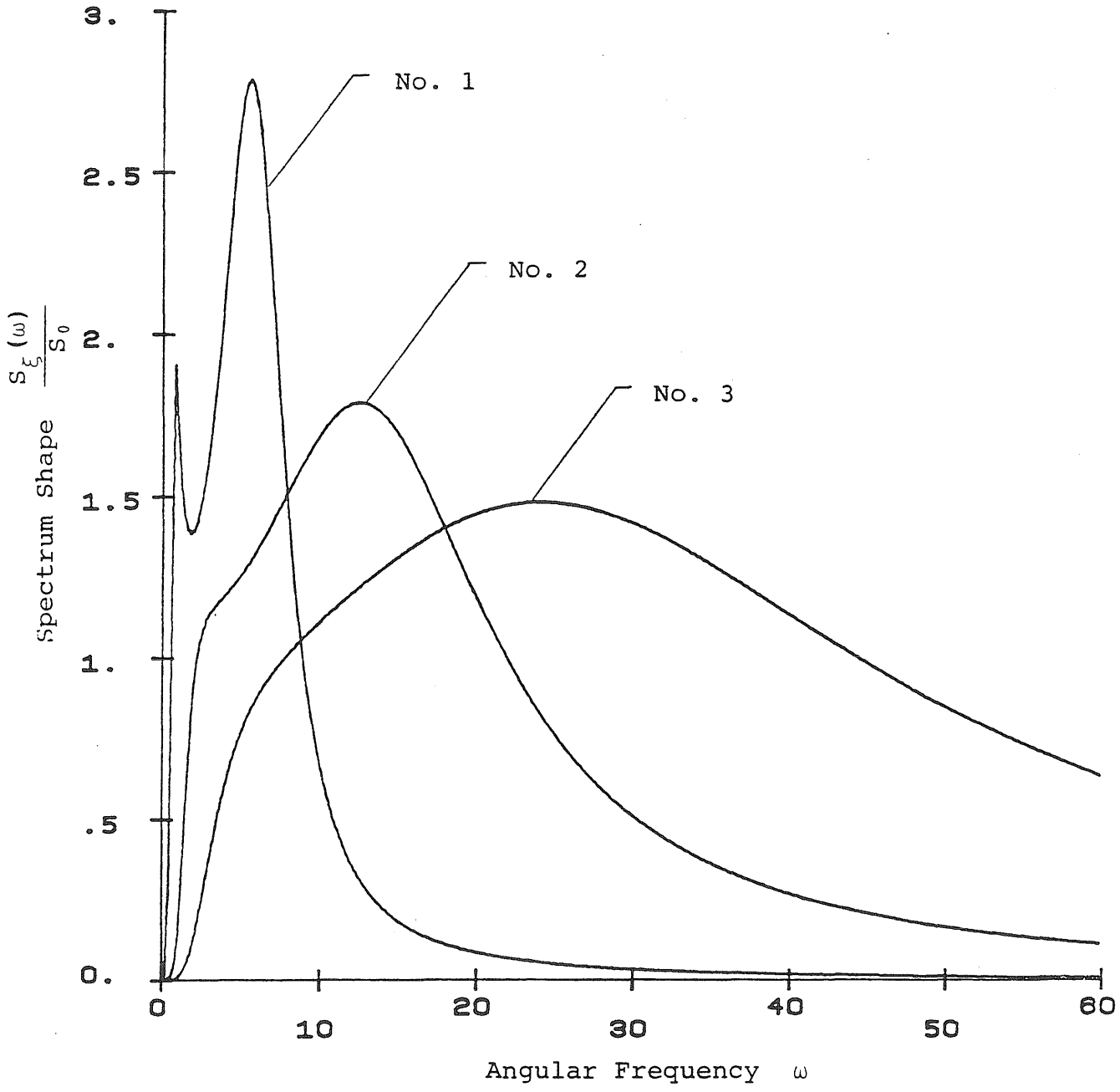

Fig. 2.7 Clough-Penzien Spectra with Different Dominant Frequencies

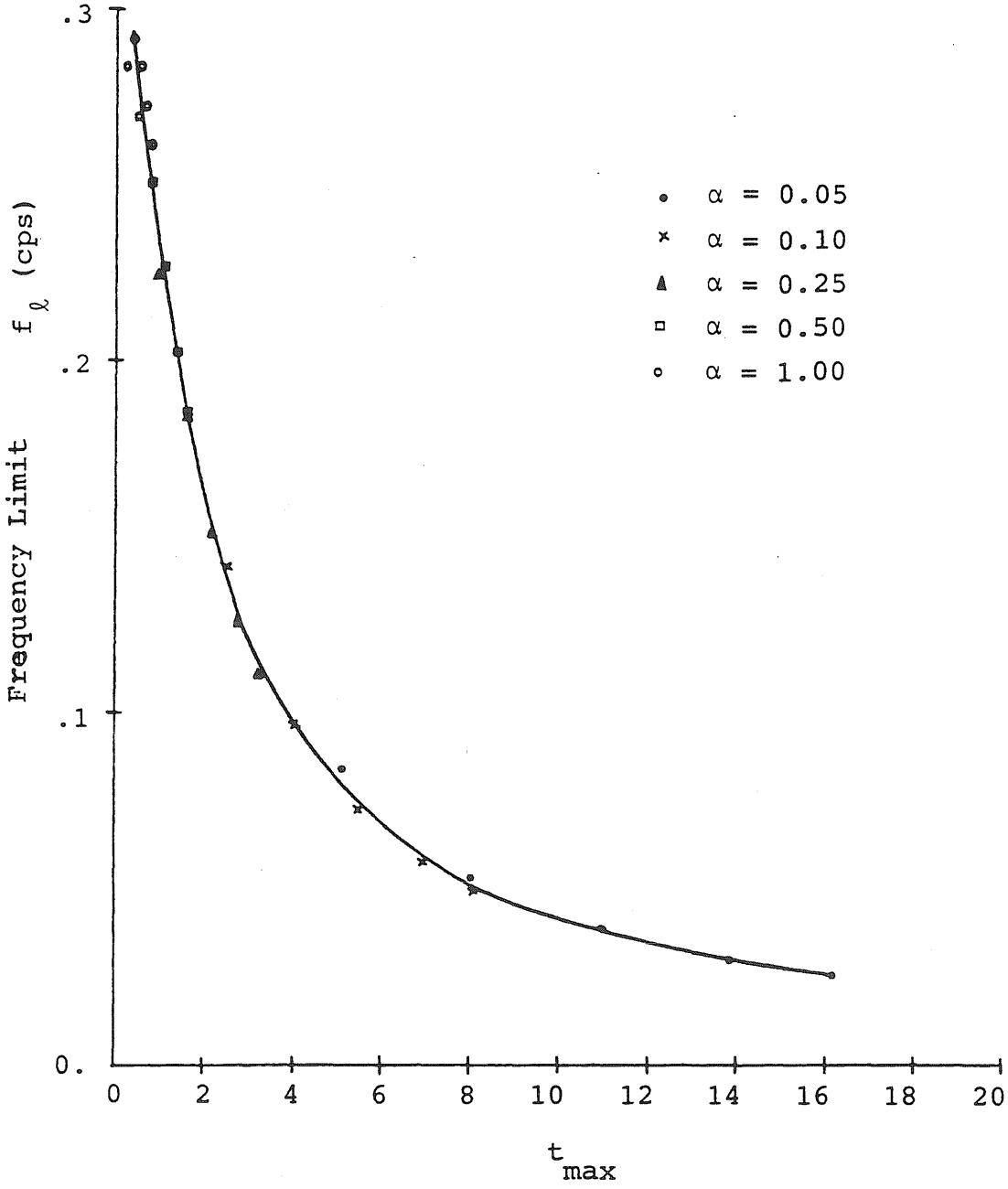

Fig. 2.10 Variation of the Low Frequency Limit f_ℓ with a Range of Values of the Envelope Parameters α and β [Table 2.1]

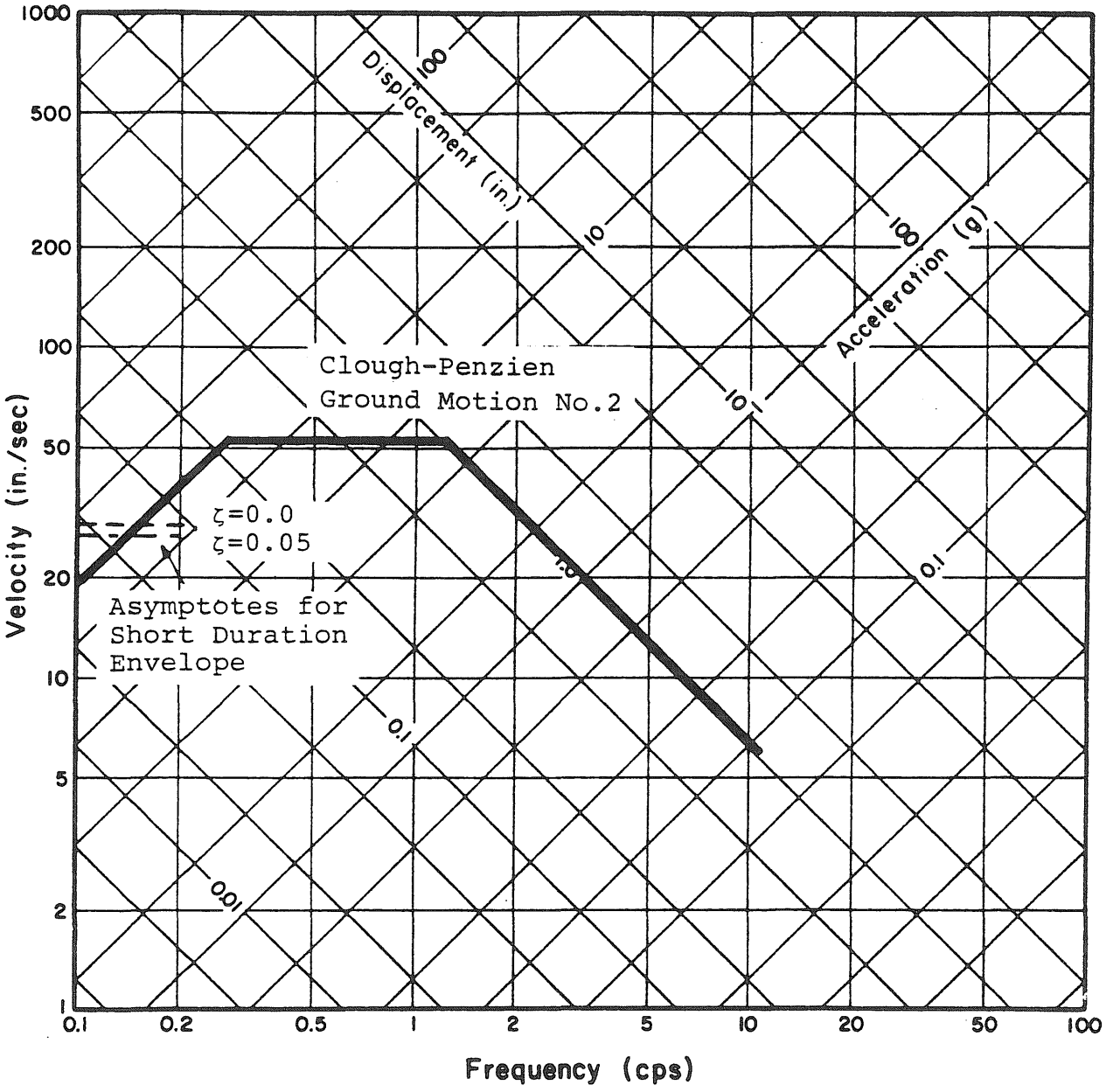

Fig. 2.9 R.M.S. Response Spectrum Asymptotes
(Clough-Penzien Ground Motion No. 2,
S_0=10000 in²/sec³, Short Duration Envelope)

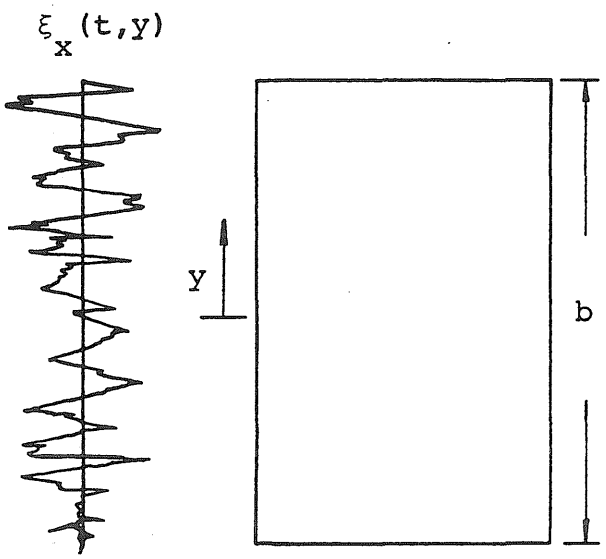

Fig. 2.13 Nonuniform Translational Base Excitation

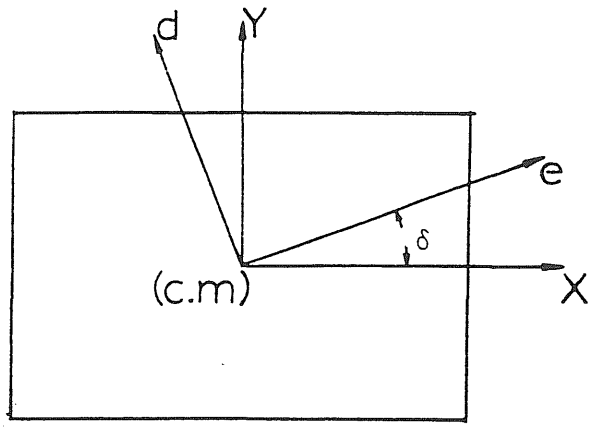

Fig. 2.11 Principal Axes of Structure and Ground Motion

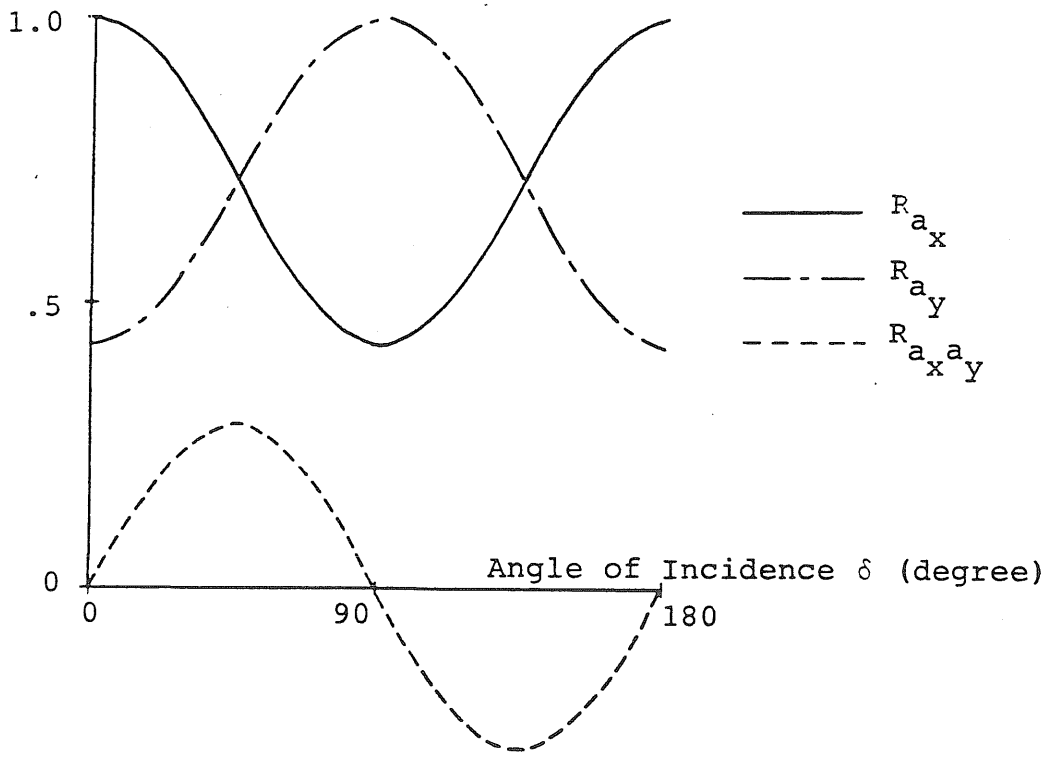

Fig. 2.12 Dependence of Ground Motion Variances in Structural Principal Axis Coordinate System on Angle of Incidence of Ground Motion (Principal Variances = 1, 0.4225)

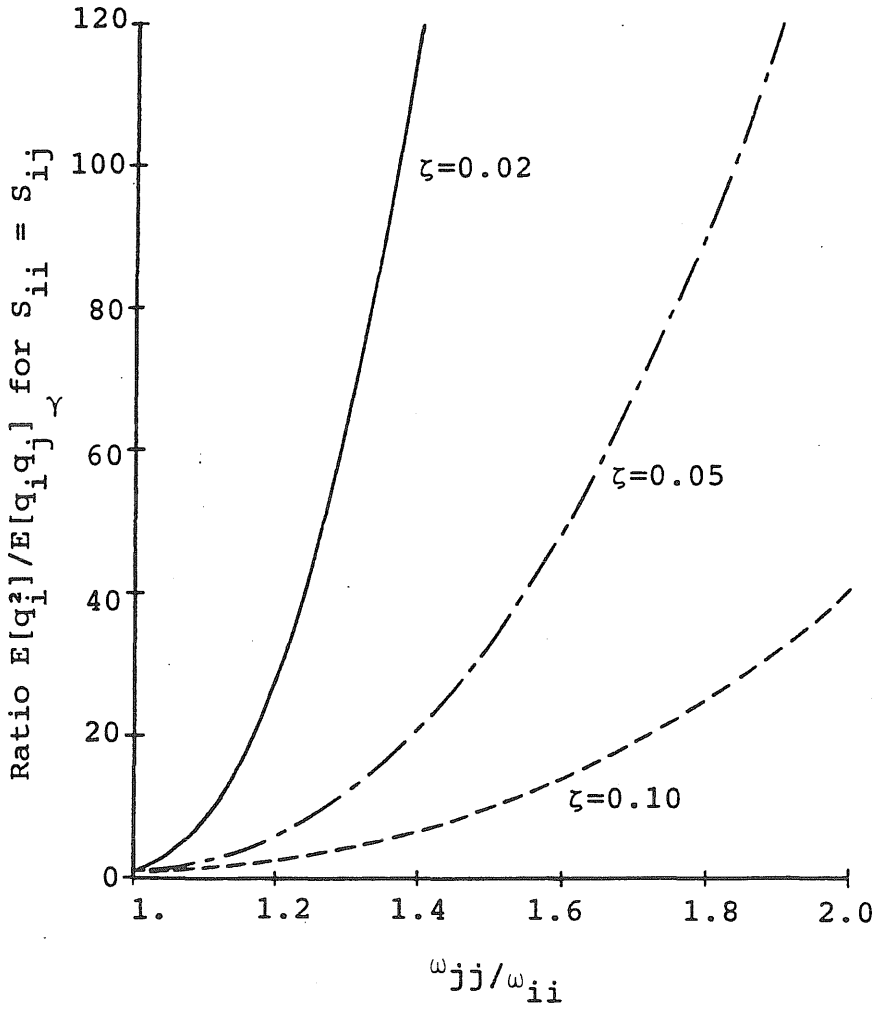

Ratio of Frequencies for two modes i, j

Fig. 3.1 Effect of Frequency Spacing on the Significance of Cross-Response

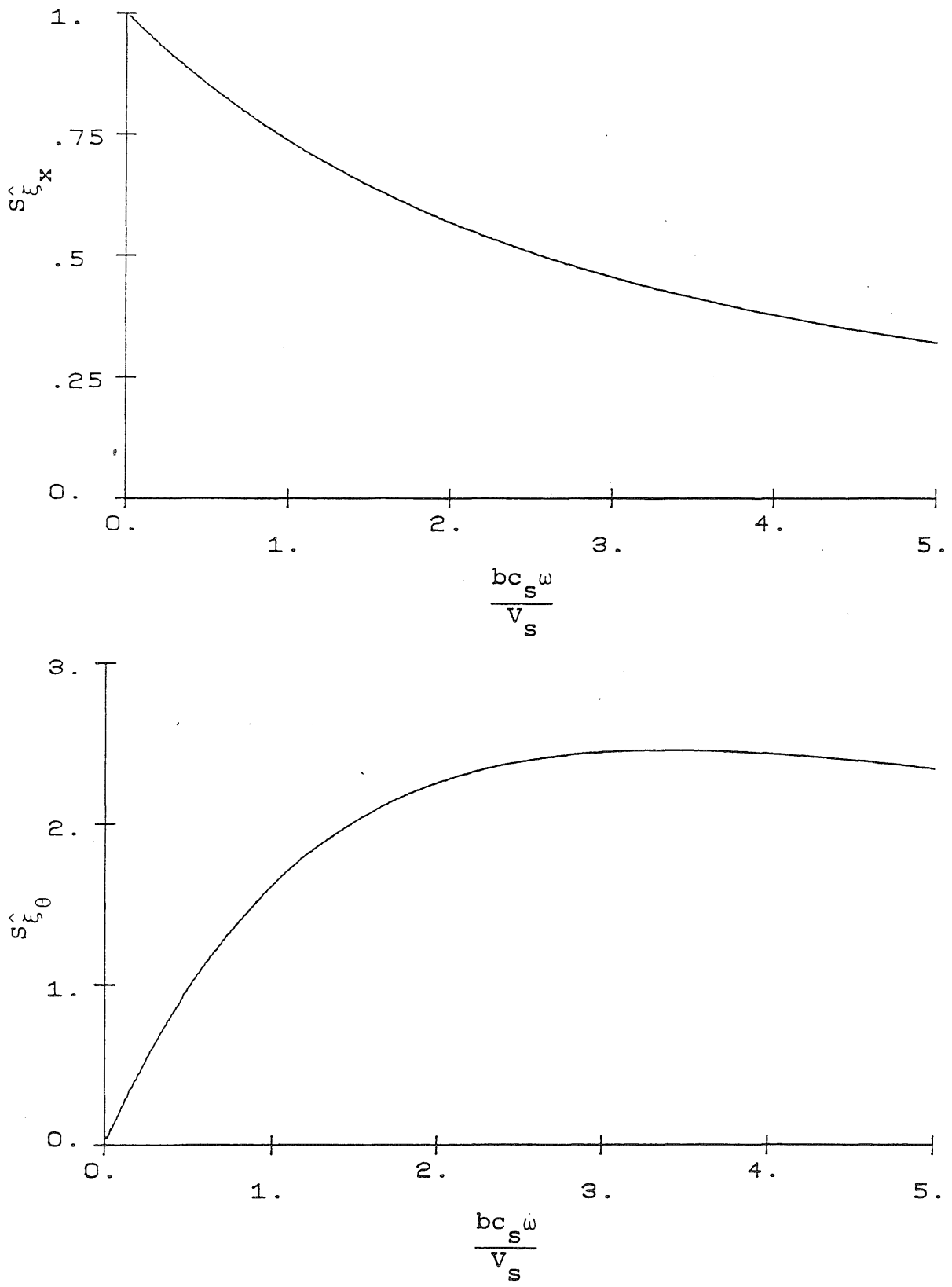

Fig. 2.14 Spectra of Effective Translational and Rotational Ground Motion with Partial Spatial Correlation

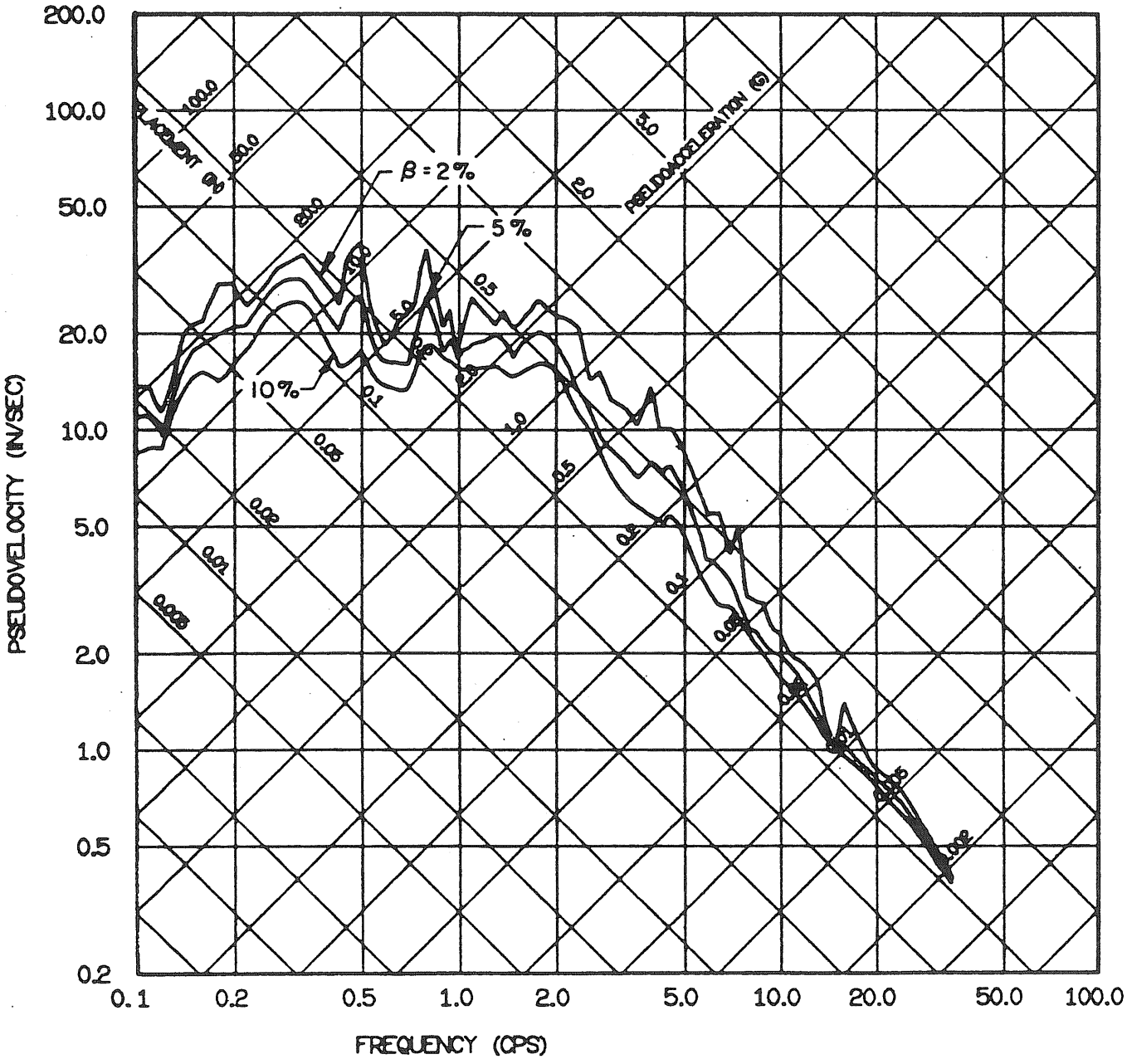

Fig. 4.1 Elastic Response Spectra for El Centro, May 18, 1940. E-W Component.

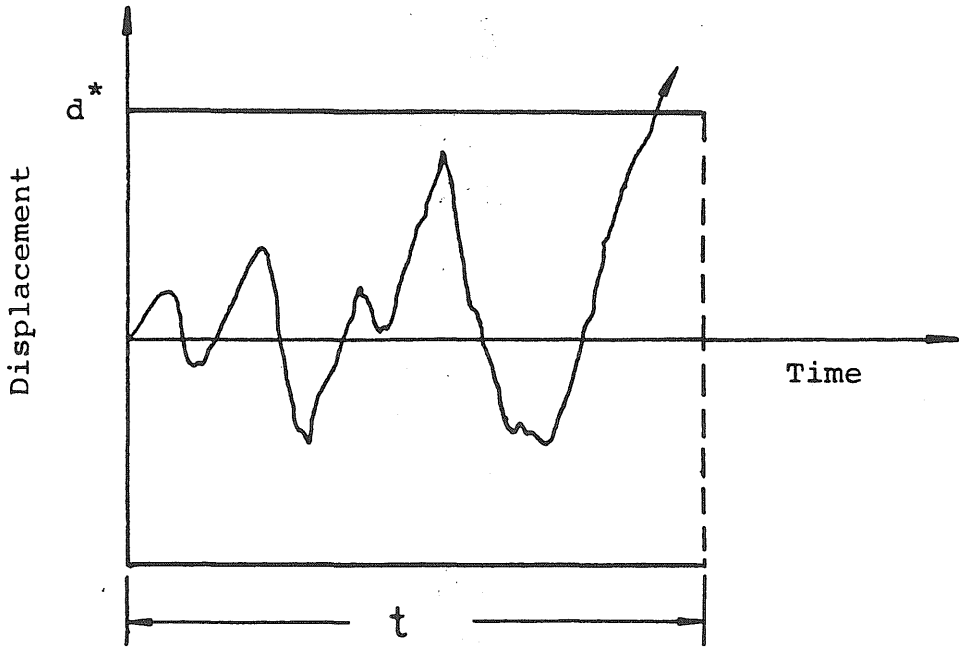

Fig. 3.2 First-Passage Problem

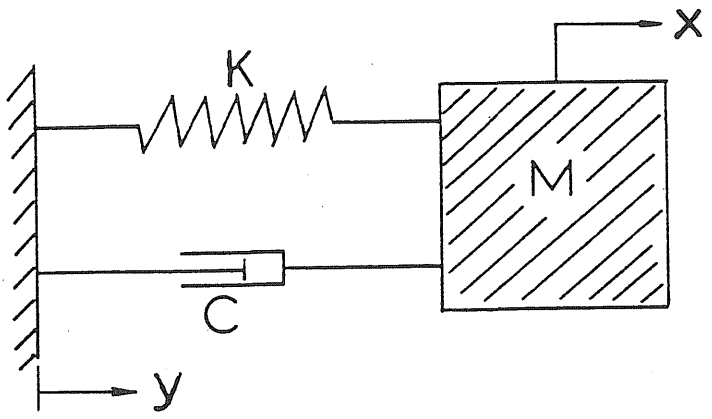

$$u = x - y$$

$$a = \ddot{y} = \frac{d^2y}{dt^2}$$

$$K = \omega_o^2 M$$

$$C = 2\zeta\omega_o M$$

Fig. 4.3 Single Degree of Freedom Elastic Oscillator

SPECTRUM AMPLIFICATION FACTORS FOR HORIZONTAL ELASTIC RESPONSE

Damping, % Critical	One Sigma (84.1%)			Median (50%)		
	A	V	D	A	V	D
0.5	5.10	3.84	3.04	3.68	2.59	2.01
1	4.38	3.38	2.73	3.21	2.31	1.82
2	3.66	2.92	2.42	2.74	2.03	1.63
3	3.24	2.64	2.24	2.46	1.86	1.52
5	2.71	2.30	2.01	2.12	1.65	1.39
7	2.36	2.08	1.85	1.89	1.51	1.29
10	1.99	1.84	1.69	1.64	1.37	1.20
20	1.26	1.37	1.38	1.17	1.08	1.01

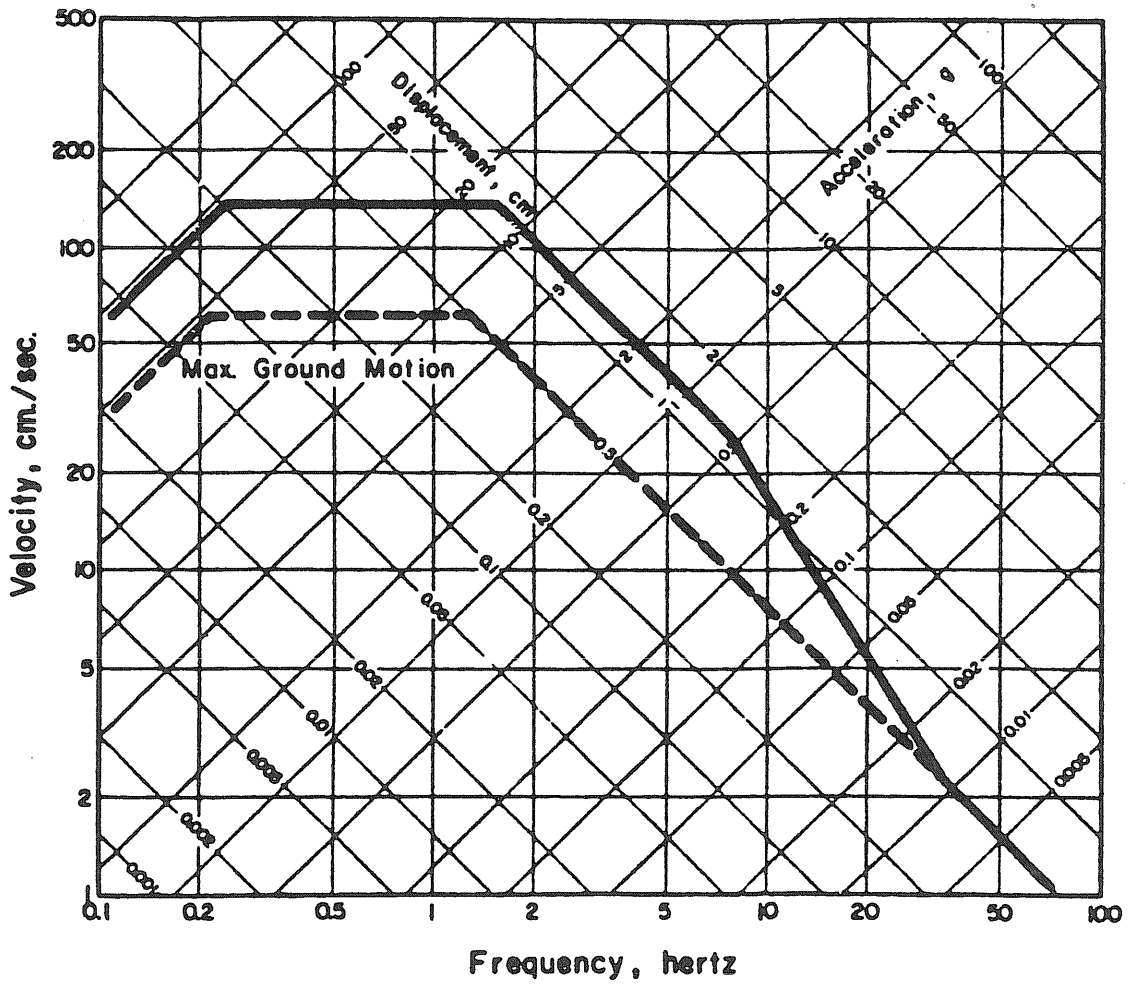

Fig. 4.2 Smoothed Earthquake Design Spectrum (0.5g Max. Accel., 5% Damping, 84.1% Cumulative Probability) (after Newmark and Hall, [61])

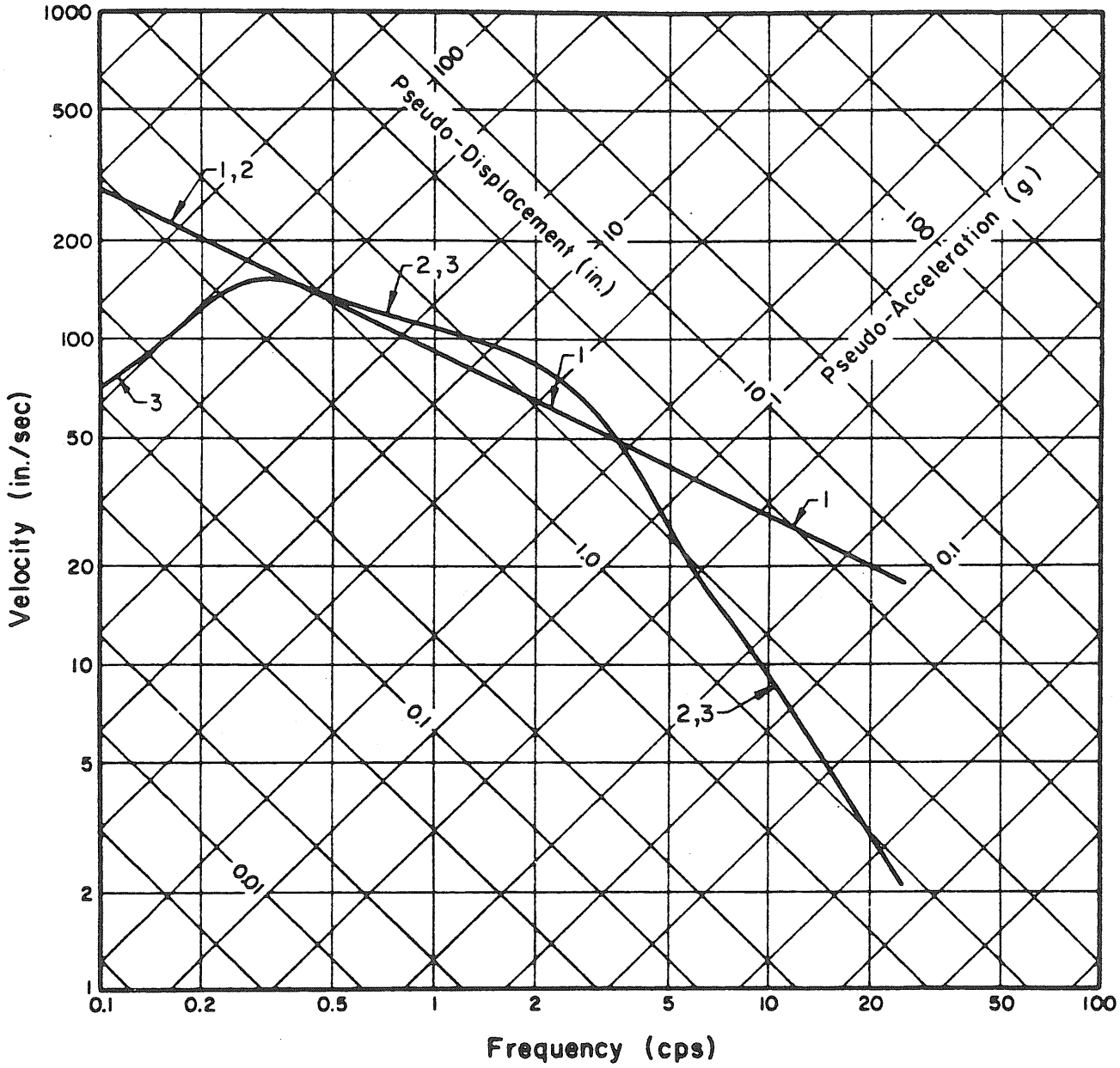

Legend:

Input Spectrum Shape		
White	Kanai-Tajimi	Clough-Penzien
1	2	3

Fig. 4.5 Effect of Ground Motion Frequency Content on Stationary Velocity Response

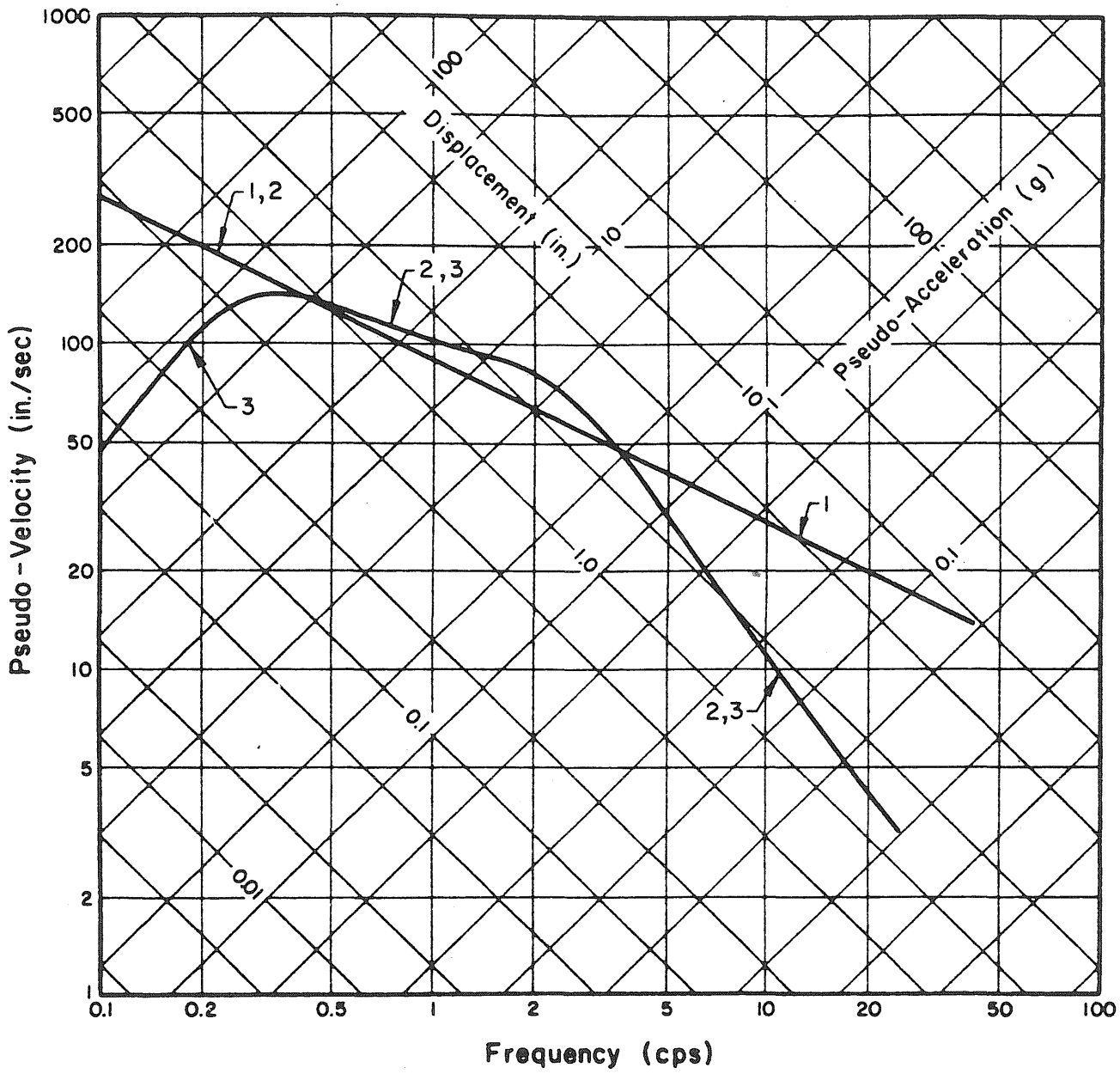

Legend:

Input Spectrum Shape		
White	Kanai-Tajimi	Clough-Penzien
1	2	3

Fig. 4.4 Effect of Ground Motion Frequency Content on Stationary Displacement Response

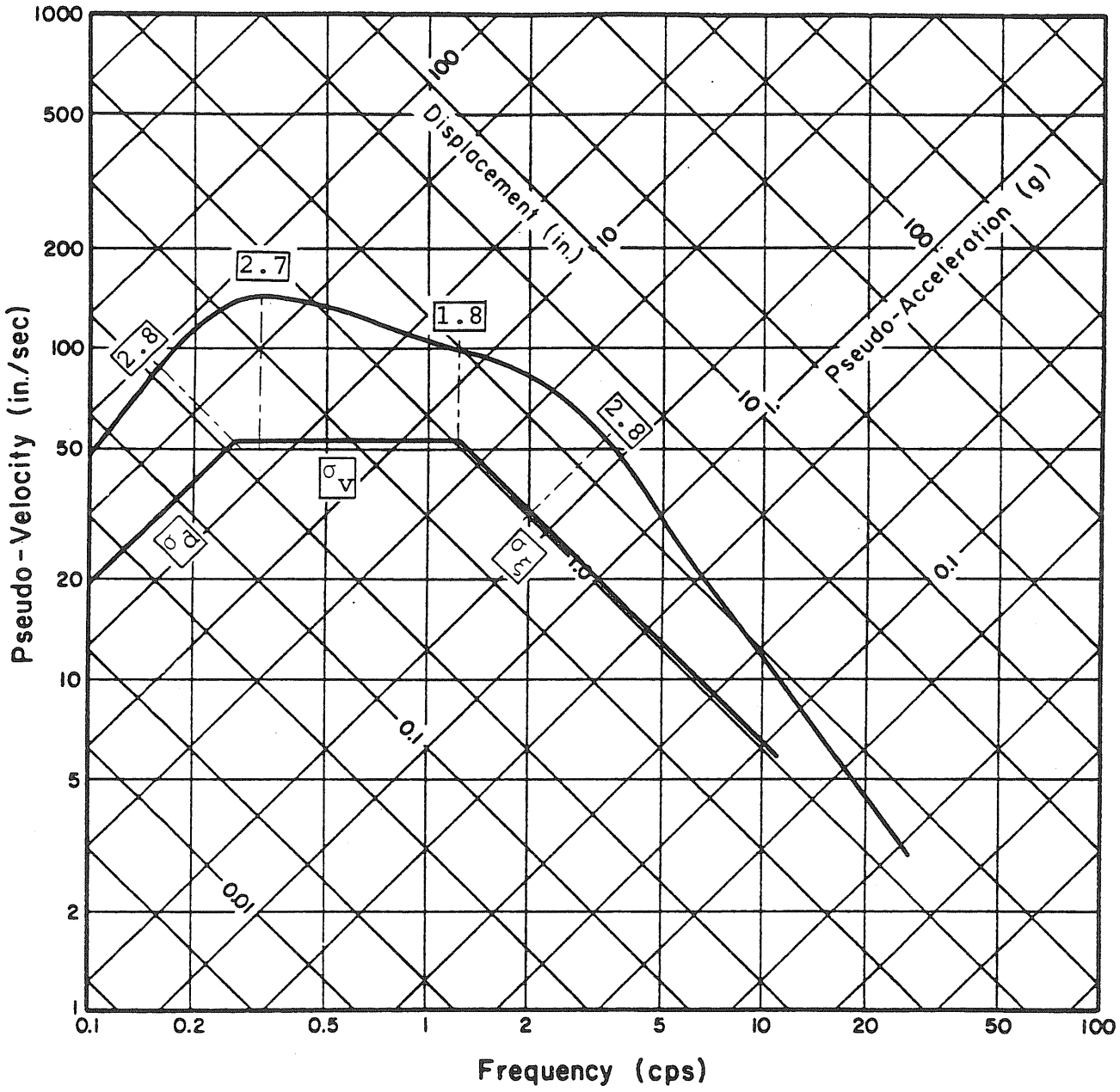

Fig. 4.7 Effect of Dominant Ground Motion Frequency on Stationary R.M.S. Displacement Response - Input: Clough-Penzien Spectrum with ω_g = 15.46 rad/sec (Ground Motion No. 2,Fig.2.7)

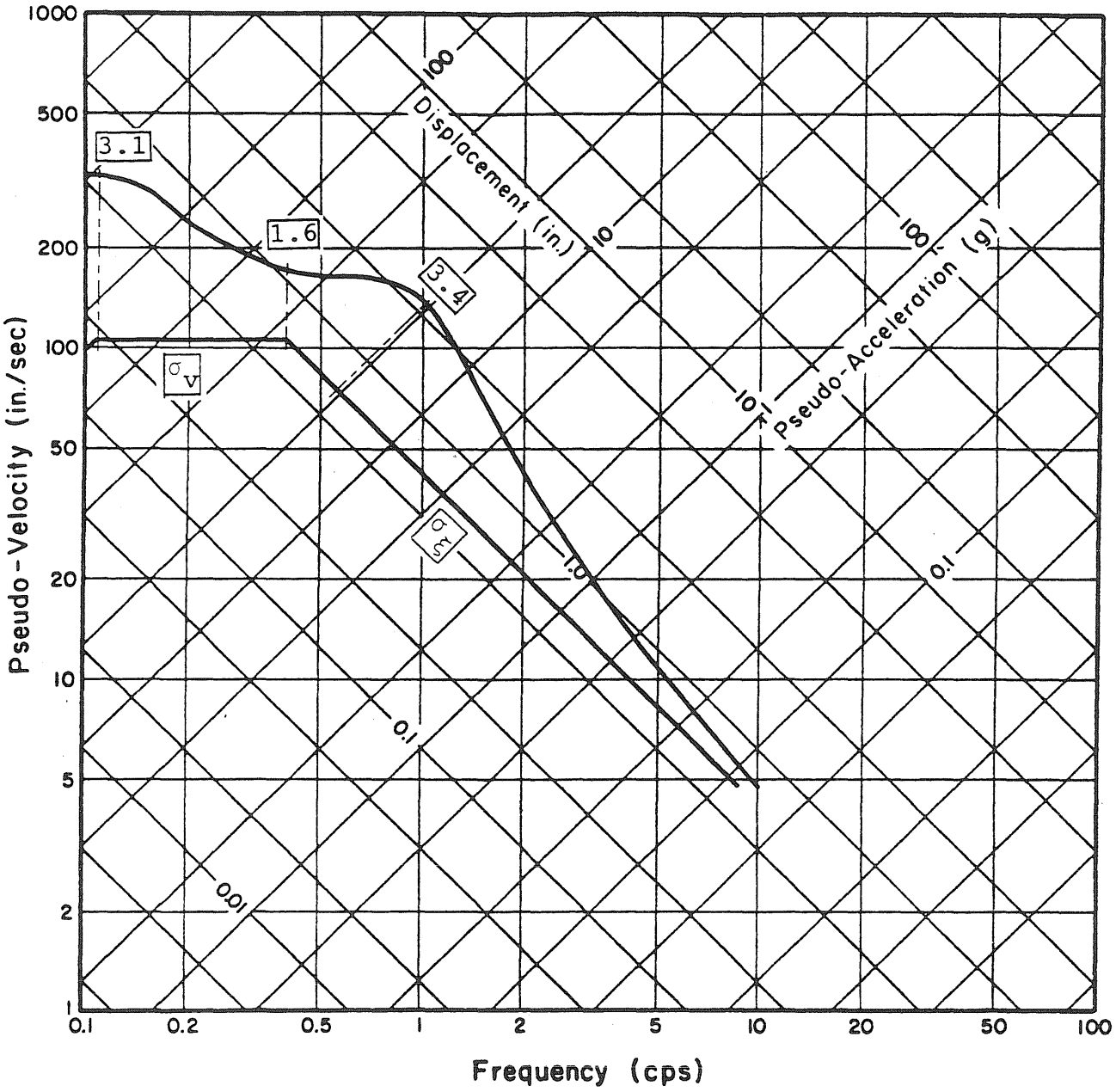

Fig. 4.6 Effect of Dominant Ground Motion Frequency on Stationary R.M.S. Displacement Response - Input: Clough-Penzien Spectrum with ω_g = 2π rad/sec (Ground Motion No. 1, Fig. 2.7)

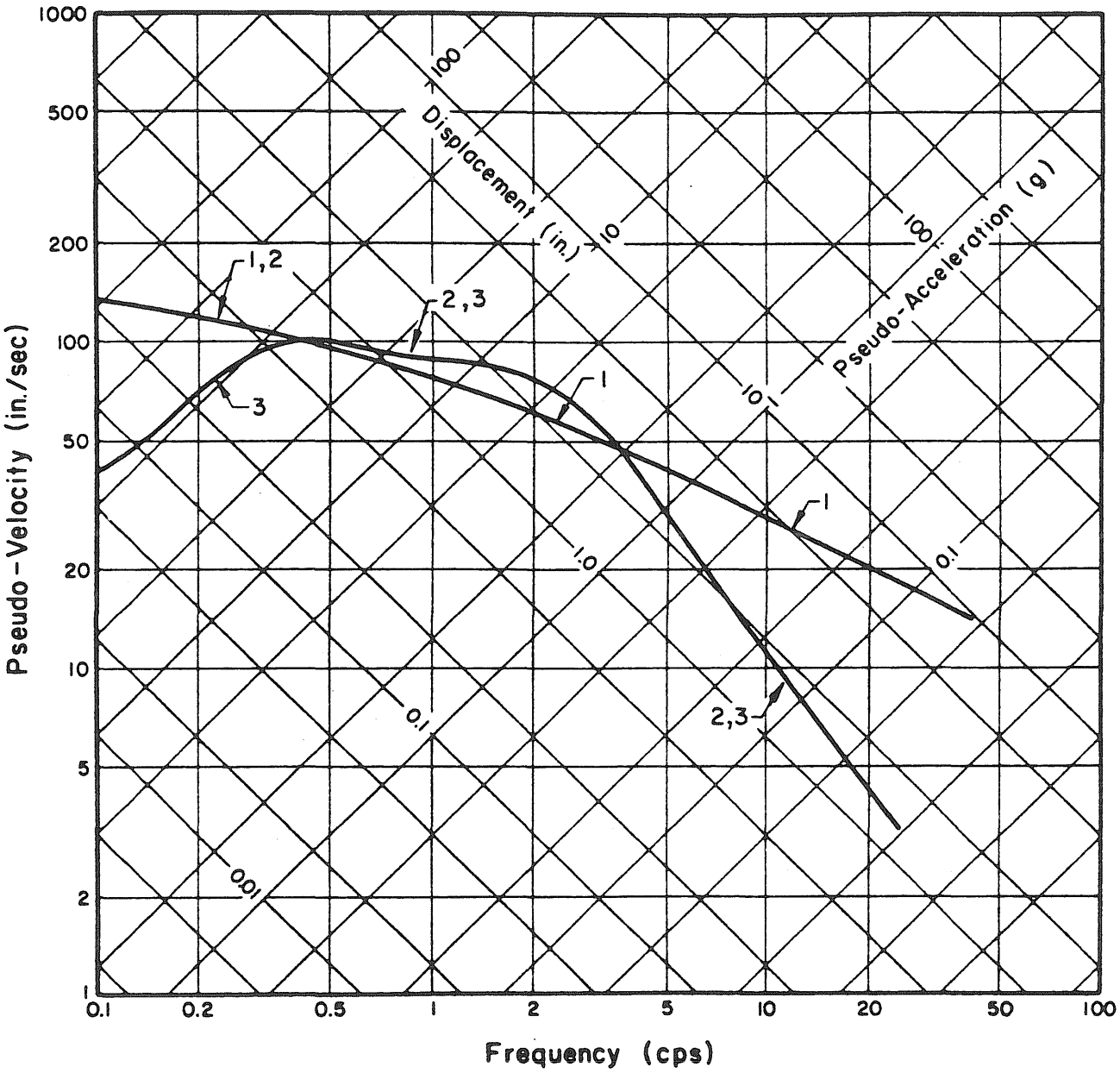

Legend:

Input Spectrum Shape		
White	Kanai-Tajimi	Clough-Penzien
1	2	3

Fig. 4.9 Effect of Ground Motion Frequency Content and Duration on Nonstationary Displacement Response ("Short Duration" Ground Motion, Trifunac-Brady Duration = 7.2 sec)

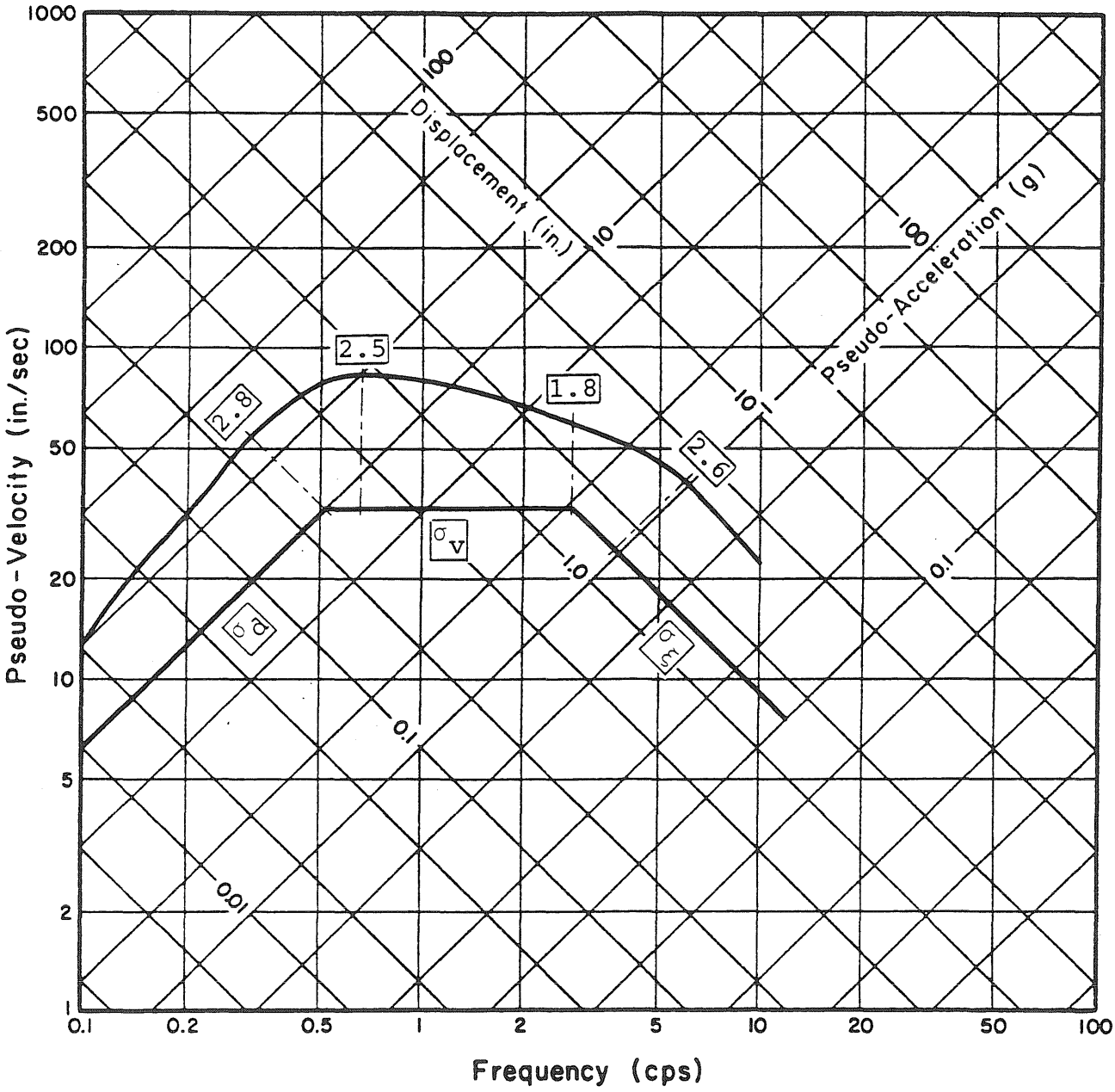

Fig. 4.8 Effect of Dominant Ground Motion Frequency on Stationary R.M.S. Displacement Response - Input: Clough-Penzien Spectrum with ω_g = 10π rad/sec (Ground Motion No. 3, Fig. 2.7)

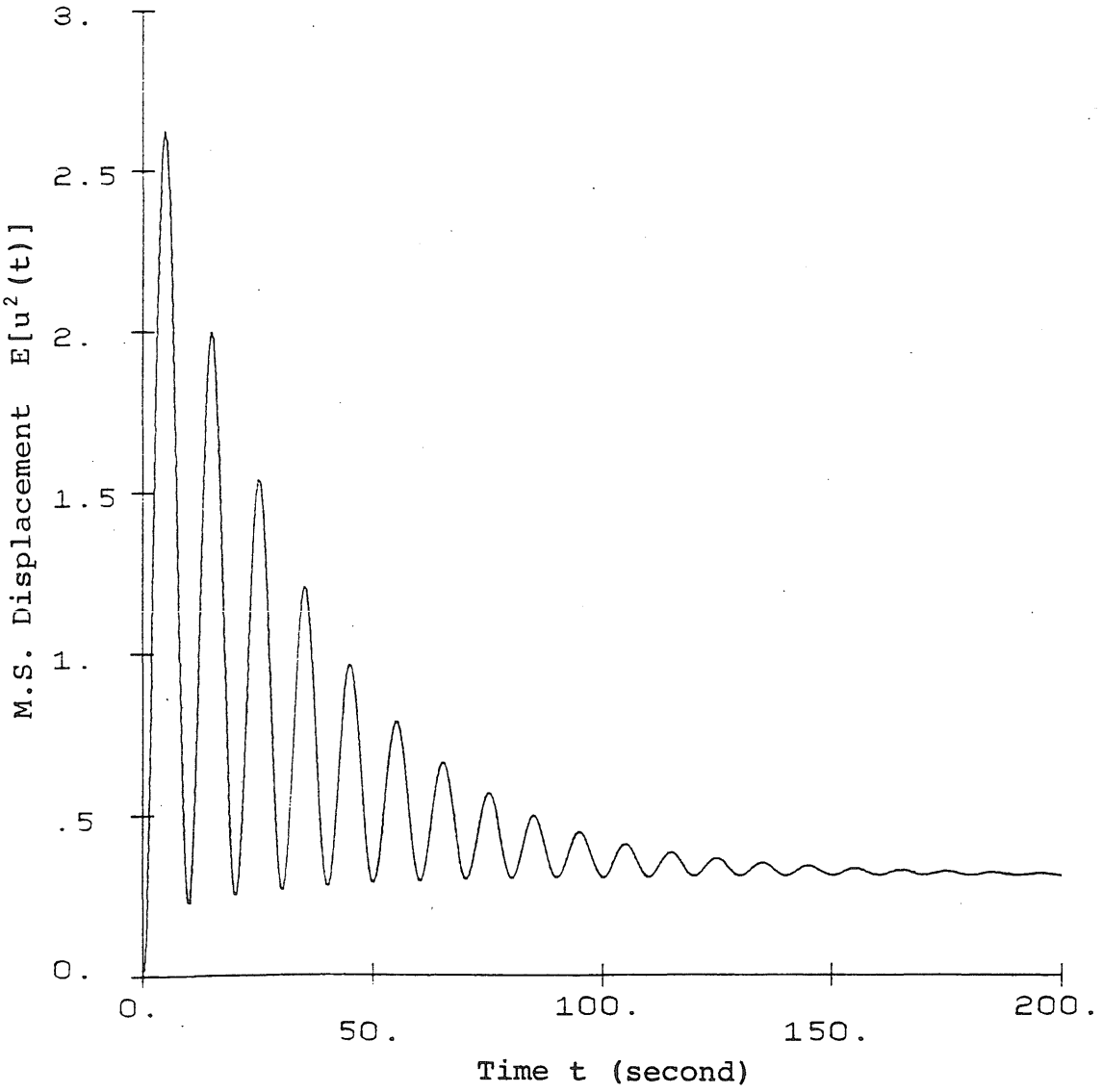

Fig. 4.11 M.S. Response History of a Low Frequency System (f_0 = 0.05 cps) to Stationary Clough-Penzien Spectrum Excitation

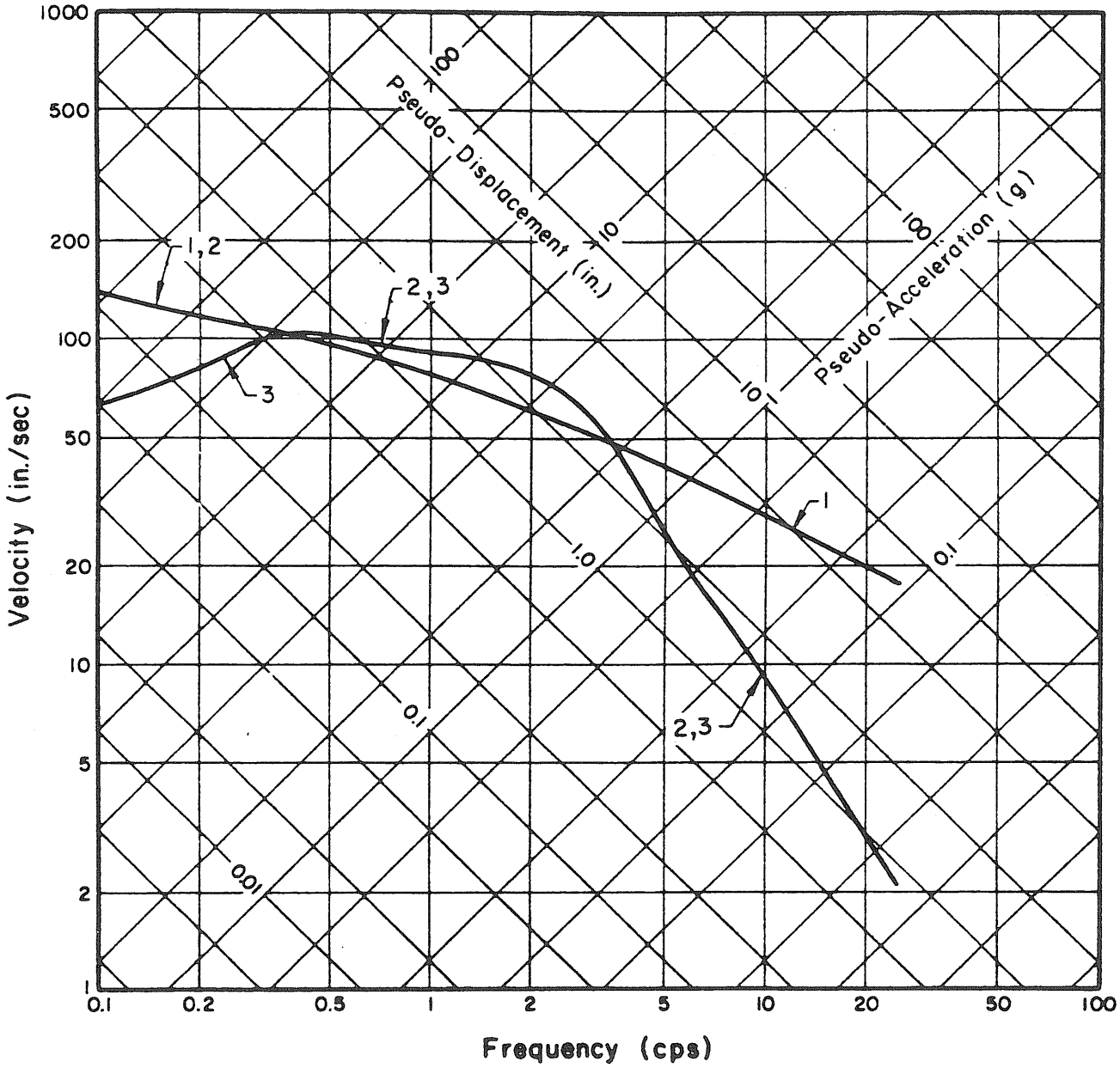

Legend:

Input Spectrum Shape		
White	Kanai-Tajimi	Clough-Penzien
1	2	3

Fig. 4.10 Effect of Ground Motion Frequency Content and Duration on Nonstationary Velocity Response ("Short Duration" Ground Motion, Trifunac-Brady Duration = 7.2 sec)

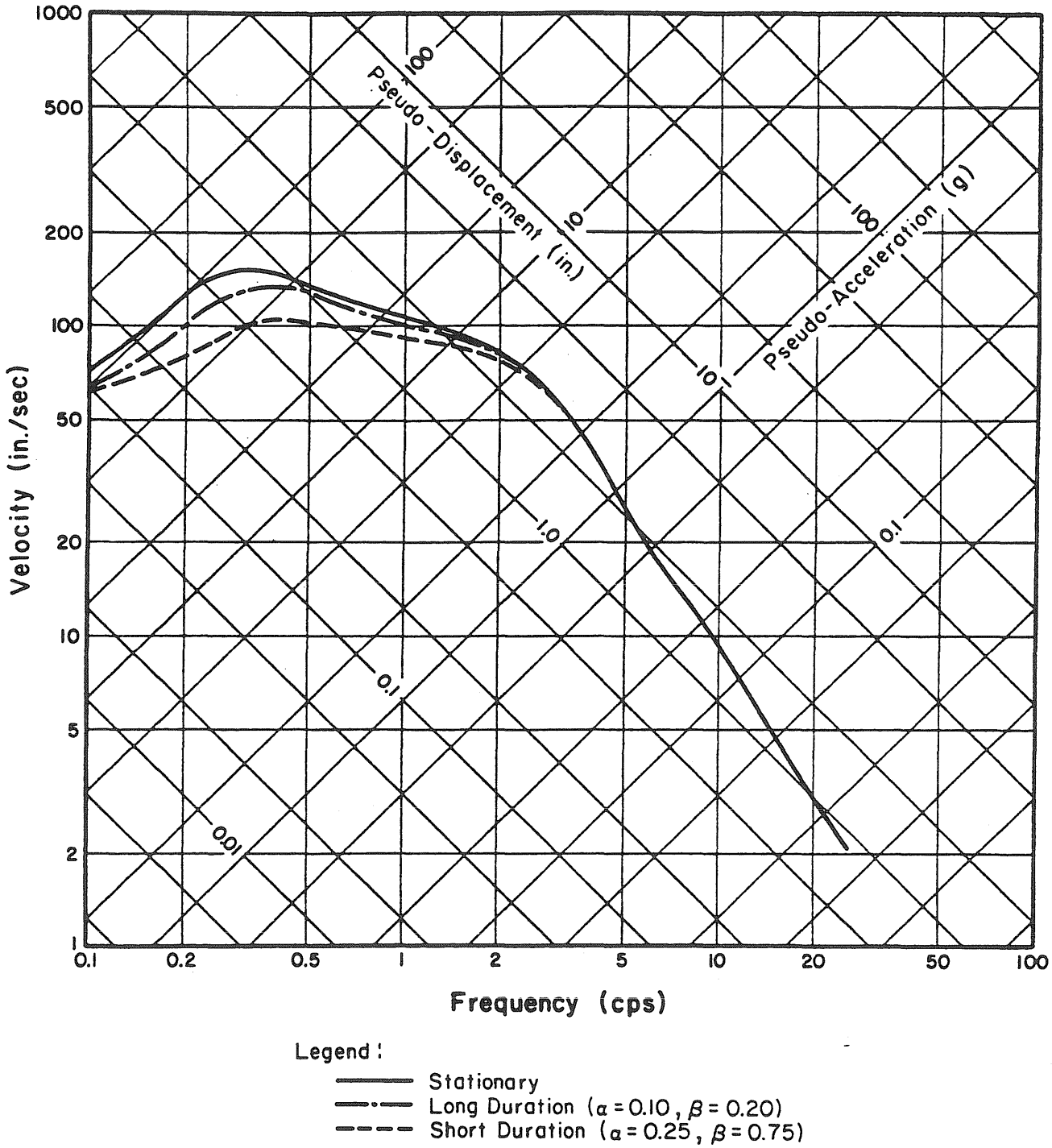

Fig. 4.13 Effect of Duration on R.M.S. Velocity Response - Clough-Penzien Spectrum Input

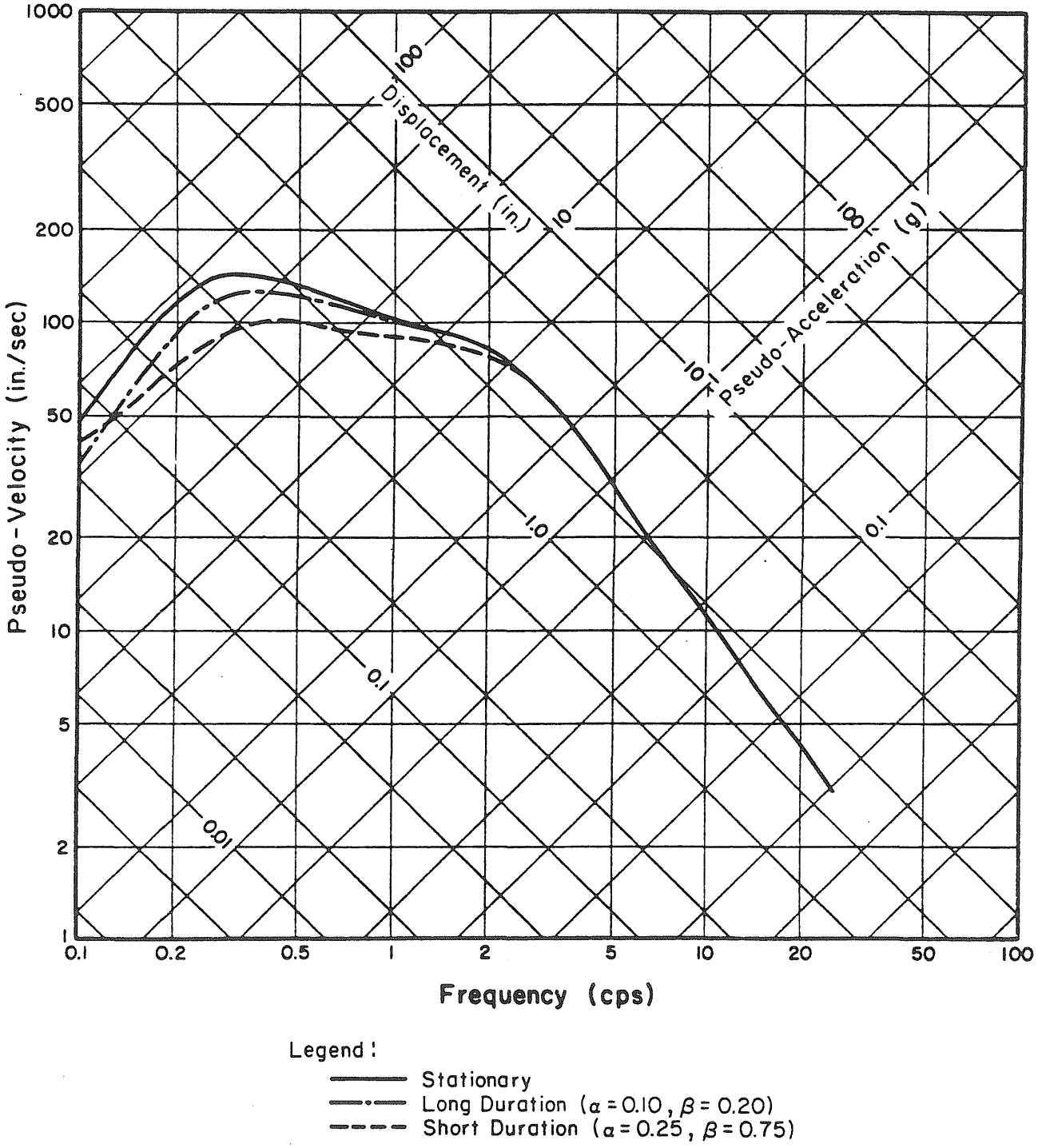

Fig. 4.12 Effect of Duration on R.M.S. Displacement Response - Clough-Penzien Spectrum Input

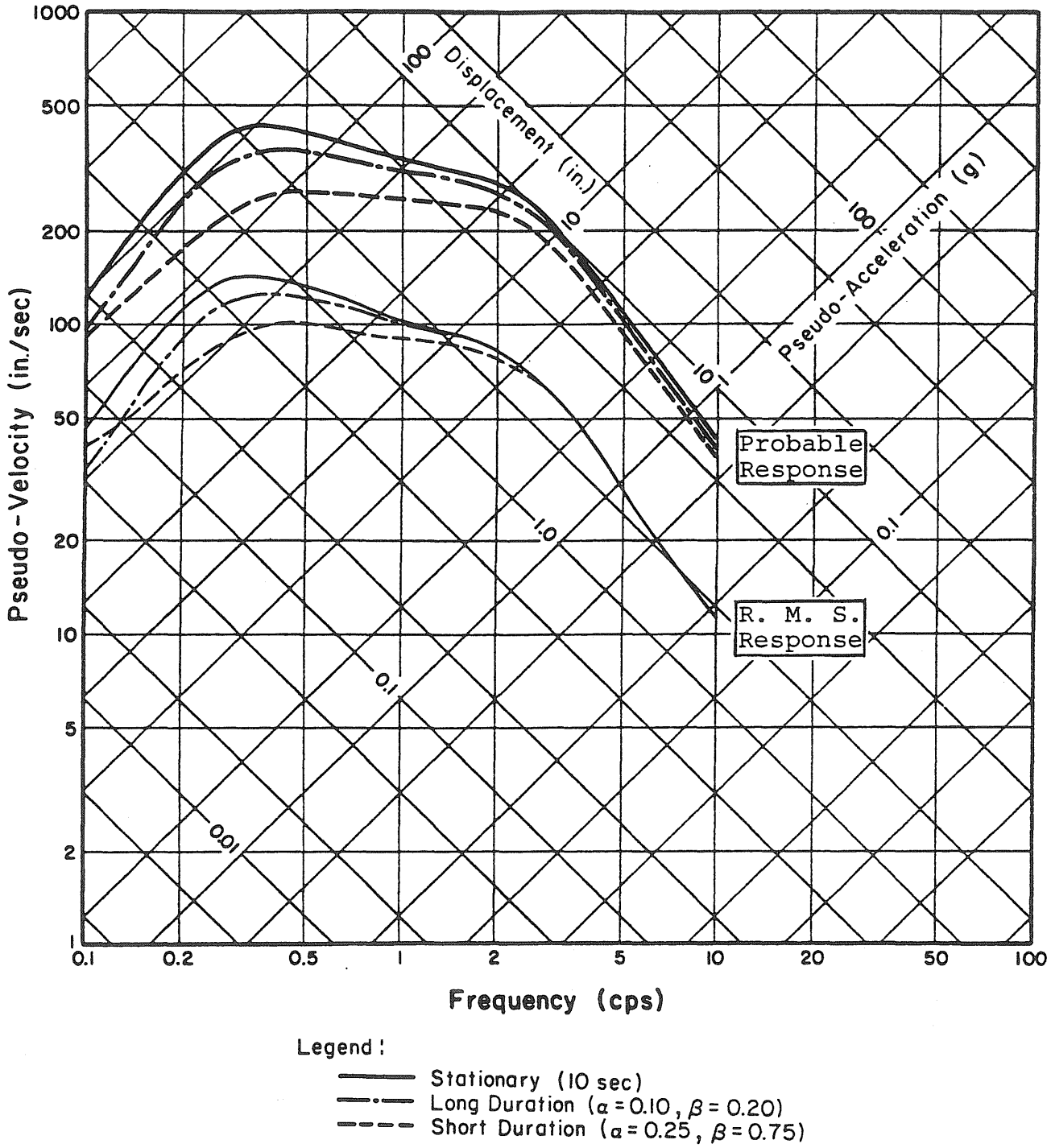

Fig. 4.15 Effect of Duration on 90% Probable Displacement Response - Clough-Penzien Spectrum Input

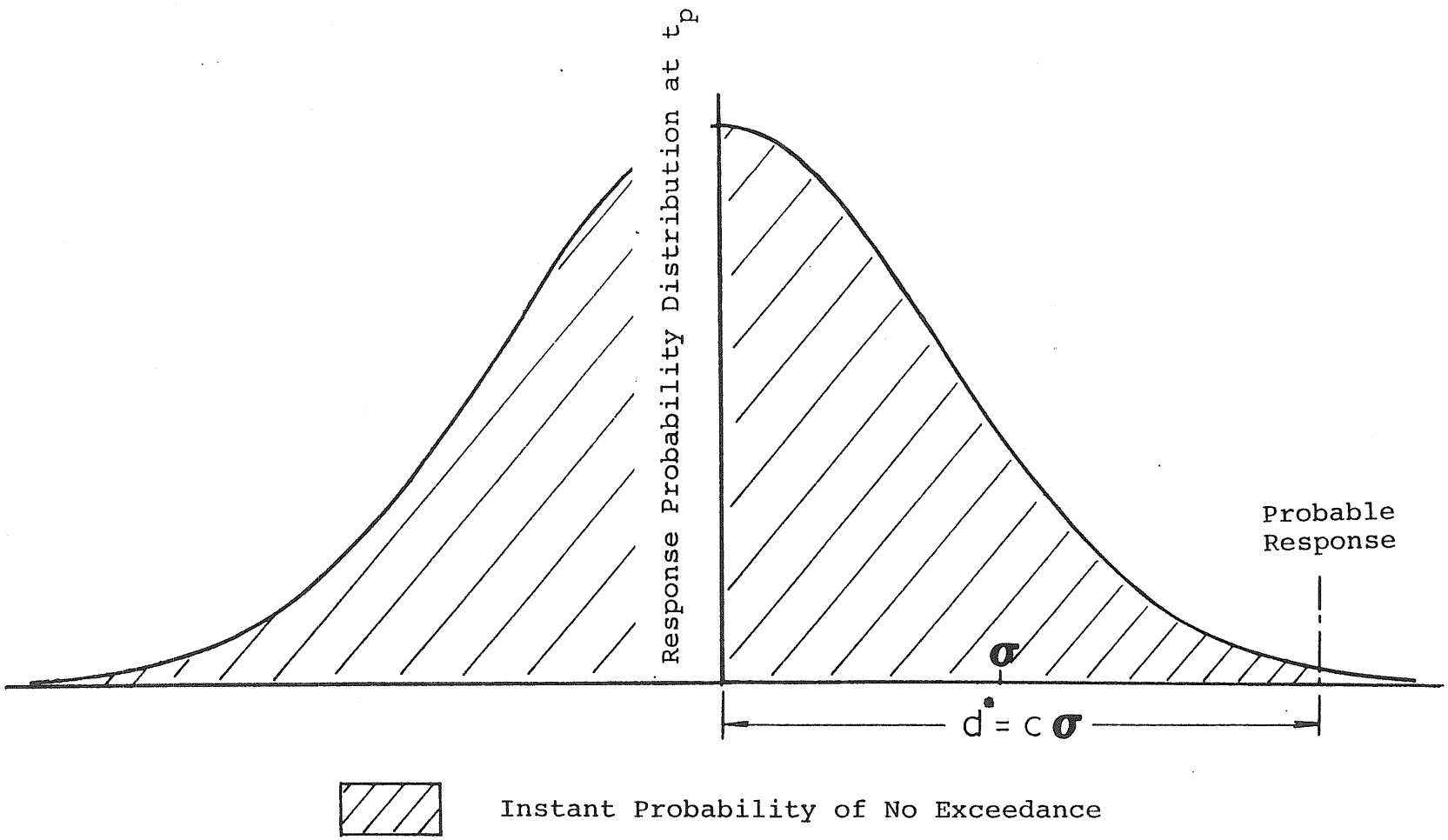

Fig. 4.14 Probability of No Exceedance for a Response Level d* Obtained Based on the Response Probability Distribution at Time t_p

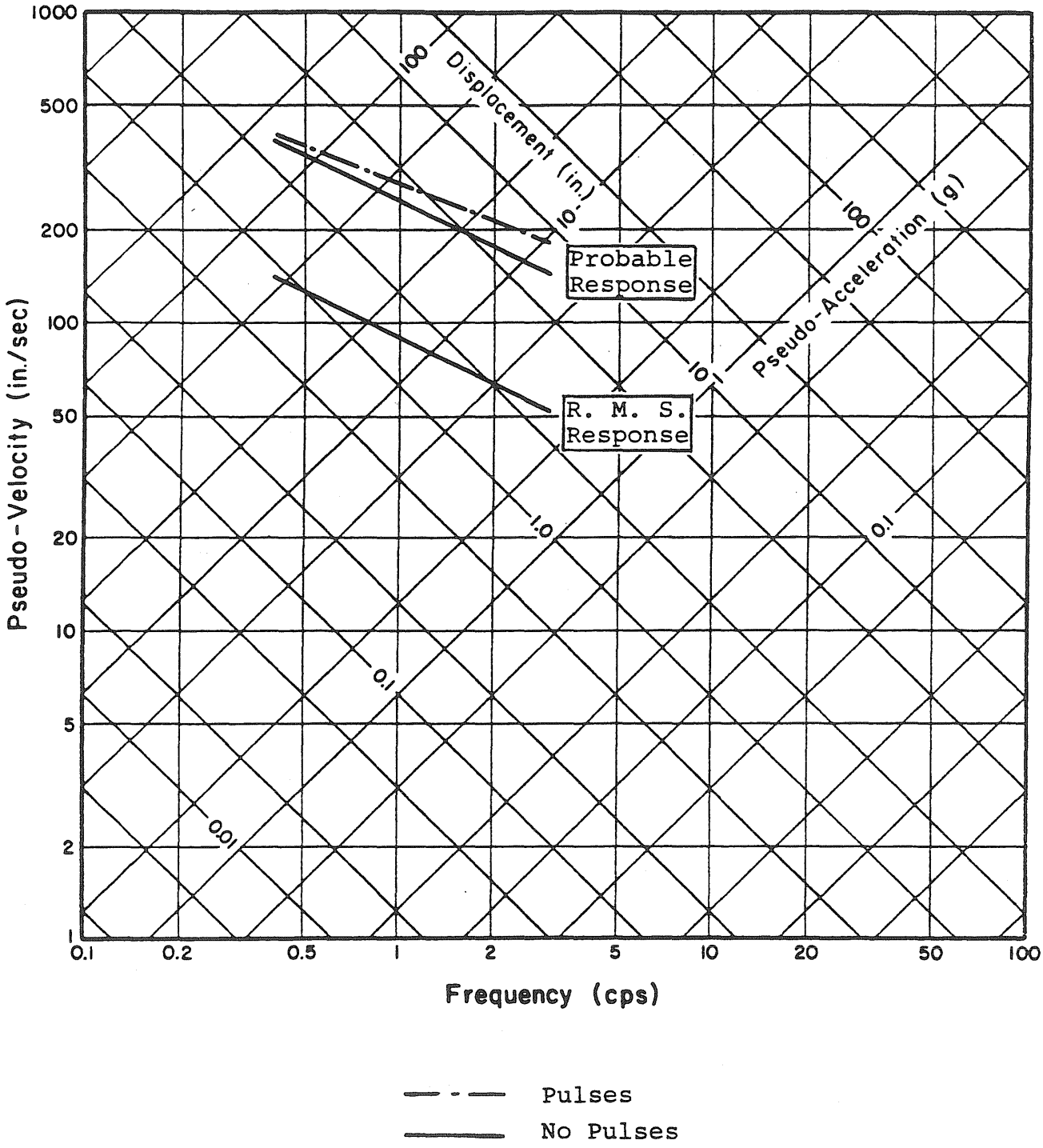

Fig. 4.17 Effect of Large Pulses in Ground Motion on Displacement Response - White Noise Spectrum Input (1/3 of Input Spectral Level Contributed by Pulses)

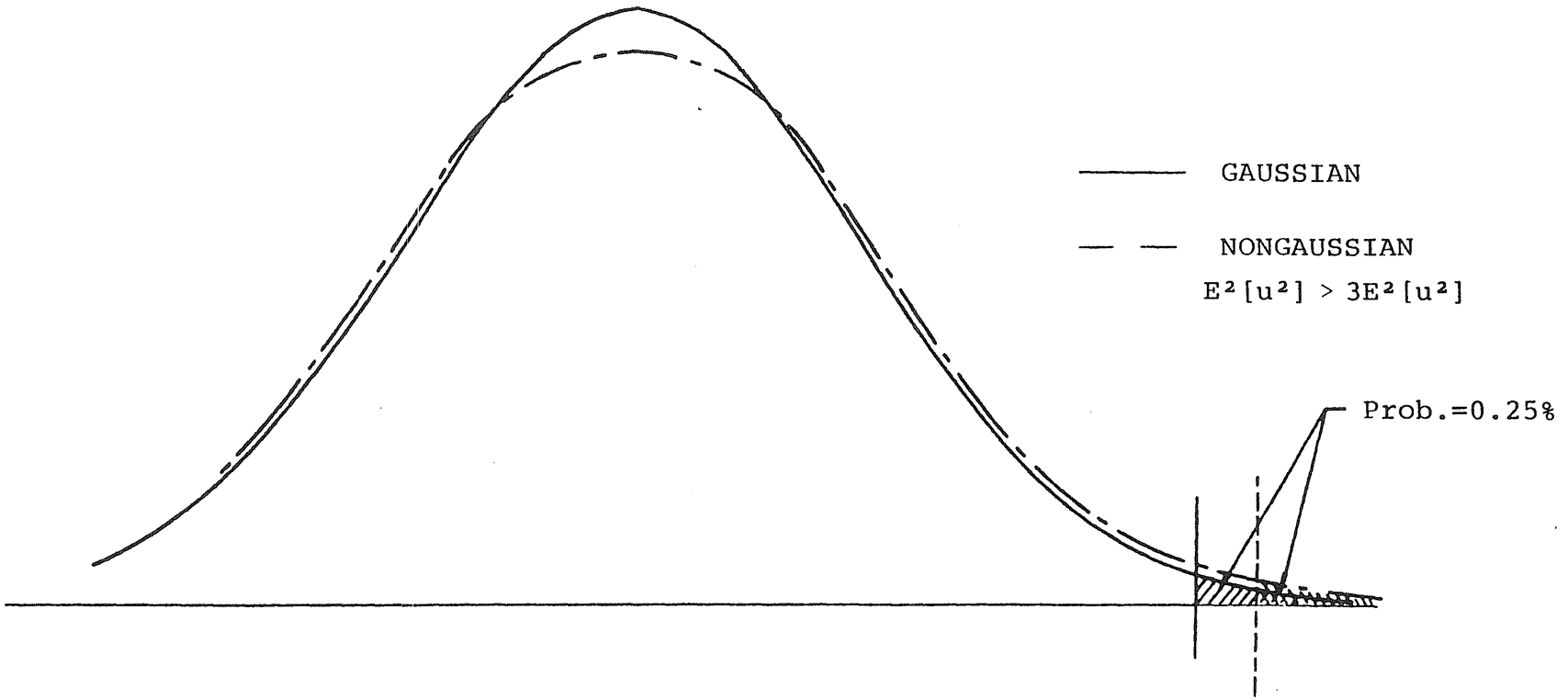

Fig. 4.16 Response Levels Corresponding to a Fixed Instant Probability of No Exceedance

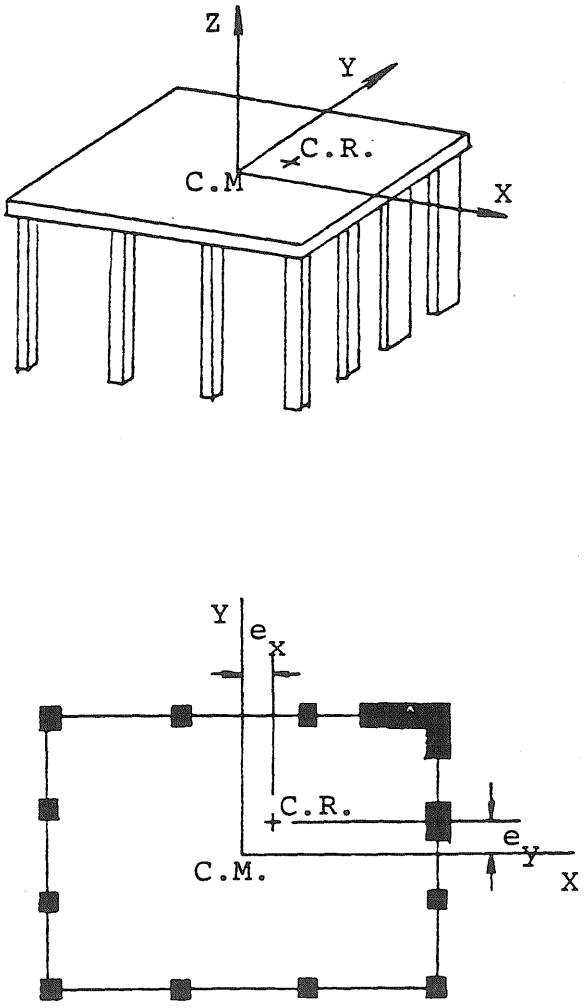

Fig. 5.1 One-Story Structural Model

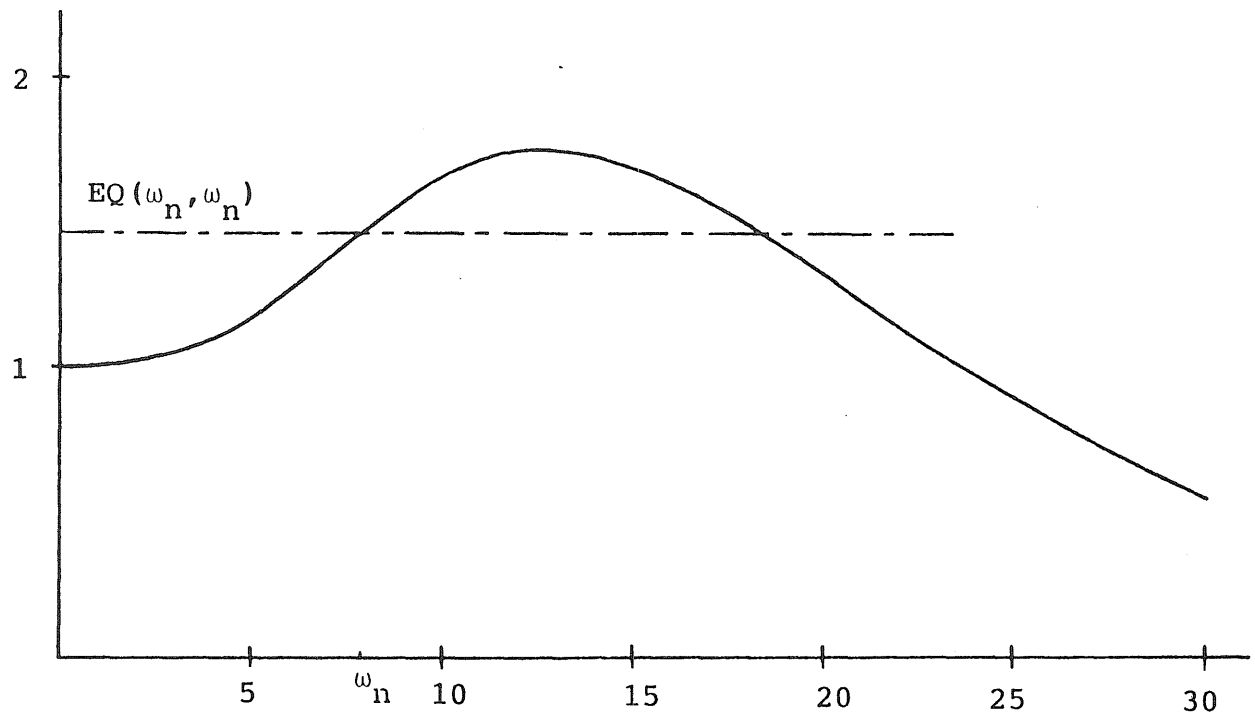

Fig. 4.18 Equivalent White Noise

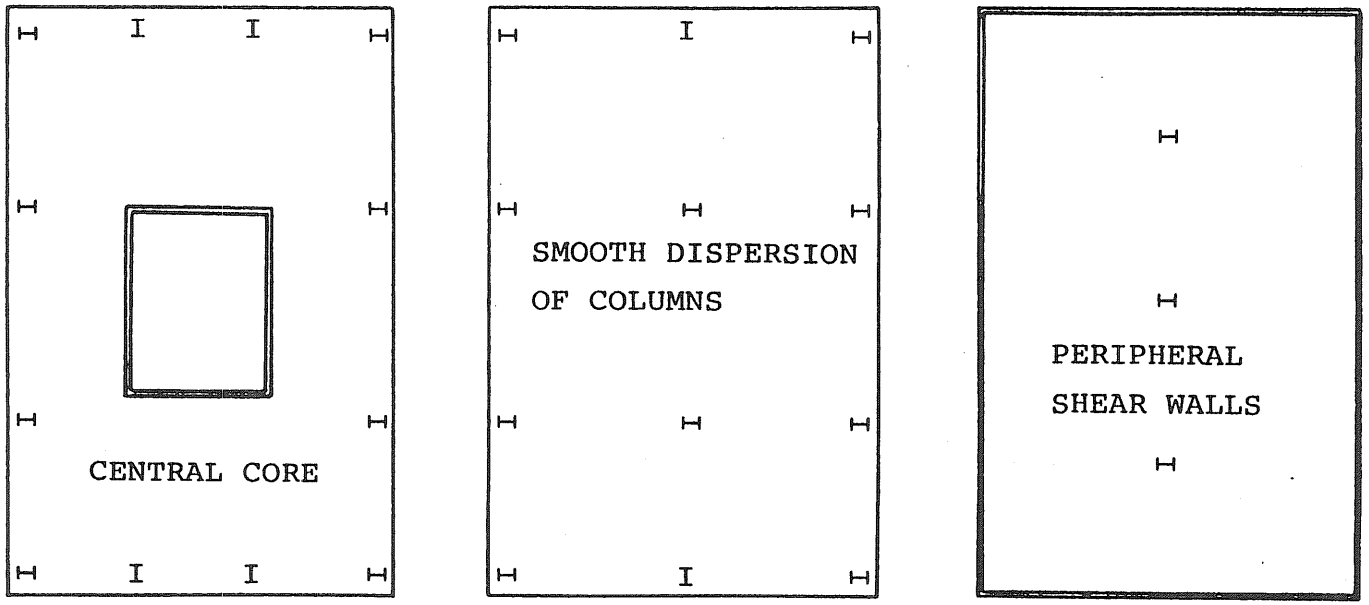

Torsional Frequencies Smaller than Corresponding Translational Frequencies

Torsional Frequencies Nearly Equal Corresponding Translational Frequencies

Torsional Frequencies Larger than Corresponding Translational Frequencies

Fig. 5.3 Common Types of Layout of the Resistance Elements of Buildings

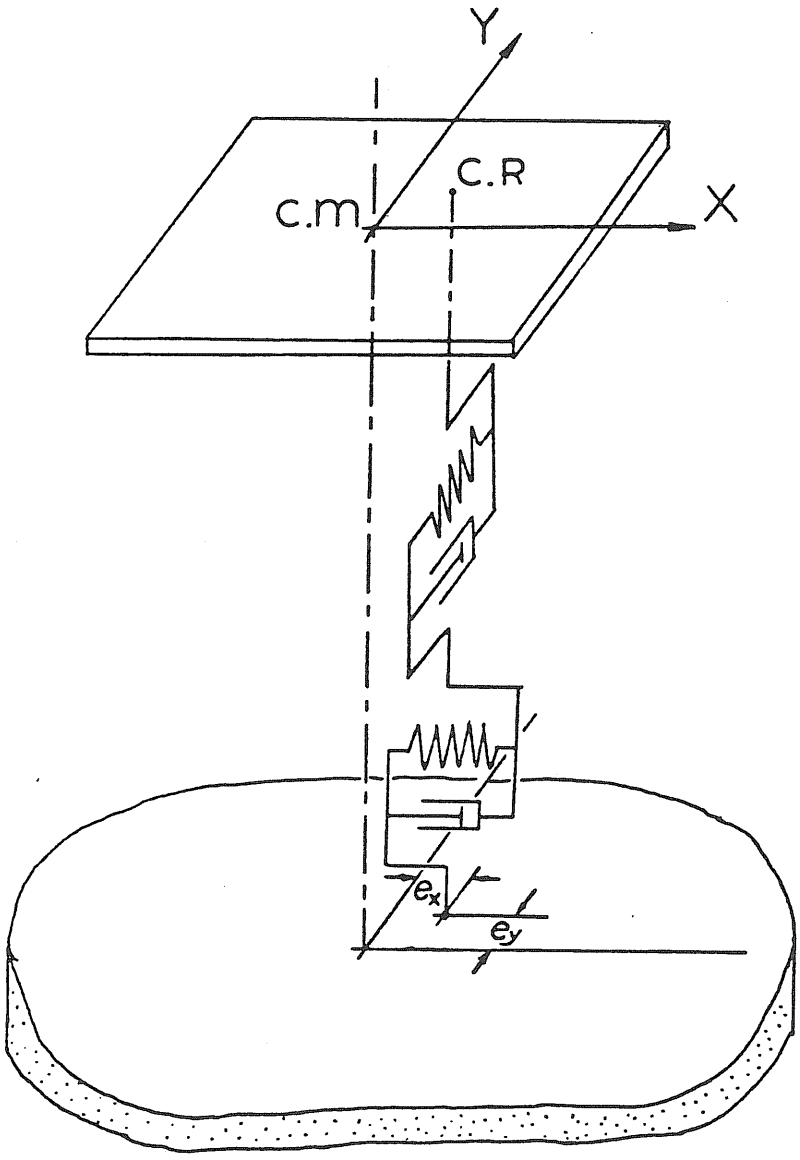

Fig. 5.2 Idealized Three Dimensional Shear Beam Model

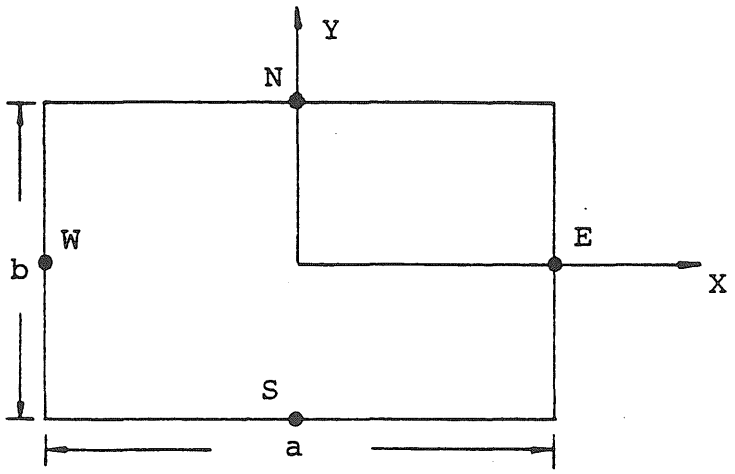

Fig. 5.5 Locations at the Perimeter of Building

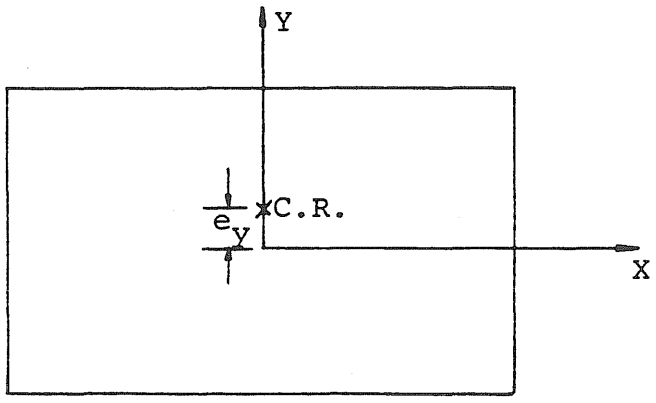

Fig. 5.6 One-Way Torsionally Coupled System

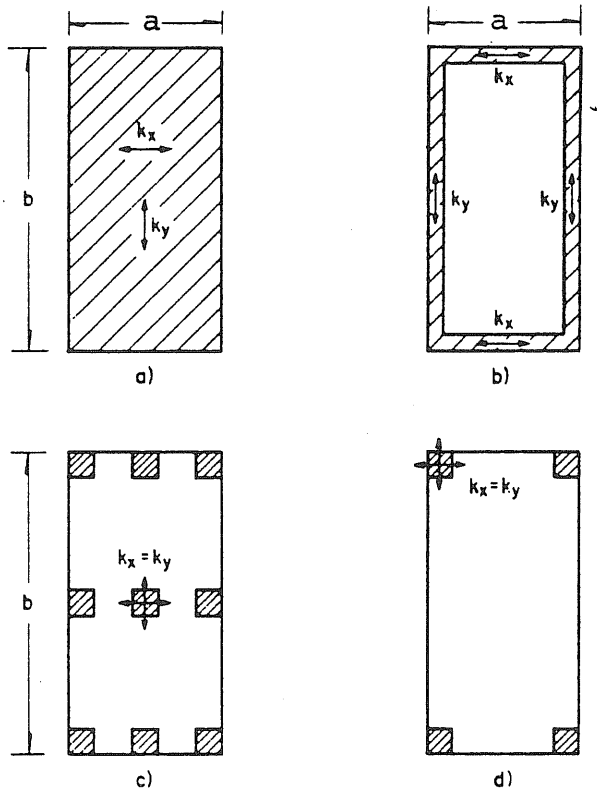

a) Uniform resistance
b) Resistance on perimeter only
c) Nine-column building
d) Four-column building

Fig. 5.4 Building Resistance Patterns after Newmark [62]

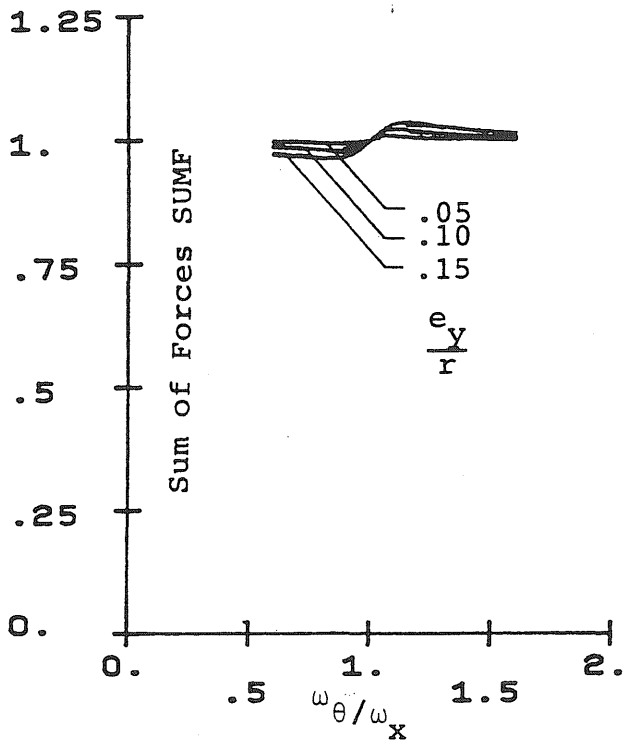

(e)

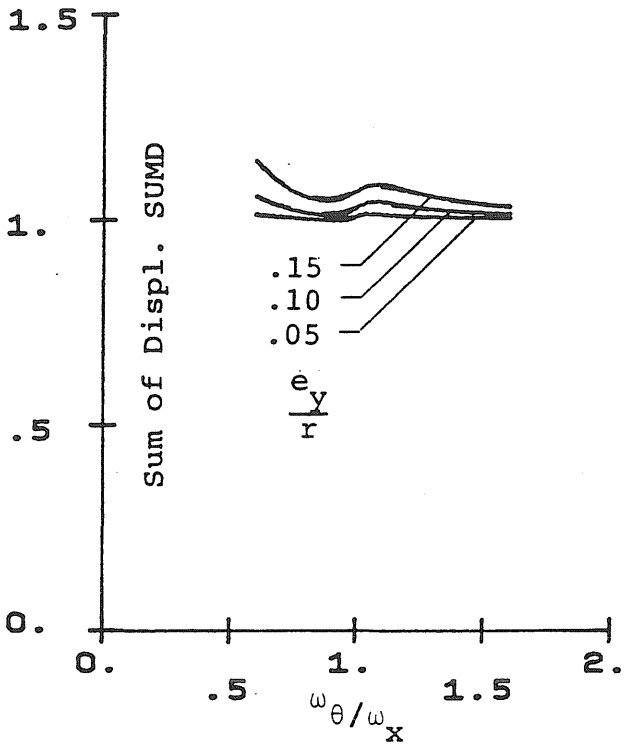

(f)

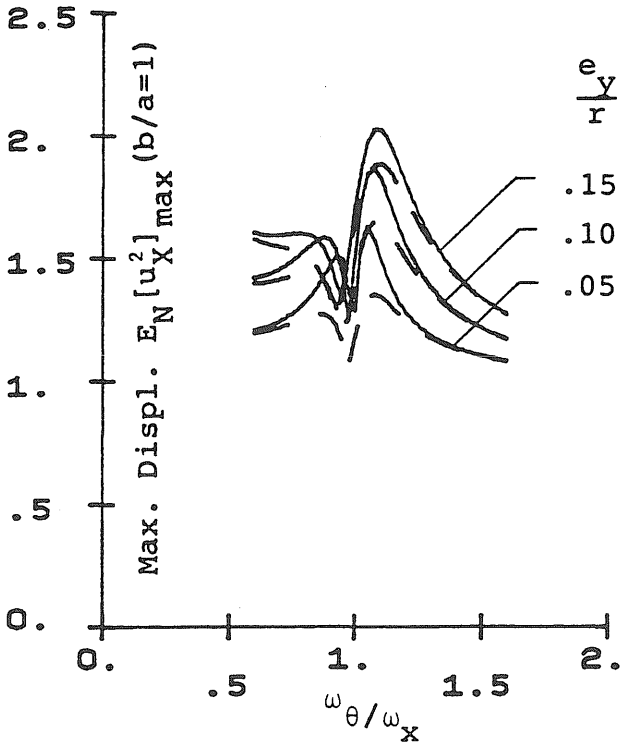

(g)

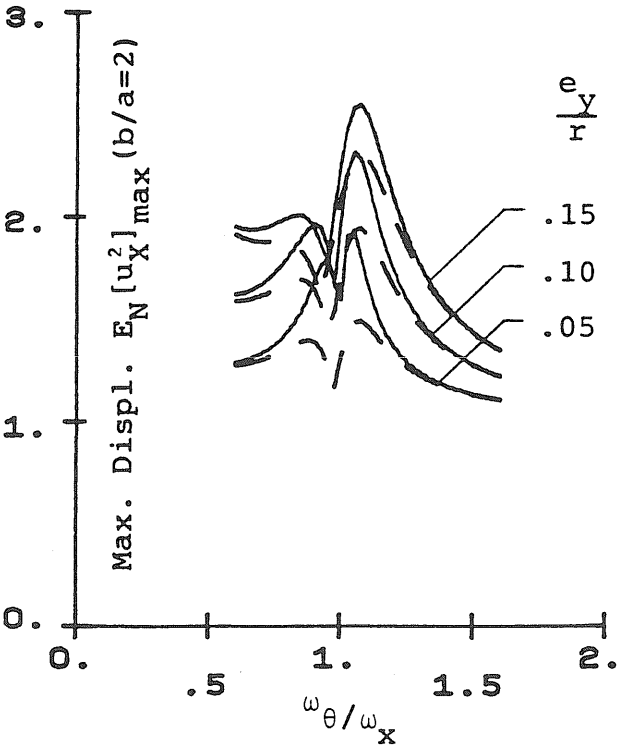

(h)

Fig. 5.7 (continued)

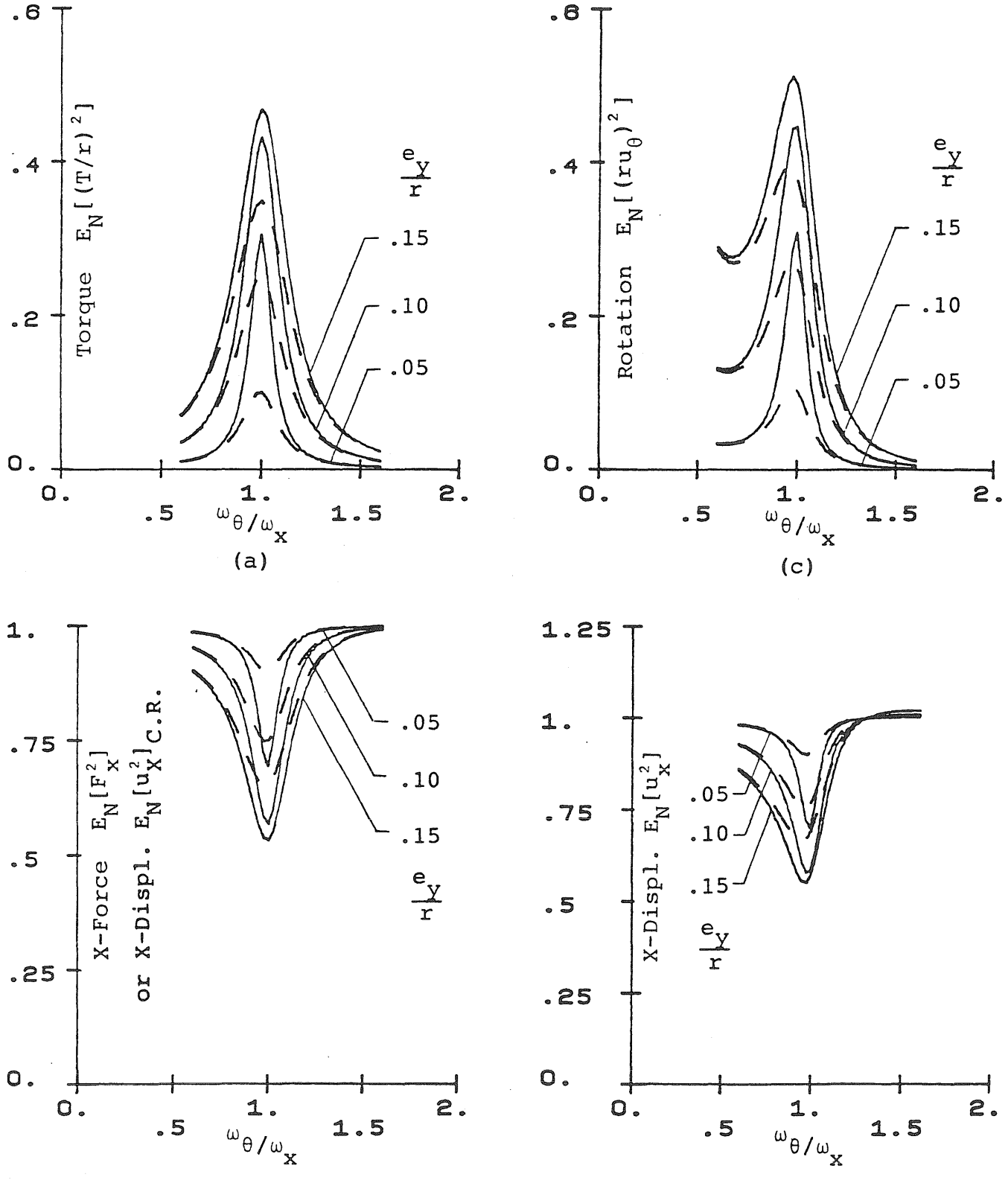

Legend: —— $\zeta = 0.02$, – – $\zeta = 0.05$

Fig. 5.7 Normalized M.S. Responses of One-Way Torsionally Coupled Systems - Input: White Noise (Special Damping)

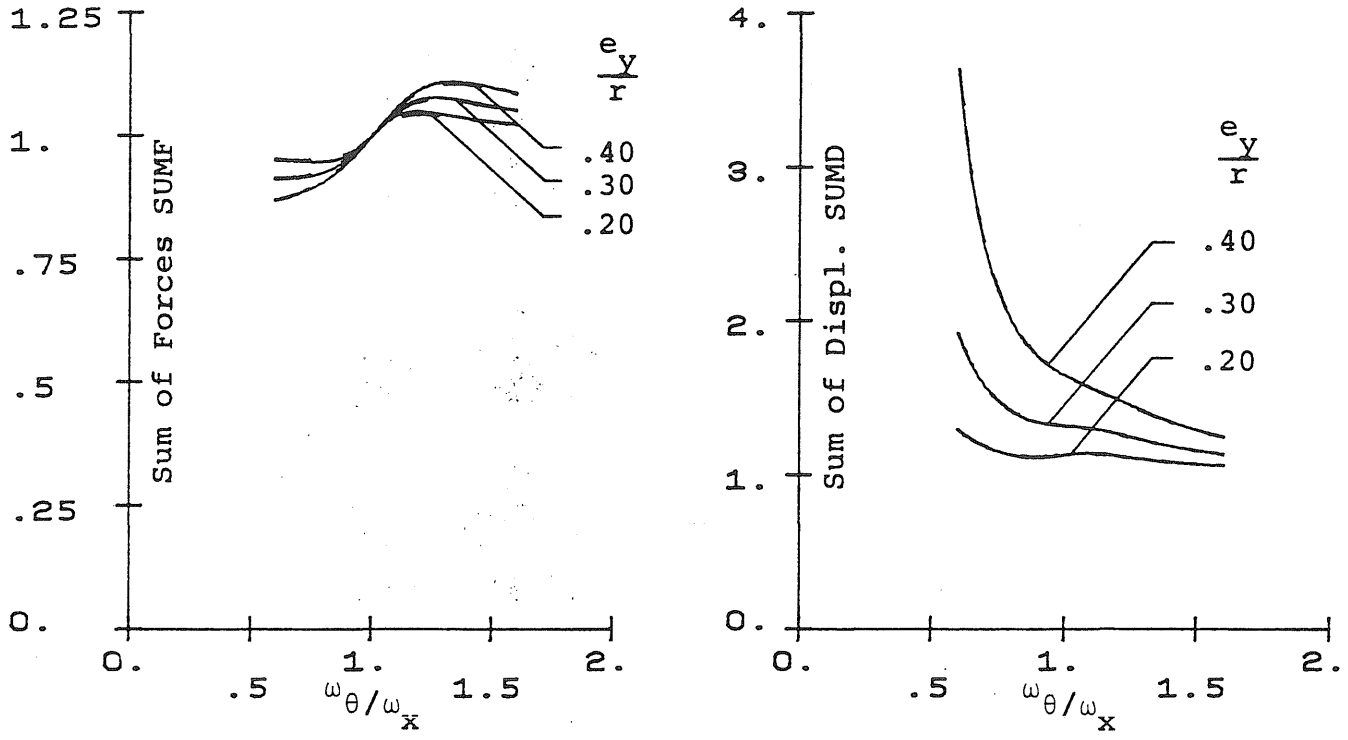

(e)

(f)

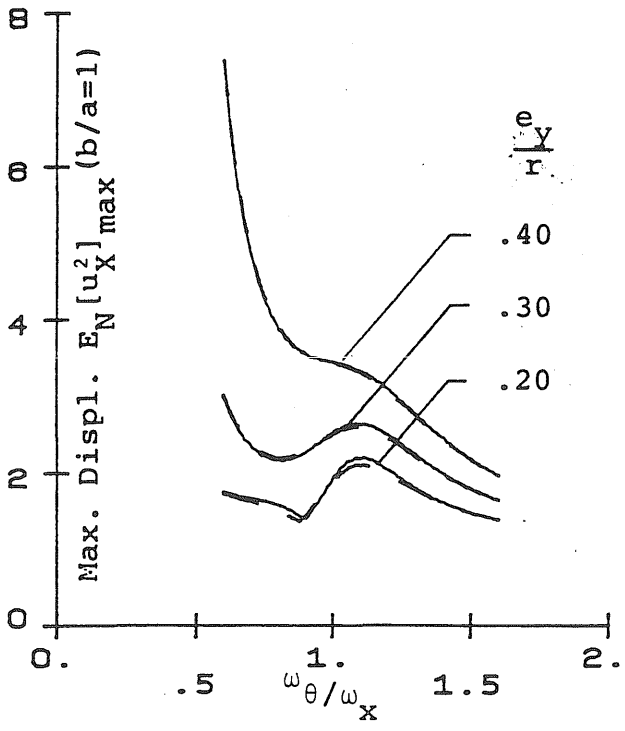

(g)

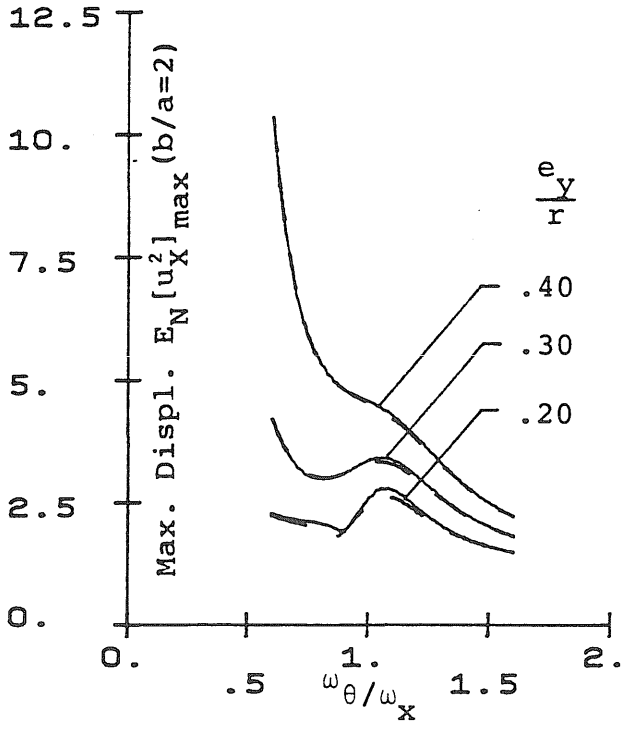

(h)

Fig. 5.8 (continued)

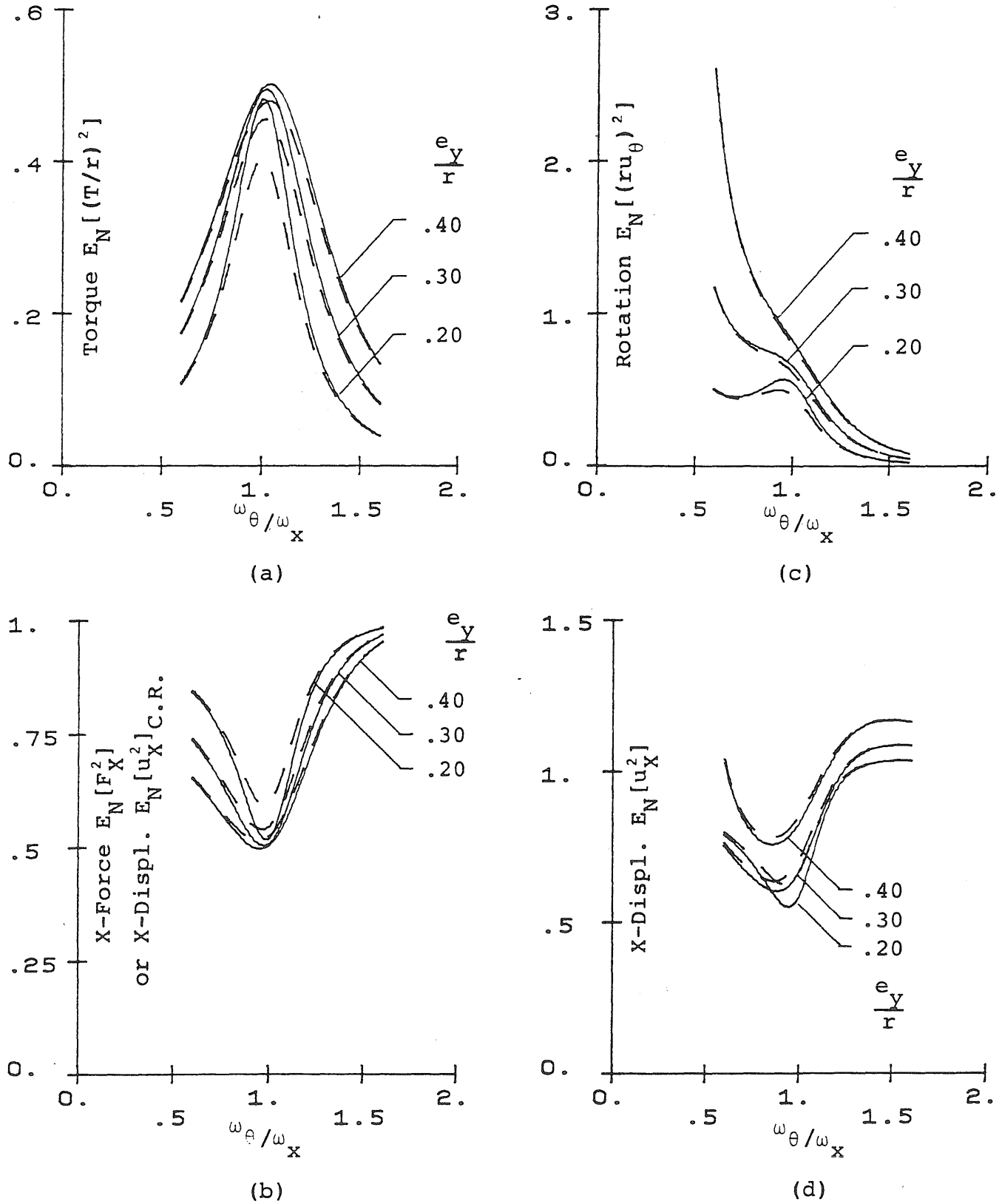

Legend: —— $\zeta = 0.02$, – – $\zeta = 0.05$

Fig. 5.8 Normalized M.S. Responses of One-Way Torsionally Coupled Systems - Input: White Noise (Special Damping)

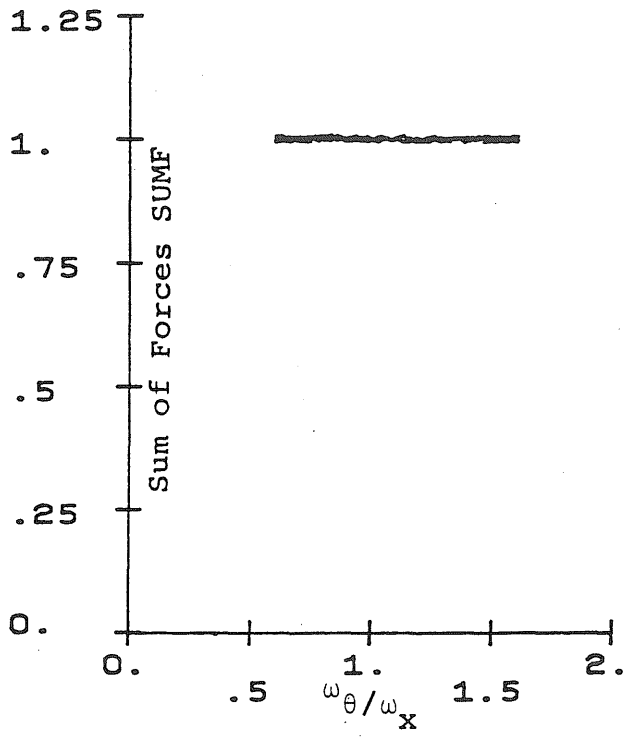

(e)

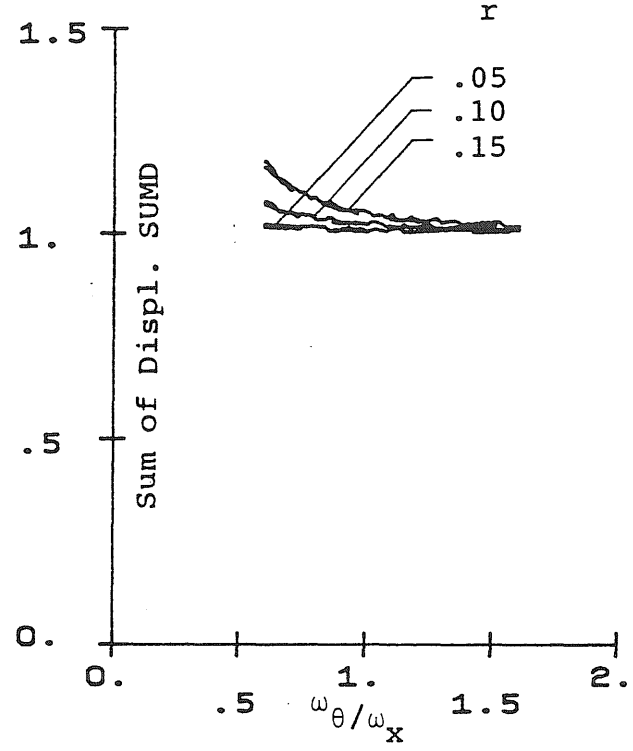

(f)

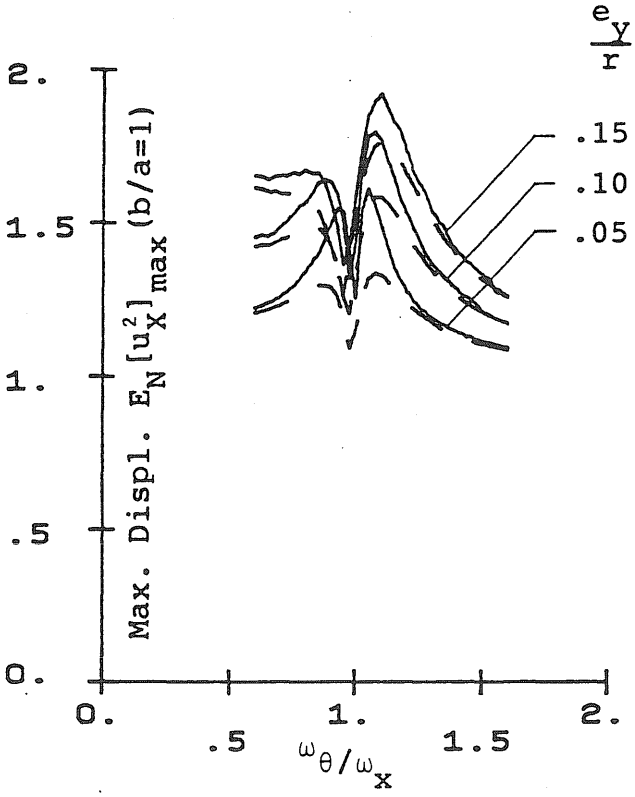

(g)

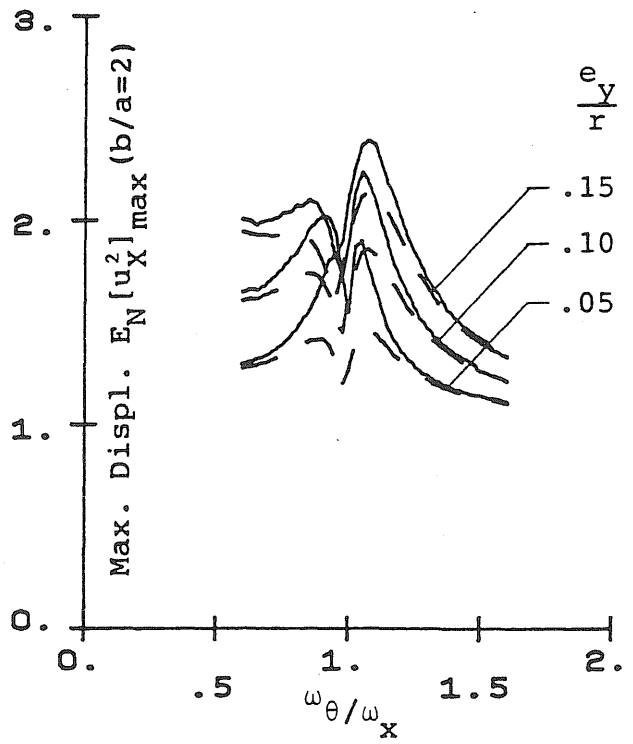

(h)

Fig. 5.9 (continued)

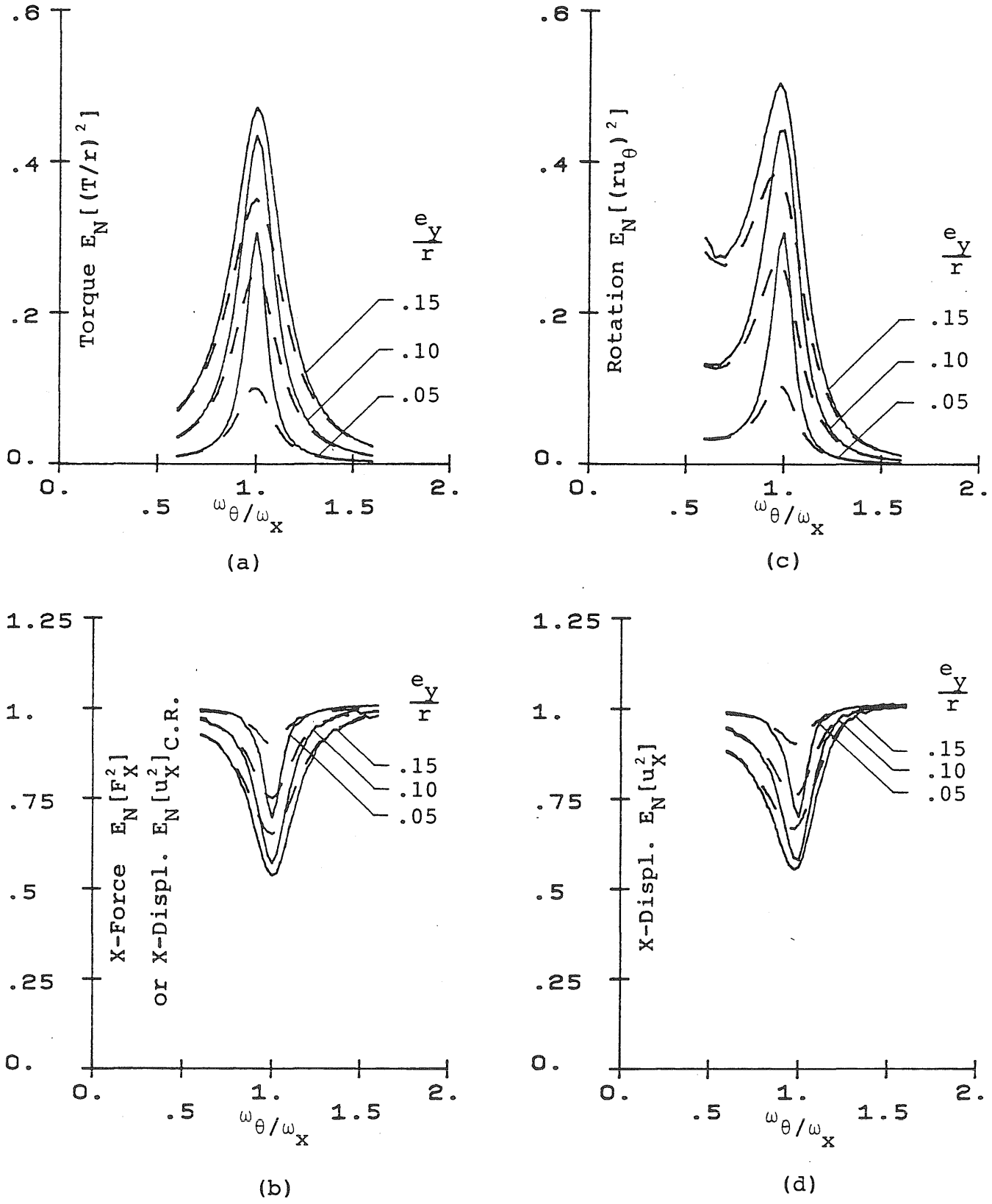

Legend: —— $\zeta = 0.02$, – – $\zeta = 0.05$

Fig. 5.9 Normalized M.S. Responses of One-Way Torsionally Coupled Systems - Input: White Noise (Modal Damping)

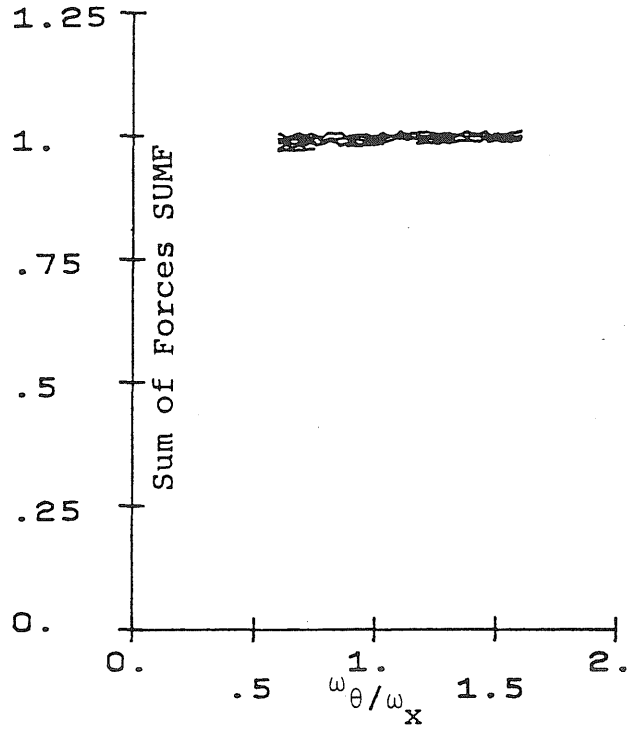

(e)

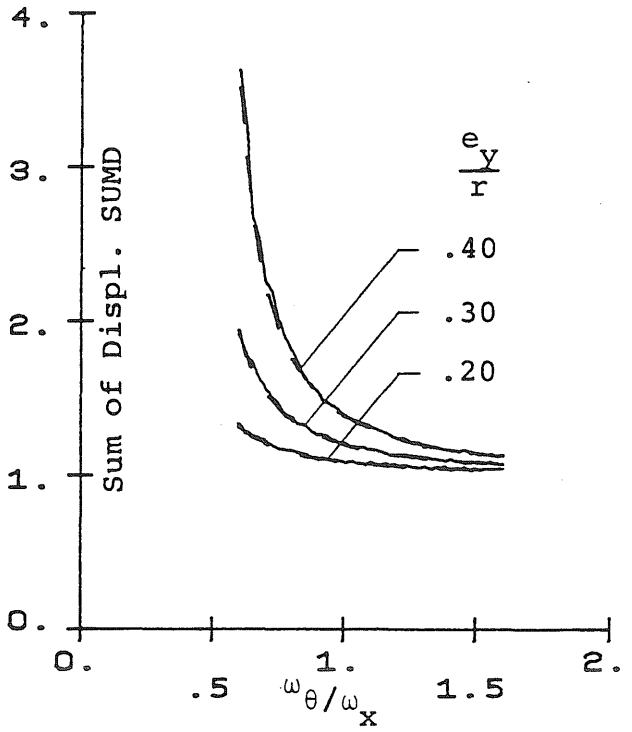

(f)

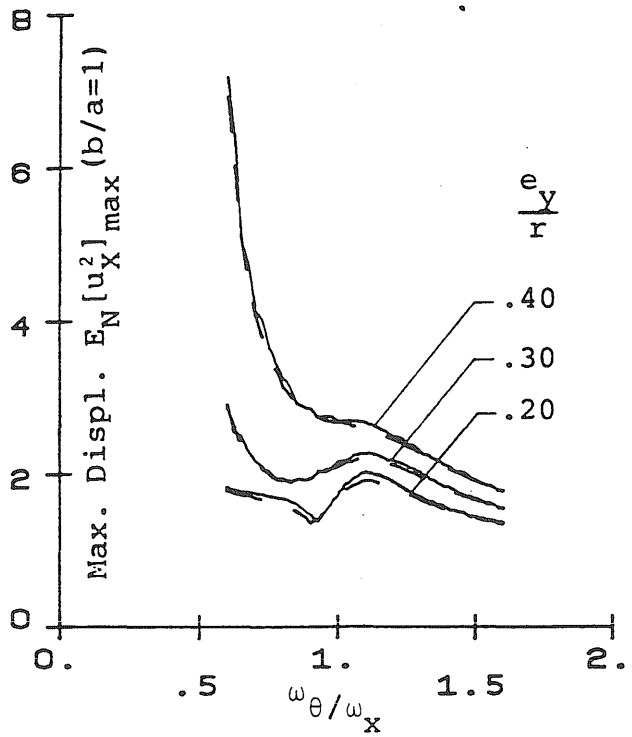

(g)

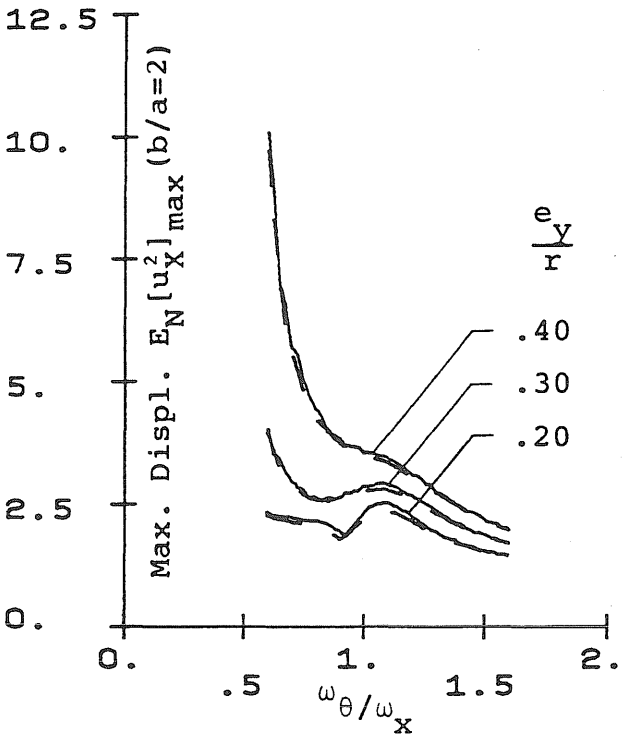

(h)

Fig. 5.10 (continued)

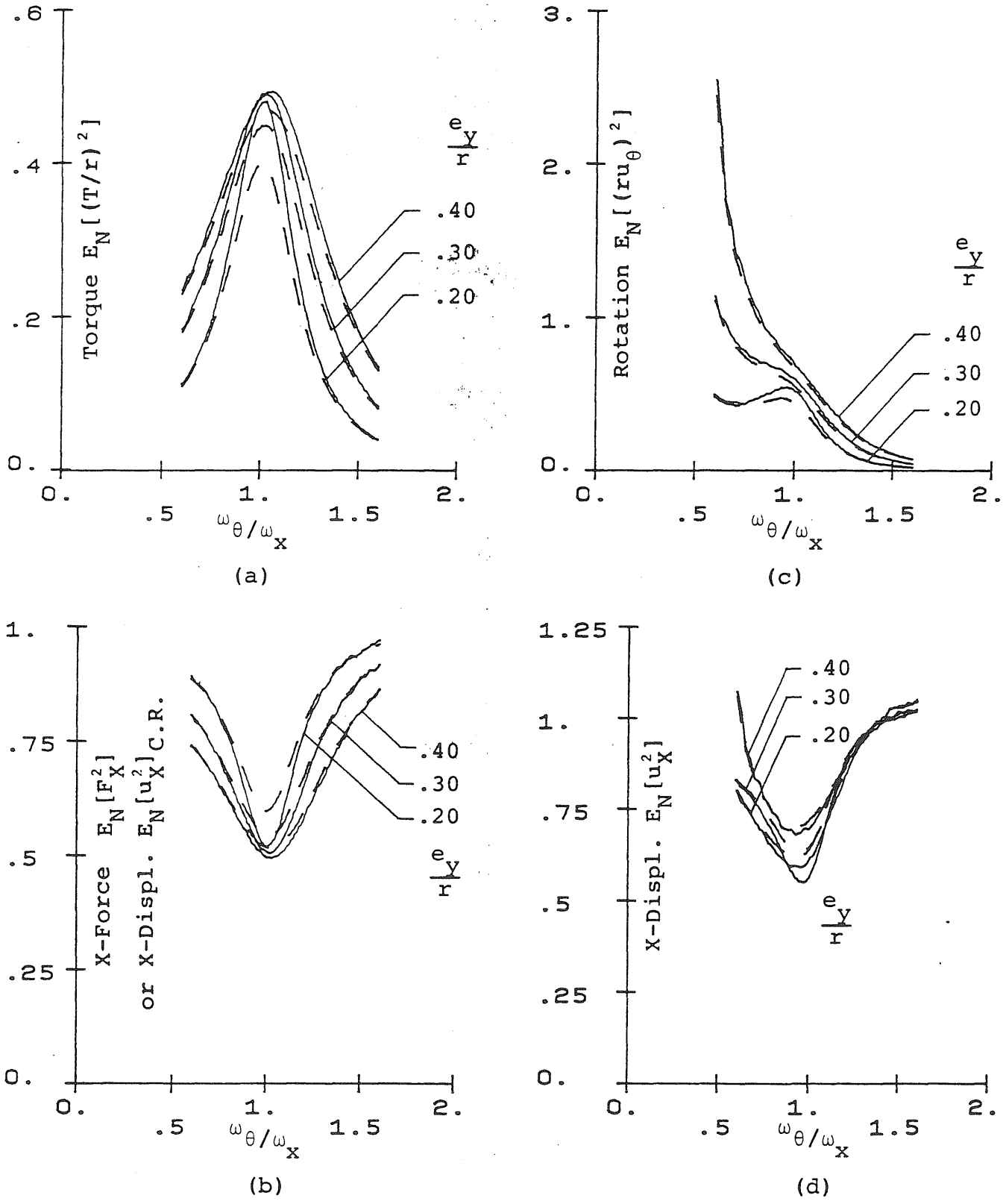

Legend: —— $\zeta = 0.02$, – – $\zeta = 0.05$

Fig. 5.10 Normalized M.S. Responses of One-Way Torsionally Coupled Systems - Input: White Noise (Modal Damping)

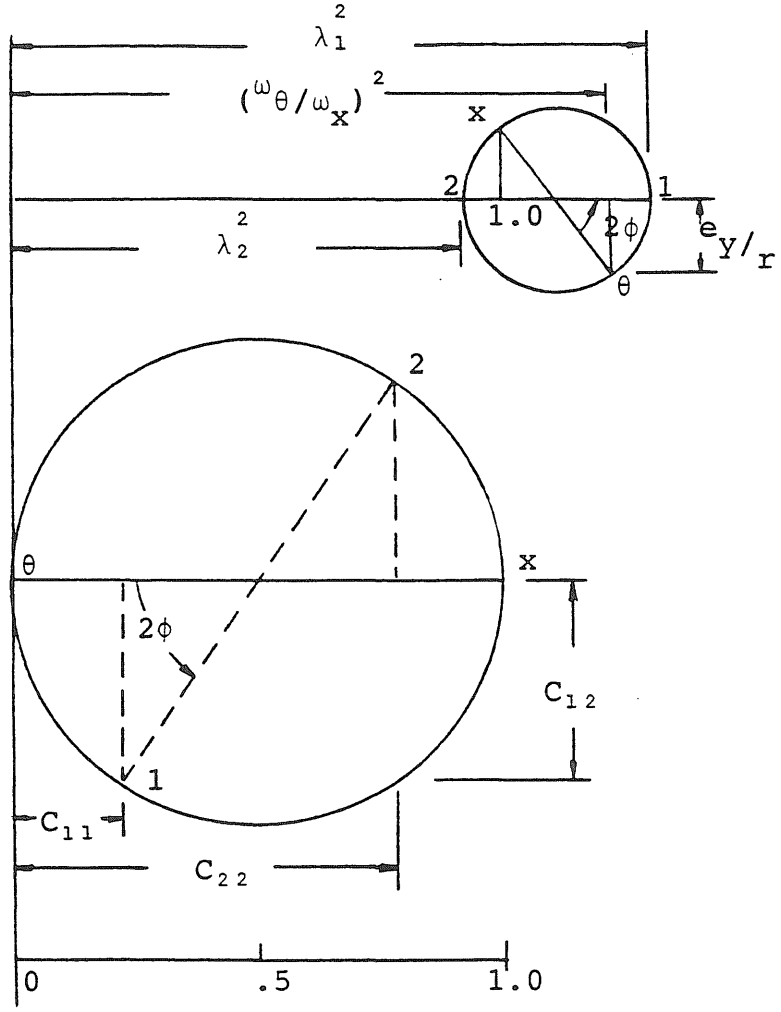

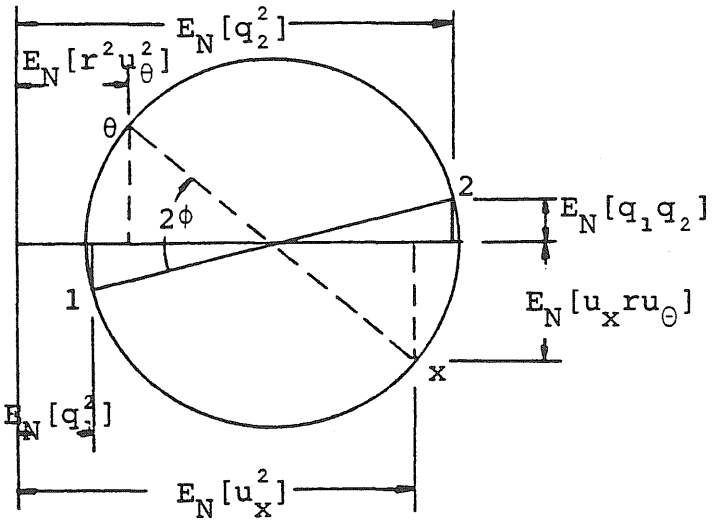

Fig. 5.12 Use of Mohr's Circle Plots for Presentation of Responses

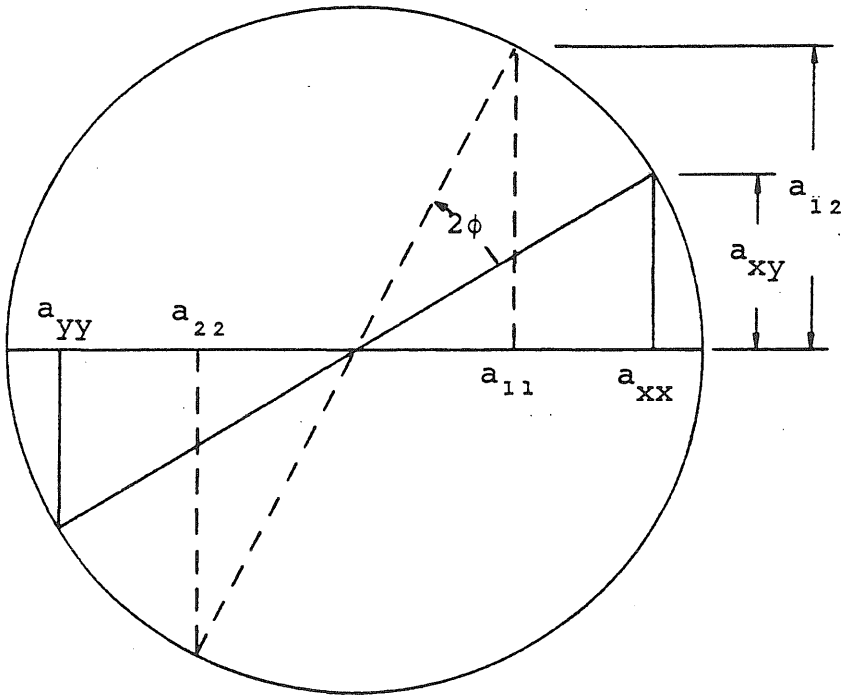

Fig. 5.11 Mohr's Circle Plot for Similarity Transformation

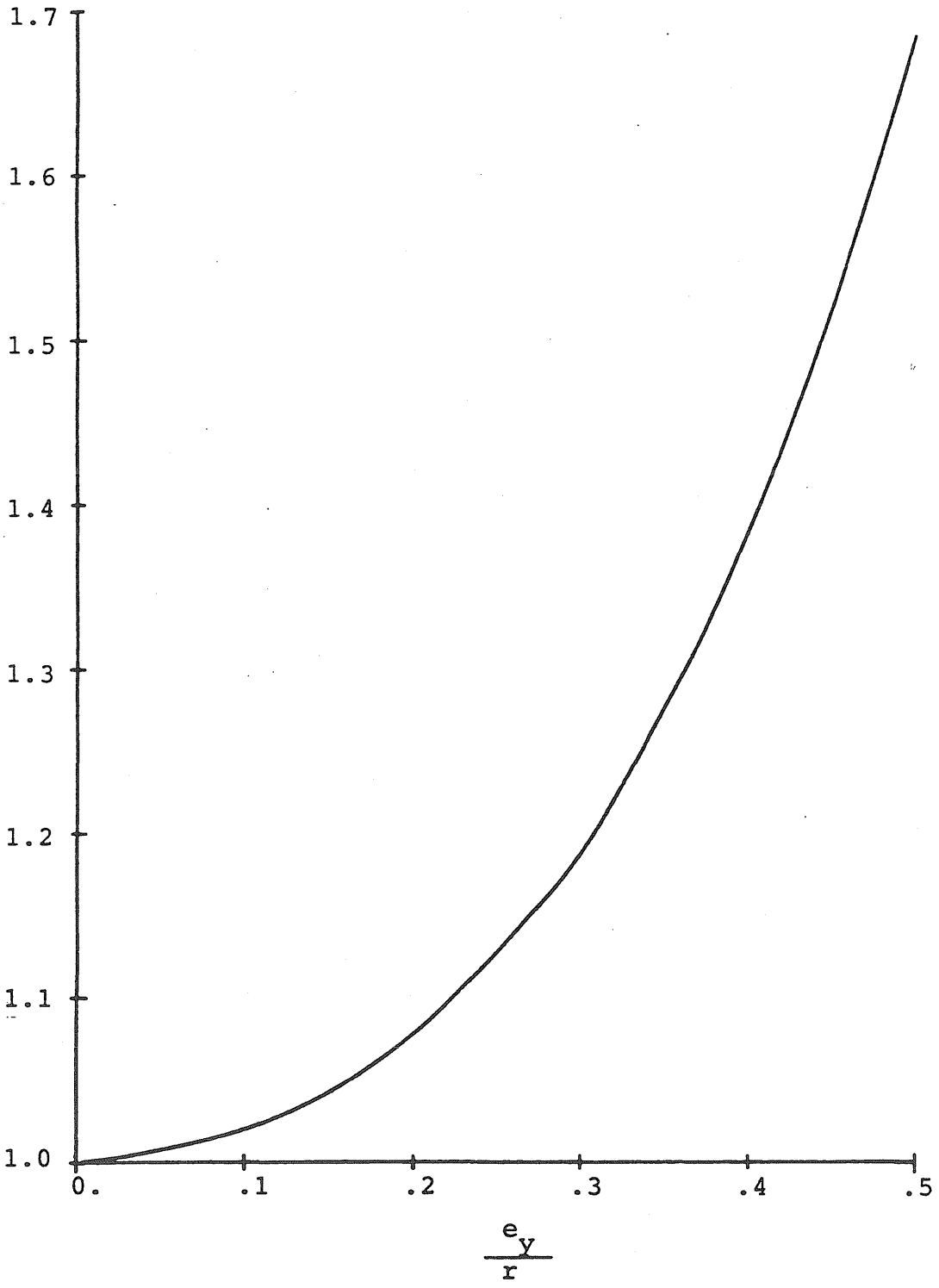

Fig. 5.14 Plot of $\frac{1}{2}\{\frac{1}{[\sqrt{1+(e_y/r)}]^3} + \frac{1}{[\sqrt{1-(e_y/r)}]^3}\}$ against $\frac{e_y}{r}$

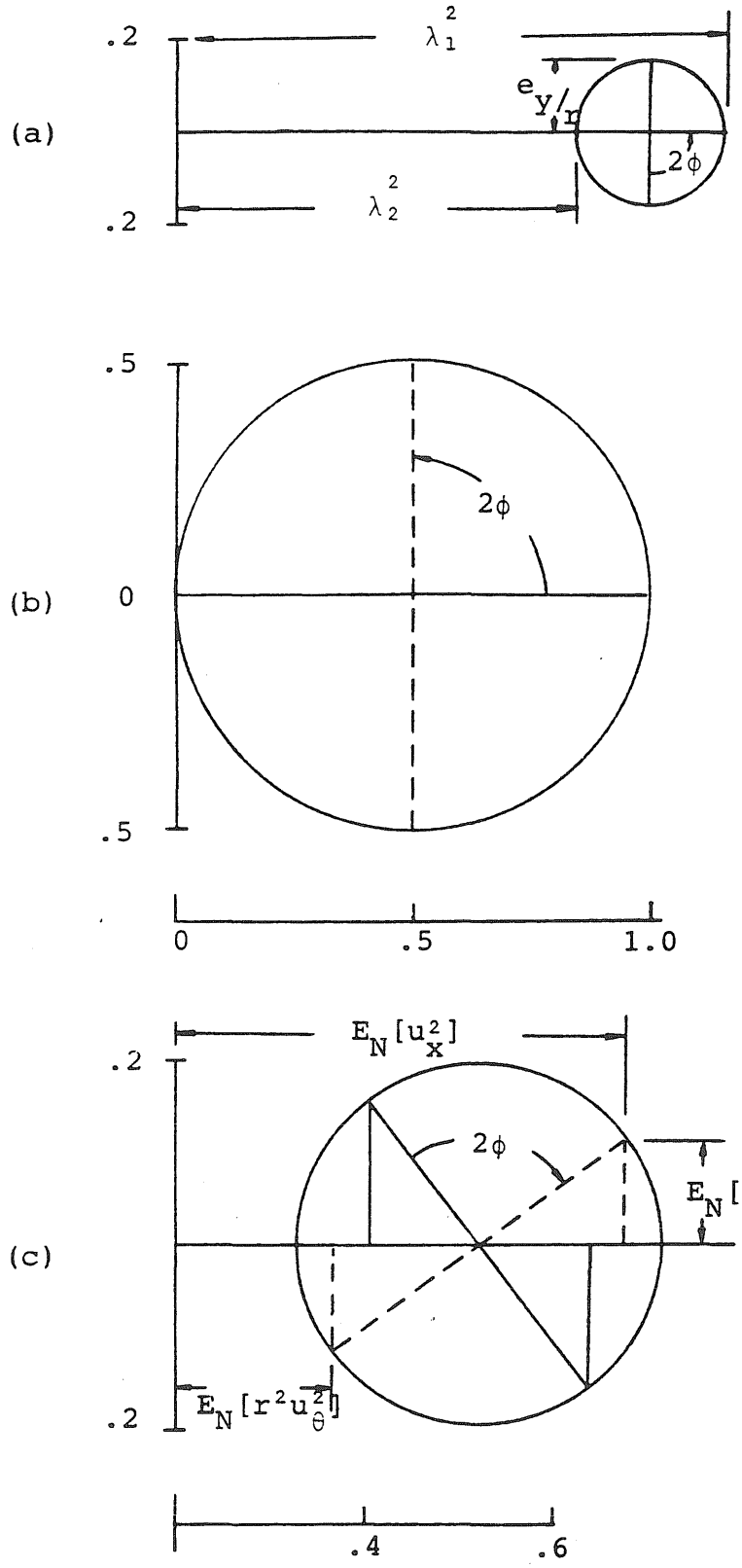

STEP 1

$\lambda_1^2 = 1.15$

$\lambda_2^2 = 0.85$

$\phi = \pi/4$

STEP 2

$C_{11} = 0.50$

$C_{22} = 0.50$

$C_{12} = -.50$

STEP 3

$E_N[q_1^2] = 0.41$

$E_N[q_2^2] = 0.64$

$E_N[q_1 q_2] = 0.15$

STEP 4

$E_N[r^2 u_\theta^2] = 0.37$

$E_N[u_x^2] = 0.68$

$E_N[u_x ru_\theta] = 0.12$

Fig. 5.13 Use of Mohr's Circle Plots for Presentation of Responses ($\omega_\theta/\omega_x = 1$, $e_y/r = 0.15$)

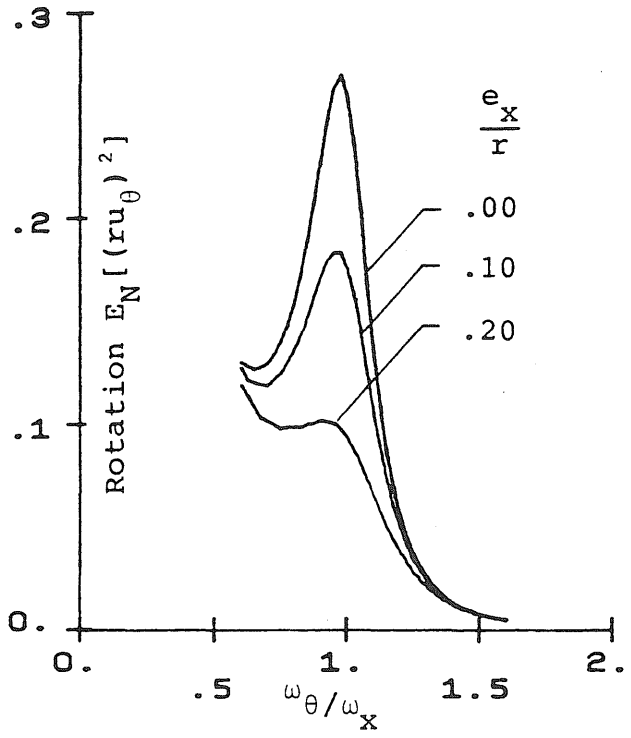

(e)

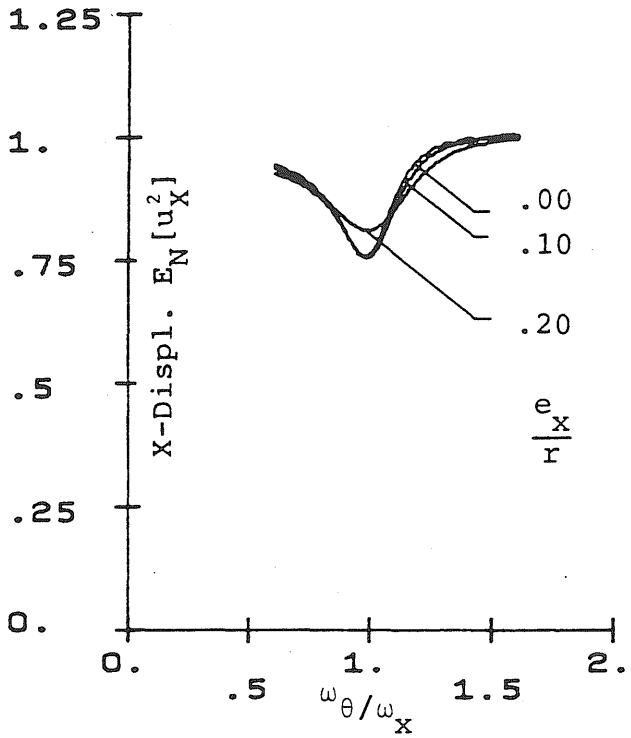

(f)

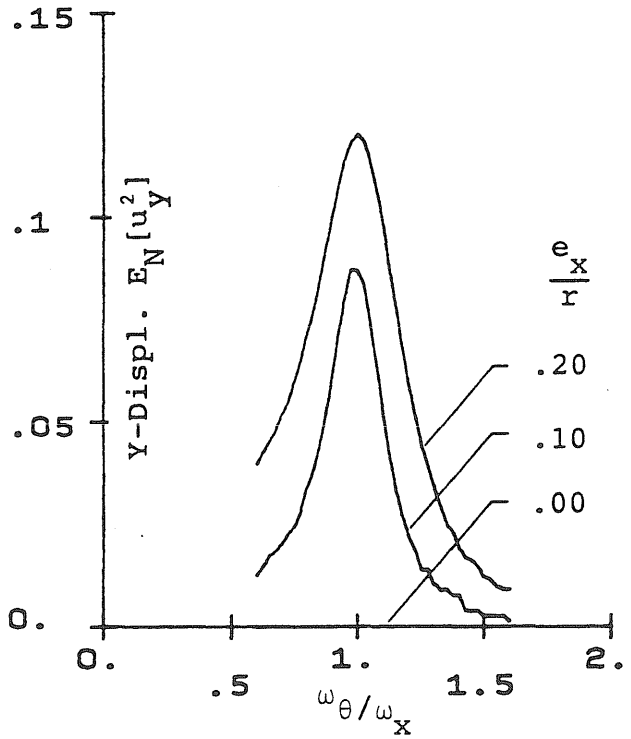

(g)

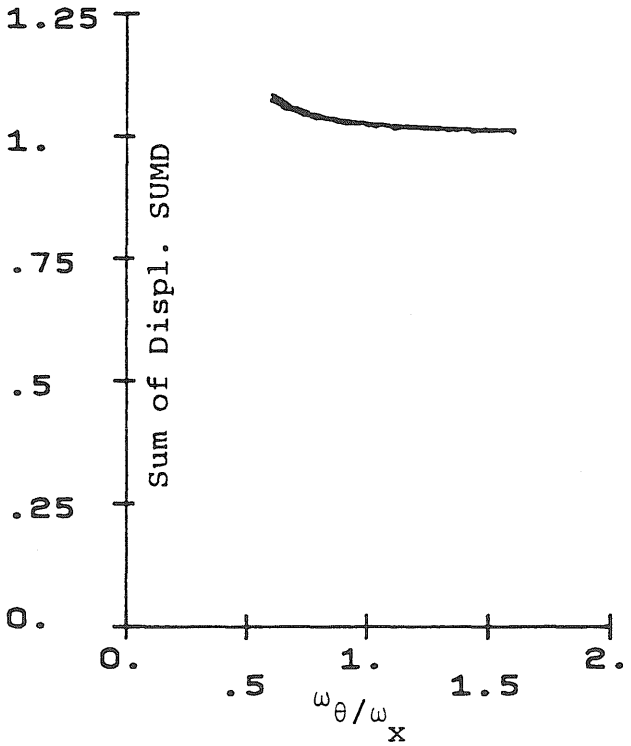

(h)

Fig. 5.15 (continued)

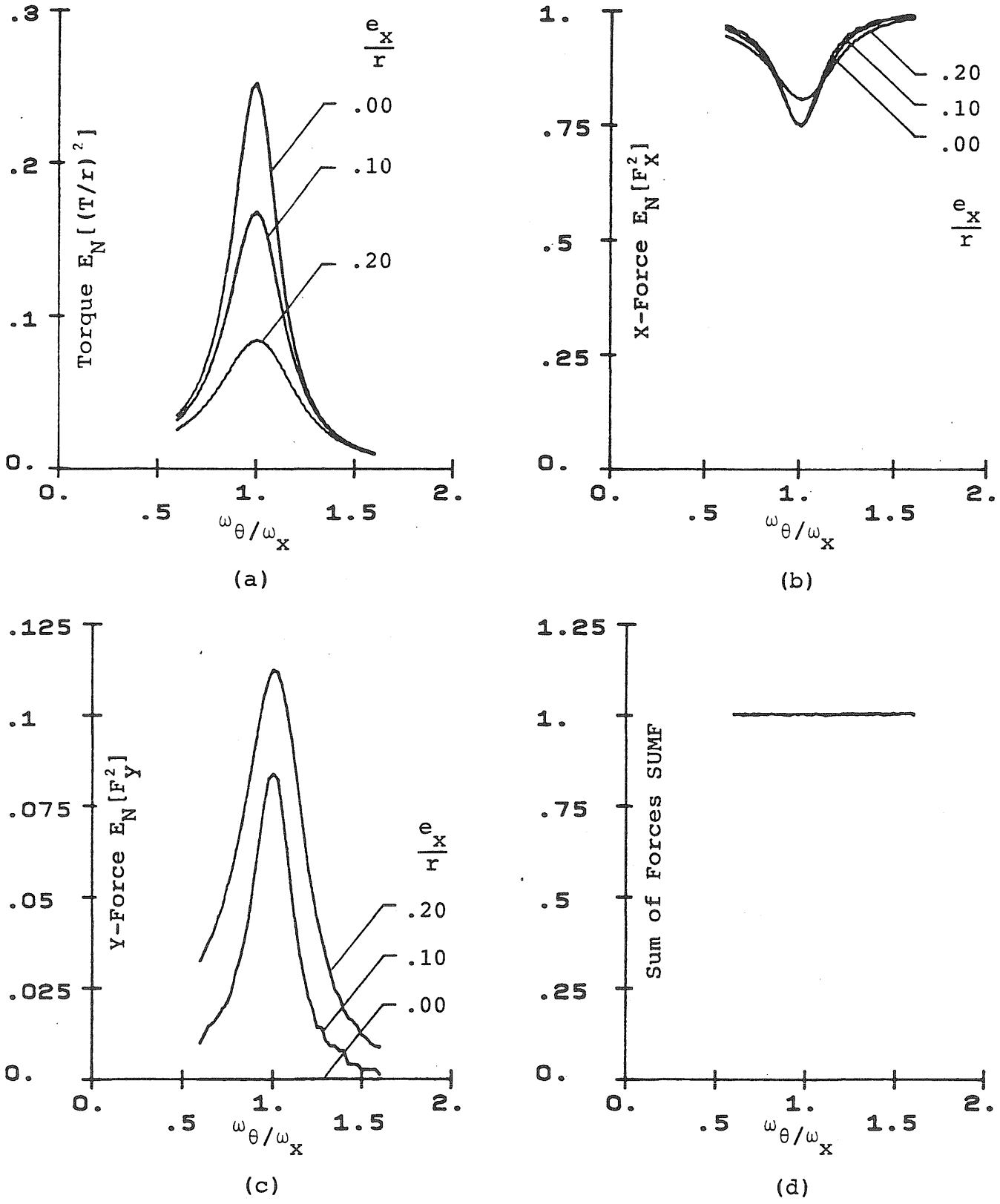

Fig. 5.15 Normalized M.S. Responses of Torsionally Coupled Systems with $\omega_y/\omega_x = 1$, $\frac{e_y}{r} = 0.1$ - Input: White Noise (S_x)

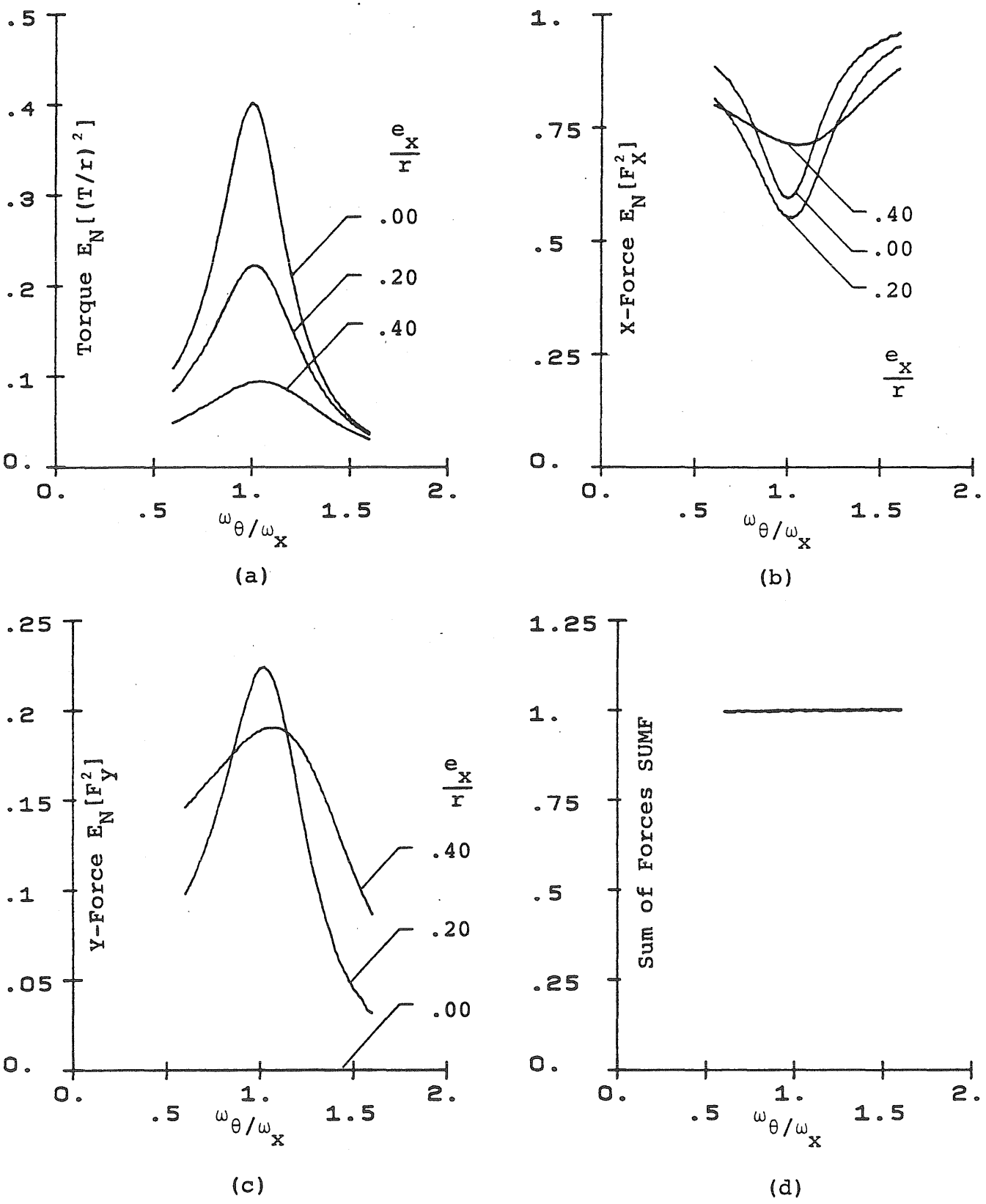

Fig. 5.16 Normalized M.S. Responses of Torsionally Coupled Systems with $\omega_y/\omega_x = 1$, $\frac{e_y}{r} = 0.2$ - Input: White Noise (S_x)

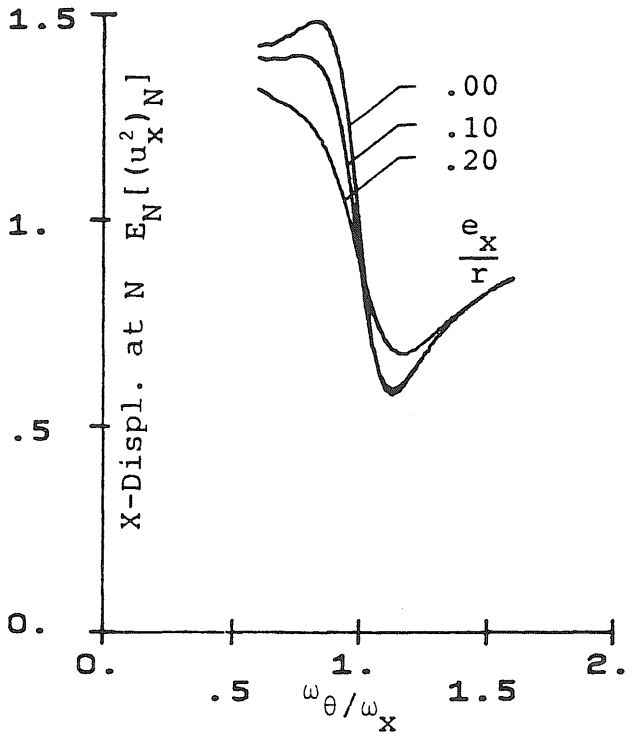

(i)

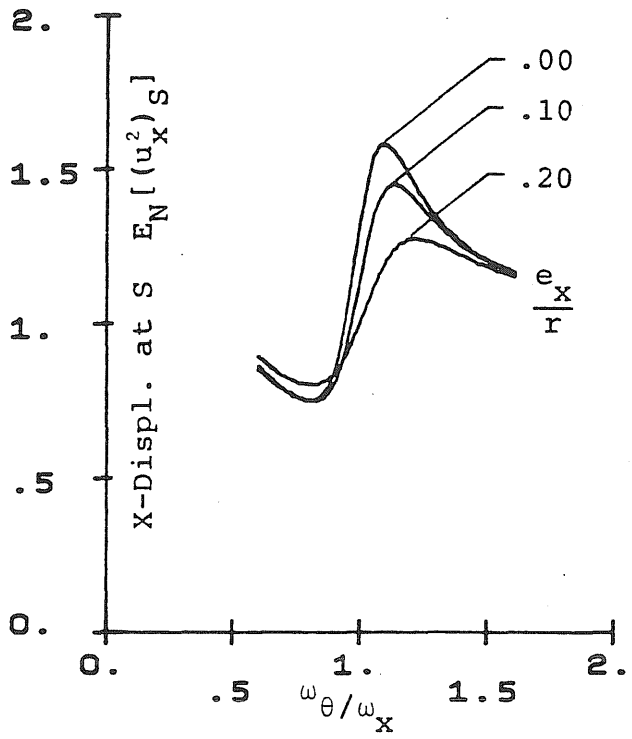

(j)

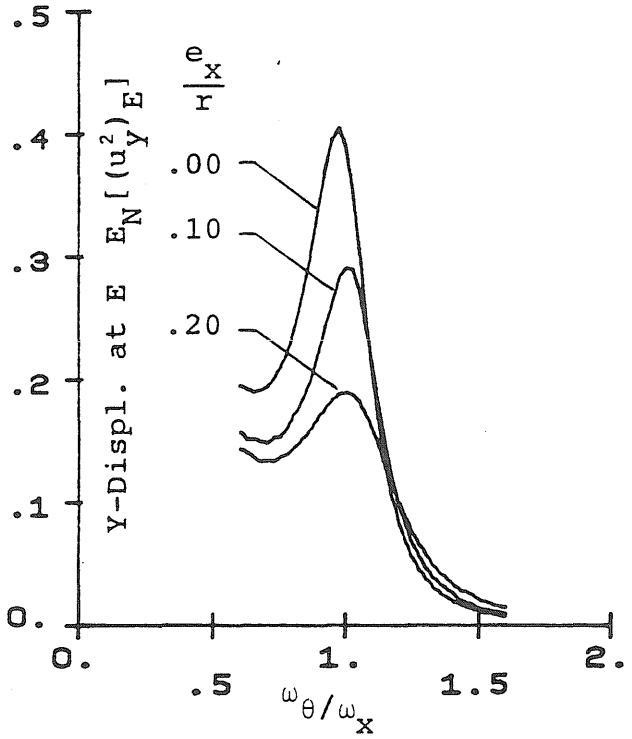

(k)

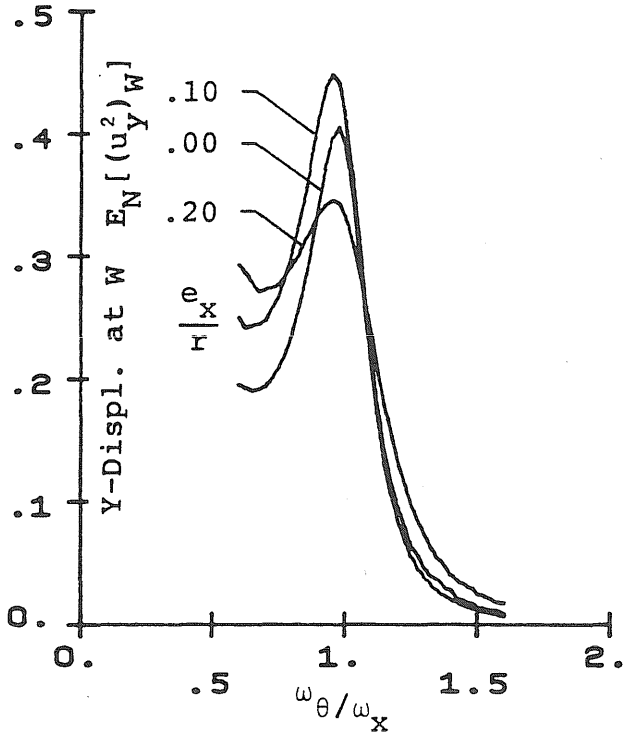

(l)

Fig. 5.15 (continued)

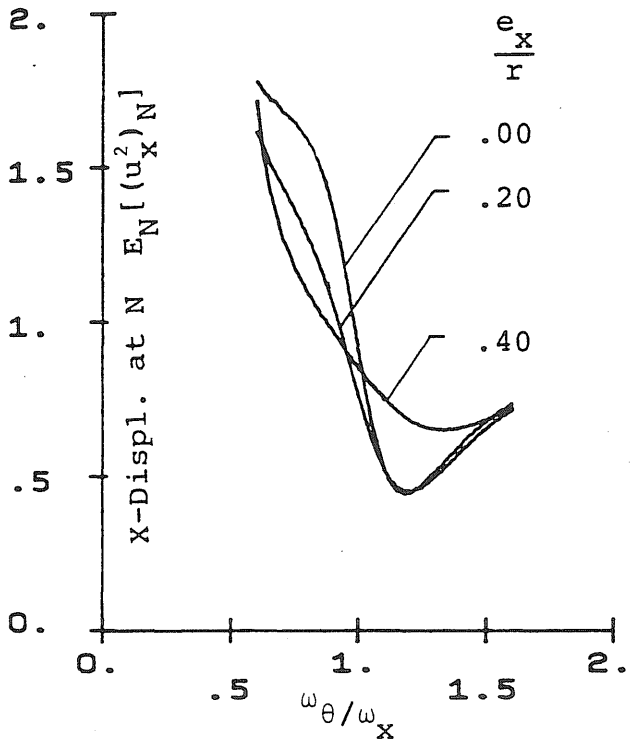

(i)

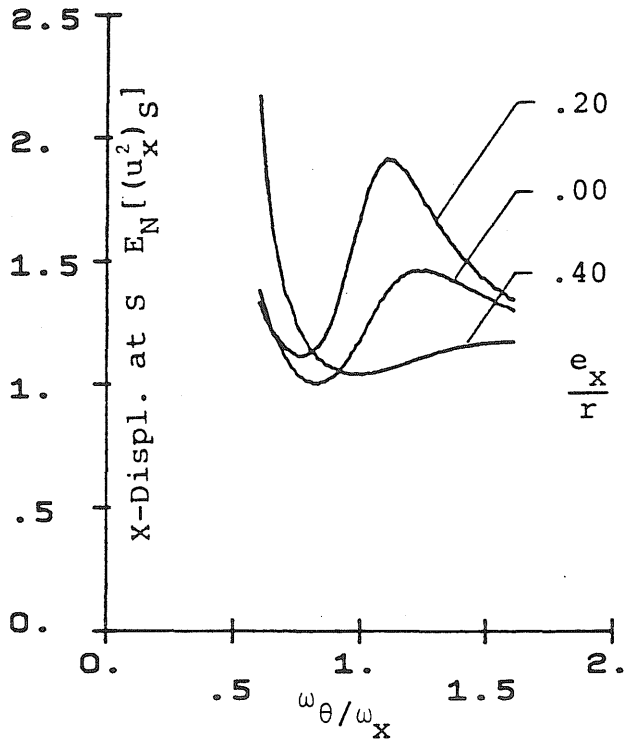

(j)

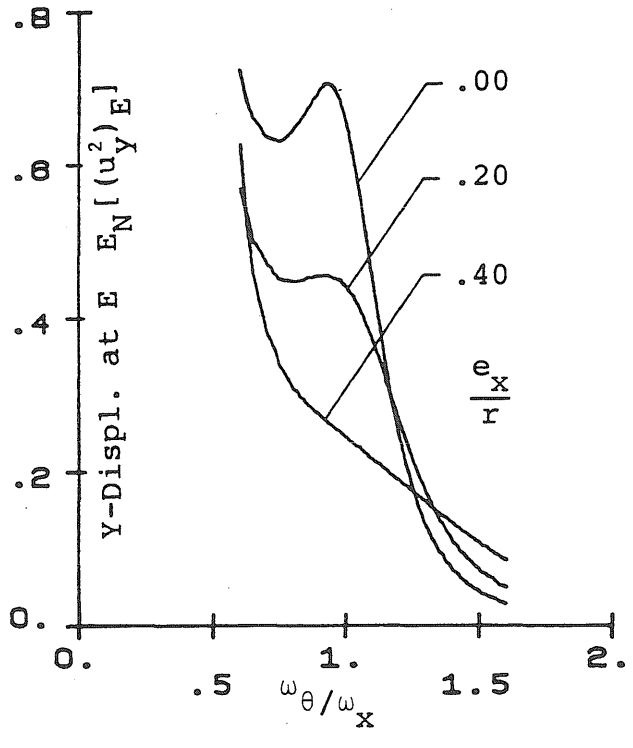

(k)

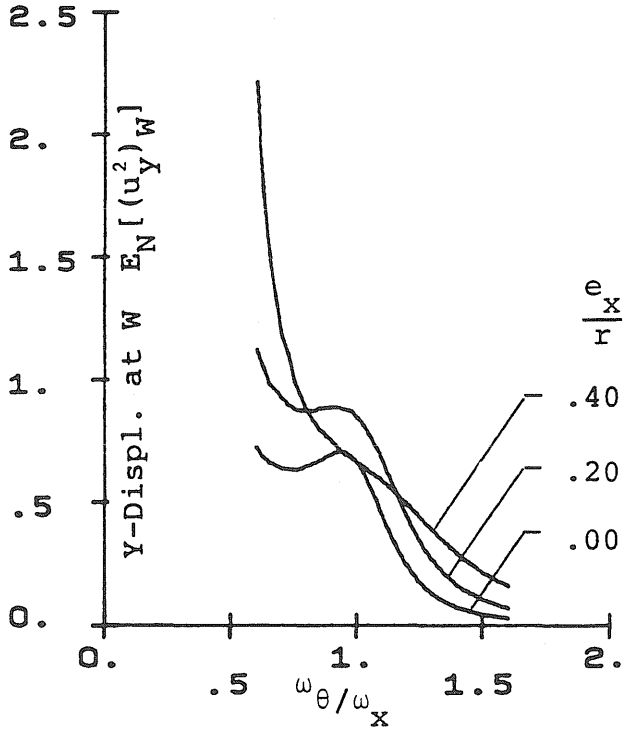

(l)

Fig. 5.16 (continued)

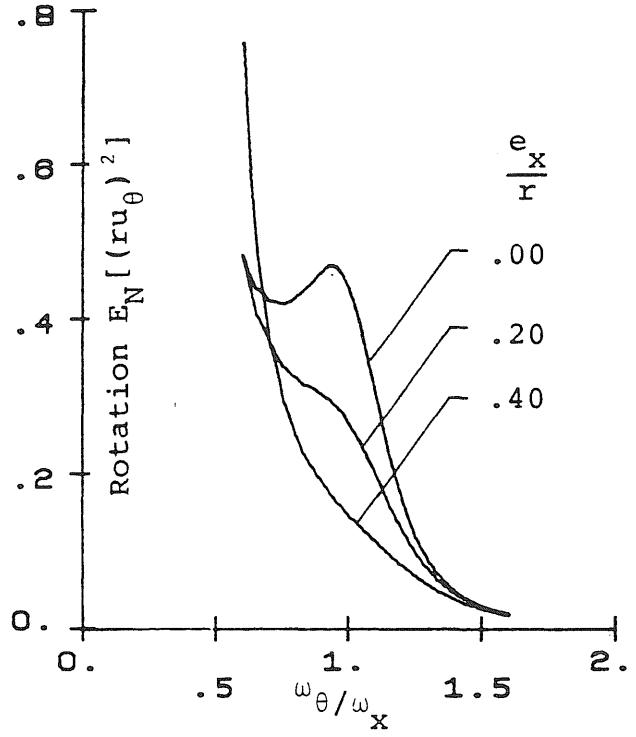

(e)

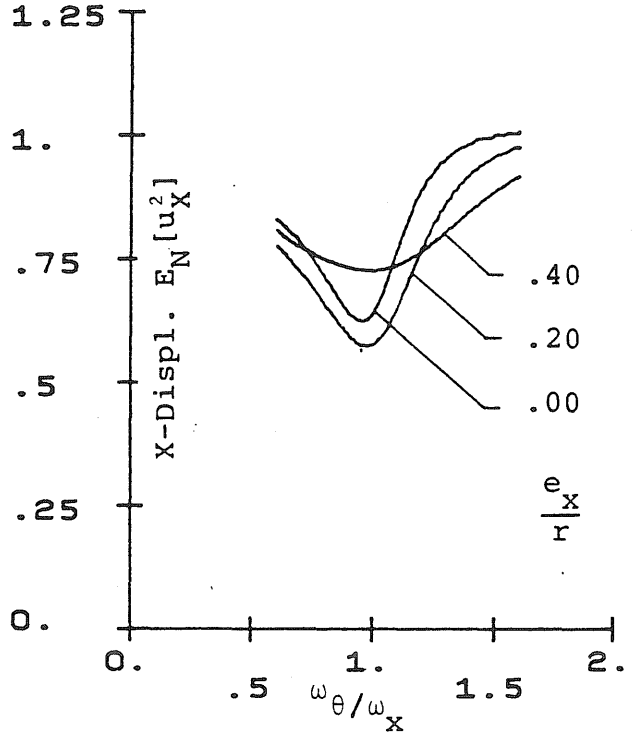

(f)

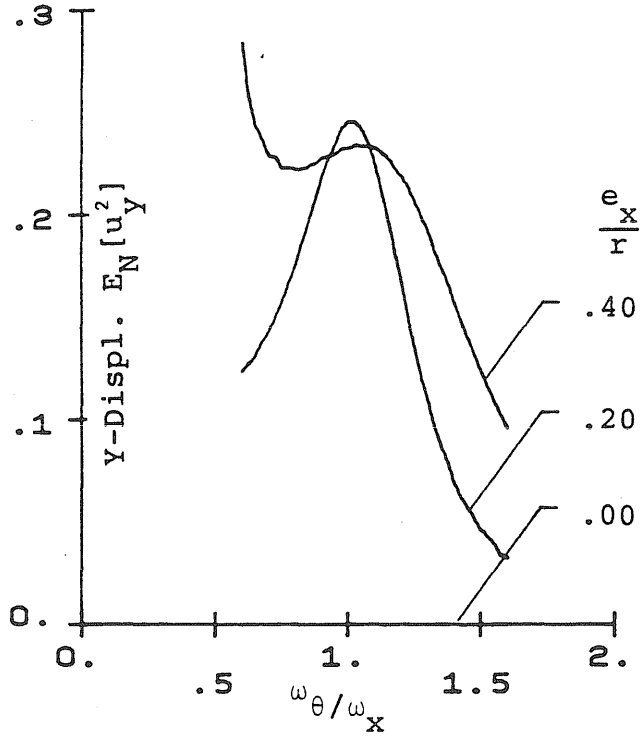

(g)

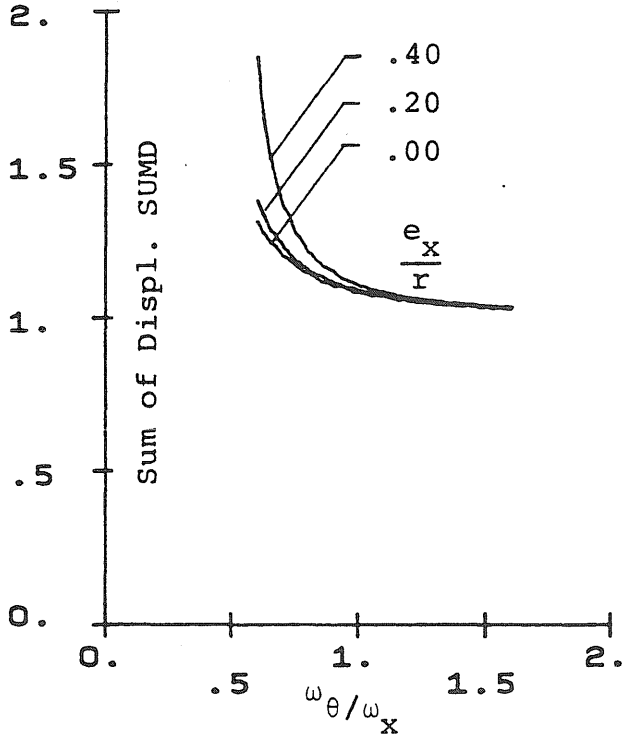

(h)

Fig. 5.16 (continued)

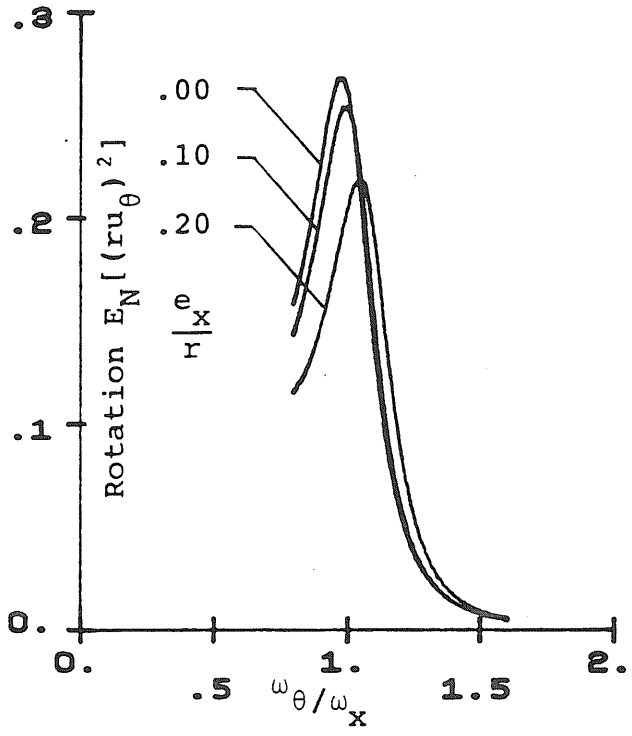

(e)

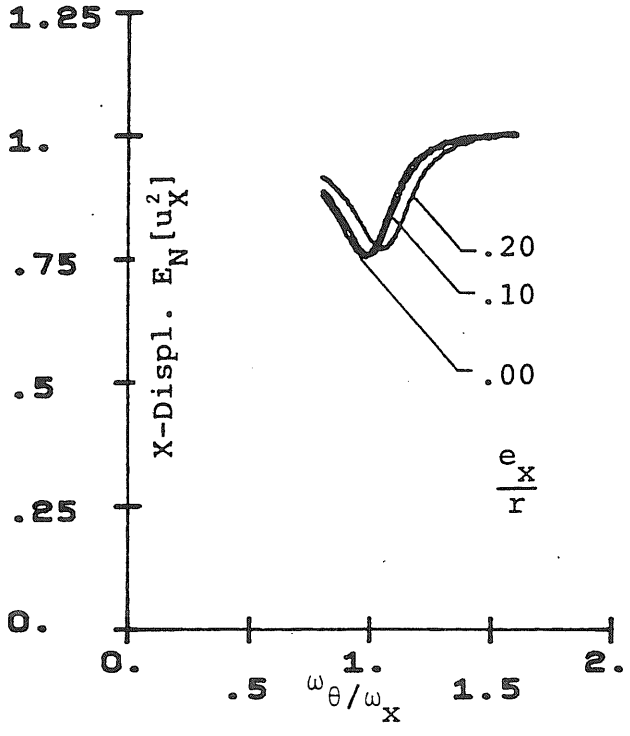

(f)

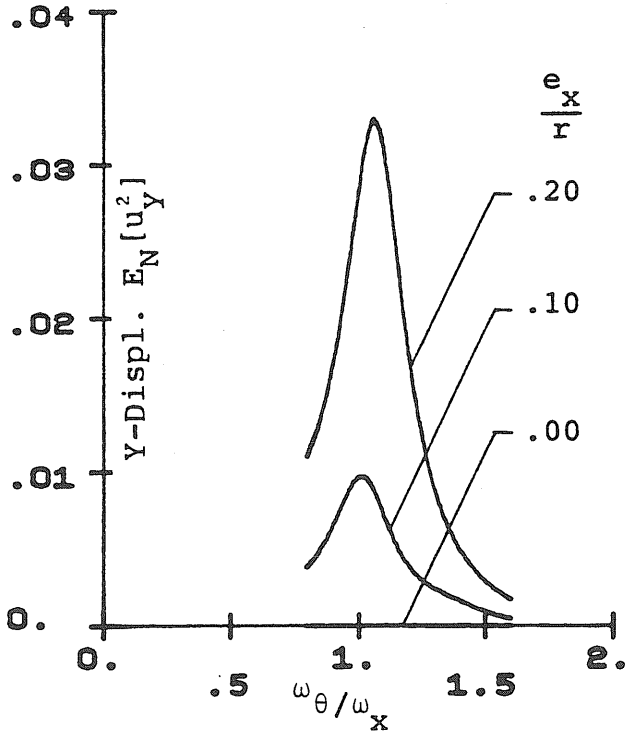

(g)

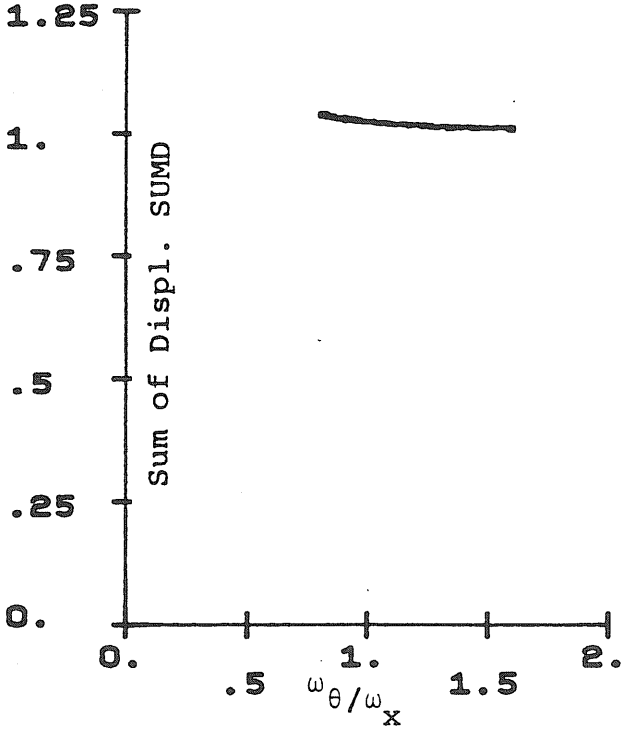

(h)

Fig. 5.17 (continued)

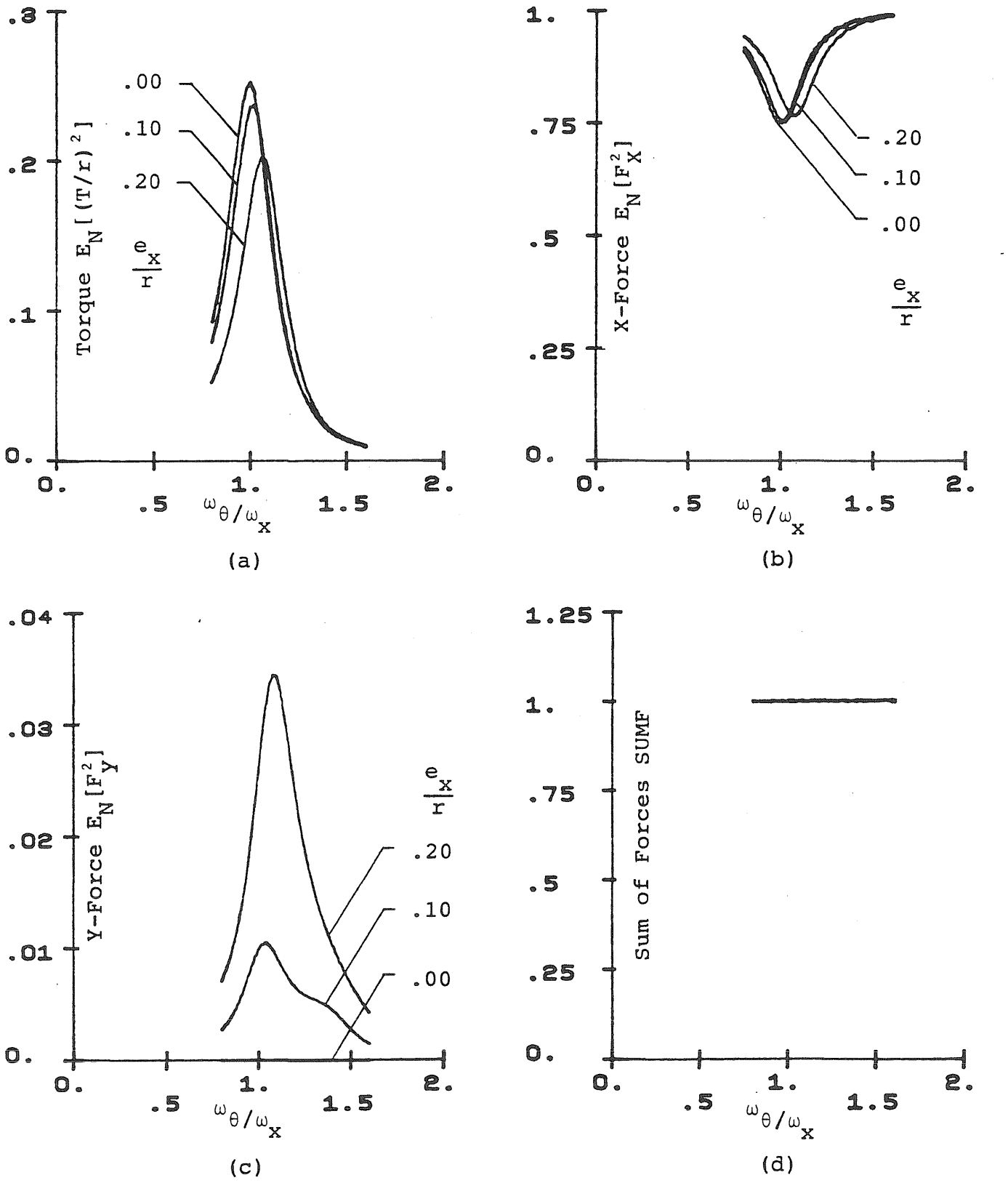

Fig. 5.17 Normalized M.S. Responses of Torsionally Coupled Systems with $\omega_y/\omega_x = \sqrt{2}$, $\frac{e_y}{r} = 0.1$ - Input: White Noise (S_x)

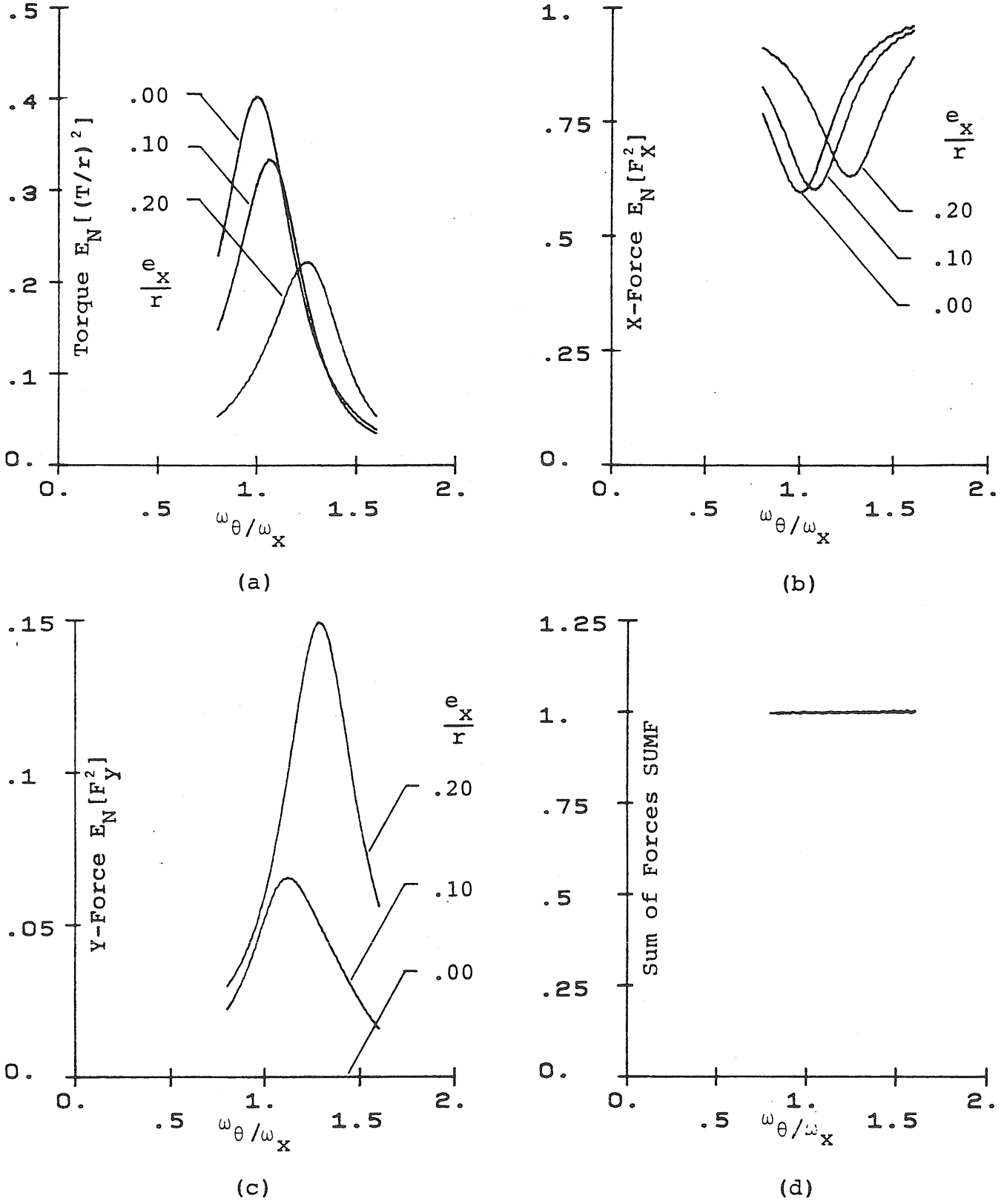

Fig. 5.18 Normalized M.S. Responses of Torsionally Coupled Systems with $\omega_y/\omega_x = \sqrt{2}$, $\frac{e_y}{r} = 0.2$ - Input: White Noise (S_x)

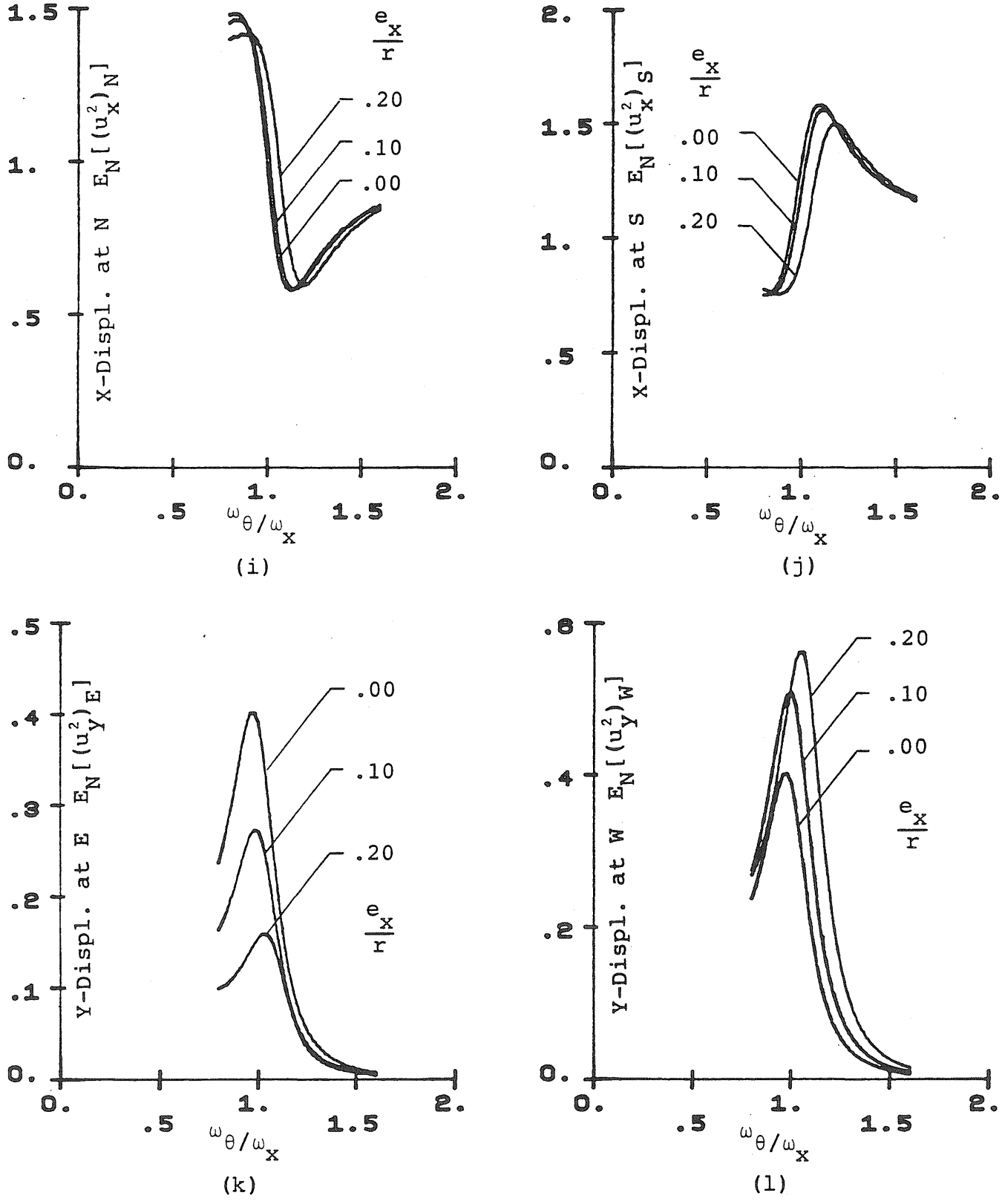

Fig. 5.17 (continued)

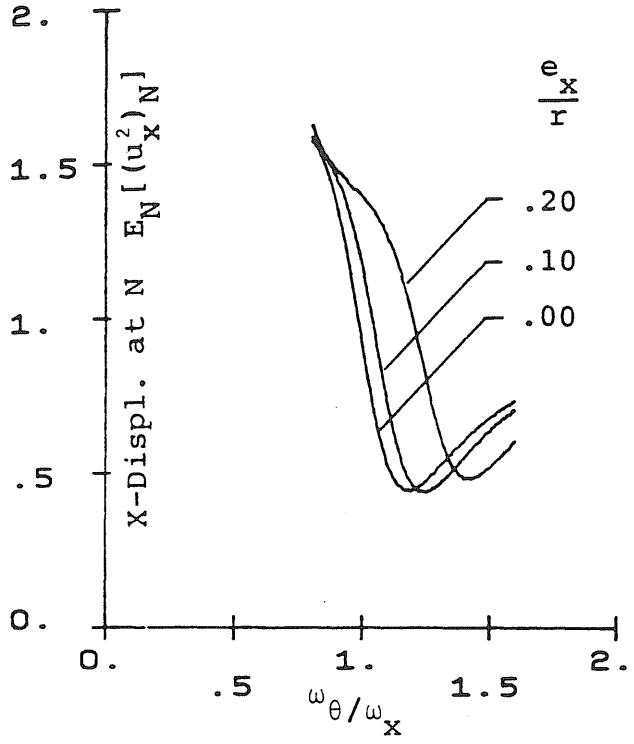

(i)

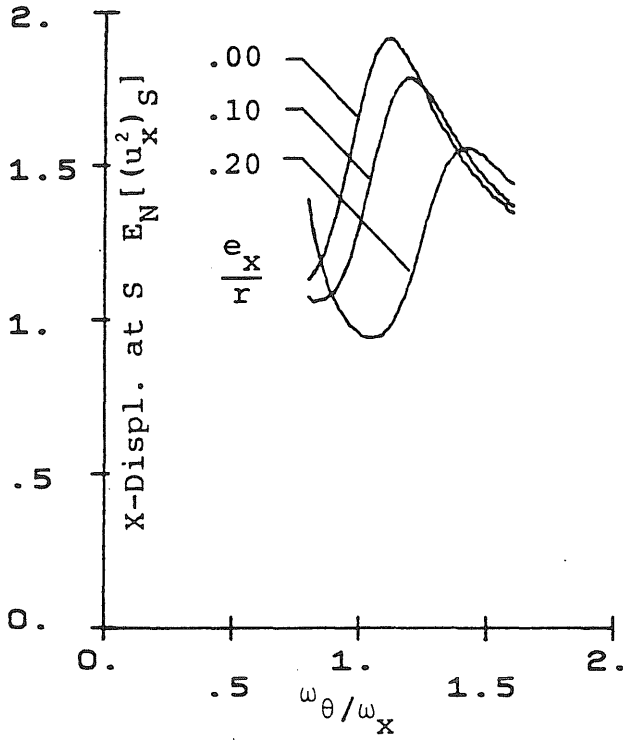

(j)

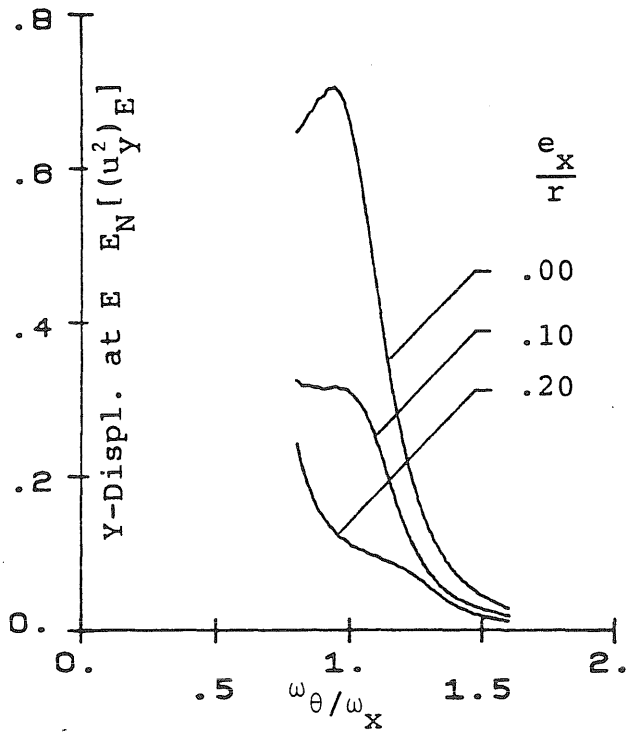

(k)

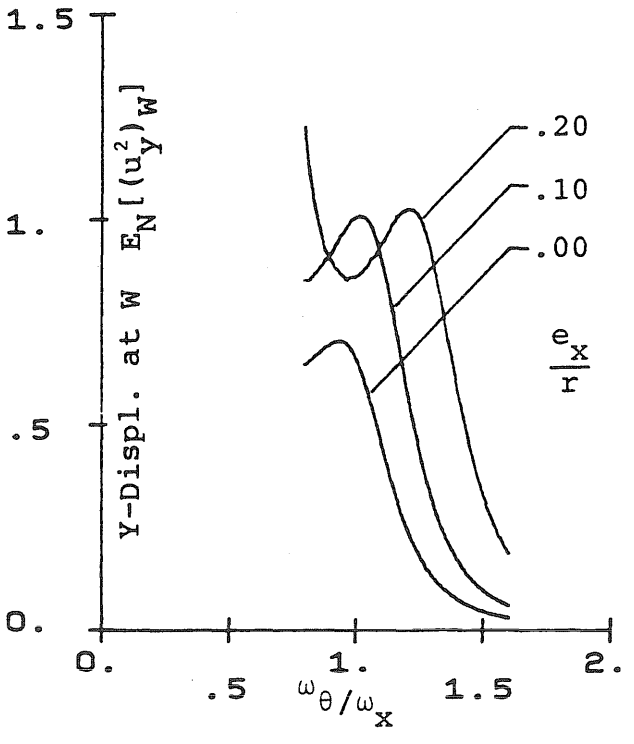

(l)

Fig. 5.18 (continued)

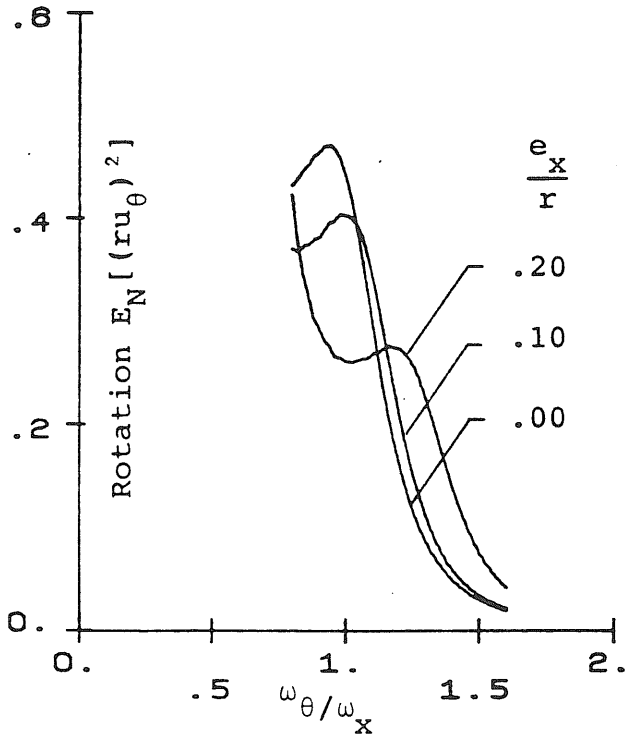

(e)

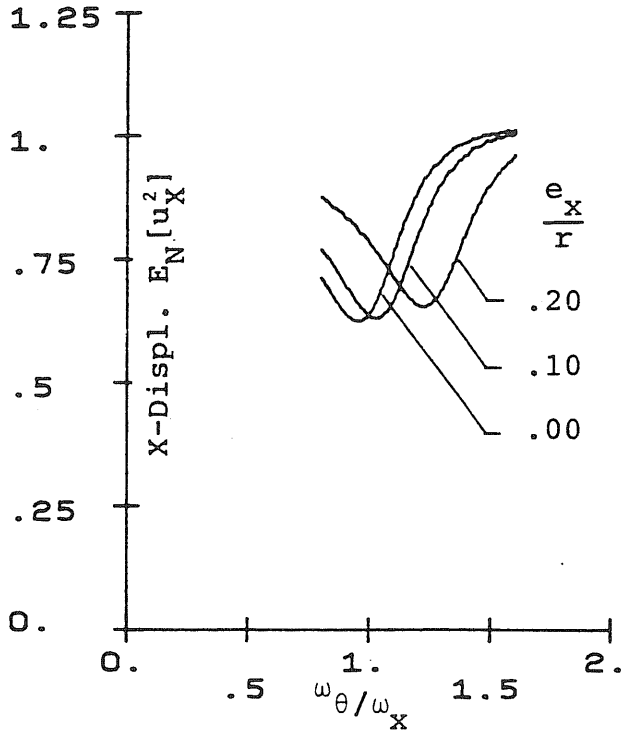

(f)

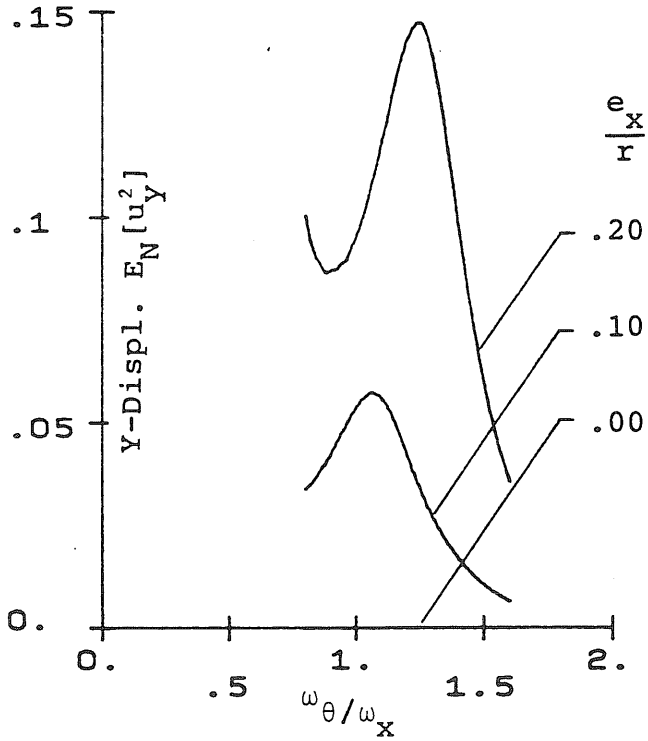

(g)

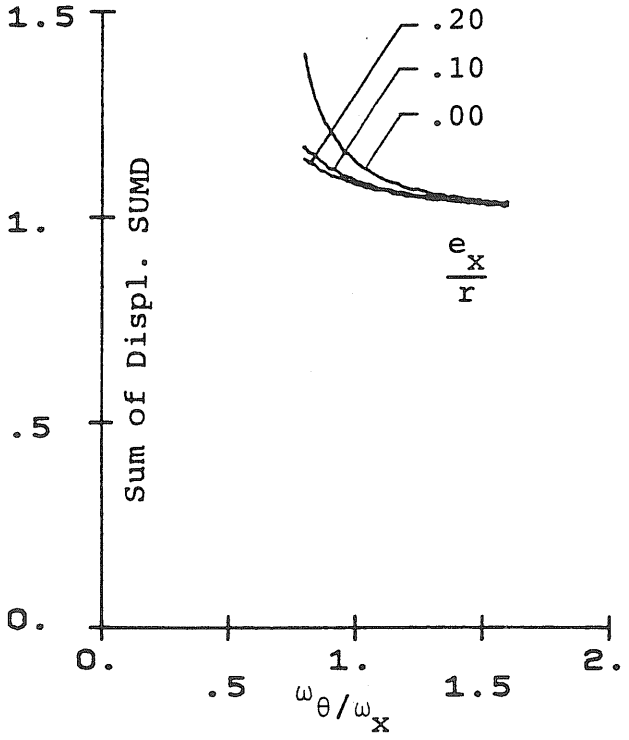

(h)

Fig. 5.18 (continued)

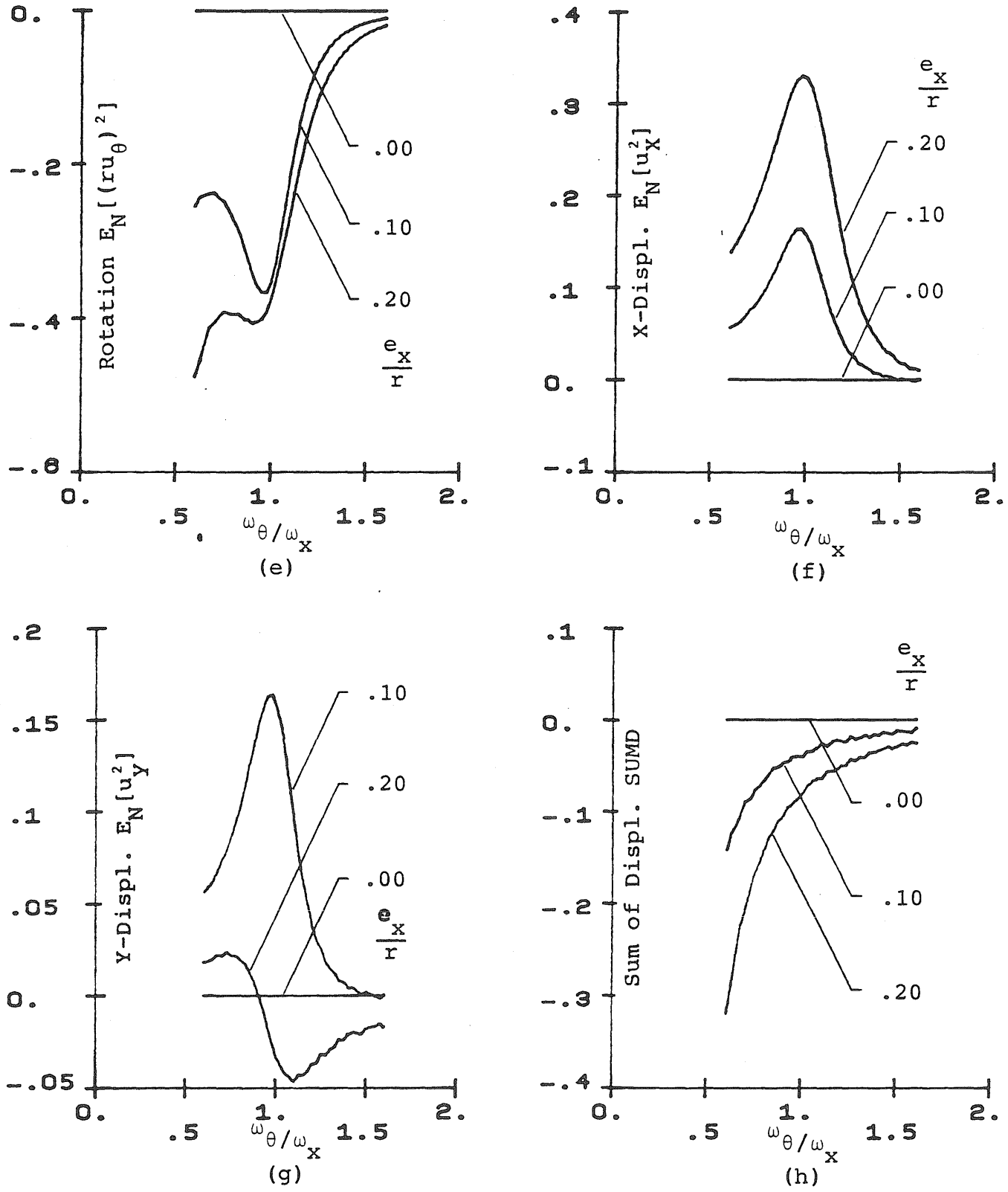

Fig. 5.19 (continued)

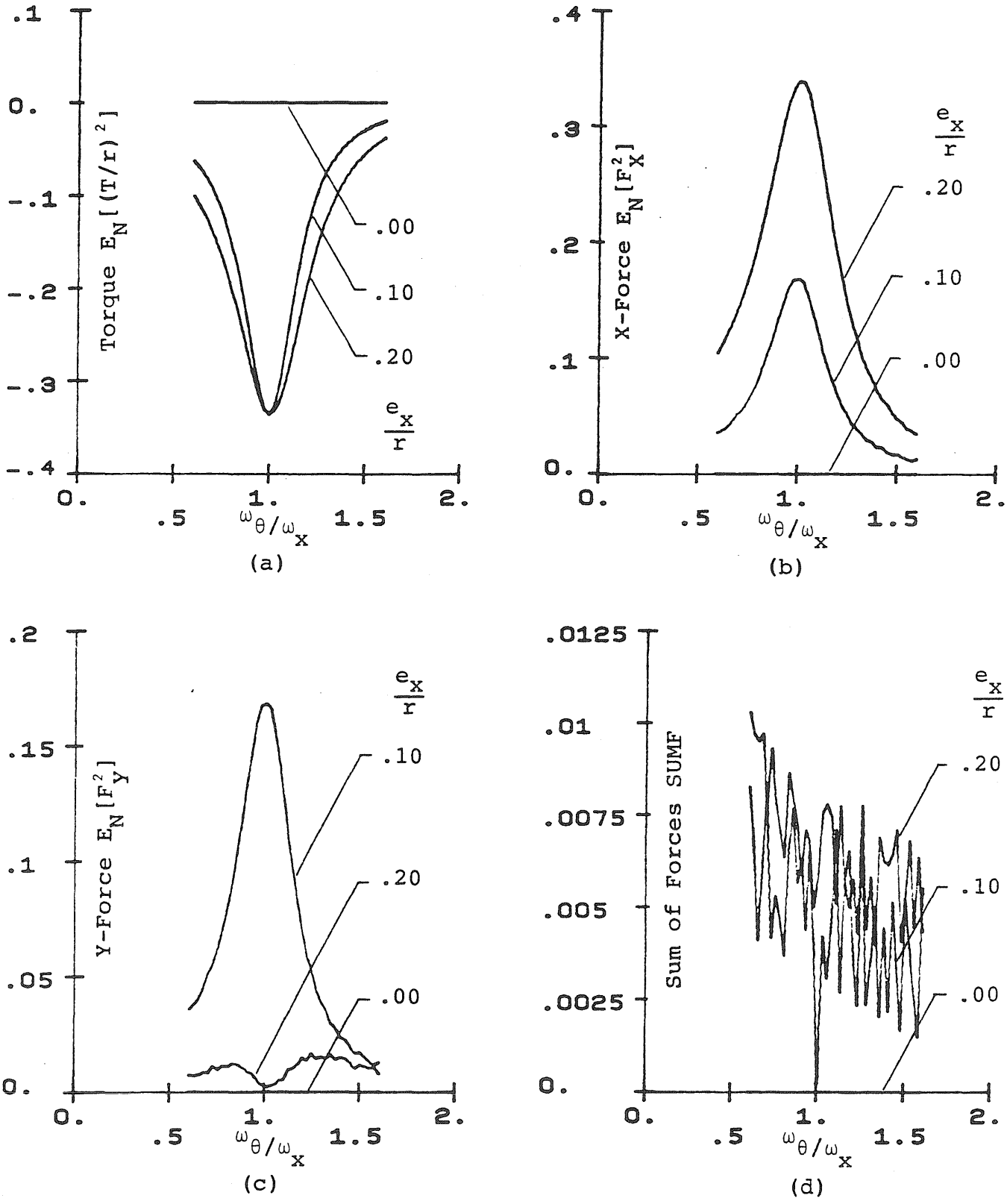

Fig. 5.19 Normalized M.S. Responses of Torsionally Coupled Systems with $\omega_y/\omega_x = 1$, $\frac{e_y}{r} = 0.1$ - Input: White Noise (S_{xy})

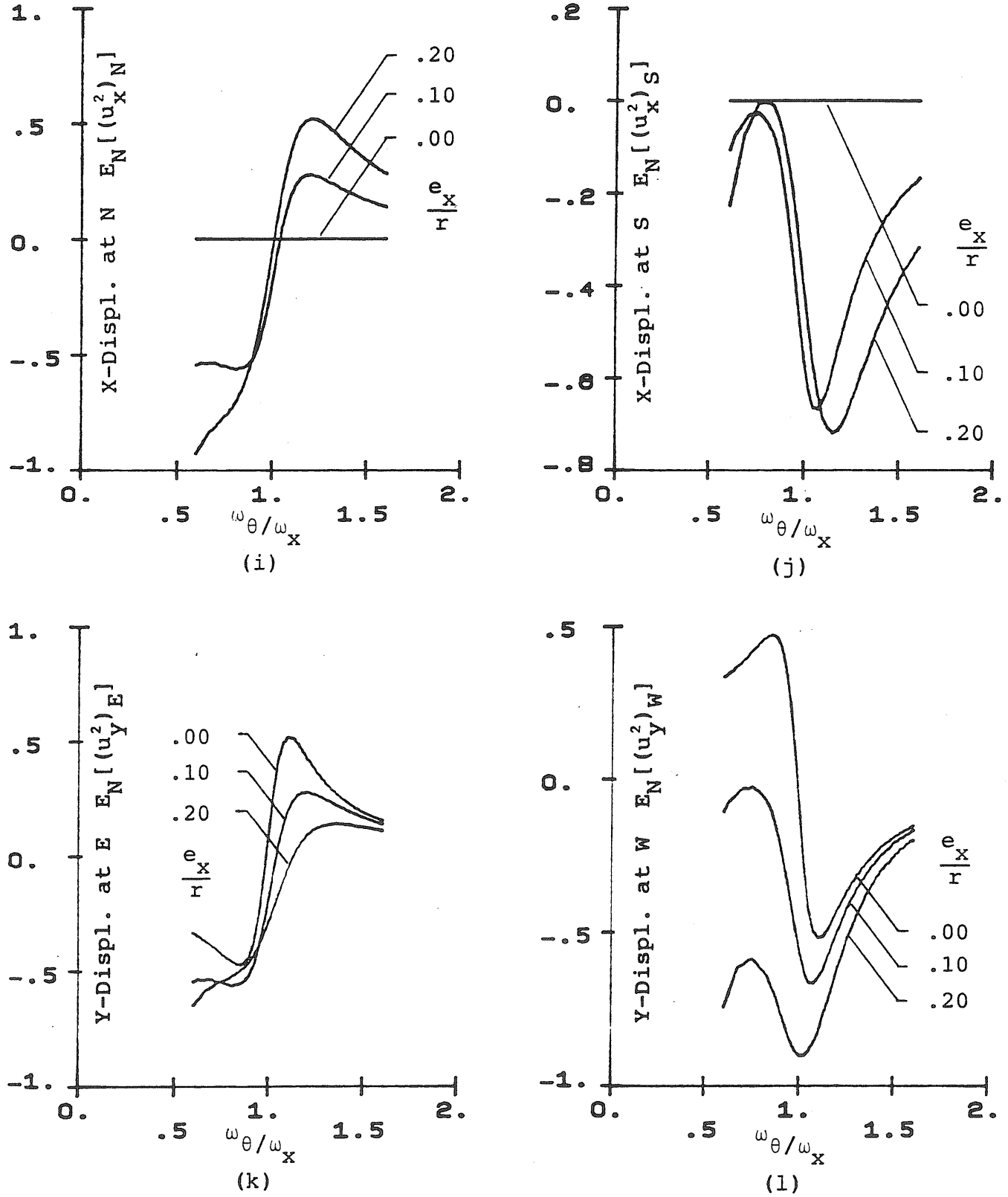

Fig. 5.19 (continued)

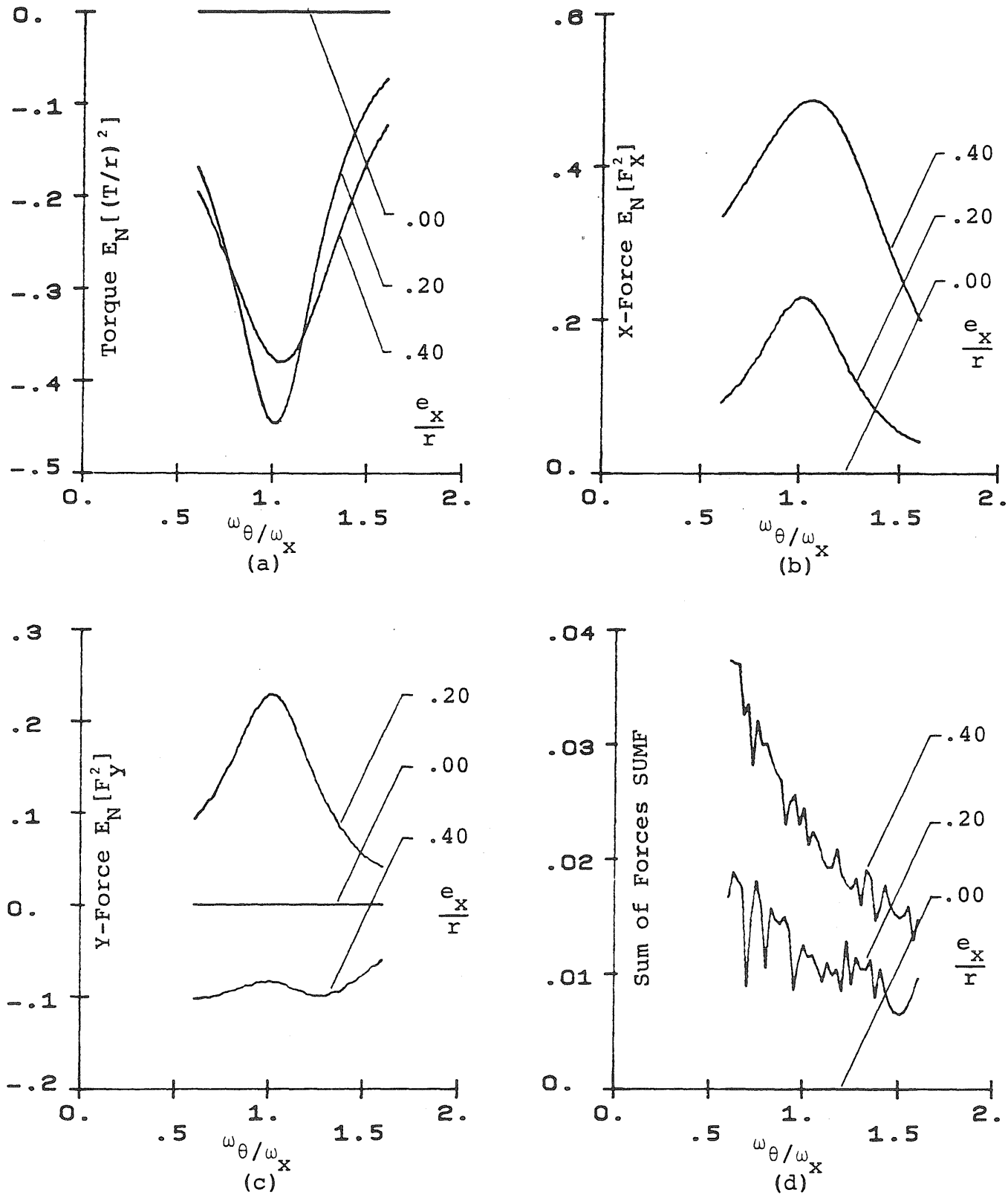

Fig. 5.20 Normalized M.S. Responses of Torsionally Coupled Systems with $\omega_y/\omega_x = 1$, $\frac{e_y}{r} = 0.2$ - Input: White Noise(S_{xy})

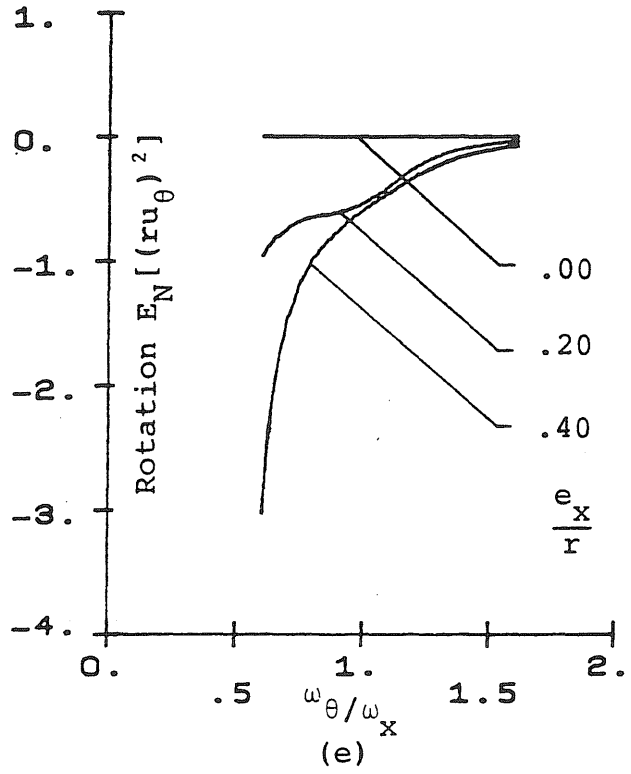

(e)

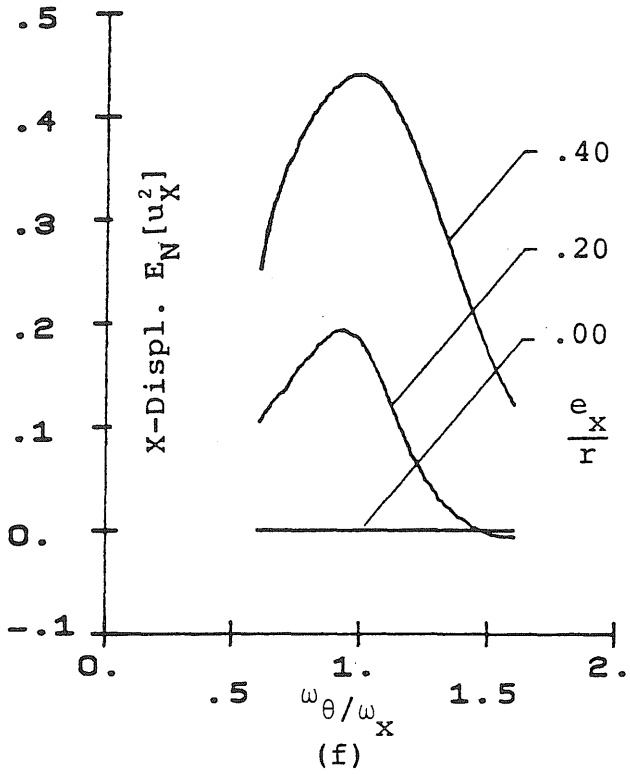

(f)

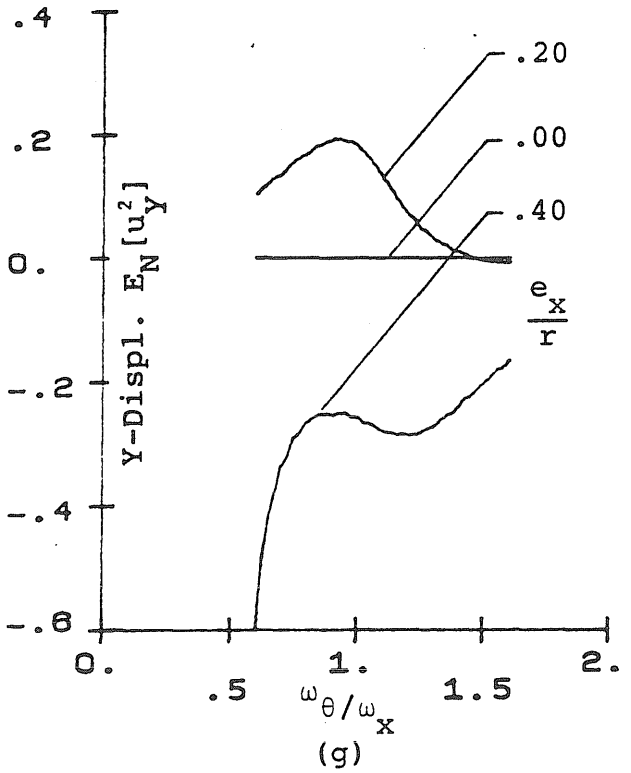

(g)

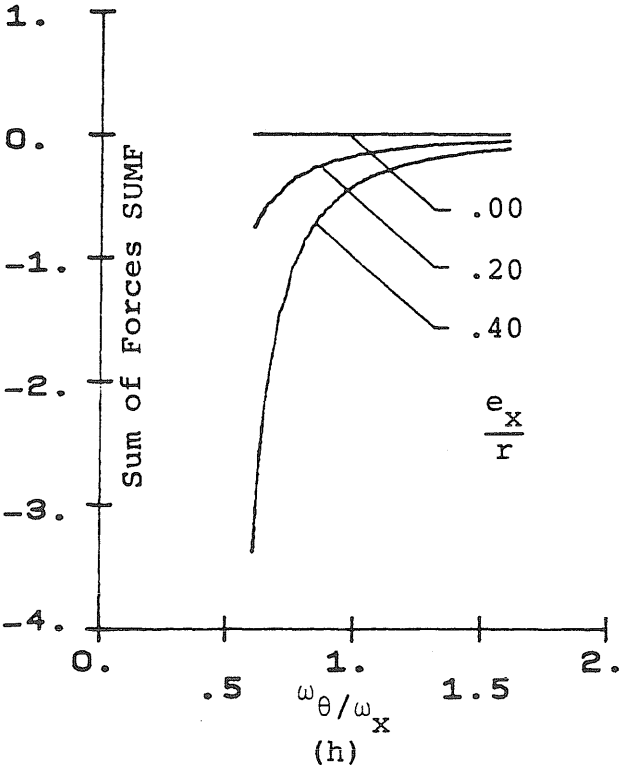

(h)

Fig. 5.20 (continued)

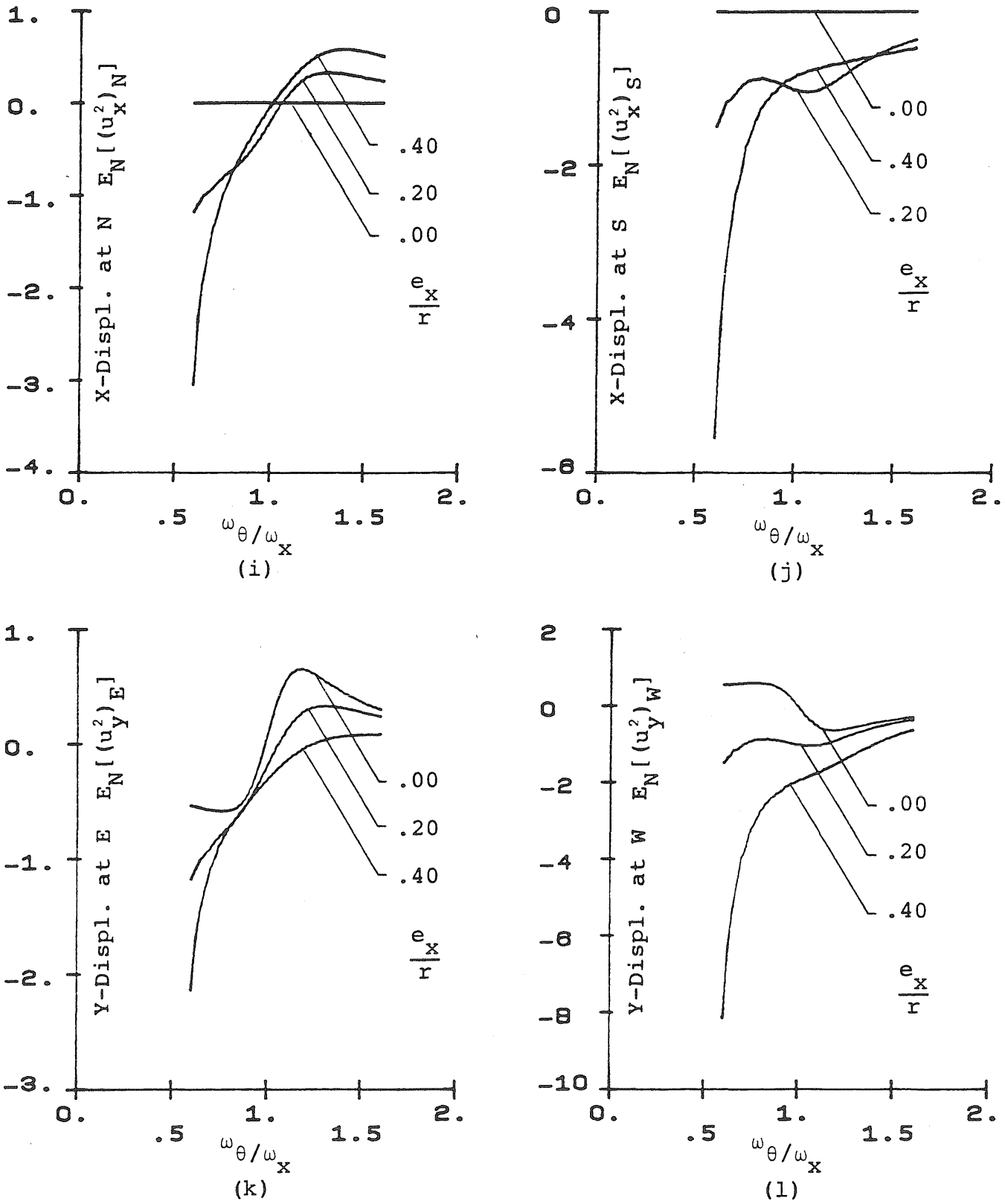

Fig. 5.20 (continued)

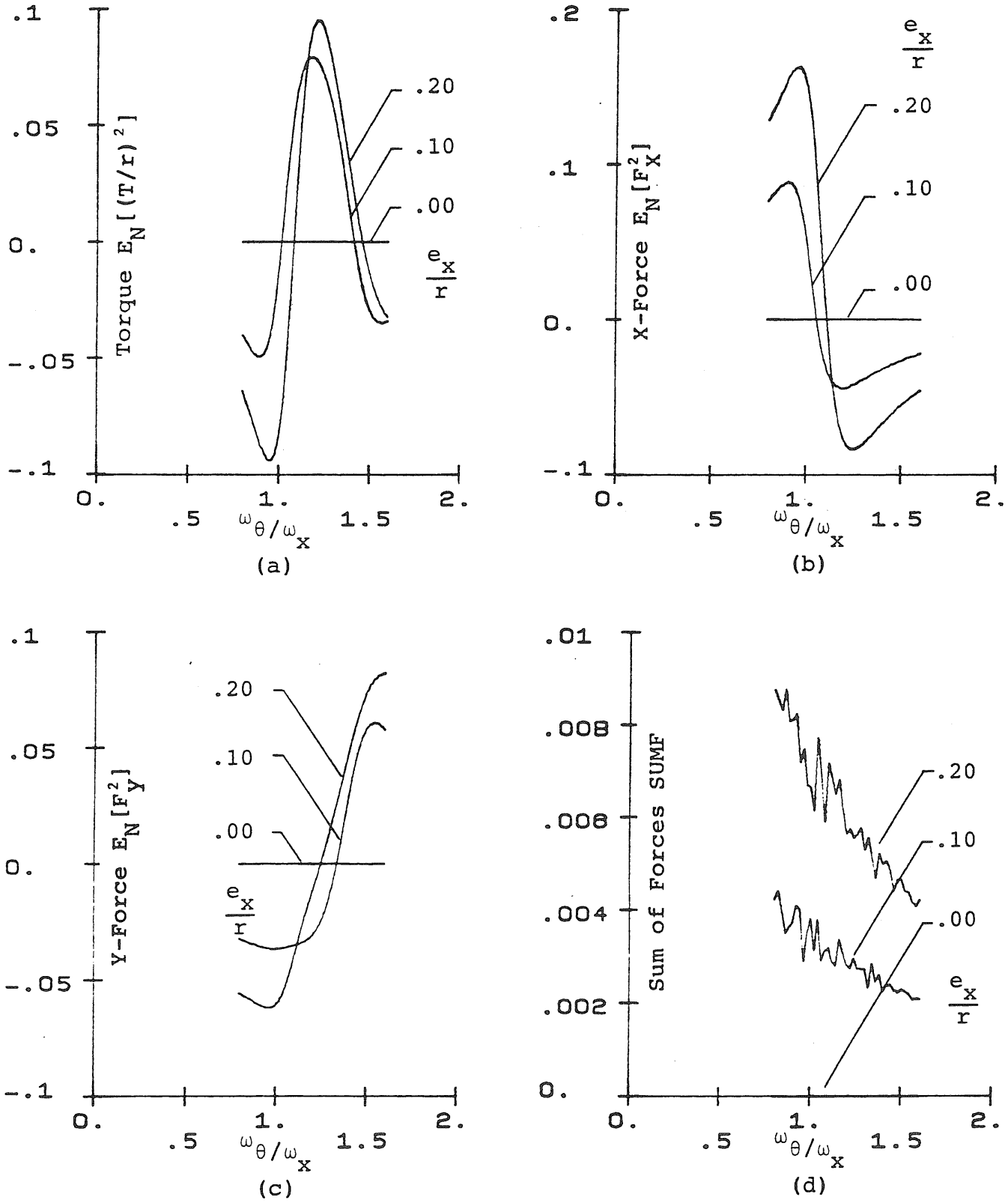

Fig. 5.21 Normalized M.S. Responses of Torsionally Coupled Systems with $\omega_y/\omega_x = \sqrt{2}$, $\frac{e_y}{r} = 0.1$ - Input: White Noise(S_{xy})

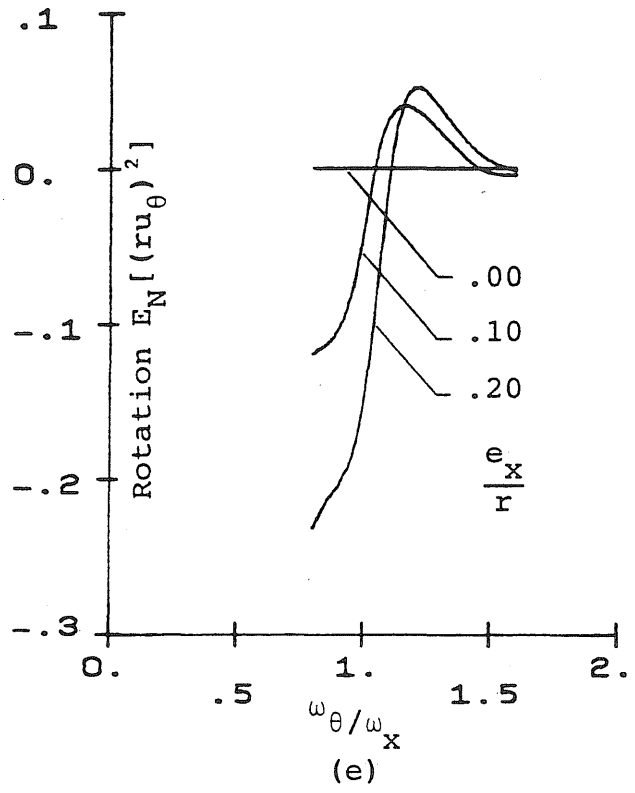

(e)

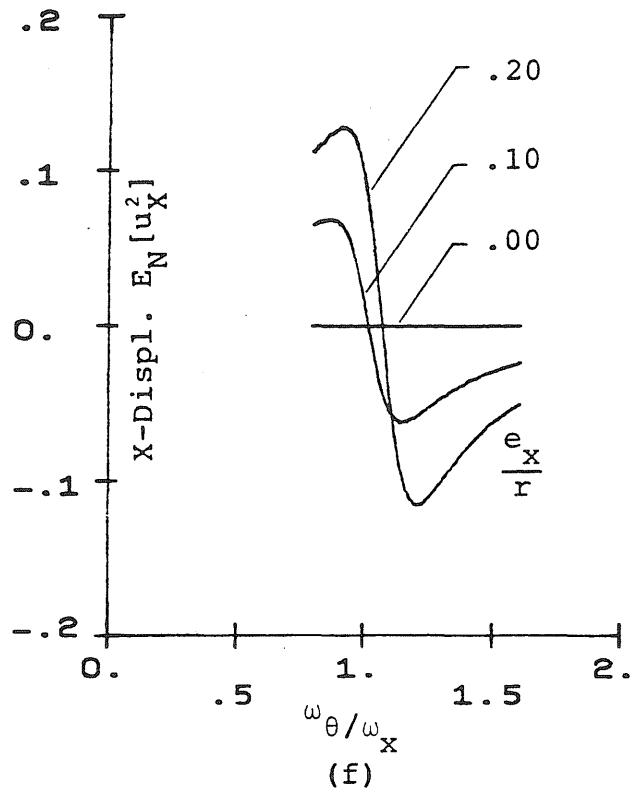

(f)

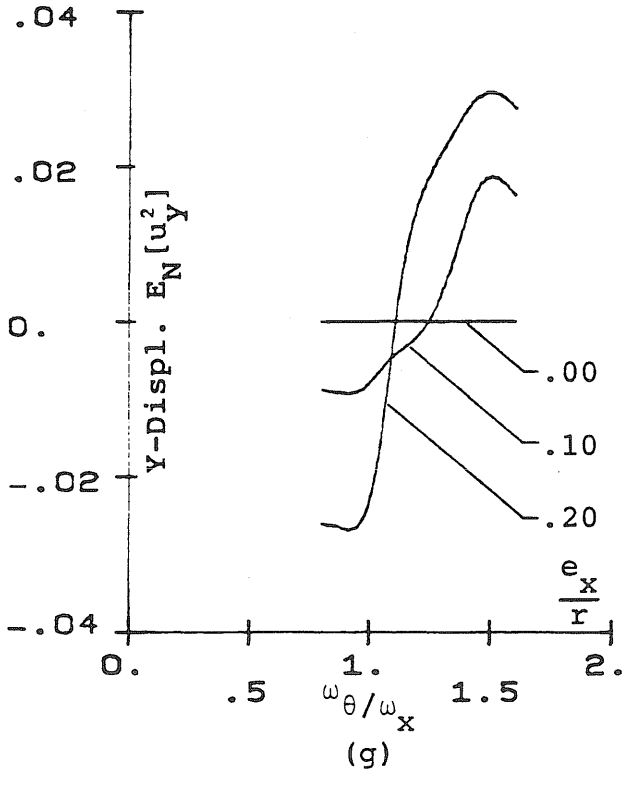

(g)

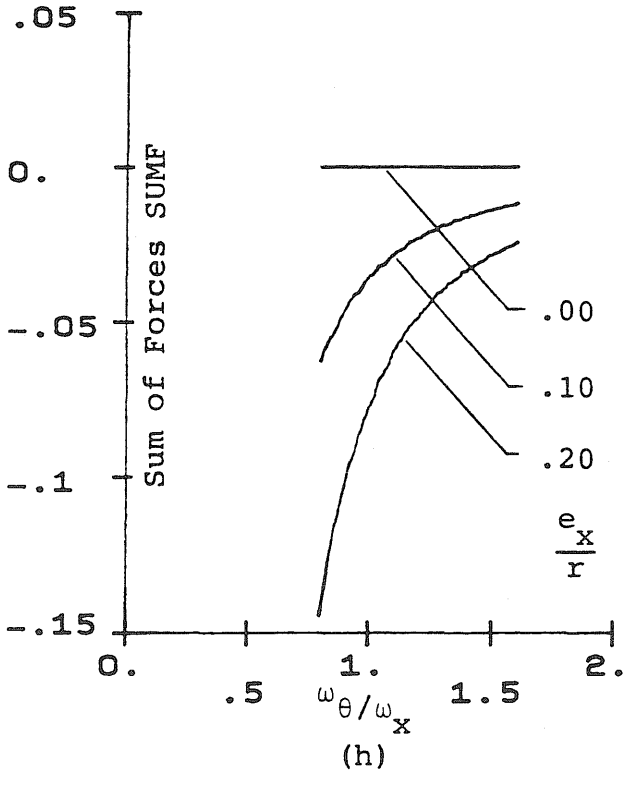

(h)

Fig. 5.21 (continued)

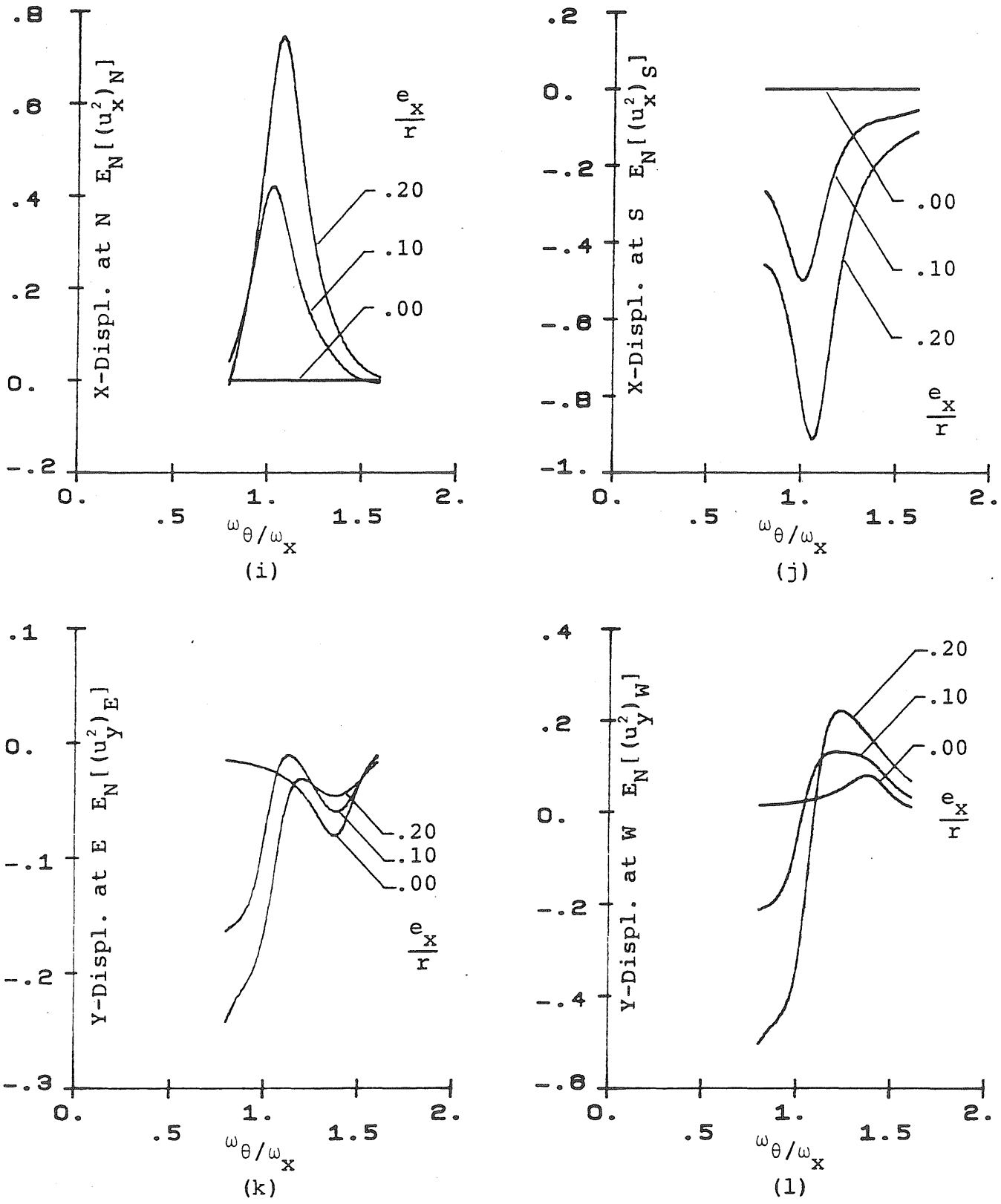

Fig. 5.21 (continued)

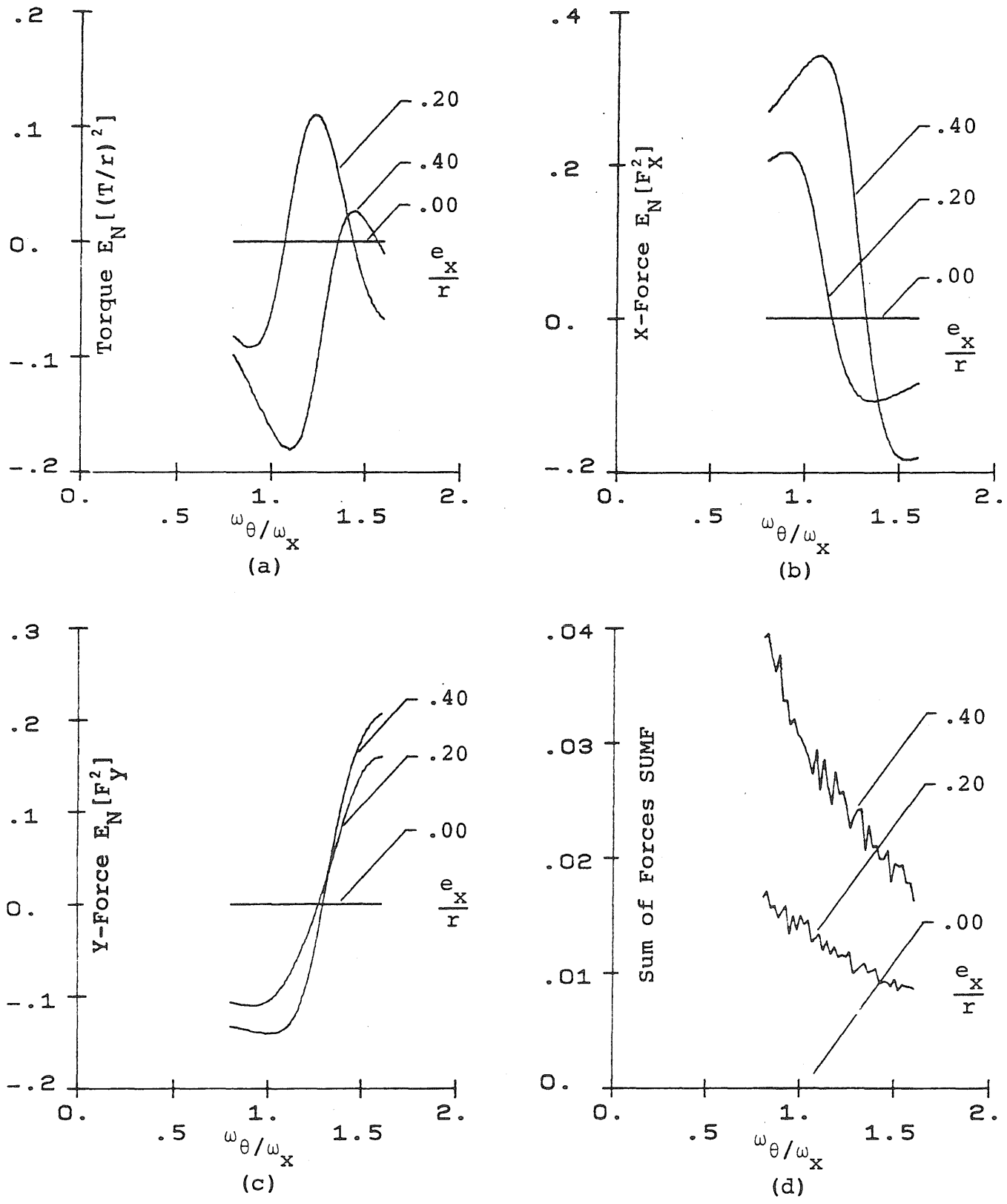

Fig. 5.22 Normalized M.S. Responses of Torsionally Coupled Systems with $\omega_y/\omega_x = \sqrt{2}$, $\frac{e_y}{r} = 0.2$ - Input: White Noise(S_{xy})

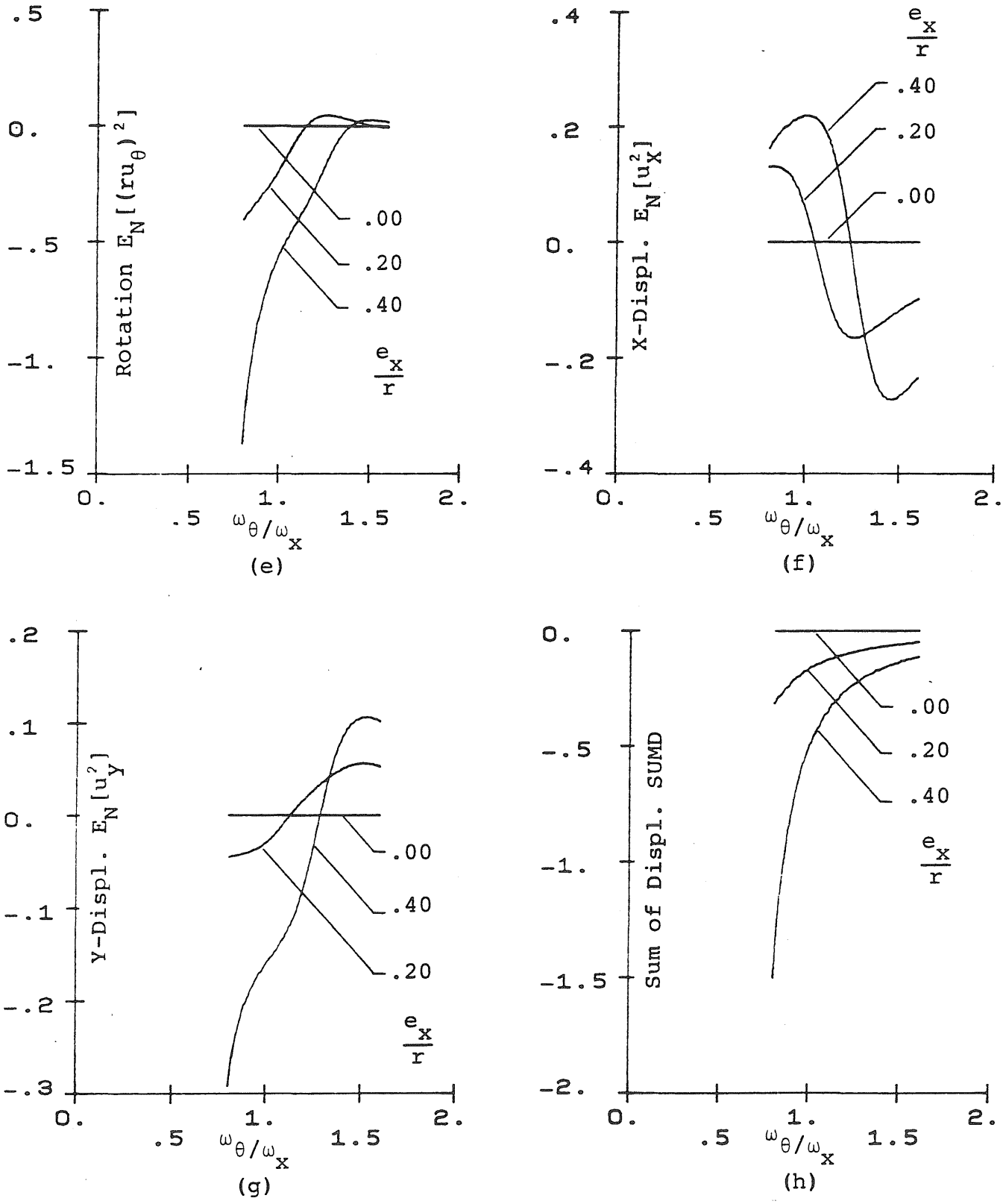

Fig. 5.22 (continued)

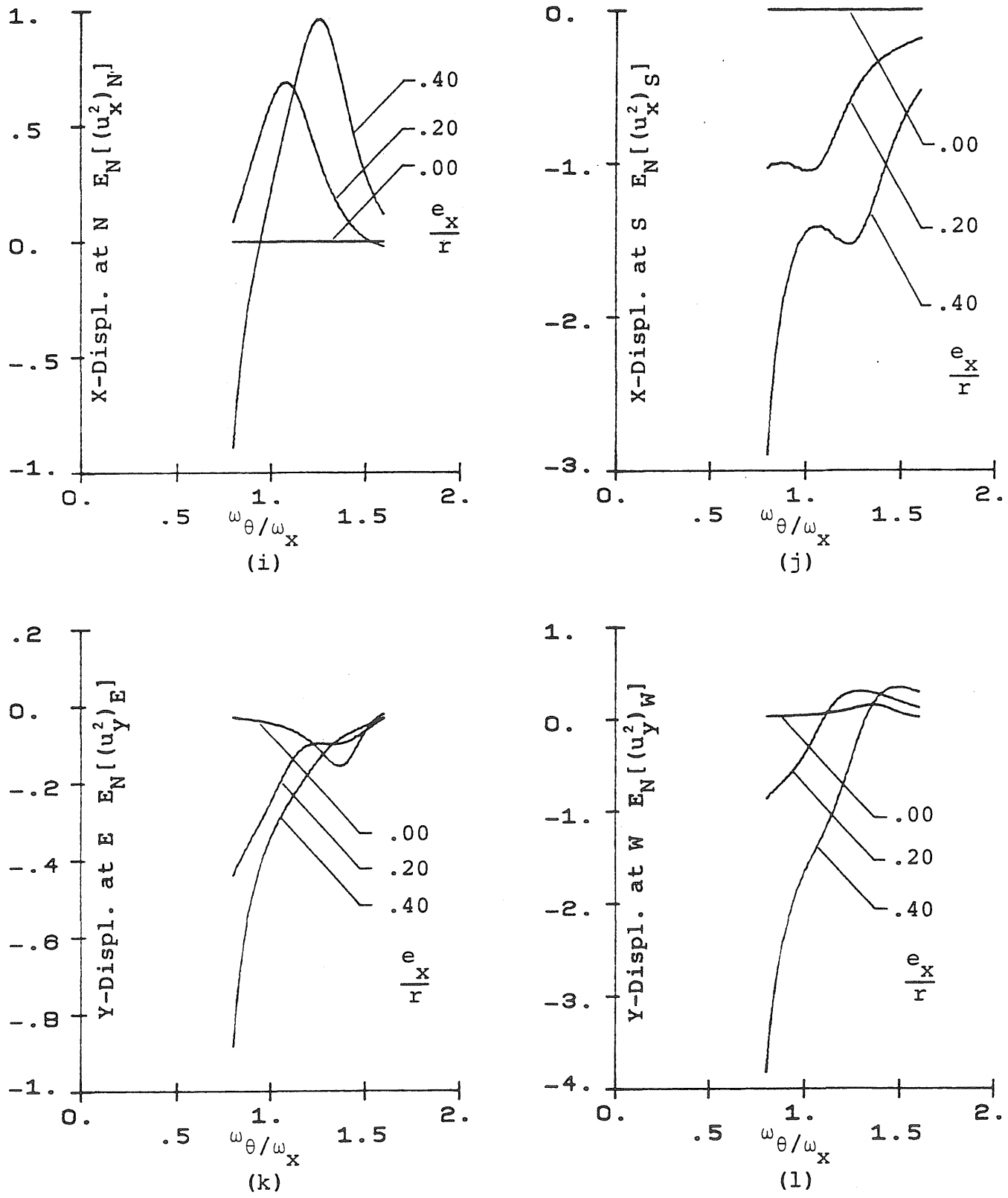

Fig. 5.22 (continued)

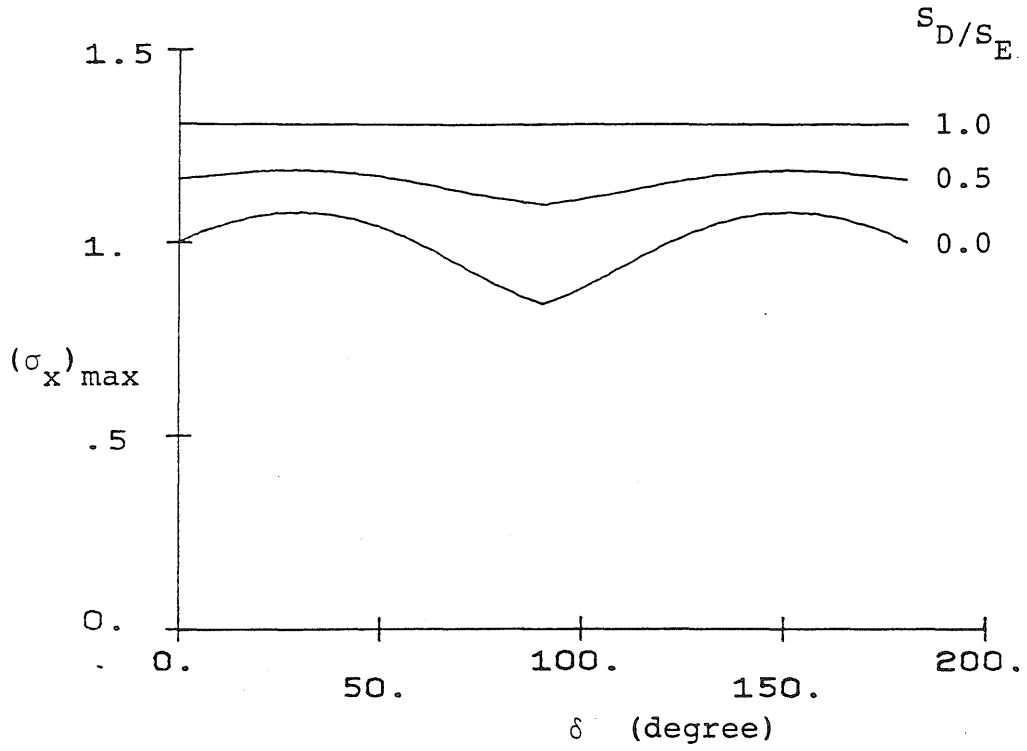

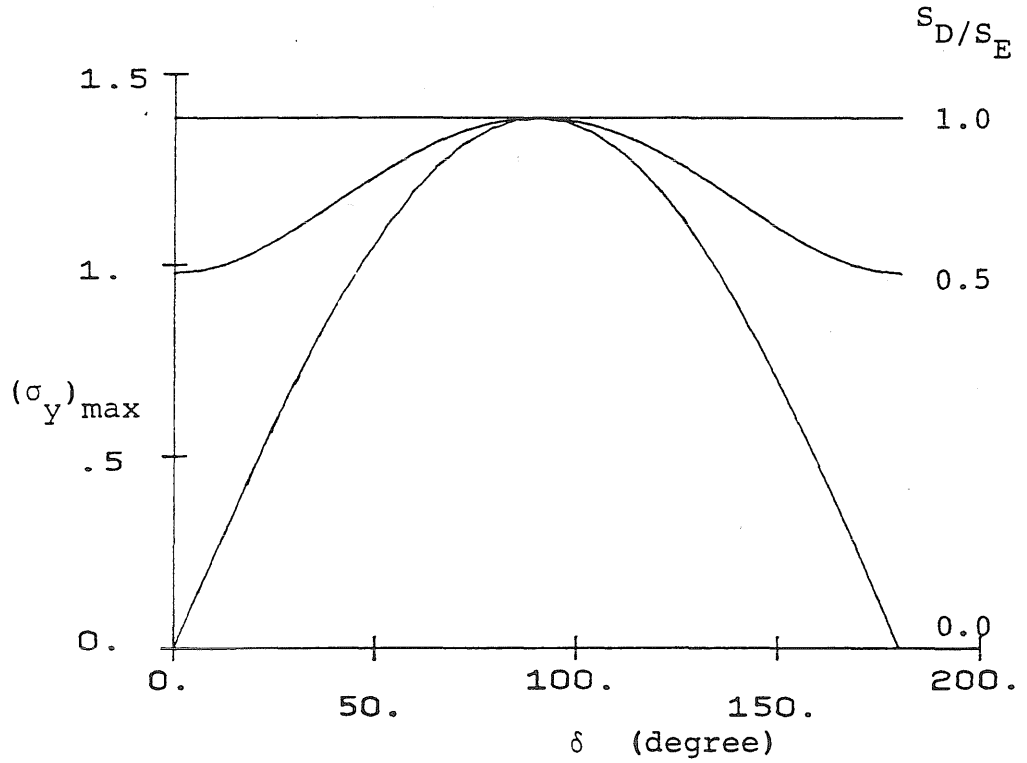

Fig. 5.23 $(\sigma_x)_{max}$ and $(\sigma_y)_{max}$ for Torsionally Coupled Systems with $e_x/r = 0.2$, $e_y/r = 0.0$, $\omega_y/\omega_x = 1$, $a/b = 1$

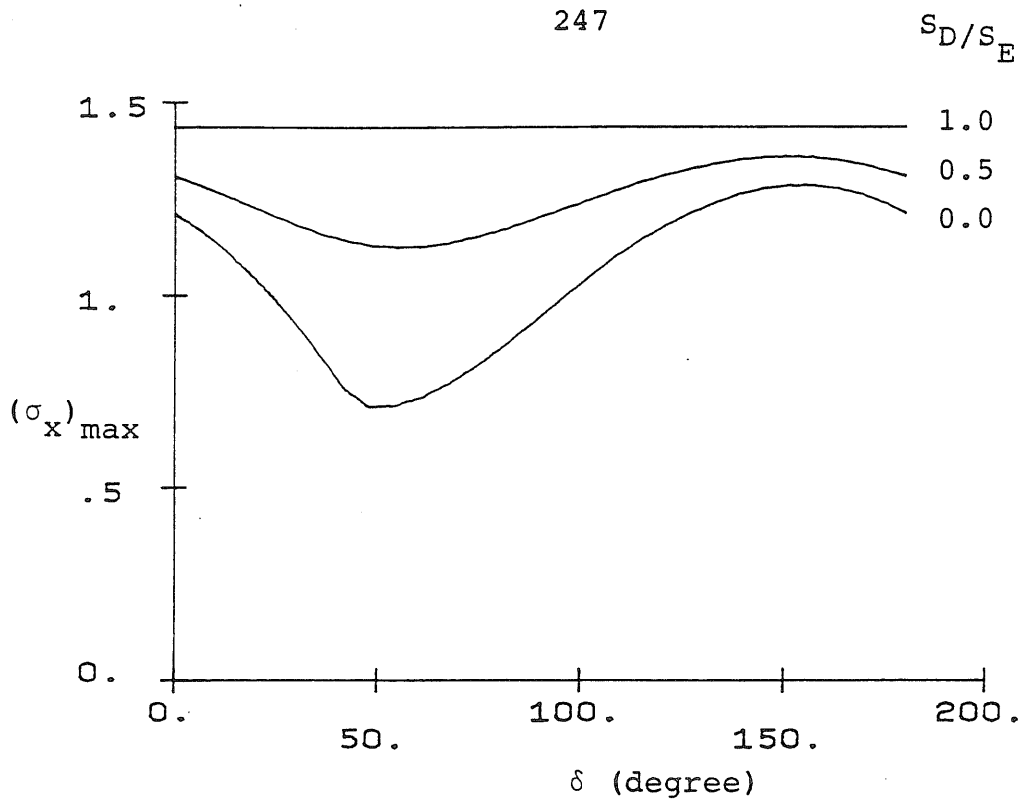

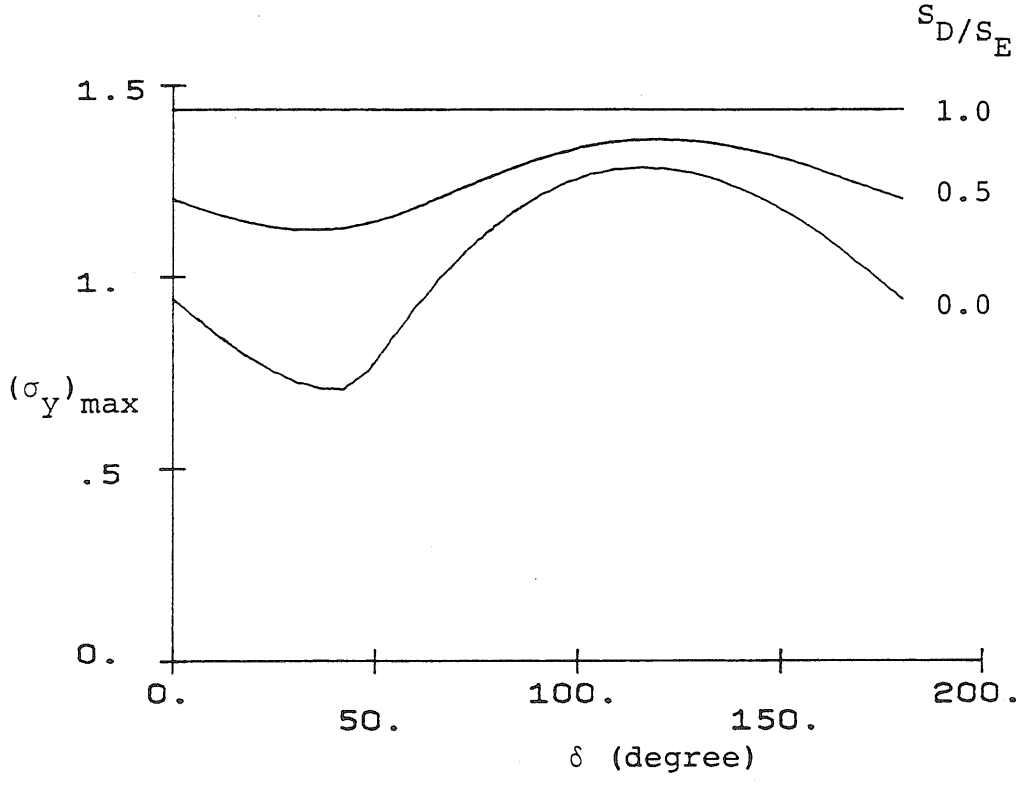

Fig. 5.24 $(\sigma_x)_{max}$ and $(\sigma_y)_{max}$ for Torsionally Coupled Systems with $e_x/r = 0.2$, $e_y/r = 0.2$, $\omega_y/\omega_x = 1$, $a/b = 1$

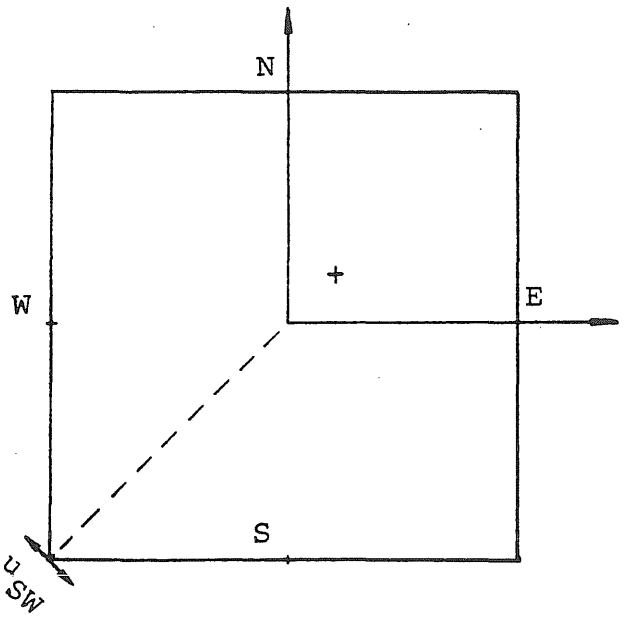

Fig. 5.25 Displacement Response at South-West Corner

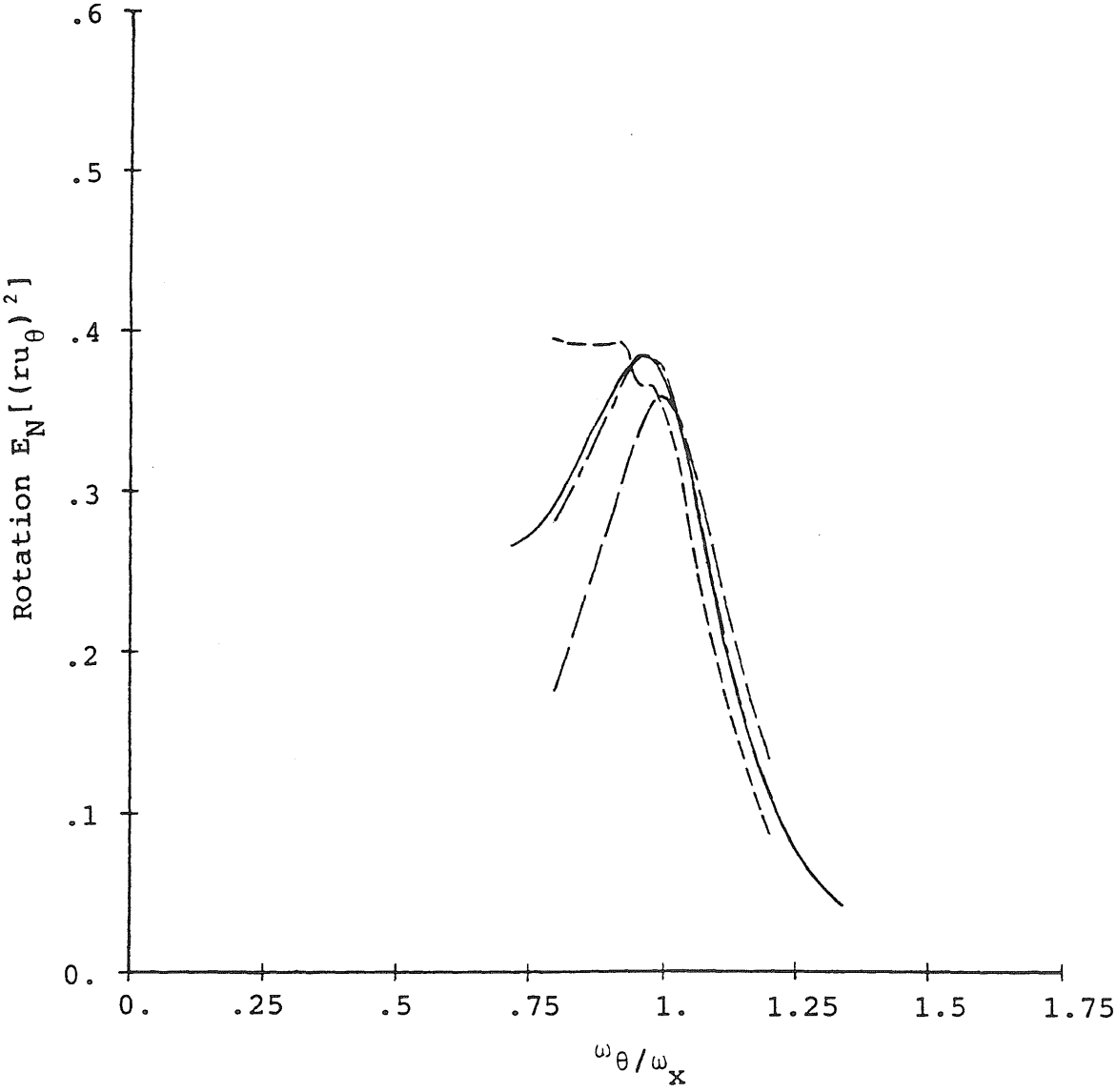

Legend:
——— Stationary White
— — f_x = 0.2 cps
— - — f_x = 1.0 cps
– – – – f_x = 5.0 cps

Fig. 5.26 Normalized Rotational Response of a Torsionally Coupled System with $\frac{e_y}{r}$ = 0.15. Input: Stationary Clough-Penzien Spectrum [No. 2 in Fig. 2.7]

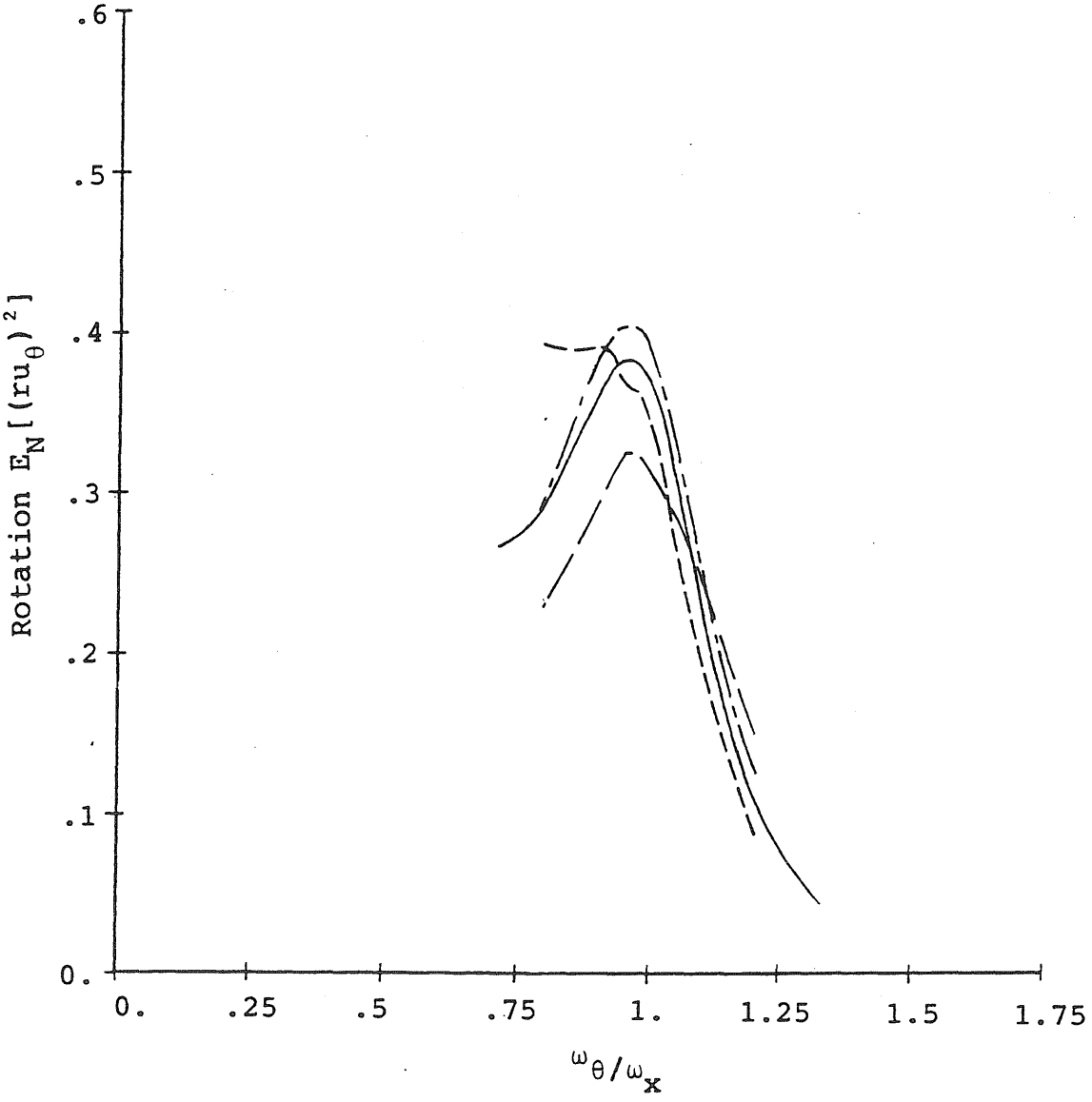

Legend:
- ——— Stationary White
- — — f_x = 0.2 cps
- —·— f_x = 1.0 cps
- – – – f_x = 5.0 cps

Fig. 5.27 Normalized Rotational Response of a Torsionally Coupled System with $\frac{e_y}{r}$ = 0.15. Input: Nonstationary Clough-Penzien Spectrum [No. 2 in Fig. 2.7]

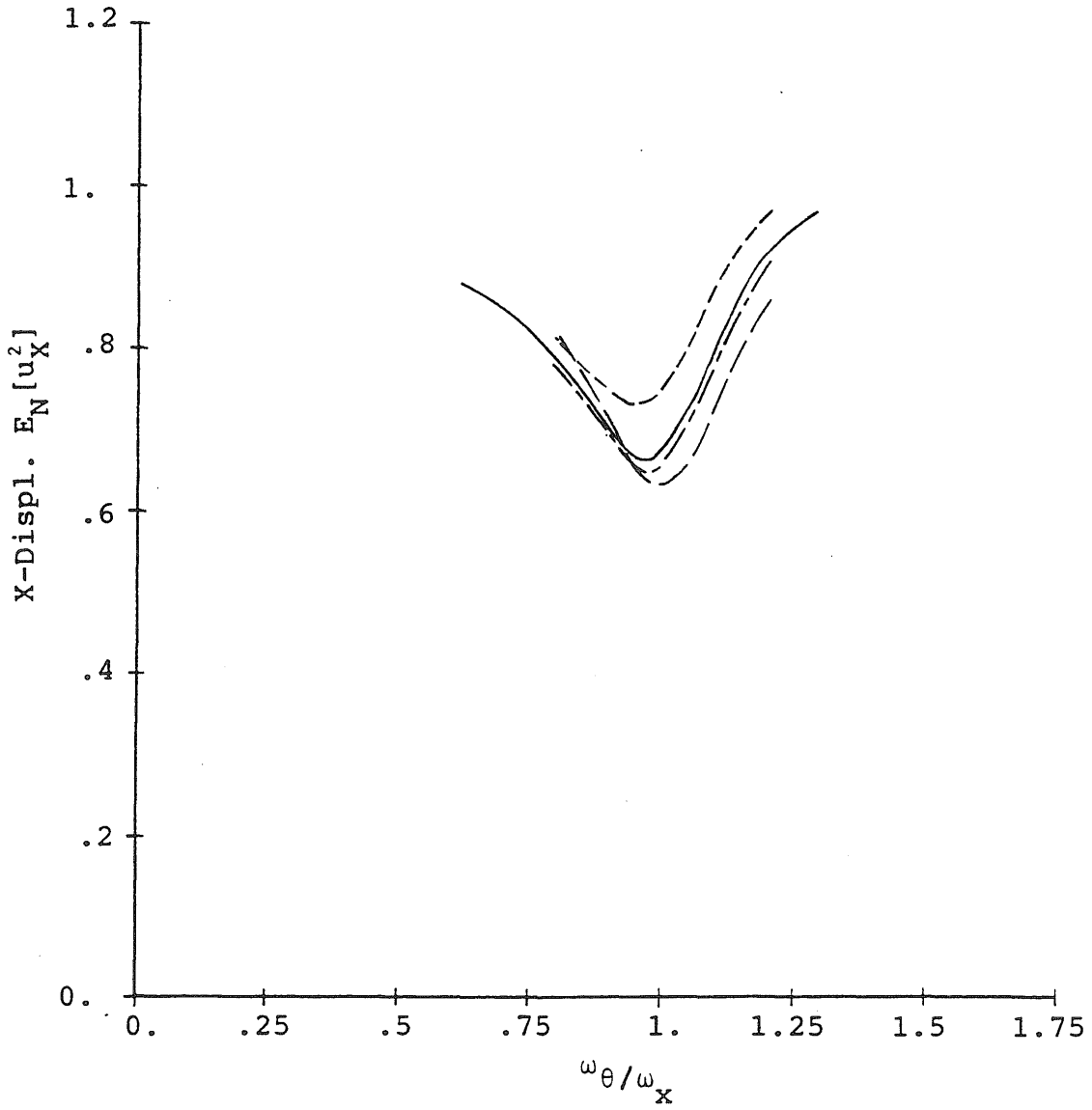

Fig. 5.28 Normalized Translational Response of a Torsionally Coupled System with $\frac{e_y}{r}$ = 0.15. Input: Stationary Clough-Penzien Spectrum [No. 2 in Fig. 2.7]

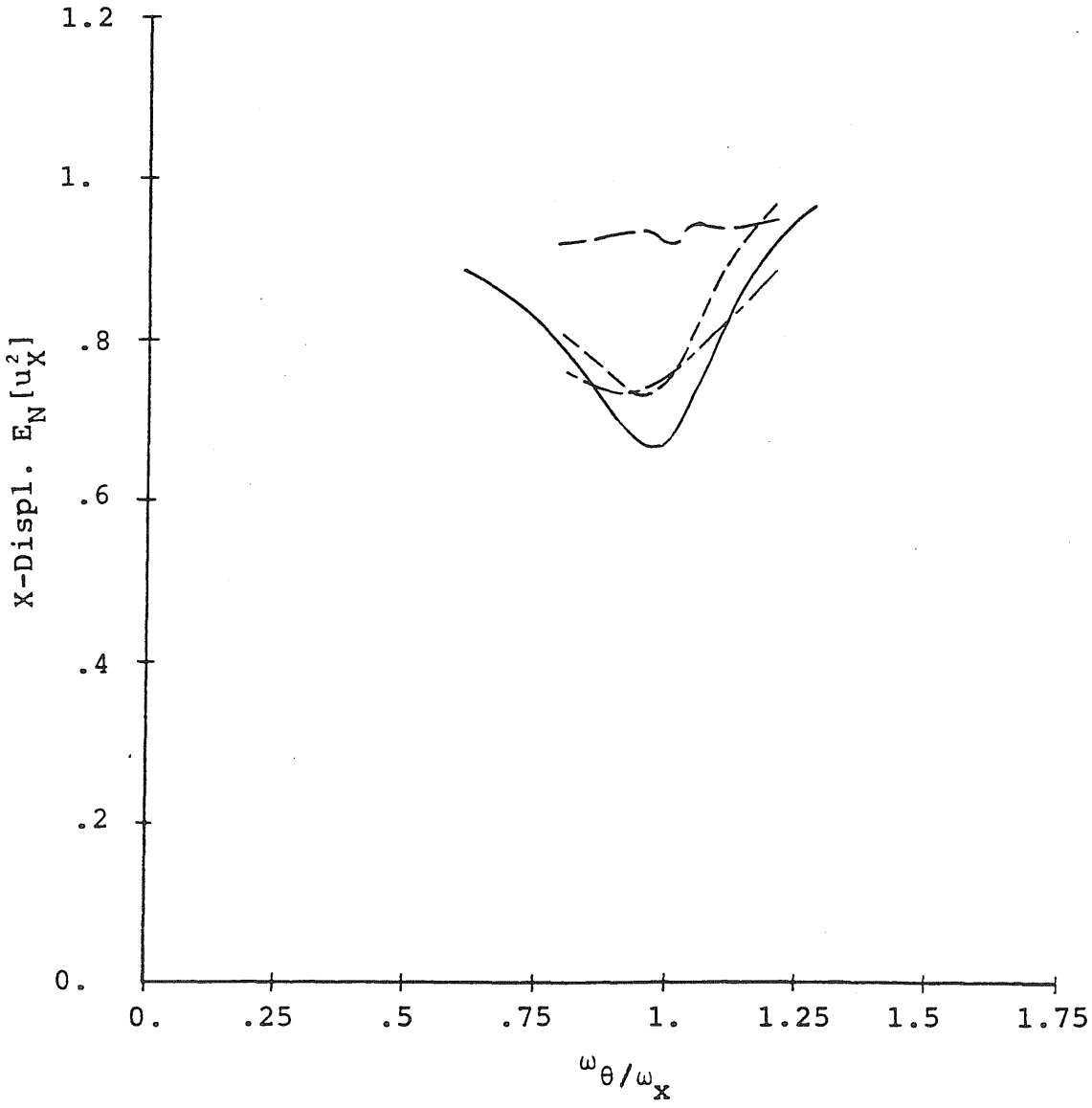

Fig. 5.29 Normalized Translational Response of a Torsionally Coupled System with $\frac{e_y}{r}$ = 0.15. Input: Nonstationary Clough-Penzien Spectrum [No. 2 in Fig. 2.7]

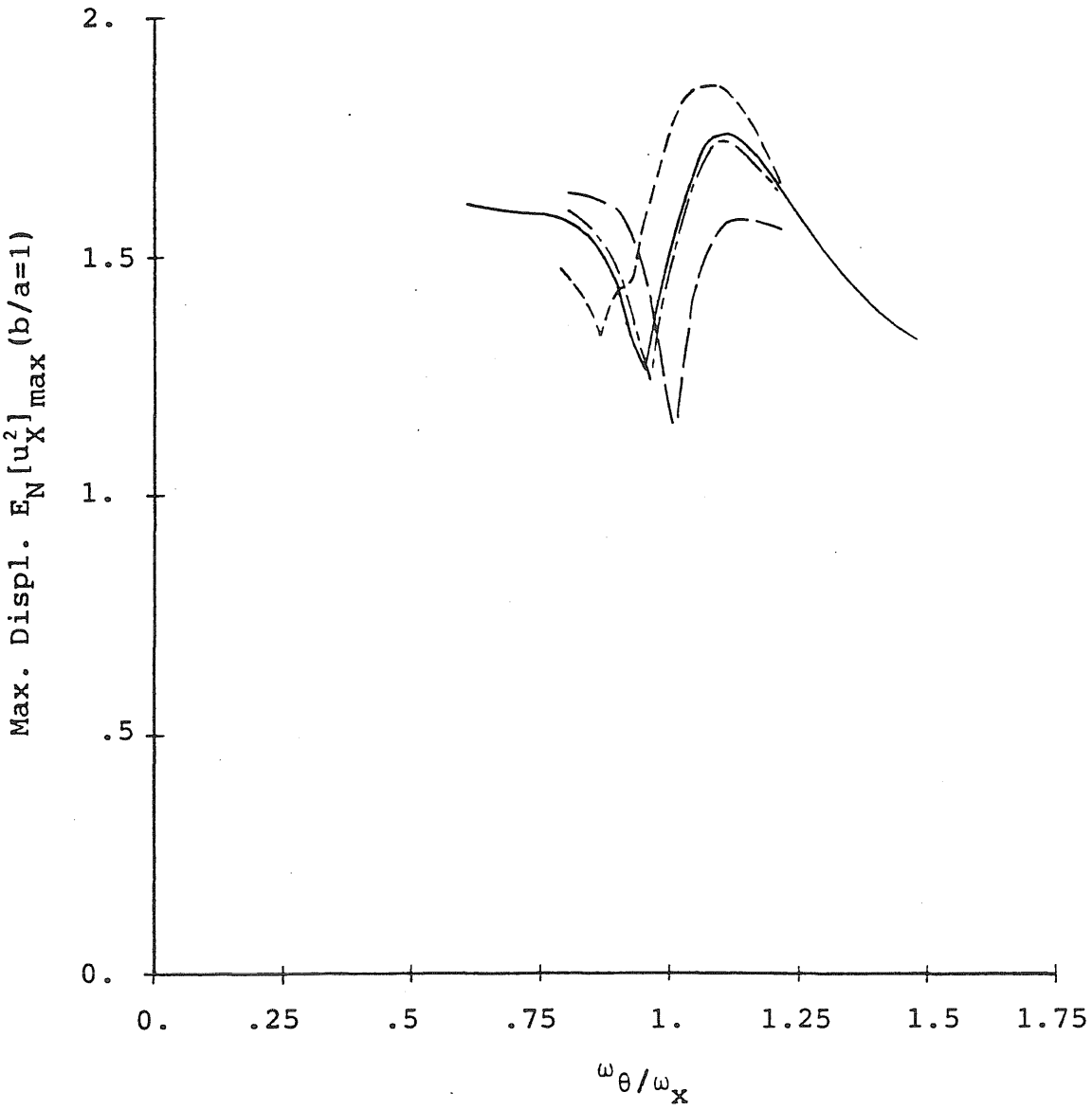

Fig. 5.30 Maximum of the Displacement Responses at N and S of a Torsionally Coupled System with $\frac{e_y}{r}$ = 0.15. Input: Stationary Clough-Penzien Spectrum [No. 2 in Fig. 2.7]

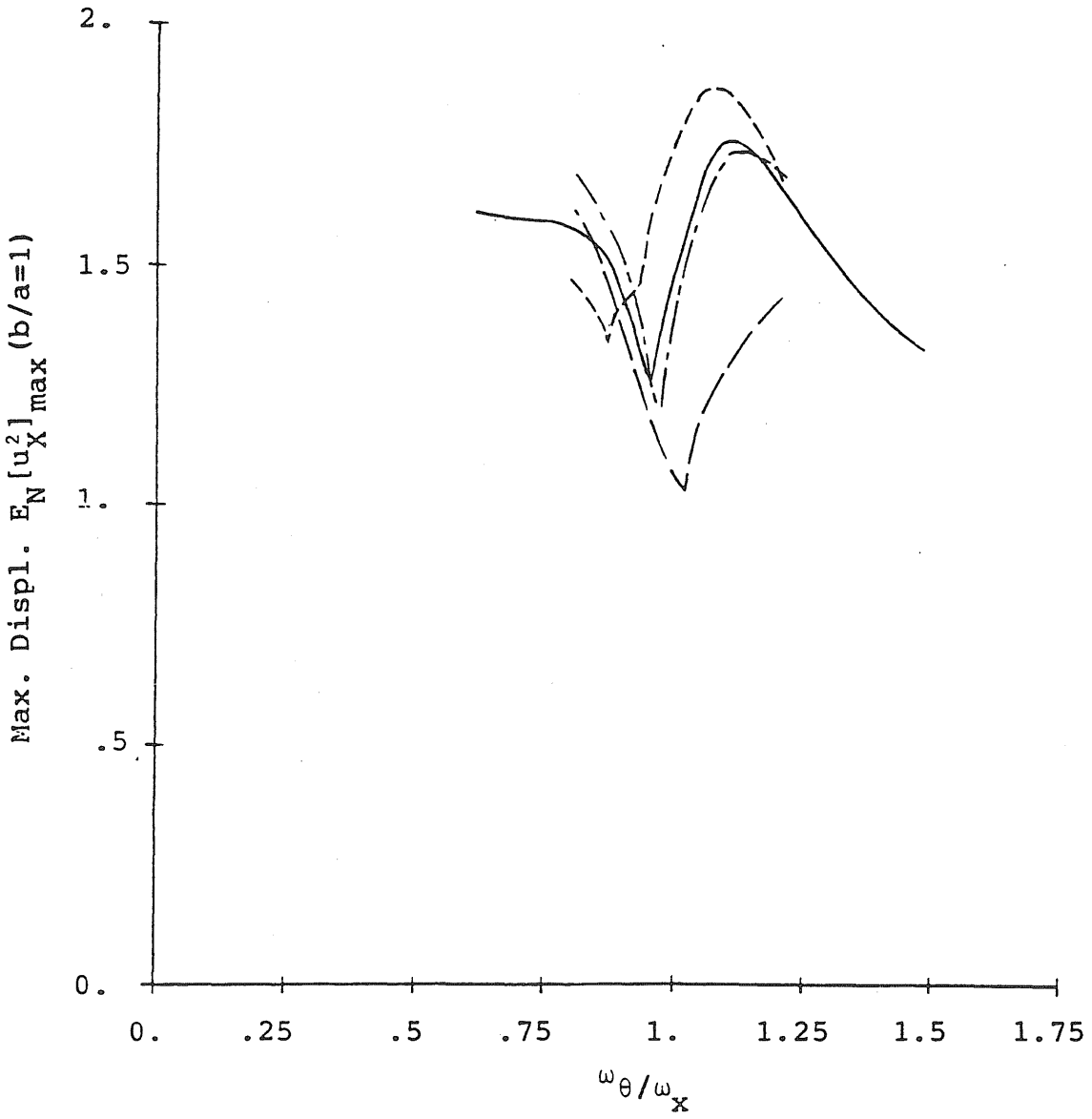

Legend:
——— Stationary White
— — f_x = 0.2 cps
— - — f_x = 1.0 cps
— - - - f_x = 5.0 cps

Fig. 5.31 Maximum of the Displacement Responses at N and S of a Torsionally Coupled System with $\frac{e_y}{r}$ = 0.15. Input: Nonstationary Clough-Penzien Spectrum [No. 2 in Fig. 2.7]

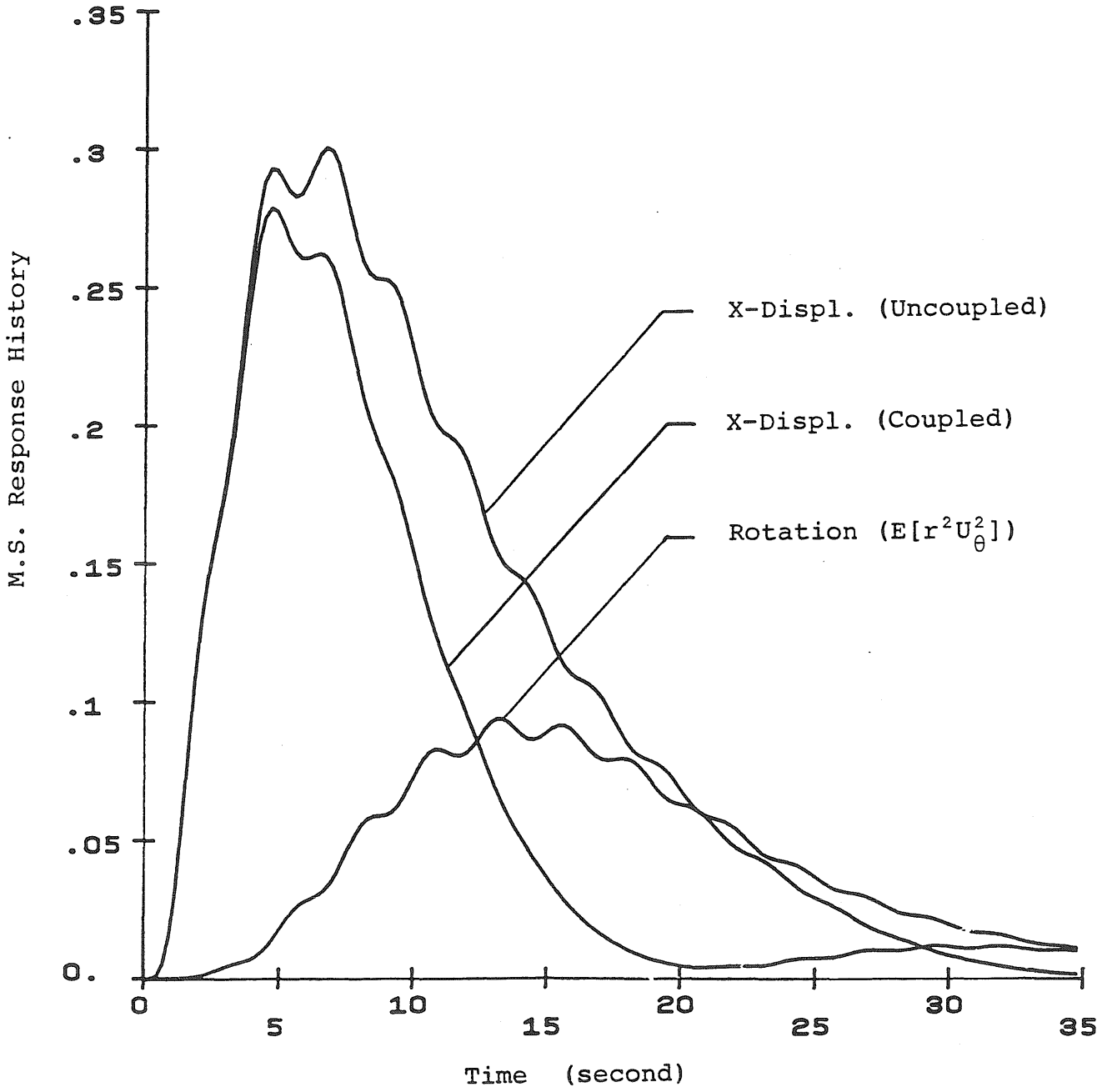

Fig. 5.32 Response History of a Torsionally Coupled System with $e_y/r = 0.15$, $\omega_\theta/\omega_x = 1.0$, $f_x = 0.2$ cps - Input: Clough-Penzien Spectrum with Short Duration Envelope [No. 2 in Fig. 2.7]

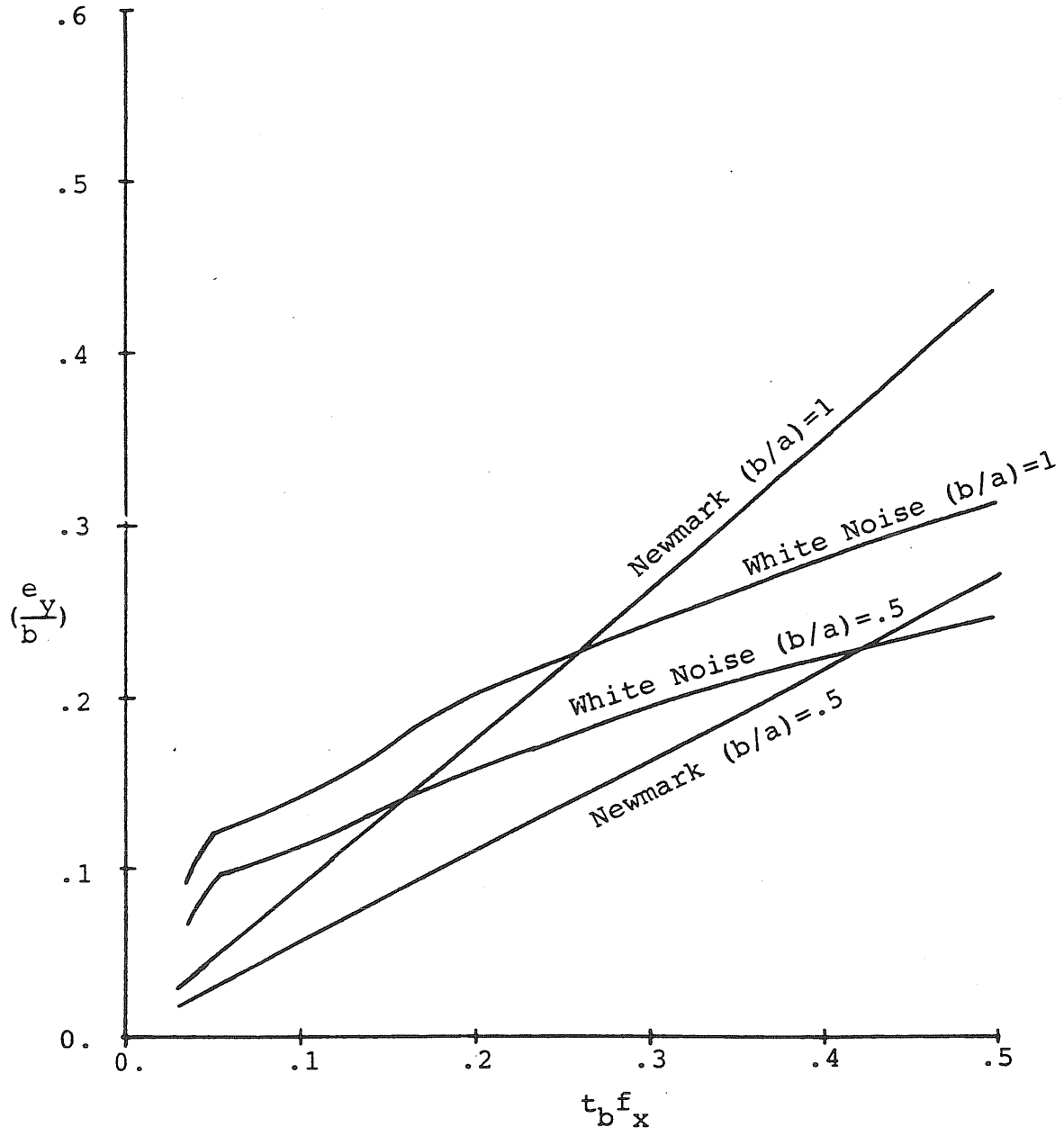

Fig. 5.33 Plots of Accidental Eccentricity as Functions of $t_b f_x$ $[(\omega_\theta/\omega_x) = 1.0]$

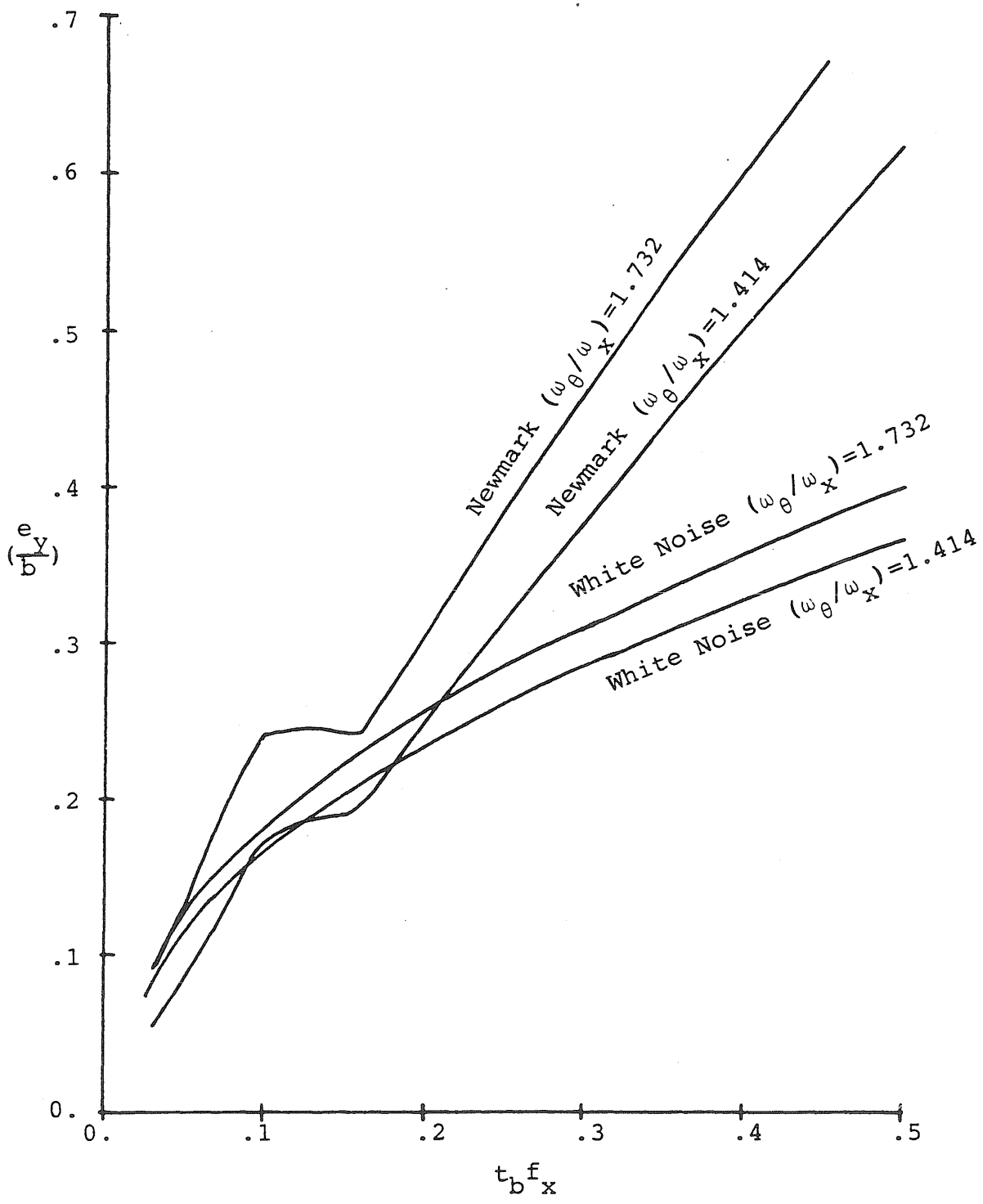

Fig. 5.34 Plots of Accidental Eccentricity as Functions of $t_b f_x$ [(b/a) = 1.0]

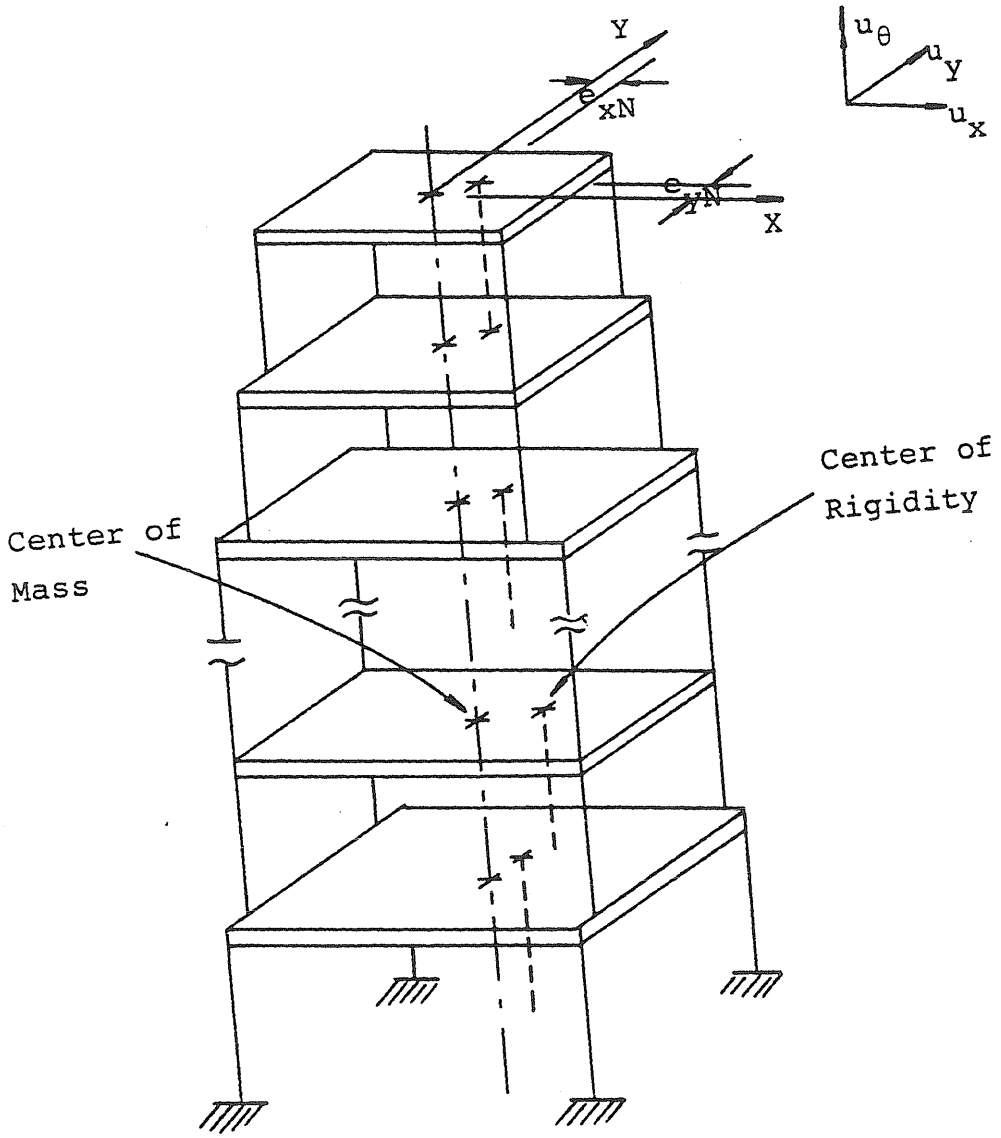

Fig. 6.1 Idealized Building

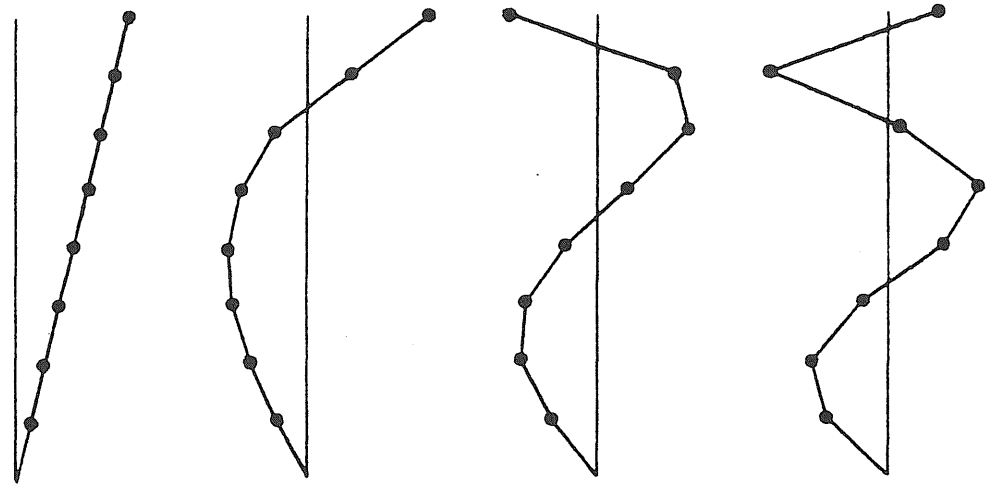

Mode	1	2	3	4
ω_{xi} (rad/sec)	5.46	13.39	21.16	28.92

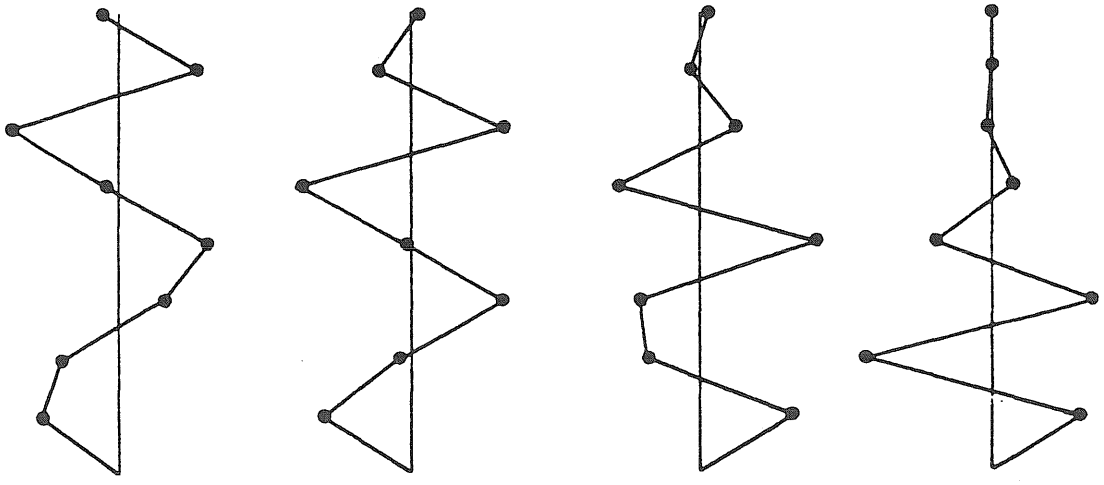

Mode	5	6	7	8
ω_{xi} (rad/sec)	36.66	44.39	52.12	59.86

Fig. 6.2 Mode Shapes and ω_{xi}'s of Uncoupled System

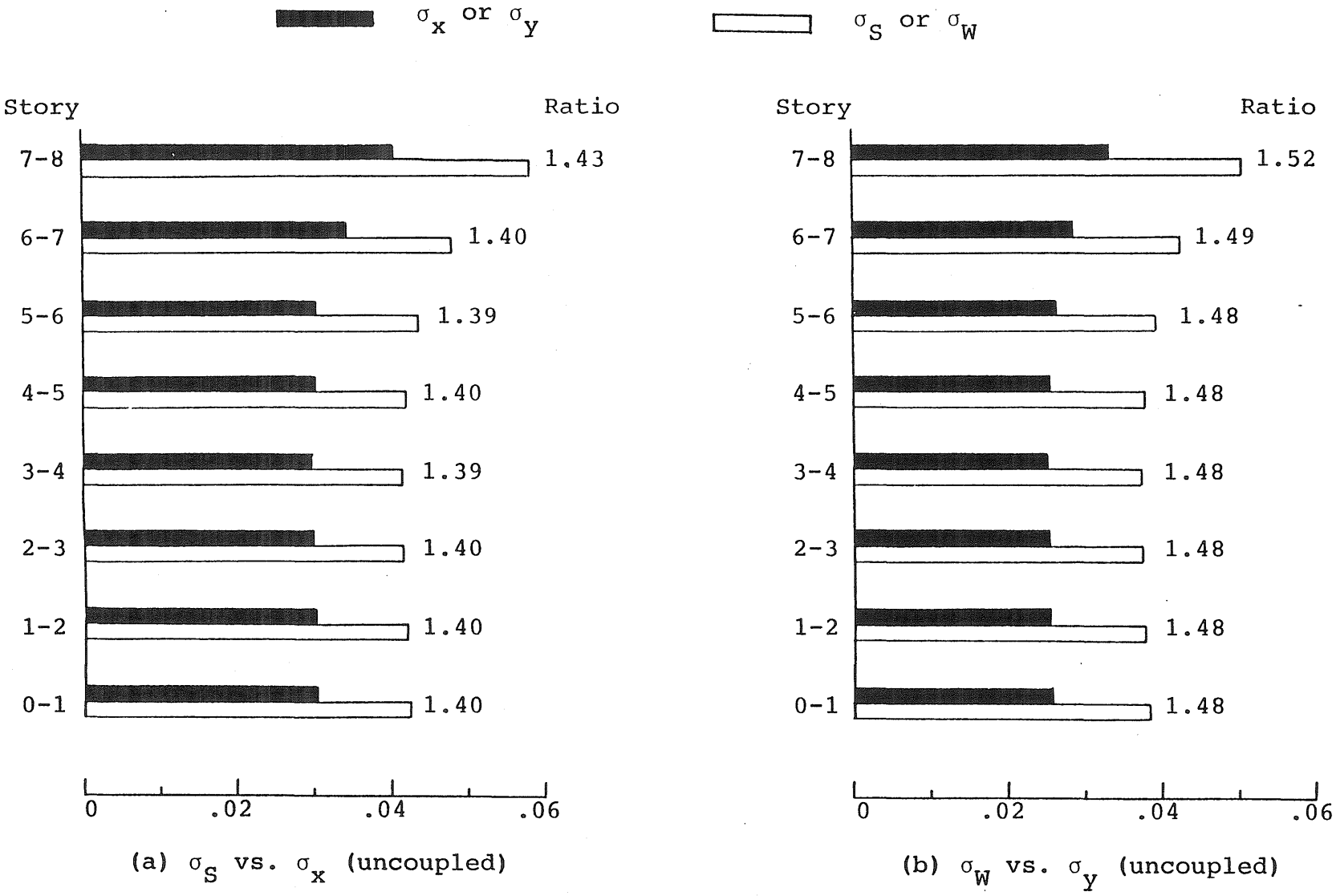

(a) σ_S vs. σ_x (uncoupled)

(b) σ_W vs. σ_y (uncoupled)

Fig. 6.3 Comparison of the Response at the Outer Edges of the Building and the Response at the Mass Center (Stationary Case)

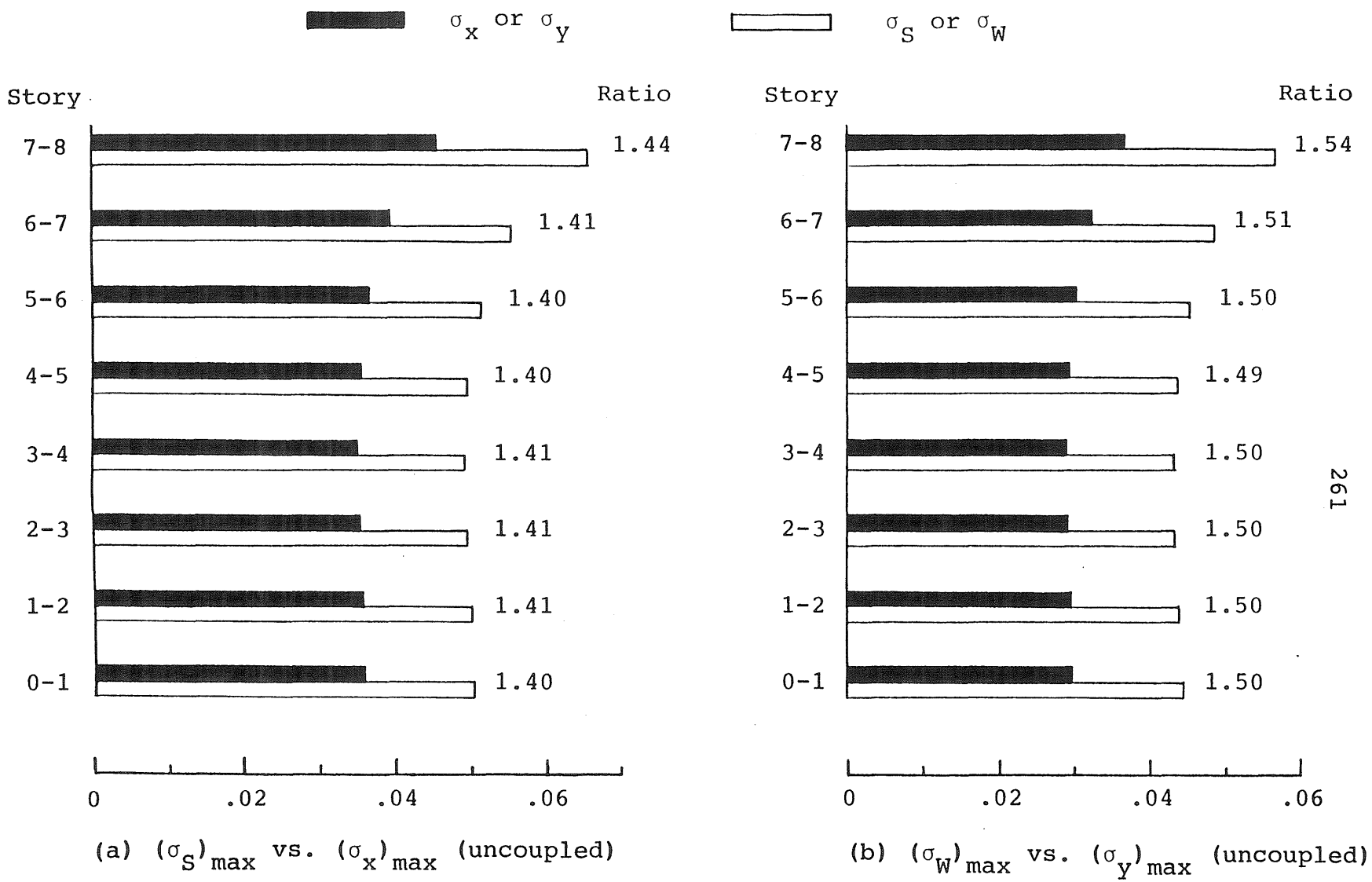

Fig. 6.4 Comparison of the Response at the Outer Edges of the Building and the Response at the Mass Center (Nonstationary Case)

APPENDIX A

CORRELATION AND POWER SPECTRAL DENSITY FUNCTION

Some basic definitions used in this study are summarized here. [64]

A.1 Mean; Cross-Correlation; Cross-Covariance

The following functions are basic in the study of stochastic processes.

The mean $\eta(t)$ of a process $\xi(t)$ is the expected value of the random variable $\xi(t)$:

$$\eta(t) = E[\xi(t)] \tag{A.1}$$

where $E[\cdot]$ denotes ensemble average.

The Cross-Correlation $R_{\xi_1\xi_2}(t_1, t_2)$ of two processes $\xi_1(t)$ and $\xi_2(t)$ is the joint moment of the random variables $\xi_1(t_1)$ and $\xi_2(t_2)$:

$$R_{\xi_1\xi_2}(t_1,t_2) = E[\xi_1(t_1)\xi_2(t_2)] \tag{A.2}$$

and their cross-covariance, $C_{\xi_1\xi_2}(t_1, t_2)$ is the joint cen-

tral moment of the random variables $\xi_1(t)$ and $\xi_2(t)$:

$$C_{\xi_1\xi_2}(t_1,t_2) = E[(\xi_1(t) - \eta_1(t))(\xi_2(t) - \eta_2(t))] \qquad (A.3)$$

If $\xi_1(t) = \xi_2(t) = \xi(t)$, then $R_{\xi_1\xi_2}(t_1,t_2) \equiv R_\xi(t_1,t_2)$, and $C_{\xi_1\xi_2}(t_1,t_2) = C_\xi(t_1,t_2)$ are respectively called the autocorrelation and autocovariance of $\xi(t)$.

In earthquake engineering, zero mean random processes are of concern. In this case, correlation is the same as covariance. Therefore, only the correlation function is discussed. For convenience, if $t_1 = t_2 = t$ then $R_\xi(t,t)$ will be called the variance of the random variable $\xi(t)$, and $R_{\xi_1\xi_2}(t,t)$ will be called the covariance of two random variables $\xi_1(t)$ and $\xi_2(t)$.

A.2 Power Spectrum of Stationary Processes

A process $\xi(t)$ is said to be stationary in the wide sense (weakly stationary), if its mean is a constant and its autocorrelation depends only on $t_2 - t_1$:

$$E[\xi(t)] = \eta = \text{constant}$$
$$E[\xi(t+\tau)\xi(t)] = R_\xi(\tau) \qquad (A.4)$$

Two processes are jointly stationary in the wide sense if each satisfies (A-4), and their cross-correlation depends only on $|t_1-t_2|$:

$$E[\xi_1(t+\tau)\xi_2(t)] = R_{\xi_1\xi_2}(\tau) \tag{A.5}$$

The power spectrum (or spectral density) $S_\xi(\omega)$ of a process $\xi(t)$ is the Fourier transform of its autocorrelation:

$$S_\xi(\omega) = \int_{-\infty}^{\infty} e^{-i\omega\tau} R_\xi(\tau)d\tau \tag{A.6}$$

and the cross-power spectrum $S_{\xi_1\xi_2}(\omega)$ of two processes $\xi_1(t)$ and $\xi_2(t)$ is

$$S_{\xi_1\xi_2}(\omega) = \int_{-\infty}^{\infty} e^{-i\omega\tau} R_{\xi_1\xi_2}(\tau)d\tau \tag{A.7}$$

From the Fourier inversion formula it follows that

$$R_\xi(\tau) = \int_{-\infty}^{\infty} e^{i\omega\tau} S_\xi(\omega)d\omega/2\pi \tag{A.8}$$

and

$$R_{\xi_1\xi_2}(\tau) = \int_{-\infty}^{\infty} e^{i\omega\tau} S_{\xi_1\xi_2}(\omega)\, d\omega/2\pi$$

physically, $S_{\xi}(\omega)$ describes the distribution of total mean square value (energy) over the frequency domain.

APPENDIX B

DIFFUSION OPERATORS

In this section, a brief summary of some fundamental background information needed for this work is presented. Emphasis is on intuitive justification rather than mathematical rigor. Interested readers may refer to [24, 28, 46, 50, 85] for fuller details.

B.1 State Variable Representation [28]

Early work in stochastic theory involved system description and analysis in the frequency domain. In contrast to these efforts, most of recent advances have involved system description in the time domain. The formulation used in this study employs state-variable notation, which is particularly useful in providing statistical descriptions of system behavior.

Many physical systems can be represented by a differential equation of the form

$$\dot{\underline{X}}_1(t) = \underline{f}(\underline{X}_1(t), \underline{X}_2(t), t) \qquad \text{(B.1)}$$

where $\underline{X}_2(t)$ is a bandlimited (nonwhite) random forcing function having bounded variance, i.e., white noise is physically

unrealizable. We shall model $\underline{X}_2(t)$ as a gaussian random process generated by the linear system

$$\dot{\underline{X}}_2(t) = [F(t)]\underline{X}_2(t) + [G(t)]\dot{\underline{W}}(t) \tag{B.2}$$

in which $\dot{\underline{W}}(t)$ is gaussian white noise and is formally expressed by

$$\dot{\underline{W}}(t) = \frac{d\underline{W}(t)}{dt} \tag{B.3}$$

where $\underline{W}(t)$ is Wiener (Brownian) process.

Combining Eqs. (B-1) and (B-2) and defining

$$\underline{X}(t) = \begin{Bmatrix} \underline{X}_1(t) \\ - - - \\ \underline{X}_2(t) \end{Bmatrix}$$

we obtain the augumented equation of motion

$$\dot{\underline{X}}(t) = \begin{Bmatrix} \underline{f}(\underline{X}_1(t),\ \underline{X}_2(t),\ t) \\ [F(t)]\underline{X}_2(t) \end{Bmatrix} + \begin{Bmatrix} 0 \\ [G(t)]\dot{\underline{W}}(t) \end{Bmatrix} \qquad (B.4)$$

or $d\underline{X}(t) = \underline{m}(\underline{X},t)dt + [\sigma(t)]d\underline{W}'(t)$

where $\underline{m}(\underline{X},t) = \begin{Bmatrix} \underline{f}(\underline{X}_1(t),\ \underline{X}_2(t),\ t) \\ [F(t)]\underline{X}_2(t) \end{Bmatrix}$

$$[\sigma(t)] = \begin{bmatrix} 0 & 0 \\ 0 & [G(t)] \end{bmatrix} \qquad \underline{W}'(t) = \begin{Bmatrix} 0 \\ W(t) \end{Bmatrix}$$

B.2 Diffusion Operators and Moment Evolutionary Equation

The conventional rules of calculus are not valid for stochastic processes because conventional calculus is based on the assumption that "Bounded Variation" exists. However, this may not be true for stochastic problems. To illustrate this, let X(t) be a scalar random process given by

$$dX = m(X,t)dt + \sigma(t)dW(t) \tag{B.5}$$

and let $Q(X)$ be any functional differentiable once with respect to t and twice with respect to X, then

$$\begin{aligned} dQ(X) &= Q(X + dX) - Q(X) \\ &= Q(X) + \frac{\partial}{\partial X} Q(X)dX + \frac{1}{2} \frac{\partial^2}{\partial X^2} Q(X)(dX)^2 + \ldots - Q(X) \\ &= \frac{\partial}{\partial X} Q(X)dX + \frac{1}{2} \frac{\partial^2}{\partial X^2} Q(X)(dX)^2 + \ldots \end{aligned} \tag{B.6}$$

The conventional differential rule holds only when all higher order terms, $(dX)^2$, $(dX)^3$, etc., are negligible when compared with dX. However, in this case

$$\begin{aligned} (dX)^2 = [m(X,t)]^2(dX)^2 &+ \sigma^2(t)(\dot{W}(t)dt)^2 \\ &+ 2m(X,t)\sigma(t)\dot{W}(t)(dt)^2 \end{aligned} \tag{B.7}$$

which has expectation

$$E[(dX)^2] = O((dt)^2) + \sigma^2(t)S_0\delta(0)(dt)^2 \tag{B.8}$$

where S_0 is white noise spectral level.

Since

$$\lim_{dt\to 0} \int_{-dt/2}^{dt/2} \delta(h)dh = 1$$

we can write formally

$$\delta(0) = \frac{1}{dt}$$

therefore

$$E[(dX)^2] = \sigma_0^2(t)S_0 dt$$

which is of the same order of magnitude as the term involving (dX). So, in Wiener process driven stochastic problems, it is necessary to carry up to second order differential terms. It can be easily verified that terms involving $(dX)^3$, $(dX)^4$, etc. can be neglected.

Consider

$$Q(X) \equiv e^{iuX}$$

then

$$dQ(X) = iue^{iuX}dX - \frac{1}{2}u^2e^{iuX}(dX)^2 \tag{B.9}$$

Let $\hat{(\cdot)}$ denote

$$E[(\cdot)|X_0] \equiv \int_{-\infty}^{\infty}(\cdot)p(X|X_0)dX$$

where $P(X|X_0)$, $t \geq t_0$, is the conditional probability density function. Then

$$\begin{aligned} d\hat{Q}(X) &= \widehat{iue^{iuX}dX} - \frac{1}{2}u^2\widehat{e^{iuX}(dX)^2} \\ &= \widehat{iue^{iuX}m(X,t)dt} - \frac{1}{2}u^2\widehat{e^{iuX}\sigma^2(t)S_0dt} \end{aligned} \tag{B.10}$$

Take the inverse Fourier transform, leading to

$$\frac{\partial}{\partial t}p(X|X_0) = -\frac{\partial}{\partial X}\{m(X,t)p(X|X_0)\} +$$

$$\frac{1}{2}\frac{\partial^2}{\partial X^2}\{\sigma^2(t)S_0 p(X|X_0)\} \qquad (B.11)$$

which is the Fokker-Planck equation.

Define the forward diffusion operator $L^*(\cdot(X))$ as

$$L^*(\cdot(X)) = -\frac{\partial}{\partial X}\{m(X,t)\cdot(X)\} + \frac{1}{2}\frac{\partial^2}{\partial X^2}\{\sigma^2(t)S_0\cdot(X)\} \qquad (B.12)$$

Then $\frac{\partial}{\partial t}\, p(X|X_0)$ satisfies the forward diffusion equation. The adjoint operator of L^* is the backward diffusion operator, L, which satisfies following relation

$$\int v(X)L(u(X))dX = \int u(X)L^*(v(X))dX \qquad (B.13)$$

It can be easily shown that

$$L(\cdot(X)) = m(X,t)\frac{\partial}{\partial X}\{\cdot(X)\} + \frac{1}{2}\sigma^2(t)S_0\frac{\partial^2}{\partial X^2}\{\cdot(X)\} \qquad (B.14)$$

Since

$$p(X_1|X_0) = \int_{-\infty}^{\infty} p(X_1|X)p(X|X_0)dX \qquad t_1 \geq t \geq t_0$$

then

$$\frac{\partial}{\partial t} p(X_1|X_0) = 0$$

$$= \int_{-\infty}^{\infty} p(X_1|X)\frac{\partial}{\partial t} p(X|X_0)dX + \int_{-\infty}^{\infty} p(X|X_0) \frac{\partial}{\partial t} p(X_1|X)dX$$

$$= \int_{-\infty}^{\infty} p(X|X_0)[L(p(X_1|X)) + \frac{\partial}{\partial t} p(X_1|X)]dX$$

thus

$$-\frac{\partial}{\partial t} p(X_1|X) = L(p(X_1|X)) \qquad \text{(B.15)}$$

The results derived above are also true for the vector case. In the vector case, let

$$dX_j = m_j(\underline{X},t)dt + \sum_{\alpha} \sigma_{j\alpha} dW_{\alpha} \qquad \text{(B.16)}$$

Repeating the same argument in Eqs. (B.9) to (B.15), the diffusion operators are

$$L^*(\cdot) = -\sum_j \frac{\partial}{\partial X_j}\{m_j(\underline{X},t)(\cdot)\} + \frac{1}{2}\sum_j\sum_k \frac{\partial^2}{\partial X_j \partial X_k}\{b_{jk}(\cdot)\}$$

$$L(\cdot) = \sum_j m_j(\underline{X},t)\frac{\partial}{\partial X_j}\{(\cdot)\} + \frac{1}{2}\sum_j\sum_k b_{jk}\frac{\partial^2}{\partial X_j \partial X_k}\{(\cdot)\} \qquad \text{(B.17)}$$

where

$$b_{jk} = \sum_\alpha \sum_\beta \sigma_{j\alpha}\sigma_{j\beta}S_{\alpha\beta}$$

Consider the conditional moment $\widehat{X_i^m X_j^n}$

$$\begin{aligned}\frac{\partial}{\partial t}(\widehat{X_i^m X_j^n}) &= \int X_i^m X_j^n \frac{\partial}{\partial t} p(\underline{X}|\underline{X}_0)d\underline{X} \\ &= \int X_i^m X_j^n L^*(p(\underline{X}|\underline{X}_0))d\underline{X} \qquad \text{(B.18)} \\ &= \int L(X_i^m X_j^n)p(\underline{X}|\underline{X}_0)d\underline{X} = \widehat{L(X_i^m X_j^n)}\end{aligned}$$

(B.18) shows that the evolution of conditional moments satisfies the backward diffusion operator.

APPENDIX C

AUTOCORRELATION FUNCTION OF RATIONAL POWER SPECTRA

C.1 Rational Power Spectra

A set of random processes of interest are stationary and have spectra that can be written as a ratio of two polynomials in ω^2.

$$S_{\xi}(\omega) = \frac{N(\omega^2)}{D(\omega^2)} \qquad (C.1)$$

in which $N(\omega^2)$ is a polynomial of order q in ω^2 and $D(\omega^2)$ is a polynomial of order p in ω^2 and $q < p$. These spectra are called rational spectra. The Kanai-Tajimi spectrum and Clough-Penzien spectrum are in this category.

C.2 Differential Equation Representation of Random Process Generation

Random processes $\xi(t)$ having rational spectra can always be obtained as stationary outputs from a linear system driven by white noise in terms of the state variable representation.

$$dX(t) = FX(t)dt + GdW(t) \qquad (C.2)$$

$$\xi(t) = CX(t) \tag{C.3}$$

where X(t) is a vector of state variable, F, G, and C are constant matrices, and W(t) is a vector of Wiener process.

C.3 State Transition Matrix

Consider the homogeneous solution of Eq. (C.2)

$$\frac{dX}{dt} = FX(t)$$

then (C.4)

$$X(t) = \Phi(t-t_0)X(t_0)$$

where $X(t_0)$ is the initial condition, $\Phi(t-t_0)$ is called the state transition matrix of the system. It can easily be shown that Φ satisfies the equation

$$\frac{d\Phi(\tau)}{d\tau} = F\Phi(\tau) \tag{C.5}$$

The solution to Eq. (C.5) is easily obtained by using coventional Laplace transform techniques.

$$\Phi(\tau) = L^{-1}\{[sI - F]^{-1}\} \tag{C.6}$$

where $L^{-1}(\cdot)$ denotes the inverse Laplace transform, and I is the identity matrix.

C.4 Autocorrelation Function

The autocorrelation function of $\xi(t)$ in Eq. (C.3) can be easily derived as

$$\begin{aligned} R_\xi(t_1,t_2) &= C\Phi(t_1-t_2)R_X(t_2,t_2)C^T && t_1 > t_2 \\ &= C\, R_X(t_1,t_1)\Phi^T(t_2-t_1)C^T && t_1 < t_2 \end{aligned} \tag{C.7}$$

where $\cdot^T$ denotes matrix transpose. Since only the stationary case is considered,

$$\begin{aligned} R_\xi(\tau) = R_\xi(t_2-t_1) &= C\Phi(-\tau) \lim_{s\to\infty} R_X(s,s)C^T && \tau < 0 \\ &= C \lim_{s\to\infty} R_X(s,s)\Phi^T(\tau)C^T && \tau > 0 \end{aligned} \tag{C.8}$$

where $\lim_{s\to\infty} R_X(s,s)$ can be obtained by applying Eq. (B.18) in Appendix B. For a real stationary process,

$$R_\xi(\tau) = R_\xi(-\tau) \tag{C.9}$$

This allows us to examine only the case $\tau > 0$.

C.4.1 Autocorrelation Function of Kanai-Tajimi Spectrum

The generating differential equation for a process having the Kanai-Tajimi spectrum can be written as

$$\begin{Bmatrix} X \\ \dot{X} \end{Bmatrix} = \begin{bmatrix} 0 & 1 \\ -\omega_g^2, & -2\zeta_g\omega_g \end{bmatrix} \begin{matrix} X \\ \dot{X} \end{matrix} dt + \begin{Bmatrix} 0 \\ dW \end{Bmatrix}$$

$$\xi(t) = S_0 \begin{Bmatrix} \omega_g^2, & 2\zeta_g\omega_g \end{Bmatrix} \begin{Bmatrix} X \\ \dot{X} \end{Bmatrix} \tag{C.10}$$

Using (C.7), after simple algebraic manipulation, one obtains

$$\Phi(\tau) = \begin{bmatrix} \Phi_{11}(\tau), & \Phi_{12}(\tau) \\ \Phi_{21}(\tau), & \Phi_{22}(\tau) \end{bmatrix} \tag{C.11}$$

where

$$\Phi_{11}(\tau) = e^{-\zeta_g \omega_g \tau} \left\{\cos(\omega_g^d \tau) + \frac{\zeta_g}{\sqrt{1-\zeta_g^2}} \sin(\omega_g^d \tau)\right\}$$

$$\Phi_{22}(\tau) = e^{-\zeta_g \omega_g \tau} \left\{\cos(\omega_g^d \tau) - \frac{\zeta_g}{\sqrt{1-\zeta_g^2}} \sin(\omega_g^d \tau)\right\}$$

$$\Phi_{12}(\tau) = e^{-\zeta_g \omega_g \tau} \left\{\frac{1}{\omega_g^d} \sin(\omega_g^d \tau)\right\}$$

$$\Phi_{21}(\tau) = e^{-\zeta_g \omega_g \tau} \left\{\frac{-\omega_g^2}{\omega_g^d} \sin(\omega_g^d \tau)\right\}$$

The steady-state covariance matrix

$$\lim_{s\to\infty} R_X(s,s) = \frac{1}{4\omega_g^3 \zeta_g} \begin{bmatrix} 1 & 0 \\ 0 & \omega_g^2 \end{bmatrix} \qquad \text{(C.12)}$$

Substitution of Eqs. (C.11) and (C.12) into (C.8), gives

$$R_\xi(\tau) = \frac{S_0\omega_g^2}{4\omega_g\zeta_g}\sqrt{\frac{1+8\zeta_g^2}{1-\zeta_g^2}}\{e^{-\omega_g\zeta_g|\tau|}\cos(\omega_g^d|\tau| - \phi)\} \qquad (C.13)$$

C.4.2 Autocorrelation Function of Clough-Penzien Spectrum

The state variable representation for random processes $\xi(t)$ having the Clough-Penzien spectrum can be obtained as

$$d\begin{Bmatrix} X_f \\ \dot{X}_f \\ X \\ \dot{X} \end{Bmatrix} = \begin{bmatrix} 0 & 1 & 0 & 0 \\ -\omega_f^2 & -2\zeta_f\omega_f & 0 & 0 \\ 0 & 0 & 0 & 1 \\ -\omega_f^2 & -2\zeta_f\omega_f & -\omega_g^2 & -2\zeta_g\omega_g \end{bmatrix} \begin{Bmatrix} X_f \\ \dot{X}_f \\ X \\ \dot{X} \end{Bmatrix} dt + \begin{Bmatrix} 0 \\ dW \\ 0 \\ dW \end{Bmatrix} \qquad (C.14)$$

$$\xi(t) = \{\, 0,\ 0,\ \omega_g^2,\ 2\zeta_g\omega_g \,\} \begin{Bmatrix} X_f \\ \dot{X}_f \\ X \\ \dot{X} \end{Bmatrix}$$

Let

$$\Phi(\tau) = [\Phi_{ij}]_{4\times4} \tag{C.15}$$

By application of Eq. (C.6), it can be shown that Φ_{ij} takes the general form

$$\begin{aligned}\Phi_{ij}(\tau) = {} & 2\, e^{-\omega_g \zeta_g \tau} \{a_{ij}\cos(\omega_g^d \tau) - b_{ij}\sin(\omega_g^d \tau)\} \\ & + 2\, e^{-\omega_f \zeta_f \tau} \{c_{ij}\cos(\omega_f^d \tau) - d_{ij}\sin(\omega_f^d \tau)\} \\ & i = 1, 2, 3, 4 \qquad j = 1, 2, 3, 4\end{aligned} \tag{C.16}$$

Let

$$\lim_{s\to\infty} R_X(s,s) = [R_{ij}]_{4\times4} \tag{C.17}$$

Substitution of Eqs. (C.17), (C.15), and (C.14) into (C.8), leads to

$$R_\xi(\tau) = \omega_g^4 \sum_{k=1}^{4} \Phi_{3k} R_{k3} + 4\zeta_g^2\omega_g^2 \sum_{i=1}^{4} \Phi_{4k} R_{k4} \tag{C.18}$$

Let

$$D = (\omega_g^2 - \omega_f^2)^2 + 4\omega_f\omega_g(\omega_f\zeta_f - \omega_g\zeta_g)(\omega_g\zeta_f - \omega_f\zeta_g) \tag{C.19}$$

then, the quantities required for evaluating Eq. (C.18) are

$$a_{31} = -c_{31} = \frac{-\omega_f^2}{2D}\{\omega_f^2 - \omega_g^2\}$$

$$b_{31} = \frac{-\omega_f^2}{2D\sqrt{1-\zeta_g^2}}\{\zeta_g(\omega_f^2 + \omega_g^2) - 2\omega_g\omega_f\zeta_f\}$$

$$d_{31} = \frac{-\omega_f^2}{2D\sqrt{1-\zeta_f^2}}\{\zeta_f(\omega_f^2 + \omega_g^2) - 2\omega_f\omega_g\zeta_g\}$$

$$a_{32} = -c_{32} = \frac{-1}{D}\{\omega_f\omega_g(\omega_f\zeta_g - \omega_g\zeta_f)\}$$

$$b_{32} = \frac{1}{2D\omega_g^d}\{(\omega_f^2 - \omega_g^2)(\omega_f^2 - 2\omega_g\zeta_g\omega_f\zeta_f)$$

$$+ 2\omega_g\omega_f(\omega_g\zeta_g - \omega_f\zeta_f)(\omega_f\zeta_g - 2\omega_g\zeta_f)\}$$

$$d_{32} = \frac{1}{2D\omega_f^d}\{\omega_f^2(\omega_g^2 - \omega_f^2) + 2\omega_f^2\omega_g\zeta_f(\omega_f\zeta_g - \omega_g\zeta_f)\}$$

$$a_{33} = 0.5$$

$$b_{33} = \frac{-\zeta_g}{2\sqrt{1-\zeta_g^2}}$$

$$c_{33} = d_{33} = 0$$

$$d_{34} = c_{34} = d_{34} = 0$$

$$b_{34} = \frac{-1}{2\omega_g^d}$$

$$a_{41} = - c_{41} = \frac{-\omega_f^2}{D} \{\omega_g \omega_f (\omega_g \zeta_f - \omega_f \zeta_g)\}$$

$$b_{41} = \frac{\omega_f^2}{2D\sqrt{1-\zeta_g^2}} \{\omega_g (\omega_g^2 - \omega^2{}_f) + 2\omega_g \omega_f \zeta_g (\omega_f \zeta_g - \omega_g \zeta_f)\}$$

$$d_{41} = \frac{\omega_f^2}{2D\sqrt{1-\zeta_f^2}} \{\omega_f (\omega_f^2 - \omega_g^2) + 2\omega_g \omega_f \zeta_f (\omega_g \zeta_f - \omega_f \zeta_g)\}$$

$$a_{42} = \frac{-1}{2D} \{(\omega_f^2-\omega_g^2)(\omega_f^2-2\omega_g\zeta_g\omega_f\zeta_f) +$$

$$2\omega_g\omega_f(\omega_g\zeta_g-\omega_f\zeta_f)(\omega_f\zeta_g-2\omega_g\zeta_f) - 2\omega_g\zeta_g[\omega_f\omega_g(\omega_f\zeta_g-\omega_g\zeta_f)]\}$$

$$b_{42} = \frac{-1}{2D\sqrt{1-\zeta_g^2}} \{\zeta_g[(\omega_f^2-\omega_g^2)(\omega_f^2-2\omega_g\zeta_g\omega_f\zeta_f) +$$

$$2\omega_g\omega_f(\omega_g\zeta_g-\omega_f\zeta_f)(\omega_f\zeta_g-2\omega_g\zeta_f) + 2\omega_g(1-\zeta_g^2)\omega_f\omega_g(\omega_f\zeta_g-\omega_g\zeta_f)\}$$

$$c_{42} = \frac{-1}{2D} \{\omega_f^2(\omega_g^2-\omega_f^2) + 2\omega_f^2\omega_g\zeta_f(\omega_f\zeta_g-\omega_g\zeta_f)$$

$$- 2\omega_f\zeta_f\omega_f\omega_g(\omega_g\zeta_f-\omega_f\zeta_g)\}$$

$$d_{42} = \frac{-1}{2D\sqrt{1-\zeta_f^2}} \{\zeta_f[\omega_f^2(\omega_g^2-\omega_f^2) + 2\omega_f^2\omega_g\zeta_f(\omega_f\zeta_g-\omega_g\zeta_f)$$

$$+ 2\omega_f(1-\zeta_f^2)\omega_f\omega_g(\omega_g\zeta_f-\omega_f\zeta_g)\}$$

$$a_{43} = c_{43} = d_{43} = 0$$

$$b_{43} = \frac{\omega_g}{2\sqrt{1-\zeta_g^2}}$$

$$a_{44} = 0.5$$

$$b_{44} = \frac{\zeta_g}{2\sqrt{1-\zeta_g^2}}$$

$$c_{44} = d_{44} = 0$$

$$R_{14} = -R_{23} = \frac{-1}{2} \frac{(\omega_g^2-\omega_f^2) + \frac{\omega_f}{\zeta_f}(\omega_g\zeta_g+\omega_f\zeta_f)}{(\omega_g^2-\omega_f^2)^2 + 4\omega_g\omega_f(\omega_g\zeta_g+\omega_f\zeta_f)(\omega_f\zeta_g+\omega_g\zeta_f)}$$

$$R_{13} = \frac{-1}{(\omega_g^2-\omega_f^2)} \{\frac{1}{4\omega_f\zeta_f} + 2(\omega_g\zeta_g+\omega_f\zeta_f)R_{14}\}$$

$$R_{24} = \frac{-1}{(\omega_g^2-\omega_f^2)} \left\{ \frac{\omega_f}{4\zeta_f} + 2\omega_g\omega_f(\omega_f\zeta_g+\omega_g\zeta_f)R_{14} \right\}$$

$$R_{33} = \frac{1}{4\omega_g\zeta_g} \left\{ 1 + \frac{\omega_f^2}{\omega_g^2-\omega_f^2} - \left[2\omega_f^2 - \frac{8\omega_f\zeta_f\omega_g\omega_f}{\omega_g^2-\omega_f^2}(\omega_f\zeta_g+\omega_g\zeta_f) \right] R_{14} \right\}$$

$$R_{34} = R_{43} = 0$$

$$R_{44} = \frac{1}{\omega_g^2} \left\{ R_{33} + 2\omega_f\zeta_f R_{14} - \omega_f^2 R_{13} \right\}$$

denote:

$$\alpha_{33} = \sum_{i=1}^{4} a_{3i} R_{i3} \qquad \beta_{33} = \sum_{i=1}^{4} b_{3i} R_{i3}$$

$$\gamma_{33} = \sum_{i=1}^{4} c_{3i} R_{i3} \qquad \delta_{33} = \sum_{i=1}^{4} d_{3i} R_{i3}$$

$$\alpha_{44} = \sum_{i=1}^{4} a_{4i} R_{i4} \qquad \beta_{44} = \sum_{i=1}^{4} b_{4i} R_{i4}$$

$$\gamma_{44} = \sum_{i=1}^{4} c_{4i} R_{i4} \qquad \delta_{44} = \sum_{i=1}^{4} d_{4i} R_{i4}$$

$$\hat{\alpha} = \omega_g^4 \alpha_{33} + 4\zeta_g^2 \omega_g^2 \alpha_{44}$$

$$\hat{\beta} = \omega_g^4 \beta_{33} + 4\zeta_g^2 \omega_g^2 \beta_{44}$$

$$\hat{\gamma} = \omega_g^4 \gamma_{33} + 4\zeta_g^2 \omega_g^2 \gamma_{44}$$

$$\hat{\delta} = \omega_g^4 \delta_{33} + 4\zeta_g^2 \omega_g^2 \delta_{44}$$

then, (c.18) becomes

$$R_\xi(\tau) = 2\, e^{-\omega_g \zeta_g \tau} \{\hat{\alpha}\cos(\omega_g^d \tau) - \hat{\beta}\sin(\omega_g^d \tau)\}$$

$$+ 2\, e^{-\omega_f \zeta_f \tau} \{\hat{\gamma}\cos(\omega_f^d \tau) - \hat{\delta}\sin(\omega_f^d \tau)\} \qquad \text{(C.20)}$$

$$= A_\xi e^{-\omega_g \zeta_g \tau} \cos(\omega_g^d \tau - \phi) + B_\xi e^{-\omega_f \zeta_f \tau} \cos(\omega_f^d \tau - \theta)$$

where

$$A_\xi = 2\sqrt{\hat{\alpha}^2 + \hat{\beta}^2} \qquad \phi = \tan^{-1} \frac{-\hat{\beta}}{\hat{\alpha}}$$

$$B_\xi = 2\sqrt{\hat{\gamma}^2 + \hat{\delta}^2} \qquad \theta = \tan^{-1} \frac{-\hat{\delta}}{\hat{\gamma}}$$

APPENDIX D

COMPOUND POISSON PROCESS

In this section, only intuitive arguments are employed in the discussion. Interested readers should refer to [50] for complete details.

D.1 Poisson Process (Poisson Counting Process)

A stochastic process by definition is a time parametered family of random variables. The Poisson process is an important class of random counting processes in which the random variables can take only integer values, i.e., the random variable is the count of the occurrence of events during a fixed time interval. The Poisson process satisfies the following assumptions:

1. Independent increment; the probability of a random occurrence is any subinterval t is independent of previous occurrence.

2. Unit jump; the probability of an occurrence in a interval $(t,t+dt)$ is $\lambda(t)dt$, where $\lambda(t)$ is positive. The probability of more than one occurrence in the interval is zero.

For a homogeneous Poisson process, $\lambda(t) = \lambda$ = constant, is independent of absolute time. A nonhomogeneous Poisson process can always be reduced to a homogeneous process by the

nonlinear time transformation

$$\tau = \int_0^t \lambda(s)ds \tag{D.1}$$

Therefore, it suffices to consider only the homogeneous case, $\lambda(t) = \lambda$. From the assumption, the probability of k occurrences in (0,t) satisfies

$$p(k;t) = p(k-1;t-dt)\lambda dt + p(k;t-dt)(1-\lambda dt) \tag{D.2}$$

Eq. (D.2) can be rearranged as

$$\frac{dp(k;t)}{dt} = \frac{p(k;t) - p(k;t-dt)}{dt} = -\lambda p(k;t) + \lambda p(k-1,t) \tag{D.3}$$

from which p(k;t) can be determined as

$$p(k;t) = \frac{(\lambda t)^k}{k!} e^{-\lambda t} \tag{D.4}$$

The parameter λ can be easily shown from assumption 2 to be the expected rate of occurrence normally referred to as intensity or incidence rate of the process.

D.2 Compound Poisson Process

A marked counting process is a counting process with an auxiliary variable, called a mark, associated with each ccurrence. If the counting process is Poisson, and the marks $\{H_i\}$ are a sequence of mutually independent, identically distributed random variables which are also independent of the counting process, then the process is termed a compound Poisson process.

It is noted that for a Poisson counting process the incidence rate, λ , is sufficient to characterize the process. For a compound Poisson process, we introduce another mark random variable H.

D.3 Moment Evolutionary Equation

Let N(t) denote a Poisson counting process having intensity λ, and P(t) = HN(t) denote a compound Poisson process with mark variable H. The Poisson impulse $\dot{P}(t)$ is formally expressed as

$$\dot{P}(t) = \frac{dP(t)}{dt} \qquad (D.5)$$

As discussed in section B-2, conventional calculus does not hold here. For Gaussian white noise, one must carry up to second-order differential terms to obtain the correct result. For a (compound) Poisson process not all higher order differential terms can be neglected. To illustrate this, consider a scalar Poisson driven process X(t) given by

$$dX(t) = aX(t)dt + \sigma(t)dP(t) \tag{D.6}$$

Since

$$\begin{aligned} E[dP(t)] &= E[H]dt \\ E[(dP(t))^2] &= E[H^2]dt \\ &\cdots\cdots \\ E[(dP(t))^n] &= E[H^n]dt \end{aligned} \tag{D.7}$$

Eq. (D-7) can be immediately obtained from assumption 2 for a poisson process and the independence assumption between the Poisson process and mark variable. Therefore, much information is contained in the higher order differential terms and should not be neglected. This is due to the highly disconti-

nuous nature of the process and is analogous to the Gibbs phenomenon in Fourier integrals or series.

The differentiation rule of Dolean-Dade and Meyer (1970) can account for this discontinuous process. Let X(t) be a scalar process described in Eq. (D-6), and Q(X) be any differentiable functional of X. The differentiation rule gives

$$dQ(X(t)) = \frac{\partial}{\partial X} Q(X(t_-)dX + d \sum_{t_0 \leq s \leq t} [Q(X_s) - Q(X_{s_-}) - \frac{\partial}{\partial X} Q(X_{s_-})(X_s - X_{s_-})] \tag{D.8}$$

The summation is carried out over those values of s where X jumps. Again, let $Q(X(t)) = e^{iuX(t)}$, and apply the differentiation rule to give

$$dQ(X(t)) = iue^{iuX(t)}[aX(t)dt + \sigma(t)dP(t)] + d \sum_{t_0 \leq s \leq t} \{e^{iu[X_{s_-} + \sigma(s_-)H} - e^{iuX_{s_-}} - iue^{iuX_{s_-}}[\sigma(s)H]\} \tag{D.9}$$

where $X_s - X_{s_-} = \sigma(s)H$ if a jump occurs at s.

Since for any function ψ, one has

$$d \sum_{t_0 \leq s \leq t} \psi(X_{s_-}) = d\int_{t_0}^{t} \psi(X_s)dN(s) = \psi(X_t)dN(t) \qquad (D.10)$$

Eq. (D.9) may be written as

$$dQ(X(t)) = iuaX(t)e^{iuX(t)}dt + e^{iuX(t)}(e^{iu\sigma(t)H} - 1)dN(t) \qquad (D.11)$$

Rearrange the right-hand side of (D-11) as

$$dQ(X(t)) = iuaX(t)e^{iuX(t)}dt + \lambda e^{iuX(t)}[e^{iu\sigma(t)H} - 1]dt + e^{iuX(t)}[e^{iu\sigma(t)H} - 1][dN(t) - \lambda dt] \qquad (D.12)$$

Let $\hat{(\cdot)}$ denote

$$E[(\cdot)|X_0] \equiv \int_{\mathcal{H}} \int_{-\infty}^{\infty} (\cdot)p(X|X_0)dXdG(H)$$

where G(H) is the distribution function of H. Then

$$\widehat{dQ(X(t))} = \widehat{iuaX(t)e^{iuX(t)}}dt + \widehat{\lambda e^{iuX(t)}[e^{iu\sigma(t)H} - 1]}dt \tag{D.13}$$

Take the inverse Fourier Transform, leading to

$$\begin{aligned}\frac{\partial}{\partial t}\, p(X|X_0) &= -\frac{\partial}{\partial X}\{aX(t)p(X|X_0)\} + \\ &\lambda\int_{-\infty}^{\infty} p(X-\sigma(t)H|X_0)dG(H) - \lambda p(X|X_0) \\ &= L^*(p(X|X_0))\end{aligned} \tag{D.14}$$

where L^* is forward diffusion operator given by

$$\begin{aligned}L^*(\cdot(X)) &= -\frac{\partial}{\partial X}\{aX[\cdot(X)]\} + \\ &\lambda\int_{-\infty}^{\infty}[\cdot(X-\sigma(t)H)]dG(H) - \lambda[\cdot(X)]\end{aligned} \tag{D.15}$$

then the backward diffusion operator L, the adjoint operator of L, is easily obtained as

$$L(\cdot(X)) = aX \frac{\partial}{\partial X} (\cdot(X)) + \lambda \int_{-\infty}^{\infty} [\cdot(X+\sigma(t)H)] dG(H) - \lambda [\cdot(X)] \tag{D.16}$$

By the same argument as used in Eq. (B.21), the conditional moment evolution satisfies backward diffusion equation. The derivation can be easily extended to vector processes.

APPENDIX E

ANALYTICAL EVALUATION OF RESPONSE COVARIANCES

This appendix gives some formulas required for the evaluation of displacement, velocity, and displacement-velocity joint response covariances $\hat{\gamma}_{jk}(t)$ in Eq. (3.24). It is sufficient to consider the following three cases.

Case I:

$$h_{xj}(\tau) = \frac{1}{\omega_j^d} e^{-\omega_j \zeta \tau} \sin(\omega_j^d \tau)$$

$$h_{yk}(\tau) = \frac{1}{\omega_k^d} e^{-\omega_k \zeta \tau} \sin(\omega_k^d \tau)$$

Case II:

$$h_{xj}(\tau) = e^{-\omega_j \zeta \tau} \cos(\omega_j^d \tau)$$

$$h_{yk}(\tau) = e^{-\omega_k \zeta \tau} \cos(\omega_k^d \tau)$$

Case III:

$$h_{xj}(\tau) = \frac{1}{\omega_j^d} e^{-\omega_j \zeta \tau} \sin(\omega_j^d \tau)$$

$$h_{yk}(\tau) = e^{-\omega_k \zeta \tau} \cos(\omega_k^d \tau)$$

The $\hat{\gamma}_{jk}(t)$ for Case I and II can be expressed as

$$\begin{aligned}\hat{\gamma}_{jk}(t) = e^{-(\omega_j \zeta + \omega_k \zeta)t} \{ & f(\omega_j, \omega_k, \alpha, \alpha) - f(\omega_j, \omega_k, \alpha, \beta) \\ & - f(\omega_j, \omega_k, \beta, \alpha) + f(\omega_j, \omega_k, \beta, \beta) \\ & + f(\omega_k, \omega_j, \alpha, \alpha) - f(\omega_k, \omega_j, \alpha, \beta) \\ & - f(\omega_k, \omega_j, \beta, \alpha) + f(\omega_k, \omega_j, \beta, \beta) \}\end{aligned} \tag{E.1}$$

where for Case I

$$f(\omega_1,\omega_2,\eta,\delta) = \frac{1}{\omega_j^d \omega_k^d}\{ e^{\lambda t}\{ W_1\cos\phi + W_2\sin\phi \}$$

$$+ e^{\nu t}\{ W_3\cos\phi_1 + W_4\sin\phi_1 \}$$

$$+ e^{\nu t}\{ W_5\cos\phi_2 + W_6\sin\phi_2 \} \qquad \text{(E.2)}$$

$$+ \{W_7\cos\phi_3+W_8\sin\phi_3+W_9\cos\phi_4+W_{10}\sin\phi_4\}$$

$$+ \{W_{11}\cos\phi_5+W_{12}\sin\phi_5+W_{13}\cos\phi_6+W_{14}\sin\phi_6\}\}$$

for Case 2

$$f(\omega_1,\omega_2,\eta,\delta) = e^{\lambda t}\{ W_{15}\cos\phi + W_{16}\sin\phi\}$$

$$+ e^{\nu t}\{ W_{17}\cos\phi_1 + W_{18}\sin\phi_1\}$$

$$+ e^{\nu t}\{ W_{19}\cos\phi_2 + W_{20}\sin\phi_2\} \qquad \text{(E.3)}$$

$$+ \{ W_7\cos\phi_3 + W_8\sin\phi_3 + W_9\cos\phi_4 + W_{10}\sin\phi_4\}$$

$$- \{ W_{11}\cos\phi_5 + W_{12}\sin\phi_5 + W_{13}\cos\phi_6 + W_{14}\sin\phi_6\}$$

The $\hat{\gamma}_{jk}(t)$ for Case III can be expressed as

$$\begin{aligned}\hat{\gamma}_{jk}(t) = e^{-(\omega_j\zeta+\omega_k\zeta)t} \{ & f_a(\omega_j,\omega_k,\alpha,\alpha) - f_a(\omega_j,\omega_k,\alpha,\beta) \\ & - f_a(\omega_j,\omega_k,\beta,\alpha) + f_a(\omega_j,\omega_k,\beta,\beta) \\ & + f_b(\omega_k,\omega_j,\alpha,\alpha) - f_b(\omega_k,\omega_j,\alpha,\beta) \\ & - f_b(\omega_k,\omega_j,\beta,\alpha) + f_b(\omega_k,\omega_j,\beta,\beta)\}\end{aligned} \tag{E.4}$$

where

$$\begin{aligned}f_a(\omega_1,\omega_2,\eta,\delta) = \frac{1}{\omega_j^d}\{ & e^{\lambda t}\{W_{21}\cos\phi + W_{22}\sin\phi\} \\ & + e^{\nu t}\{W_4\cos\phi_1 - W_3\sin\phi_1\} \\ & + e^{\nu t}\{-W_6\cos\phi_2 + W_5\sin\phi_2\} \\ & + \{-W_8\cos\phi_3 + W_7\sin\phi_3 - W_{10}\cos\phi_4 + W_9\sin\phi_4\} \\ & + \{W_{12}\cos\phi_5 - W_{11}\sin\phi_5 + W_{14}\cos\phi_6 - W_{13}\sin\phi_6\}\}\end{aligned} \tag{E.5}$$

$$f_b(\omega_1,\omega_2,\eta,\delta) = \frac{1}{\omega_j^d}\{e^{\lambda t}\{W_{23}\cos\phi + W_{24}\sin\phi\}$$

$$+ e^{\nu t}\{-W_{18}\cos\phi_1 + W_{17}\sin\phi_1\}$$

$$+ e^{\nu t}\{W_{20}\cos\phi_2 - W_{19}\sin\phi_2\} \qquad \text{(E.6)}$$

$$+ \{W_8\cos\phi_3 - W_7\sin\phi_3 + W_{10}\cos\phi_4 - W_9\sin\phi_4\}$$

$$+ \{W_{12}\cos\phi_5 - W_{11}\sin\phi_5 + W_{14}\cos\phi_6 - W_{13}\sin\phi_6\}\}$$

The parameters used in (E.1) to (E.6) are defined as follows:

$$\mu_\eta = \omega_g\zeta_g + \omega_2\zeta - \eta$$

$$\nu_\delta = -\delta - (\omega_g\zeta_g - \omega_1\zeta)$$

$$\lambda = \mu_\eta + \nu_\delta$$

$$C_p = \frac{1}{\mu_\eta^2 + (\omega_2^d + \omega_g^d)^2}$$

$$C_M = \frac{1}{\mu_\eta^2 + (-\omega_2^d + \omega_g^d)^2}$$

$$F_1 = \frac{C_e^2 C_p \mu_\eta}{4}$$

$$F_2 = \frac{C_e^2 C_p (\omega_2^d + \omega_g^d)}{4}$$

$$F_3 = \frac{C_e^2 C_M \mu_\eta}{4}$$

$$F_4 = \frac{C_e^2 C_M (\omega_2^d - \omega_g^d)}{4}$$

$$D_1 = \frac{1}{\lambda^2 + (-\omega_1^d + \omega_2^d)^2}$$

$$D_2 = \frac{1}{\lambda^2 + (\omega_1^d + \omega_2^d)^2}$$

$$E_1 = \frac{1}{\nu_\delta^2 + (\omega_1^d + \omega_g^d)^2}$$

$$E_2 = \frac{1}{\nu_\delta^2 + (-\omega_1^d + \omega_g^d)^2}$$

$$a_1 = (D_1 - D_2)\lambda$$

$$a_2 = D_1(-\omega_1^d + \omega_2^d) - D_2(\omega_1^d + \omega_2^d)$$

$$a_3 = (E_2 - E_1)\nu_\delta$$

$$a_4 = E_2(-\omega_1^d + \omega_g^d) - E_1(\omega_1^d + \omega_g^d)$$

$$a_5 = - D_1\lambda + E_1\nu_\delta$$

$$a_6 = - D_1(-\omega_1^d + \omega_2^d) - E_1(\omega_1^d + \omega_g^d)$$

$$a_7 = D_2\lambda - E_2\nu_\delta$$

$$a_8 = - D_2(\omega_1^d + \omega_2^d) - E_2(-\omega_1^d + \omega_g^d)$$

$$a_9 = - D_1\lambda + E_2\nu_\delta$$

$$a_{10} = - D_1(-\omega_1^d + \omega_2^d) + E_2(-\omega_1^d + \omega_g^d)$$

$$a_{11} = D_2\lambda - E_1\nu_\delta$$

$$a_{12} = E_1(\omega_1^d + \omega_g^d) - D_2(\omega_1^d + \omega_2^d)$$

$$a_{13} = D_2(\omega_1^d + \omega_2^d) - D_1(\omega_1^d - \omega_2^d)$$

$$a_{14} = -(D_1 + D_2)\lambda$$

$$a_{15} = E_2(\omega_g^d - \omega_1^d) + E_1(\omega_g^d + \omega_1^d)$$

$$a_{16} = -(E_1 + E_2)\nu_\delta$$

$$W_1 = (F_1 + F_3)a_1 - (F_2 + F_4)a_2$$

$$W_2 = (F_1 - F_3)a_2 + (F_2 - F_4)a_1$$

$$W_3 = F_1a_3 + F_2a_4$$

$$W_4 = F_1a_4 - F_2a_3$$

$$W_5 = -F_3a_3 + F_4a_4$$

$$W_6 = - F_3 a_4 - F_4 a_3$$

$$W_7 = F_1 a_5 - F_2 a_6$$

$$W_8 = F_1 a_6 + F_2 a_5$$

$$W_9 = F_3 a_9 - F_4 a_{10}$$

$$W_{10} = F_3 a_{10} + F_4 a_9$$

$$W_{11} = F_1 a_7 + F_2 a_8$$

$$W_{12} = F_1 a_8 - F_2 a_7$$

$$W_{13} = F_3 a_{11} + F_4 a_{12}$$

$$W_{14} = F_3 a_{12} - F_4 a_{11}$$

$$W_{15} = -(F_1 + F_3) a_{14} - (F_2 + F_4) a_{13}$$

$$W_{16} = (F_1 - F_3) a_{13} + (-F_2 + F_4) a_{14}$$

$$W_{17} = F_1 a_{16} - F_2 a_{15}$$

$$W_{18} = -F_1 a_{15} - F_2 a_{16}$$

$$W_{19} = F_3 a_{16} + F_4 a_{15}$$

$$W_{20} = - F_3 a_{15} + F_4 a_{16}$$

$$W_{21} = -(F_2 + F_4)\, a_1 - (F_1 + F_3) a_2$$

$$W_{22} = (-F_2 + F_4) a_2 + (F_1 - F_3) a_1$$

$$W_{23} = -(F_2 + F_4) a_{14} + (F_1 + F_3) a_{13}$$

$$W_{24} = (F_2 - F_4) a_{13} + (F_1 - F_3) a_{14}$$

$$\phi_1 = (\omega_2^d + \omega_g^d) t - \phi$$

$$\phi_2 = (-\omega_2^d + \omega_g^d) t - \phi$$

$$\phi_3 = (\omega_1^d - \omega_2^d) t + \phi$$

$$\phi_4 = (\omega_1^d - \omega_2^d) t - \phi$$

$$\phi_5 = (\omega_1^d + \omega_2^d)t - \phi$$

$$\phi_6 = (\omega_1^d + \omega_2^d)t + \phi$$

APPENDIX F

THE SECOND AND FOURTH MOMENTS OF RESPONSE OF SDOF SYSTEMS TO WHITE NOISE EXCITATION

F.1 Second Moments

Eq. (4.5) can be integrated as follows for the envelope function described in Eq. (2.3)

$$E[u^2(t)] = \frac{C_e^2}{2\omega_0^2(1-\zeta^2)}\{h(2\alpha)+h(2\beta)-2h(\alpha+\beta)-f(2\alpha)-f(2\beta)$$

$$+2f(\alpha+\beta)\}$$

$$E[u(t)\dot{u}(t)] = \frac{C_e^2}{\omega_0^2(1-\zeta^2)}\{\frac{\omega_0\zeta}{2}[f(2\alpha)+f(2\beta)-2f(\alpha+\beta)-h(2\alpha)-h(2\beta)$$

$$+2h(\alpha+\beta)+\frac{\omega_0\sqrt{1-\zeta^2}}{2}[g(2\alpha)+g(2\beta)-2g(\alpha+\beta)]\}$$

$$E[\dot{u}^2(t)] = \frac{C_e^2}{(1-\zeta^2)}\{\frac{(1-2\zeta^2)}{2}[f(2\alpha)+f(2\beta)-2f(\alpha+\beta)] -$$

$$\zeta\sqrt{1-\zeta^2}[g(2\alpha)+g(2\beta)-2g(\alpha+\beta)+\frac{1}{2}[h(2\alpha)+h(2\beta)-2h(\alpha+\beta)]\}$$

in which

$$h(\xi) = \int_0^t e^{-2\omega_0\zeta(t-\zeta)}\, e^{-\xi\tau} d\tau$$

$$= \frac{1}{2\omega_0\zeta-\xi}\{ e^{-\xi t} - e^{-2\omega_0\zeta t} \}$$

$$f(\xi) = \int_0^t e^{-2\omega_0\zeta(t-\tau)}\, e^{-\xi\tau}\cos(2\omega_0\sqrt{1-\zeta^2}(t-\tau))\, d\tau$$

$$= \frac{1}{\xi^2-4\omega_0\zeta\xi+4\omega_0^2}\{(2\omega_0\zeta-\xi)e^{-\xi t} - e^{-2\omega_0\zeta t}[(2\omega_0\zeta-\xi)\cos(2\omega_0\sqrt{1-\zeta^2}t)$$

$$-2\omega_0\sqrt{1-\zeta^2}\sin(2\omega_0\sqrt{1-\zeta^2}t)]\}$$

$$g(\xi) = \int_0^t e^{-2\omega_0\zeta(t-\tau)}\, e^{-\xi\tau}\sin(2\omega_0\sqrt{1-\zeta^2}(t-\tau))\, d\tau$$

$$= \frac{1}{\xi^2-4\omega_0\zeta\xi+4\omega_0^2}\{(2\omega_0\sqrt{1-\zeta^2})\, e^{-\xi t} -$$

$$e^{-2\omega_0\zeta t}[2\omega_0\sqrt{1-\zeta^2}\cos(2\omega_0\sqrt{1-\zeta^2}t) + (2\omega_0\zeta-\xi)\sin(2\omega_0\sqrt{1-\zeta^2}t)]\}$$

F.2 Fourth Moment

Eq. (4.11) is obtained in a straightforward manner as

$$E[u^4(t)]_p = F(4\alpha)-4F(3\alpha+\beta)+6F(2\alpha+2\beta)-4F(\alpha+3\beta)+F(4\beta) \qquad (F.2)$$

where

$$F(\xi) = \frac{1}{\omega_0^4(1-\zeta^2)^2}\left\{\frac{1}{8}F_1(\xi) - \frac{1}{2}F_2(\xi) + \frac{3}{8}F_3(\xi)\right\}$$

$$F_1(\xi) = \frac{1}{\xi^2-8\omega_0\zeta\xi+16\omega_0^2}\{(4\omega_0\zeta-\xi)e^{-\xi t} - e^{-4\omega_0\zeta t}[(4\omega_0\zeta-\xi)\cdot$$

$$\cos(4\omega_0\sqrt{1-\zeta^2}t) - 4\omega_0\sqrt{1-\zeta^2}\sin(4\omega_0\sqrt{1-\zeta^2}t)]\}$$

$$F_2(\xi) = \frac{1}{\xi^2-8\omega_0\zeta\xi+4\omega_0^2+12\omega_0^2\zeta^2}\{(4\omega_0\zeta-\xi)e^{-\xi t} - e^{-4\omega_0\zeta t}[(4\omega_0\zeta-\xi)$$

$$\cos(2\omega_0\sqrt{1-\zeta^2}t) - 2\omega_0\sqrt{1-\zeta^2}\sin(2\omega_0\sqrt{1-\zeta^2}t)]\}$$

$$F_3(\xi) = \frac{1}{4\omega_0\zeta-\xi}\{e^{-\xi t} - e^{-4\omega_0\zeta t}\}$$

APPENDIX G [32, 45]

PEARSON DISTRIBUTIONS

Frequently, there are insufficient theoretical grounds for selecting appropriate probability distributions. In this situation, very often empirical distributions are used in evaluating system performance. Standard probability distribution models do lead to a wide variety of distribution shapes. However, they do not provide the degree of generality that is frequently desirable. Therefore it is useful to have available more general techniques for representing data.

A group of distribution families due to Karl Pearson, which is defined by the first four central moments of a random variable, is employed in this work.

G.1 The Pearson Law

It can be easily verified that the probability density function p(X) of the Gaussian distribution is the solution to

$$\frac{1}{p(X)} \frac{dp(X)}{dX} = - \frac{X-u}{\sigma^2} \qquad (G.1)$$

The law, therefore, has the properties that dp(X)/dX vanishes

in the limit when p(X) tends to 0, and at one intermediate value of X, namely, μ. If we consider the generalized form

$$\frac{1}{p(X)} \frac{dp(X)}{dX} = - \frac{X - a}{b_0 + b_1 X + b_2 X^2} \tag{G.2}$$

the same properties will usually hold, but we now have two more parameters available and are able to represent a wider range of probability distribution shapes. The integral of Eq. (G.2) can in general be written in the form

$$p(X) = C_0 (X-c_1)^{m_1} (c_2-X)^{m_2} \tag{G.3}$$

where C_0 will be fixed by the condition that the integral of p(X) is 1, and c_1 and c_2 are the zeros of the denominator in Eq. (G.2).

This generalized law was proposed by Karl Pearson [32]. The solution of Eq. (G.3) leads to a large number of distribution families including all the standard probability distributions. A plot of the regions in the (β_1, β_2) plane corresponding to various Pearson distributions is shown in Fig.

G.1, where

$$\beta_1 = \frac{u_3^2}{u_2^3} \qquad \beta_2 = \frac{u_4}{u_2^2}$$

and μ_n denotes the n-th central moment of a random variable. This chart shows the wide diversity of Pearson distribution shapes and may be used to select the appropriate approximation for a given variate, based on knowledge of β_1 and β_2. The expressions for the probability density functions for the various Pearson distributions are given in [45].

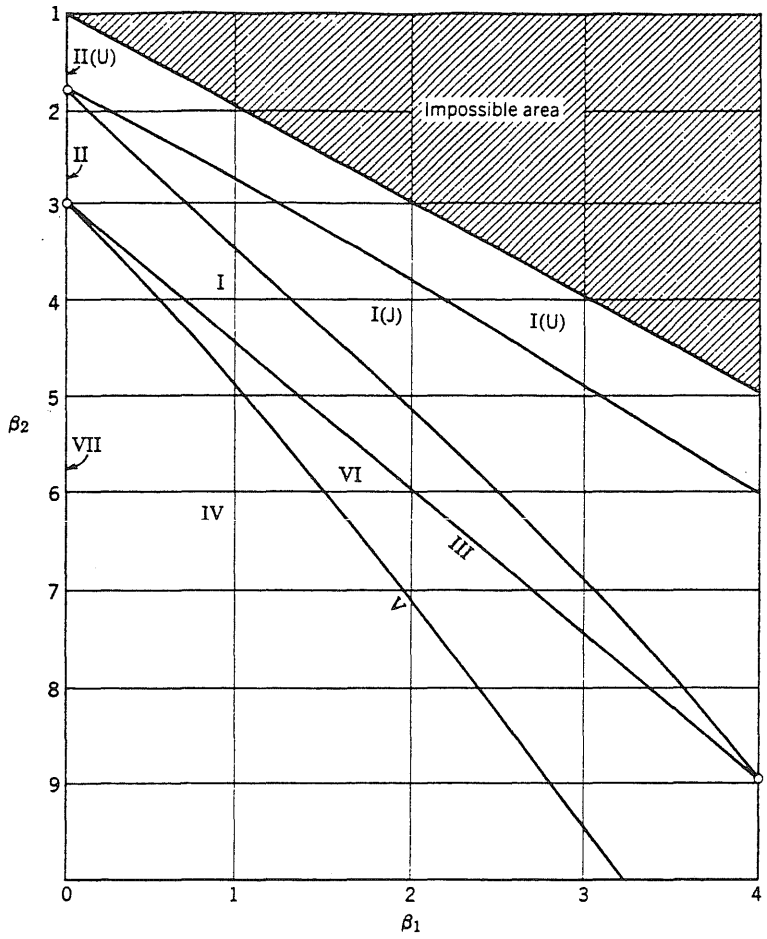

Fig. G.1 Region in (β_1, β_2) Plane for Various Type Pearson Distributions. Letters U and J Denote U-Shaped and J-Shaped Distribution. (From E.S. Pearson, Seminars, Princeton University, 1960)

APPENDIX H

COEFFICIENTS OF MATRIX [Γ]

Applying Eq.(B.18), a set of 21 evolutionary equations are obtained for second moments. If the stationary displacement responses are considered, Eq.(5.6) is obtained by condensing out all terms other than displacement responses. The coefficients of matrix [Γ] in Eq.(5.6) are as follows:

$$\Gamma_{11} = \omega_x^3 \{ 2\zeta + \frac{u_1'}{2\zeta\Delta'} (\frac{e_y}{r})^2 \}$$

$$\Gamma_{12} = \omega_x^3 \{ 2\zeta (\frac{e_y}{r})^2 + \frac{1}{2\zeta\Delta'} [-u_1' (\frac{e_y}{r})^2 - u_2' \beta_y^2 (\frac{e_x}{r}) (\frac{e_y}{r})] \}$$

$$\Gamma_{13} = \omega_x^3 \{ \frac{u_2' \beta_y^2}{2\zeta\Delta'} (\frac{e_x}{r}) (\frac{e_y}{r}) \}$$

$$\Gamma_{14} = \omega_x^3 (\frac{e_y}{r}) \{ -4\zeta + \frac{1}{2\zeta\Delta'} [(-u_1') (\beta_\theta^2 - 1) - u_3' \beta_y^2 (\frac{e_x}{r})] \}$$

$$\Gamma_{15} = \omega_x^3 (\frac{e_y}{r}) \{ \frac{1}{2\zeta\Delta'} [-u_3' (\beta_y^2 - 1) - u_1' \beta_y^2 (\frac{e_x}{r}) - u_2' (\frac{e_y}{r})] \}$$

$$\Gamma_{16} = \omega_x^3 (\frac{e_y}{r}) \{ \frac{1}{2\zeta\Delta'} [-u_2' (\beta_y^2 - \beta_\theta^2) - u_3' (\frac{e_y}{r})] \}$$

$$\Gamma_{22} = \omega_x^3 \{ 2\beta_\theta^3 \zeta + \frac{1}{2\zeta\Delta'} [u_1' (\frac{e_y}{r})^2 + 2u_2' \beta_y^2 (\frac{e_x}{r}) (\frac{e_y}{r}) + v_2' \beta_y^4 (\frac{e_x}{r})^2] \}$$

$$\Gamma_{23} = \omega_x^3 (\frac{e_x}{r}) \{ 2\beta_y^3 \zeta (\frac{e_x}{r}) + \frac{1}{2\zeta\Delta'} [-v_2' \beta_y^4 (\frac{e_x}{r}) - u_2' \beta_y^2 (\frac{e_y}{r})] \}$$

$$\Gamma_{24} = \omega_x^3 \{ -2\beta_\theta \zeta (\frac{e_y}{r}) (1+\beta_\theta) + \frac{1}{2\zeta\Delta'}[(1-\beta_\theta^2) (-u_1' (\frac{e_y}{r}) - u_2' \beta_y^2 (\frac{e_x}{r})$$

$$+ \omega_2' \beta_y^4 (\frac{e_x}{r})^2 + u_3' \beta_y^2 (\frac{e_x}{r}) (\frac{e_y}{r})] \}$$

$$\Gamma_{25} = \omega_x^3 \{ -2\beta_y \zeta (\frac{e_x}{r}) (\frac{e_y}{r}) (1+\beta_y) + \frac{1}{2\zeta\Delta'}[(1-\beta_y^2) (-u_3' (\frac{e_y}{r}) - \omega_2' \beta_y^2 (\frac{e_x}{r}))$$

$$+ (u_1'+v_2') \beta_y^2 (\frac{e_x}{r}) (\frac{e_y}{r}) + u_2' ((\frac{e_y}{r})^2 + \beta_y^4 (\frac{e_x}{r})^2)] \}$$

$$\Gamma_{26} = \omega_x^3 \{ 2\beta_y \beta_\theta \zeta (\beta_\theta+\beta_y) (\frac{e_x}{r}) + \frac{1}{2\zeta\Delta'}[(\beta_y^2-\beta_\theta^2) (u_2' (\frac{e_y}{r}) + v_2' \beta_y^2 (\frac{e_x}{r}))$$

$$+ u_3' (\frac{e_y}{r})^2 + \omega_2' (\beta_y^2 (\frac{e_x}{r}) (\frac{e_y}{r})] \}$$

$$\Gamma_{33} = \omega_x^3 \{ 2\beta_y^3 \zeta + \frac{1}{2\zeta\Delta'}[v_2' \beta_y^4 (\frac{e_x}{r})^2] \}$$

$$\Gamma_{34} = \omega_x^3 (\frac{e_x}{r}) \{ \frac{1}{2\zeta\Delta'}[(1-\beta_\theta^2) (u_2' \beta_y^2) - \omega_2' \beta_y^4 (\frac{e_x}{r})] \}$$

$$\Gamma_{35} = \omega_x^3 (\frac{e_x}{r}) \{ \frac{1}{2\zeta\Delta'}[(1-\beta_y^2) (\omega_2' \beta_y^2) - u_2' \beta_y^4 (\frac{e_x}{r}) - v_2' \beta_y^2 (\frac{e_y}{r})] \}$$

$$\Gamma_{36} = \omega_x^3 (\frac{e_x}{r}) \{ 4\beta_y^3 \zeta + \frac{1}{2\zeta\Delta'}[(\beta_\theta^2-\beta_y^2) (v_2' \beta_y^2) - \omega_2' \beta_y^2 (\frac{e_y}{r})] \}$$

$$\Gamma_{44} = \omega_x^3 \{ 2\beta_\theta \zeta (1+\beta_\theta) + 4\zeta (\frac{e_y}{r})^2 + \frac{1}{2\zeta\Delta'} [u_1' (1-\beta_\theta^2)^2 -$$

$$2(1-\beta_\theta^2)(u_3' \beta_y^2 (\frac{e_x}{r})) + \omega_3' \beta_y^4 (\frac{e_x}{r})^2] \}$$

$$\Gamma_{45} = \omega_x^3 \{ 2\beta_y \zeta (\frac{e_x}{r})(1+\beta_y) + \frac{1}{2\zeta\Delta'} [u_3' (1-\beta_\theta^2)(1-\beta_y^2) +$$

$$(1-\beta_\theta^2)(-u_1' \beta_y^2 (\frac{e_x}{r}) - u_2' (\frac{e_y}{r})) + (\beta_y^2 - 1)(\omega_3' \beta_y^2 (\frac{e_x}{r}))$$

$$+ u_3' \beta_y^4 (\frac{e_x}{r})^2 + \omega_2' \beta_y^2 (\frac{e_x}{r})(\frac{e_y}{r})] \}$$

$$\Gamma_{46} = \omega_x^3 \{ -2\beta_y \zeta (1+\beta_y)(\frac{e_x}{r})(\frac{e_y}{r}) + \frac{1}{2\zeta\Delta'} [u_2' (1-\beta_\theta^2)(\beta_\theta^2 - \beta_y^2) +$$

$$(1-\beta_\theta^2)(-u_3' (\frac{e_y}{r})) + (\beta_y^2 - \beta_\theta^2)(\omega_2' \beta_y^2 (\frac{e_x}{r})) + \omega_3' \beta_y^2 (\frac{e_x}{r})(\frac{e_y}{r})] \}$$

$$\Gamma_{55} = \omega_x^3 \{ 2\beta_y \zeta (1+\beta_y) + \frac{1}{2\zeta\Delta'} [\omega_3' (1-\beta_y^2)^2 + 2(1-\beta_y^2)(-\omega_2' (\frac{e_y}{r}) -$$

$$u_3' \beta_y^2 (\frac{e_x}{r})) + (2u_2' \beta_y^2 (\frac{e_x}{r})(\frac{e_y}{r}) + u_1' \beta_y^4 (\frac{e_x}{r})^2 + v_2' (\frac{e_y}{r})^2)] \}$$

$$\Gamma_{56} = \omega_x^3 \{ -2\beta_y \zeta (1+\beta_y)(\frac{e_y}{r}) + \frac{1}{2\zeta\Delta'} [\omega_2' (1-\beta_y^2)(\beta_\theta^2 - \beta_y^2) - \omega_3' (1-\beta_y^2)(\frac{e_y}{r})$$

$$+ (\beta_y^2 - \beta_\theta^2)(u_2' \beta_y^2 (\frac{e_x}{r}) + v_2' (\frac{e_y}{r})) + (\omega_2' (\frac{e_y}{r})^2 + u_3' \beta_y^2 (\frac{e_x}{r})(\frac{e_y}{r}))] \}$$

$$\Gamma_{66} = \omega_x^3 \{ 2\beta_y\beta_\theta\zeta(\beta_\theta+\beta_y) + 4\beta_y^3\zeta(\frac{e_x}{r})^2 + \frac{1}{2\zeta\Delta'}[v_2'(\beta_\theta^2-\beta_y^2)^2 -$$

$$2\omega_2'(\beta_\theta^2-\beta_y^2)(\frac{e_y}{r}) + \omega_3'(\frac{e_y}{r})^2]\}$$

where $\Delta' = (1+\beta_\theta)(\beta_\theta+\beta_y)(1+\beta_y) - \beta_y^2(\beta_\theta+\beta_y)(\frac{e_x}{r})^2 - (1+\beta_\theta)(\frac{e_y}{r})^2$

$$u_1' = (\beta_\theta+\beta_y)(1+\beta_y) - (\frac{e_y}{r})^2$$

$$v_2' = (1+\beta_y)(1+\beta_\theta) - \beta_y^2(\frac{e_x}{r})^2$$

$$\omega_2' = (1+\beta_\theta)(\frac{e_y}{r})$$

$$\omega_3' = (1+\beta_\theta)(\beta_\theta+\beta_y)$$

$$u_2' = -\beta_y(\frac{e_x}{r})(\frac{e_y}{r})$$

$$u_3' = -(\beta_\theta+\beta_y)\beta_y(\frac{e_x}{r})$$

REFERENCES

1. Aki, K. "Scattering of P Waves under the Montana Lasa," Journal of Geophysical Research, Vol. 78, No.8, March, 1973.

2. Amin, M. and A. H. Ang, "A Nonstationary Stochastic Model for Strong-Motion Earthquake," Structural Research Series 306, University of Illinois, Urbana, Illinois.

3. API RP2A, "API Recommended Practice for Planning, Designing and Constructing Fixed Offshore Platforms," 11th Edition, Jan. 1980.

4. Ariaratnam, S. T., "Course Notes on Probabilistic Structural Dynamics," Department of Aeronautical and Astronautical Engineering, University of Illinois, Urbana, Illinois.

5. Arias, A., "A Measure of Earthquake Intensity," In Seismic Design for Nuclear Power Plants, R. Hansen, Editor, Massachusetts Institute of Technology Press, Cambridge, Massachusetts, 1970.

6. ATC-3 Code, "Tentative Provisions for the Development of Seismic Regulations for Buildings, "Prepared by Applied Technology Council, ATC Pub, ATC 3-06, NSF Pub, 78-8.

7. Ayre, R. S., "Interconnection of Translational and Torsional Vibrations in Buildings," Bulletin of the Seismological Society of America, Vol. 28, No. 2, April 1938, pp. 89-130.

8. Ayre, R. S., "Experimental Response of an Asymmetric, one-Story Building Model to An Idealized Transient Ground Motion," Bulletin of the Seismological Society of America, Vol. 33, No. 2, April 1943, pp. 91-119.

9. Bathe, K. J., and Wilson, E. L., "Numerical Methods in Finite Element Analysis," Prentice-Hall, Inc. Englewood Cliffs, New Jersey, 1976, pp. 494-506.

10. Barstein, M. F., "Application of Probability Methods for Design. The Effect of Seismic Forces on Engineering Structures," Proceedings of the 2nd World Conference on Earthquake Engineering, Tokyo and Kyoto, July, 1960.

11. Bertero, V. V., "An overview of the State-of-the-Art in Earthquake-Resistant Reinforced Concrete Building Construction," Proceedings of the 2nd U.S. National Conference on Earthquake Engeering, Aug. 22-24, 1979, Stanford, pp. 838-852.

12. Bertero, V. V., "State-of-the-Art in Establishing Design Earthquakes," Earthquake-Resistant Reinforced Concrete Building Construction, Proceedings of a Workshop Held at the University of California at Berkeley, July 11-15,1977, Vol. II, pp. 315-345, University of California Extension, Berkeley, June 1978.

13. Bogdanoff, J. L., Goldberg, J. E., and Bernard, M. C., "Response of a Simple Structure to a Random Earthquake-Type Disturbance," Bulletin of the Seismological Society of America, Vol. 51, No. 2, April 1961.

14. Bolotin, V.V., "Statistical Theory of the Asiesmic Design of Structures," Proceedings of the 2nd World Conference on Earthquake Engineering, Tokyo and Kyoto, July 1960.

15. Bucy, R., "Realization of Nonlinear Filters," Second Symposium on Nonlinear Estimation, San Diego, 1971.

16. Bustamante, J. I. and Rosenblueth, E., "Building Code-Provisions on Torsional Oscillation," Proceedings of the Second World Conference on Earthquake Engineering, Vol. 2. Tokyo, Japan, 1960, pp. 879-894.

17. Bycroft, G. N., "White Noise Representation of Earthquake," Journal of Engineering Mechanics Division, ASCE, Vol. 86, No. EM6, April 1960.

18. Chopra, A., and Lopez, O. A., "Evaluation of Simulated Ground Motions for Predicting Elastic Response of Long Period Structures and Inelastic Response of Structures," Earthquake Engineering and Structural Dynamics, Vol. 7, 1979, pp. 383-402.

19. Clough, R. W. and Penzien, J., "Dynamics of Structures," McGraw-Hill Book Co., New York, New York, 1975.

20. Coleman, J. J., "Reliability of Aircraft Structures in Resisting Chance Failures," Operation Research, Vol. 7, No. 5. 1959, pp.539-645.

21. Cramer, H., "On the Intersections between the Trajectories of a Normal Stationary Stochastic Process and a High Level," Arkiv. fur Matematik, 6, 20, 1966, pp. 337-349.

22. Dempsey, K., M., and Irvine, H., M., "Envelopes of Maximum Seismic Response for a Partially Symmetric Single Story Building Model," Earthquake Engineering and Structural Dynamics, Vol. 7, 1979, pp. 161-180.

23. Der Kiureghian, A., "On Response of Structures to Stationary Excitation," Report No. EERC 79-32, Earthquake Engineering Research Center, University of California, Berkeley. 1979.

24. Dolean-Dade, C. and Meyer, P., "Integrales Stochastiques Par Rapport aux Martingales Locales," In Seminaire de probabilities IV, Lecture Notes in Math., Vol. 124, Springer, Berlin, 1970.

25. Dobry, R., Idriss, I. M. and Ng, E. "Duration Characteristics of Horizontal Components of Strong Motion Earthquake Records," Bulletin of the Seismological Society of America, Vol. 68, No. 4, Oct. 1978, pp. 1487-1520.

26. Douglas, B. M., and Trabert, T. E., "Coupled Torsional Dynamic Analysis of Multi-story Buildings," Bulletin of Seismological Society of America, Vol. 63, No. 3, June 1973, pp. 1025-1039.

27. Gasparini, D. A., and DebChaudhury, A., "Dynamic Response to Nonstationary Nonwhite Excitation," Journal of Engineering Mechanics Division, ASCE, Vol. 106, No. EM6, December 1980.

28. Gelb, A., "Applied Optimal Estimation," M. I. T. PRESS, Massachusetts Institute of Technology, Cambridge, Massachusetts, and London, England, 1974.

29. Gibson, R. E., Moody, M. L. and Ayre, R. S., "Free Vibration of an Unsymmetrical Multistoried Building Modelled as a Shear-Flexible Cantilever Beam," Bulletin of the Seismological Society of America, Vol. 62, No. 1, February 1972, pp. 195-213.

30. Hall, W. J., Mohraz, B., and Newmark, N. M., "Statistical Analyses of Earthquake Response Spectra," 3rd International Conference of Structural Mechanics and Reactor Technology, BAM, Berlin, Paper No. K 1/6, 11 pp., Sept. 1975.

31. Hadded, A. H., "Course Notes on Nonlinear Filtering," Department of Electrical Engineering, University of Illinois. Urbana, Illinois.

32. Hahn, G. J., and Shapiro, S. S., "Statistical Models in Engineering," John Wiley, New York, New York, 1967.

33. Hindy, A. and Novak, M., "Pipeline Response to Random Ground Motion," Journal of the Engineering Mechanics Division, ASCE, April 1980, pp. 339-360.

34. Hoerner, J. B., "Modal Coupling and Earthquake Response of Tall Buildings," Report No. EERL 71-07, Earthquake Engineering Research Laboratory, California, Institute of Technology, Pasadena, California, May, 1971.

35. Housner, G. W., "Characteristics of Strong-Motion Earthquakes," Bulletin of the Seismological Society of America, Vol. 37, No. 1, 1974.

36. Housner, G. W., "Behavior of Structures during Earthquakes," Journal of the Engineering Mechanics Division, ASCE, Vol. 85, No. EM4, Proc. paper 2220, Oct., 1959, pp. 109-129.

37. Housner, G. W. and Jennings, P. C., "Generation of Artificial Earthquakes," Journal of the Engineering Mechanics Division, ASCE, Vol. 90, No. EM1, February 1964, pp. 113-150.

38. Housner, G. W., "Calculating the Response of an Oscillator to Arbitrary Ground Motion," Bulletin of the Seismological Society of America, Vol. 31, No. 2, April 1941, pp. 143-149.

39. Housner, G. W., "Intensity of Ground Motion during Strong Earthquakes," Report No. 52-80 Earthquake Engineering Research Laboratory, California Institute of Technology.

40. Husid, R. L., "Analisis de Terremotos: Analisis General," Revista del IDIEM, Santiago, Chile, Vol. 8, No. 1, May 1969, pp. 21-42.

41. Irvine, H. M., and Kountouris, G. E., "Inelastic Seismic Response of a Torsionally Unbalanced Single-Story Building," Publication No. R79-31, Massachusetts Institute of Technology, Cambridge, Massachussetts, 1979.

42. Idriss, I. M., "Characteristics of Earthquake Ground Motions," Proceedings of the ASCE Geotechnical Engineering Division Special Conference, Vol. III, Earthquake Engineering and Soil Dynamics, June 19-21, 1978., Pasadena, California.

43. Iyengar, R. N., and Iyengar K. T. S. R., "A Nonstationary Random Process Model for Earthquake Accelerograms," Bulletin of Seismological Society of America, Vol. 59, No. 3, June 1969, pp. 1163-1188.

44. Jeffreys, H. "Theory of Probability," 3rd ed. Oxford University Press, Oxford, 1961.

45. Johnson, E. L., Nixon, E., and Amos, D. E., "Table of Percentage Points of Pearson Curves, for Given $\sqrt{\beta_1}, \beta_2$, Expressed in Standard Measure," Biometrika, 1963, pp. 50, 459.

46. Kailath, T., "Linear Systems," Prentice-Hall, Inc. Englewood Cliffs, New Jersey, 1980.

47. Kan, C. L., and Chopra, A. K., "Coupled Lateral Torsional Response of Buildings to Ground Shaking," Report No. EERC 76-13, May 1976, University of California, Berkeley.

48. Kanai, K., "Semi-Empirical Formula for the Seismic Characteristics of the Ground Motion," Bulletin of the Earthquake Research Institute, University of Tokyo, Japan, Vol. 35, June 1967, pp. 308-325.

49. Kubo, T., and Penzien, J., "Time and Frequency Domain Analyses of Three Dimensional Ground Motions San Fernando Earthquake," Report No. EERC 76-6, March 1976, University of California, Berkeley.

50. Kwakernaak, H., "Filter for Systems Excited by Poisson White Noise," pp. 463-492 in A. Bensonssan and J. L. Lion, Ed., Control Theory Numerical Methods and Computer Systems Modelling,Lecture Notes in Economics and Math. Systems. Vol. 107, Springer-Verlag, Berlin, 1975.

51. Lin, Y. K., "Probabilistic Theory of Structural Dynamics," McGraw-Hill Book Co., New York, New York, 1967.

52. Lin, Y. K., "Application of Nonstationary Shot Noise in the Study of System Response to a Class of Nonstationary Excitations," Journal of Applied Mechanics, Vol. 30. Series E, No. 4, 1963.

53. Liu, S. C., "Evolutionary Power Spectral Density of Strong Motion Earthquake," Bulletin of Seismological Society of America, Vol. 60, No. 3, 1970, pp. 891-900.

54. Lutes, L. D., Chen, Y. T., and Tsung, S. H., "First-Passage Approximations for Simple Oscillators," Journal of Engineering Mechanics Division, ASCE, Vol. 106, No. EM6, December 1980.

55. Morgan, J., Hall, W. J. and Newmark, N. M., "Response of Simple Structural Systems to Traveling Seismic Wave," UILU-ENG-79-2015, University of Illinois, 1979.

56. Newmark, N. M., "Design Criteria for Nuclear Reactors Subjected to Earthquake Hazards," Proc. LAEA Panel on Aseismic Design and Testing of Nuclear Facilities, Tokyo: Japan Earthquake Engineering Promotion Society, 1969, pp. 90-113.

57. Newmark, N. M., and Hall, W. J., "Seismic Design Criteria for Nuclear Reactor Facilities," Proceedings of the Forth World Conference on Earthquake Engineering, Santiago, Chile, 2, B-4, 1969, pp. 37-50.

58. Newmark, N. M., "Torsion in Symmetric Buildings," Proceedings of the Fourth World Conference on Earthquake Engineering, Vol. 2, Santiago, Chile, 1969, pp A3-19 to A3-32.

59. Newmark, N. M., Hall, W. J., and Morgan, J., "Comparison of Building Response and Free-Field Motion in Earthquakes," Proc. 6th World Conference on Earthquake Engineering, New Delhi, India, V. 11, Topic 3, 1977, pp. 972-978.

60. Newmark, N. M., "A Rationale for Development of Design Spectra for Diablo Canyon Reator Facility," A Report to the U. S. Nuclear Regulatory Commission, Nathan M. Newmark Consulting Engineering Services, 1211 Civil Engineering Building, Urbana, Illinois, Sep. 1976.

61. Newmark, N. M., and Hall, W. J., "Development of Criteria for Seismic Review of Selected Nuclear Power Plants," N. M. Newmark Consulting Engineering Service. Sep. 1977.

62. Newmark, N. M., and Rosenblueth, E., "Fundamentals of Earthquake Engineering," Prentice Hall, Inc. Englewood Cliffs, New Jersey, 1971.

63. Oppenheim, A. V., and Schafer, R. W., "Digital Signal Processing," Alan V. Oppenheim and Bell Telephone Laboratories, Inc. 1975.

64. Papoulis, A., "Probability, Random Variables, and Stochastic Processes," McGraw-Hill, New York, New York 1965.

65. Pecknold, D. A., and Riddell, R., "Effect of Initial Base Motion on Response Spectra," Journal of the Engineering Mechanics Division, ASCE, Vol. 104, No. EM2, April 1978, pp. 485-491.

66. Penzien, J., "Earthquake Response of Irregular Shaped Buildings," Proceedings of the Fourth World Conference on Earthquake Engineering, Vol. 2, Santiago, Chile, 1969, pp. A3-75 to A3-89.

67. Penzien, J., and Watabe, M., "Characteristics of 3-Dimensional Earthquake Ground Motions," Earthquake Engineering and Structural Dynamics, Vol. 3, 1975, pp. 365-373.

68. Priestley, M. B., "Evolotionary Spectra and Nonstationary Processes," Journal of the Royal Statistical Society, Vol. 27, 1965, pp. 204-228.

69. Priestley, M. B., "Power Spectral Analyses of Nonstationary Random Processes," Journal of Sound and Vibration, Vol. 6, 1967, pp. 86-97.

70. Rice, S. O., "Mathematical Analysis of Random Noise," Bell System Technical Journal, 23, 1941, pp. 282-332; 24, 1945, pp. 46-156.

71. Rosenblueth, E., and Elorduy, J., "Response of Linear Systems to Certain Transient Disturbance," Proceedings of the Fourth World Conference on Earthquake Engineering, Vol. 1, Chile, pp. A1-185 to A1-196.

72. Rosenblueth, E., and Contreras, H., "Approximate Design for Multi-component Earthquakes," Journal of Engineering Mechanics Division, ASCE, Vol. 103, No. EM5, Oct. 1977.

73. Rosenblueth, E., "some Applications of Probability Theory in Aseismic Design," World Conference on Earthquake Engineering, Berkeley, California, June 1956.

74. Rosenblueth, E., and Bustamante, J. I., "Distribution of Structural Responses to Earthquakes," Journal of the Engineering Mechanics Division, ASCE, Vol. 88, No. EM3, June 1962, pp. 75-106.

75. Ruiz, P., and Penzien, J., "Probabilistic Study of the Behavior of Structures During Earthquakes," Report of Earthquake Engineering Research Center, EERC 69-3, University of California, Berkeley, 1969.

76. Shiga, T., "Torsional Vibrations of Multi-Storied Buildings," Proceedings of the Third World Conference on Earthquake Engineering, Vol. 2, Auckland and Wellington, New Zealand, 1965, pp. 569-584.

77. Shephard, R., and Donald, R. A. H., "Seismic Response of Torsionally Unbalanced Buildings," Journal of Sound and Vibration, Vol. 6., No. 1, 1967, pp. 2037.

78. Shinozuka, M., and Sato, Y., "Simulation of Nonstationary Random Processes," Journal of the Engineering Mechanics Division, ASCE, Vol. 93, No. EM1, February 1967, pp. 11-40.

79. Skinner, R. I., Skilton, D. W. C., and Laws, D. A., "Unbalanced Buildings and Buildings with Light Towers under Earthquake Forces," Proceedings of the Third World Conference on Earthquake Engineering, Vol. 2, Auckland and Wellington, New Zealand, 1965, pp. 586-602.

80. Snyder, D., "Random Point Processes," John Wiley, New York, New York, 1975.

81. Tajimi, H., "Basic Theories on Aseismic Design of Structures," Institute of Industrial Science, University of Tokyo, Vol. 8, No. 4, 1959.

82. Trifunac, M. D., and Bardy, A. G., "A Study of the Duration of Strong Earthquake Ground Motions," Bulletin of the Seismological Society of America, Vol. 65, No. 3, June, pp. 581-626.

83. Toki, K., "Simulation of Earthquake Motion and its Application," Bulletin of the Disaster Prevention Research Institute, Kyoto University, Vol. 11-A, March 1968.

84. Vanmarcke, E. H., "On the Distribution of the First Passage Time for Normal Stationary Random Processes," Journal of Applied Mechanics Transactions ASME, Vol. 42, March 1975, pp. 215-220.

85. Van Trees, H. L., "Detection, Estimation, and Modulation Theory," Part I and Part III, John Wiley, New York, New York.

86. Ward, H. S., "Analog Simulation of Earthquake Motions," Journal of the Engineering Mechanics Division, ASCE, Vol. 91, No. EM5, Oct. 1965.

87. Wilkinson, J. H., "The Algebraic Engenvalue Problem," Oxford University Press, Oxford, 1965.

88. Wong, E., "Recent Progress in Stochastic Processes - a Survey," IEEE Trans. Information Theory, Vol. IT-19, No. 3, 1973.